Airborne noise characterisation of a complex machine using a dummy source approach

Anders Sven Axel Lindberg

N°ordre: 2015ISAL0082

THÈSE

AIRBORNE NOISE CHARACTERISATION OF A COMPLEX MACHINE USING A DUMMY SOURCE APPROACH

présentée devant
l'Institut National des Sciences Appliquées de Lyon

par
Anders S. A. LINDBERG
Civ. Ing., Civil Engineering, Chalmers University of Technology
M. Sc., Sound and Vibration, Chalmers University of Technology
B. Sc., Civil Engineering, Chalmers University of Technology

pour obtenir
le GRADE DE DOCTEUR

École doctorale:
Mécanique, Énergétique, Génie Civil, Acoustique
Spécialité : Acoustique

Juillet 2015
Novembre 2015 édition révisée

Thèse préparée au Laboratoire Vibrations Acoustique
soutenue le 28/09/2015 devant la Commission d'examen

Jury

Goran PAVIĆ	Prof. Emer.	INSA de Lyon	Directeur de Thèse
Anders NILSSON	Prof. Emer.	Università degli Studi di Brescia	Rapporteur
Paul SAS	Prof.	Katholieke Universiteit Leuven	Rapporteur
Charles PEZÉRAT	Prof.	Université de Maine	Examinateur
Quentin LECLÈRE	MCF HDR	INSA de Lyon	Examinateur

SIGLE	ECOLE DOCTORALE	NOM ET COORDONNEES DU RESPONSABLE
CHIMIE	**CHIMIE DE LYON** **http://www.edchimie-lyon.fr** Sec : Renée EL MELHEM Bat Blaise Pascal 3e etage 04 72 43 80 46 Insa : R. GOURDON secretariat@edchimie-lyon.fr	M. Jean Marc LANCELIN Université de Lyon – Collège Doctoral Bât ESCPE 43 bd du 11 novembre 1918 69622 VILLEURBANNE Cedex Tél : 04.72.43 13 95 directeur@edchimie-lyon.fr
E.E.A.	**ELECTRONIQUE, ELECTROTECHNIQUE, AUTOMATIQUE** **http://edeea.ec-lyon.fr** Sec : M.C. HAVGOUDOUKIAN Ecole-doctorale.eea@ec-lyon.fr	M. Gérard SCORLETTI Ecole Centrale de Lyon 36 avenue Guy de Collongue 69134 ECULLY Tél : 04.72.18 60.97 Fax : 04 78 43 37 17 Gerard.scorletti@ec-lyon.fr
E2M2	**EVOLUTION, ECOSYSTEME, MICROBIOLOGIE, MODELISATION** **http://e2m2.universite-lyon.fr** Sec : Safia AIT CHALAL Bat Atrium- UCB Lyon 1 04.72.44.83.62 Insa : S. REVERCHON Safia.ait-chalal@univ-lyon1.fr	M. Fabrice CORDEY Laboratoire de Géologie de Lyon Université Claude Bernard Lyon 1 Bât Géode – Bureau 225 43 bd du 11 novembre 1918 69622 VILLEURBANNE Cédex Tél : 04.72.44.83.74 Sylvie.reverchon-pescheux@insa-lyon.fr fabrice.cordey@ univ-lyon1.fr
EDISS	**INTERDISCIPLINAIRE SCIENCES-SANTE** **http://www.ediss-lyon.fr** Sec : Safia AIT CHALAL Bat Atrium – UCB Lyon 1 04 72 44 83 62 Insa : Safia.ait-chalal@univ-lyon1.fr	Mme Emmanuelle CANET-SOULAS INSERM U1060, CarMeN lab, Univ. Lyon 1 Bâtiment IMBL 11 avenue Jean Capelle INSA de Lyon 696621 Villeurbanne Tél : 04.72.11.90.13 Emmanuelle.canet@univ-lyon1.fr
INFOMATHS	**INFORMATIQUE ET MATHEMATIQUES** **http://infomaths.univ-lyon1.fr** Sec :Renée EL MELHEM Bat Blaise Pascal 3e etage infomaths@univ-lyon1.fr	Mme Sylvie CALABRETTO LIRIS – INSA de Lyon Bat Blaise Pascal 7 avenue Jean Capelle 69622 VILLEURBANNE Cedex Tél : 04.72. 43. 80. 46 Fax 04 72 43 16 87 Sylvie.calabretto@insa-lyon.fr
Matériaux	**MATERIAUX DE LYON** **http://ed34.universite-lyon.fr** Sec : M. LABOUNE PM : 71.70 –Fax : 87.12 Bat. Direction 1er et. Ed.materiaux@insa-lyon.fr	M. Jean-Yves BUFFIERE INSA de Lyon MATEIS Bâtiment Saint Exupéry 7 avenue Jean Capelle 69621 VILLEURBANNE Cedex Tél : 04.72.43 71.70 Fax 04 72 43 85 28 Ed.materiaux@insa-lyon.fr
MEGA	**MECANIQUE, ENERGETIQUE, GENIE CIVIL, ACOUSTIQUE** **http://mega.universite-lyon.fr** Sec : M. LABOUNE PM : 71.70 –Fax : 87.12 Bat. Direction 1er et. mega@insa-lyon.fr	M. Philippe BOISSE INSA de Lyon Laboratoire LAMCOS Bâtiment Jacquard 25 bis avenue Jean Capelle 69621 VILLEURBANNE Cedex Tél : 04.72 .43.71.70 Fax : 04 72 43 72 37 Philippe.boisse@insa-lyon.fr
ScSo	**ScSo*** **http://recherche.univ-lyon2.fr/scso/** Sec : Viviane POLSINELLI Brigitte DUBOIS Insa : J.Y. TOUSSAINT viviane.polsinelli@univ-lyon2.fr	Mme Isabelle VON BUELTZINGLOEWEN Université Lyon 2 86 rue Pasteur 69365 LYON Cedex 07 Tél : 04.78.77.23.86 Fax : 04.37.28.04.48 isavonb@dbmail.com

*ScSo : Histoire, Géographie, Aménagement, Urbanisme, Archéologie, Science politique, Sociologie, Anthropologie

You came here to sit and think,
but all you do is shit and stink…

Velimir Salamon,
brother-in-law of Goran Pavić

Résumé

La caractérisation des sources sonores dues aux vibrations est un défi dans le domaine du bruit et des vibrations. Dans cette thèse, une approche expérimentale pour caractériser la propagation du son d'une machine complexe a été étudiée. Pour caractériser de manière appropriée la source sonore placée dans un environnement quelconque, il a été indispensable de prendre en compte les phénomènes de rayonnement et de diffraction. Cela permet de prédire une pression acoustique. Une technique particulière, appelée *source mannequin*, a été développée pour répondre à cette problématique. Le mannequin est une enceinte fermée de taille similaire mais qui a une forme simplifiée par rapport à la machine complexe, et sert de modèle de diffraction sonore. Le mannequin est équipé d'une série de haut-parleurs alignés dans le prolongement de la surface de l'enceinte. La superposition du champ acoustique créé par chaque haut-parleur modélise le rayonnement acoustique de la machine complexe.

Cette thèse introduit donc le concept de source mannequin et traite de trois problèmes émanant de la mise en pratique de celui-ci : (1) l'estimation du transfert d'impédance dans l'espace (fonction de Green), (2) les spécifications de l'enceinte et de la série de haut-parleurs, et (3) l'estimation des sources équivalentes en termes de débit volumique. L'approche est étudiée au travers de cas d'études expérimentaux et numériques.

Mots clés : rayonnement acoustique par un corps vibrant, diffraction du son par un corps vibrant, principe de superposition, estimation des fonctions de transfert d'impédance, estimation de débit volumique des sources équivalentes, approche par source mannequin, approche par la fonction de Green.

Abstract

The characterisation of vibrating sound sources is a challenge in noise and vibration engineering. In this thesis, an experimental approach to the characterisation of air-borne sound from a complex machine is investigated. A proper characterisation has to account for both radiation and diffraction phenomena in order to describe the sound source when inserted into an arbitrary space which enables prediction of sound pressure. A particular technique — *a dummy source* — has been conceived to deal with this problem. The dummy is a closed cabinet of similar size but much simpler shape than the complex machine, and it serves as a model of sound diffraction. The dummy is equipped with a flush-mounted array of loudspeaker drivers. The superposition of sound fields created by the individual drivers models sound radiation of the complex machine.

This thesis introduces the concept of a dummy source and discusses three problems that need to be addressed for its practical application: (1) estimation of the transfer impedance of the space (the Green's function), (2) the specification of the cabinet and the driver array, and (3) the estimation of the equivalent source strengths in terms of volume velocity. The approach is investigated via experimental and numerical case studies.

Keywords: sound radiation by a vibrating body, sound diffraction by a vibrating body, the superposition principle, transfer impedance estimation, equivalent source strength estimation, the dummy source approach, Green's function approach.

Sammanfattning

Karakterisering av ljudkällor är en utmaning inom teknisk akustik. I denna avhandling undersöks en experimentell metod för karakterisering av luftburet ljud från den vibrerande ytan av en komplex maskin. En korrekt karakterisering måste ta hänsyn till både utstrålning och diffraktion för att beskriva ljudkällan oberoende av rum. Detta kan nyttjas till att förutsäga ljudtryck i ett annat rum. En särskild ansats — *en källmannekäng* — har utvecklats för att tackla problemet. Mannekängen är en sluten högtalarlåda av samma storlek som den ursprungliga maskinen men den är enklare formad och modellerar diffraktion. Mannekängen är vidare utrustad med en serie av högtalare monterade i plan med högtalarlådans yta. Maskinens utstrålning modelleras genom att superponera ljudfälten ifrån de individuella högtalarna.

Avhandlingen introducerar idén om en källmannekäng och diskuterar tre problem som måste hanteras för att praktiskt tillämpa den: (1) uppskattning av överföringsimpedanser i ett rum (Greenfunktioner), (2) specificering av högtalarlåda och serien av högtalare, och (3) uppskattning av ekvivalenta källstyrkor uttryckt i volymflöde. Metoden undersöks i en serie av experimentella och numeriska fallstudier.

Nyckelord: ljudutstrålning från en vibrerande kropp, ljuddiffraktion från en vibrerande kropp, superpositionsprincipen, uppskattning av överföringsimpedanser, uppskattning av ekvivalenta källstyrkor, ansats med källmannekäng, ansats med Greenfunktioner.

Acknowledgements

I want to acknowledge Klas Nilson, a teacher of mine a long time ago at Polhemsskolan in Lund in Sweden. Without you I would not have ventured into engineering and science. I would also like to acknowledge Wolfgang Kropp and Patrik Höstmad at Teknisk Akustik at Chalmers Tekniska Högskola in Göteborg in Sweden for teaching me sound and vibration during my engineering studies. Wolfgang, during your short stay in Lyon, you puzzled out the last detail needed to realise the dummy source. Tusen tack!

The work has been carried out at Laboratoire Vibrations Acoustique at Institut National des Sciences Appliquées de Lyon in France. This thesis has been supervised by Goran Pavić who originally came up with the idea of a dummy source. Goran, I am grateful for your patience, encouragement, and advice on my ideas about how to approach a dummy source experimentally and numerically.

The dummy source prototypes as well as the dual purpose array are to a large extent the work of Patrick Blachier and Antoine "Tonio" Godoy. Without you, the experimental work in this thesis would not have been possible. I also acknowledge Quentin Leclère, Jérôme Antoni, and Bernard Laulagnet for your advice. In particular regarding rotating machines and regularisation. I would also like to thank Anders Nilsson and Paul Sas for their remarks on the thesis.

The work has been financially supported by Volvo Construction Equipment, which is gratefully acknowledged. I appreciate the past years' discussions with Nicklas Frenne, Jonas Larsson, Catalin Badau and Didier Baligand at Volvo in Eskilstuna, Sweden, and Belley, France, who inspired the development of what will hopefully become a practicable engineering approach to air-borne sound characterisation of complex machines. Nonetheless, the conducted work has been, while being industrially applicable, oriented towards basic aspects of a dummy source.

I express my gratitude to my friends, beer buddies, visitors, hiking guides and colleagues in Lyon and southern France during the past few years: Romain Nicolas, Grégory and Ann Michel, Aurelié Jactard, Itziar Serrano, Clio Chene, Konstantinos Gryllias, Antonio Pereira, Michael Vannier, Xin Zhao, Liangfen Du, Liang Yu, Ha Dong Wang, Fulbert Mbailassem, Hadrien and Ulysse Dhomé, Laurent Brocolini and Roch Scherrer among others. Without you it would have been a lonely stay. I want to thank Maxime Chuche who helped me translate the abstract. Also, I want to thank my friends in Sweden for supporting me and in particular Emeli Nilsson for proof reading the thesis.

I send a hug to Sven, Britt-Marie and Karl Lindberg and Gunilla, Johannes and Beatrice Lindén for your support. Last but not least, my stay in France would not have been the same without my girlfriend Diane Dhomé and her family in Finistère. Trugarez vras!

Contents

Chapter 1

Discussion

Overview

The discussion concerns how airborne sound from a vibrating source can be conceptually modelled and predicted using an array of loudspeaker drivers flush-mounted in the surface of a loudspeaker cabinet — a so called dummy source. The loudspeaker assembly is, however, virtual and the sound pressure is predicted with the help of a personal computer.

The need of noise source characterisation is explained in section 1. This is followed by a statement of the research questions in section 2. Thereafter, an overview of the state-of-the-art in acoustic prototyping and characterisation of sources is given in section 3. After that airborne characterisation is reviewed and the dummy source is conceptualised in section 4. Following that, a discussion on the implementation and simulation of the proposed dummy source approach will follow. The modelling of a driver - cabinet assembly is discussed in section 5. Arguing that the driver array consists of small drivers only, the simple source formulation is discussed in section 6. To implement a dummy source prototype the electrodynamic loudspeaker driver and its use to measure transfer impedances is discussed in section 7. After that a criterion for the number of drivers on the surface of the dummy source as required for accurate sound reproduction is introduced in section 8. A remaining problem is the estimation of the drivers' source strengths which, apart from the measurement of transfer impedances in a space, requires measurement of operating sound pressure responses of the vibrating source in the same space using a microphone array. The microphone array is discussed in section 9. The experimental procedure is summarised in section 10. Thereafter the estimation of the drivers' source strengths is discussed in section 11. The implementation is closed by an explanation on how the approach has been assessed in section 12. Thereafter the discussion changes subject to the simulation of the dummy source approach using the substitute source method. The simulation of a dummy source in section 13 is not only used for assessing the approach, but will be applied in hybrid characterisation of a vibrating source using computed transfer impedances. Following the discussion on the dummy source approach, the main findings from a series of experimental and numerical case studies are presented in section 14. The findings are followed by concluding remarks on the dummy source in section 15. After the concluding remarks, an overview of the supplementary material in Appendices I, II, III, IV and V is found.

1 INDUSTRIAL BACKGROUND

Sound and vibration comfort is an important aspect of the design of earth-moving machines. Heavy-duty vehicle manufactures face the challenge to improve upon their existing machine designs to meet the requirements of international and national laws as well as to successfully compete on the market. Ideally a machine operator should never be fatigued by harsh noise and vibration, which would result in an improved working environment and more efficient machine usage.

Since no commonly employed design tool for the perception of sound and vibration in a mechanical assembly exist, operator comfort at the current state often involves costly trial and error engineering after a physical machine prototype has been designed and built. There are, however, attempts to move towards

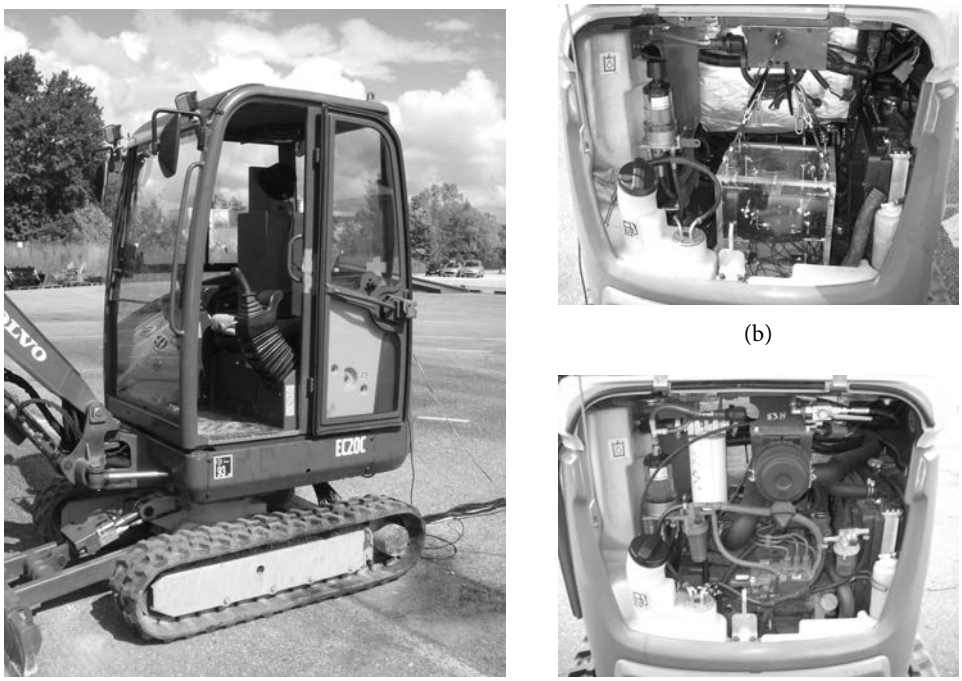

(a) (b) (c)

Figure 1: Reciprocal measurement of transfer impedances using (a) a known volume velocity source placed at the operator's ear using a dummy machine operator, (b) a dummy source implemented as an optically transparent box equipped with a microphone array and (c) the view of the engine compartment with the original diesel engine.

virtual acoustical prototyping [1, 2, 3, 4], which could be used to incorporate operator comfort in the design phase of heavy-duty vehicles. In plain words, to listen at the machine operator's ears inside of vehicle designs that are yet to be built.

Most existing computational engineering software treats the transmission of sound in the frequency domain. It is underlining the obvious, but the time domain is required for subjective evaluation. Moreover, the modelling of sound transmission is not sufficient for the purpose of virtual acoustical prototyping, which also requires one or more sound source models. Seemingly less attention has been paid to the latter problem: little is publicly known about sound modelling of an active complex machine component such as a diesel engine, although the scientific literature can be extensive on details.

It is *not* considered practicable to scrupulously model a complex machine as it is in reality. Instead such a source of sound will have to be replaced by a greatly simplified equivalent acoustical model. Such a model has to incorporate radiation and diffraction phenomena of the industrial sound source, while being independent of the acoustical space into which the complex machine is inserted.

This work investigates one procedure for *experimental characterisation* of airborne sound by a complex machine. The equivalent acoustical model, named the dummy source, is conceived to be a passive closed loudspeaker cabinet equipped with an active array of loudspeaker drivers. The cabinet - driver array assembly simulates both sound diffraction and sound radiation of the complex machine. Such a characterisation procedure is independent of the surrounding space, provided that the radiation is produced by vibration.

The investigation has been carried out as a series of experimental and numerical case studies. The dummy source approach will be demonstrated on both academic and industrial sound sources. Notably, a Yanmar 3TNV76-WVE diesel engine installed in an engine test rig. The diesel engine was commercially used in the Volvo CE EC20C compact excavator.

The dummy source approach is applicable to sources radiating sound by vibration of its housing, such as an electric engine, a hydraulic pump or an air compressor. The airborne characterisation needs to be

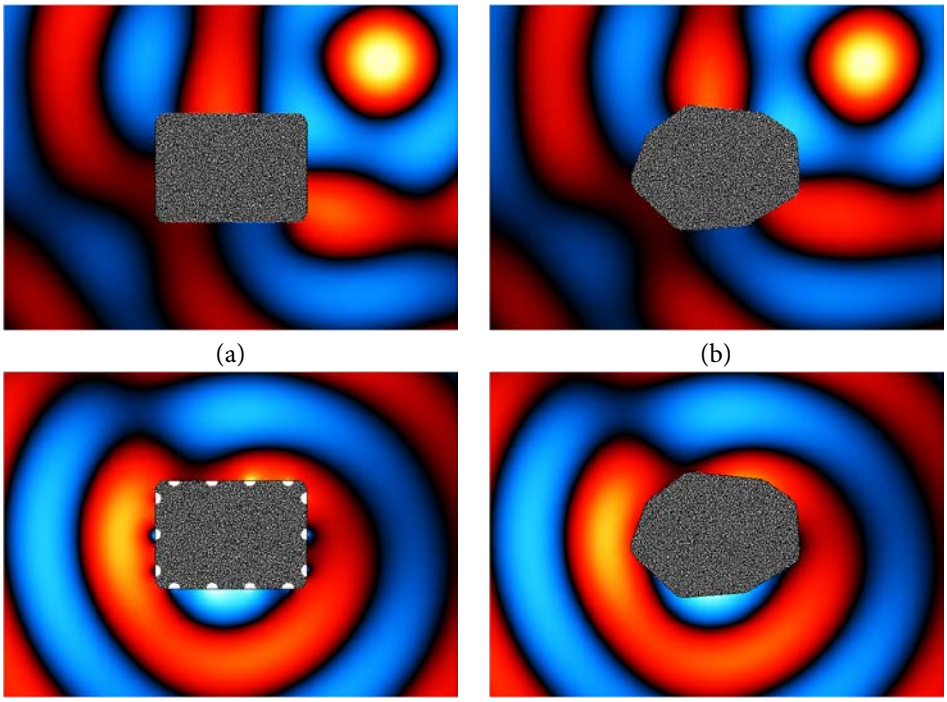

Figure 2: The dummy source approach: equivalence in diffraction of sound illustrated by (a) a spherical wave incident on the dummy, and (b) a spherical wave incident on an irregular body; equivalence in radiation of sound illustrated by (c) the sound field created by a dummy source, and (d) the sound field created by an original source. The drivers are illustrated along the contour of the dummy source by white half-circles. (G. Pavić) (Color)

complemented in regards to structureborne sound and fluidborne sound contributions to the overall noise. This will hopefully, in combination with existing finite element models or experimental models of the passive machine frame, become an engineering tool which enables designs with improved operator comfort in the future. An example of the application of the dummy source in industrial conditions, for the measurement of acoustic transfer impedances between a dummy source and a dummy operator in a compact excavator, can be seen in Fig. 1. Such a measurement can be used as a part of a noise synthesis scheme. In the next section, the research questions will be outlined.

2 RESEARCH QUESTIONS

The proposed dummy source approach has originally been conceived by Goran Pavić, and was inherited in this research work as a potential approach to the characterisation of airborne sound from a vibrating source, Fig. 2. The instantaneous sound fields at a constant frequency illustrate two essential assumptions of the approach: (1) The dummy source has a simpler shape than the vibrating source but is of similar volume, and (2) The dummy source is equipped with a limited number of drivers spread across its surface.

The research conducted within the project has focused on implementation and validation of the dummy source approach as a characterisation technique. The research questions have therefore been oriented towards experimental work: (1) *How to implement the dummy source approach?* The implementation concerns the design of the loudspeaker cabinet, the design of the loudspeaker driver array, the design of the microphone array and the estimation of the drivers' source strengths as required for accurate sound reproduction.; and (2) *Is the dummy source approach a viable characterisation method?* The viability concerns the use of the dummy source as an engineering tool to predict the operating sound pressure response inside of an acoustical space. These questions have been assessed through a series of experimental and numerical

case studies. In the next section, a literature survey on prototyping and source characterisation will be presented.

3 PROTOTYPING, CHARACTERISATION AND LOCALISATION

Moorhouse [3] reviewed virtual acoustical prototyping and substructuring into passive and active components on a refrigerator, among other examples. It is argued that a virtual acoustical prototype can not be fully virtual since the sound sources are little known and needs for the time being to be experimentally characterised. The measured equivalent source strengths can then be combined with computed impulse responses to listen to virtual source - receiver assemblies. The process is similar to auralisation techniques in which the dry sound, which is recorded in anechoic conditions, can be "played up" inside of a living room or concert hall by knowledge of the room impulse response. The primary advantages of virtual acoustical prototyping is that it gives insight to why and how a machine makes sound, as well as provides a tool to communicate the effect of design changes on the sound to non-specialists.

Pavić [4] reviewed a general framework for modelling sound of a complex machine assembly. In this framework sound sources are represented by a set of equivalent source strengths, which are intrinsic to the source and independent of the machine frame, and the passive machine frame by frame conductivity functions, which represents a transfer function between an equivalent source and sound at a point in space. In the case of airborne sound synthesis, the latter transfer function is a transfer impedance if the source strength is described in terms of volume velocity. The sound sources can not be described in terms of sound power because such a descriptor removes the radiation pattern of the source and depends on the surrounding. Nor can they be described by elementary substitute sources because in this case the source strengths depend on the surrounding space. Instead it is proposed that sound sources are characterised by blocked pressure and internal impedance at an enveloping surface as done in [5].

Bobrovnitskii and Pavić [5] proposed a technique to characterise airborne sound sources based on blocked pressure and source impedance. These source quantities were defined in terms of analytical spherical functions, but the technique requires a spherical chamber to be carried out in practice.

Berckmans et al. [6] compared by simulation equivalent source methods with the aim of auralising sound. The equivalent sources were either rigid pistons or monopoles. The equivalent sources were mounted on a cavity backed plate. The quantification of the equivalent source strengths was evaluated using several different quantities. Among them pressure, particle velocity, and normal component of particle velocity taken in the vicinity of the vibrating body. The source strength was also deduced using structural velocity on the surface of the vibrating body. It was found that the modelling accuracy is linked to the number and location of equivalent sources as well as to the structural and acoustical wavelengths. The choice of a monopole array, with its source strengths quantified from structural velocities, was found to be the best source model.

Moorhouse and Seiffert [7] characterised airborne contributions of a sound source for a virtual acoustical prototype. An active electric motor was separated from the passive machine frame of a white goods appliance, using the substitute source method implemented by an internal line array of monopoles along the engine's axis. The model neglects diffraction since the physical source was small compared to the wavelength. The characterisation was carried out in an anechoic environment. The transfer functions of the sound source model, coupled to the machine frame, were then measured using reciprocity. This enabled prediction of sound from the assembly.

Moorhouse [8] characterised structureborne contributions of a sound source, an electric engine, for use in a virtual acoustical prototype using a mobility approach. The characterisation, in which the excitation is assumed independent of the machine frame, express the equivalent contact forces between the active source and the passive frame as a function of free velocities and source and receiver mobilities. The radiated sound pressure is then calculated by transfer functions relating the sound pressure in a listening position to the equivalent contact forces. The modelling was validated by calculating and measuring the coupled velocity. Uncertainty analysis showed that successful reconstruction of the sound field strongly depends on the choice of equivalent contact forces.

Moorhouse et al. [9] showed that the blocked force of a vibration source, a quantity of the source which is independent of the passive frame, can be deduced from operational forces measured with the source

installed on a structure. The advantage of this approach to structureborne sound source characterisation is that there is no need of a special test rig.

Pavić [10] later developed an alternative formulation of the sound source characterisation in [5] based on patch averaged blocked pressure and patch averaged source impedance. In this case, the measurement of blocked pressure is not restricted to a chamber of any particular shape. The advantage of the developed approaches [5, 10] is that they are general and can be applied to any sound source. The disadvantage is that the measurement of blocked pressure is rather elaborate in practice.

Vogt et al. [11] identified sound sources on the surface of a diesel engine mock-up by an inverse boundary element approach. A custom made microphone array was used, which enclosed the sound source. The advantage of this optimisation procedure is that it allows for the construction of efficient sound synthesis models. The disadvantage is that such a model involves hundreds or thousands of degrees of freedom which needs to be quantified. This is deemed not to be feasible for experimental work.

Weber et al. [12] proposed an inverse finite element approach for the identification of sound sources embedded in the surface of a complex cavity at low frequencies. The cavity represents a section of an airplane cabin. The finite element model was experimentally validated and thereafter combined with inverse methods. The advantage is that the forward model accounts for the boundary conditions of the interior space. The disadvantage is that more than 7000 microphone positions were measured using a loudspeaker as a mock-up source, which is hardly feasible.

Frenne and Johansson [13] compared source models for time-domain quantification of partial sources on a diesel engine, the engine was represented by a combination of several point sources distributed on its surface, for the purpose of sound quality assessment. The advantage is the limited number of degrees of freedom, and that the transfer functions were measured so that the appropriate boundary conditions of the test cell were fulfilled. The disadvantage is that the source model needs to be carefully selected. In the next section, the dummy source approach will be outlined.

4 THE EQUIVALENT ACOUSTICAL MODEL — THE DUMMY SOURCE

The *dummy source* aims at characterising airborne sound from a *vibrating source*. The dummy source is an engineering tool used to both *predict the sound pressure level* and to listen to the *sound pressure response* of the vibrating source in a *listening space*. The vibrating source will sometimes be referred to as the *original source*.

4.1 Limitations

The total sound from a vibrating source, such as a diesel engine in a mechanical assembly, is only in part due to airborne sound from vibration of the housing. Alternative transmission is due to structureborne sound via the mounts, or fluidborne sound from the exhaust. Characterisation of structureborne sound and fluidborne sound is, however, outside the scope of this work. Airborne sound is of importance in some machine assemblies where, for example, the vibrating source is not completely shielded off from the machine operator.

The sound pressure radiated from housing vibration is considered to be of small amplitude. Moreover, the housing vibration is considered to be invariant to radiation loading from the surrounding sound field. The vibrating source is installed in a *characterisation space* and assumed to operate in steady-state conditions. Furthermore, the vibrating source is presumed to be the only source of sound inside of the characterisation space. Finally, the characterisation space is assumed to be a damped space such as a semi-anechoic room. The assumption of a damped space is not necessary but it simplifies the approach, especially for hybrid characterisation.

4.2 Airborne characterisation — existing approaches

The normal velocity distribution across the surface of the housing of the vibrating source is the ideal characteristic, satisfying the acoustic boundary-value problem and guaranteeing a unique sound field [14, pp. 100 - 103, 153 - 207]. However, in practice the irregular surface of the housing prevents direct measurement

of the vibration. Moreover, the vibration pattern is presumably complex. Consequently, it is not feasible to assess the velocity distribution as it is in reality.

The difficulties motivate the use of *simplified source models* which are deduced from the resulting sound field rather than the vibration field. The presumed complexity of the vibration field results, however, in that the sound field close to the surface of the vibrating source in turn is complicated. Therefore a feasible deduction needs to be carried out from operating sound pressure responses recorded at a distance away from the original source.

The choice of source model is often made in view of the volume of the vibrating source. Whether the volume is small or large depends on the acoustic wavelength compared to some typical dimension l of the vibrating source.

At long wavelengths ($l \ll \lambda$), at which the original source is negligible in size compared to the acoustic wavelength, the sound source, in an anechoic space, can be described in terms of a few elementary sources: a monopole, a dipole, and a quadrupole [14, pp. 159 - 171]. In a reflective space, such as a semi-anechoic test cell, reflections can be accounted for by the method of images [14, pp. 208 - 211].

A source model which is based on elementary sources assumes that sound diffraction can be neglected. The consequence is that a change of acoustical space, for example from a test cell to an engine compartment, is erroneous. There is, however, a technique which aims at correcting for the surface velocity distribution of the source model in the listening space and thus allowing for predictions in another space [4]. This requires modification of the source strengths of the elementary sources, in order to match the identified surface velocity of the vibrating sound source in the characterisation space as closely as possible in the listening space.

At short wavelengths ($l \gg \lambda$), in which the original source is several times larger than the acoustic wavelength, the vibrating source may be characterised it terms of its sound power output [15, pp. 71 - 81]. Sound power can, however, not be used for sound synthesis and auralisation since it removes information of both directivity and phase of the sound field. Moreover, heavy-duty machines are often problematic due to booming noise at long wavelengths. At long wavelengths, the power output of a vibrating source depends strongly on the surrounding space [14, pp. 39 - 47]. Finally, sound power does not allow for source - receiver (de)coupling. Thus sound power is not applicable for the purpose of airborne characterisation.

In the mid-frequency range, the complex machines are comparable in size to the acoustic wavelength ($l \sim \lambda$). In this range the prevailing source model is to deduce the velocity distribution [16, 17]. This can be achieved using holography methods [18, pp. 9 - 20], such as the inverse boundary element method [11], the inverse finite element method [12], or an inverse equivalent source method [18, pp. 24 - 28]. The dummy source belongs to this family of sound source modelling.

There are alternative formal sound source models in this frequency range. Bobrovnitskii et al. [16] proposed a procedure based on Huygens' principle using a smooth enclosing surface around the original source. The sound source is described by a smear of monopoles and dipoles on this enclosing surface. A finite number of such secondary sources is used as an airborne sound source model. This technique accounts for reflections in the measurement room, diffraction from the housing and radiation by the complex machine and can be formulated to be invariant of the environment [17].

Bobrovnitskii and Pavić [5] proposed a characterisation procedure based on blocked pressure and source impedance. These source parameters were written in terms of analytical spherical functions, but the technique requires a spherical chamber to be carried out in practice. Pavić later proposed [10] a further refined source model based on patch averaged blocked pressure, and patch averaged source impedance. In this case the measurement of blocked pressure is not restricted to a chamber of any particular shape. The advantage of the developed approaches is that they are general and can be applied to any noise source. The disadvantage is that the measurement of blocked pressure and source impedance is rather elaborate in practice.

4.3 The dummy source

The approach was originally developed as an experimental technique to characterise the diesel engine shown in Fig. 3, but it applies to vibrating sources in general. To achieve a source model, hereafter *the dummy source*, which is suitable for experimental characterisation of a diesel engine, hereafter *the complex machine*, both the complex machine and the dummy source have to be located at the same position in the

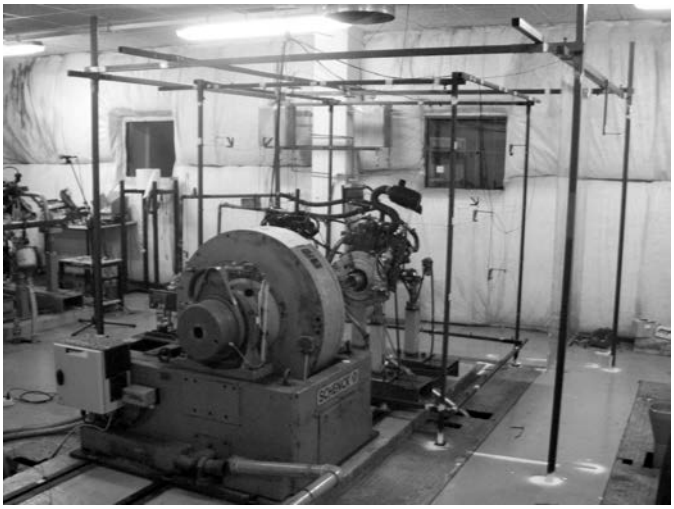

Figure 3: A diesel engine installed in a test cell.

same characterisation space. This is a basic requirement for the measurement of transfer impedances of the dummy source which has profound consequences for the approach.

In order to maintain the overall acoustical features of the characterisation space, the dummy source needs to be representative of the complex machine. Therefore, the dummy source has to be a physical object of similar volume and shape as the complex machine. Moreover, the acoustical properties of the surface of the dummy source has to be representative of the surface of the housing of the complex machine.

Since the housing of a diesel engine is a hard surface, it follows that the surface of the dummy source should be a hard surface. Whether a hard surface is a reasonable assumption depends, however, on the complex machine that should be characterised. The *dummy* will now be defined as a rigid closed cabinet which represents the passive complex machine. The dummy approximates the region of the characterisation space which is originally occupied by the complex machine.

Regarding the design of the dummy, the geometrical discrepancy between the complex machine and the dummy should be small compared to the shortest acoustical wavelength of interest. If the discrepancy is small enough, the dummy source should be equivalent in terms of sound diffraction. The equivalence in sound diffraction is not elaborated upon in this thesis but can be assessed in future applications of the dummy source approach. The assessment can be done by computation, with respective body being subject to an incident wave. Such a computation was shown in the beginning of the discussion, and will be illustrated later on in App. II.

A remark is that a single dummy may represent not only one complex machine but an entire class of complex machines. A trade-off exists in the design of the dummy between on the one hand accurate geometrical representation of a particular complex machine and on the other hand capturing common features between several complex machines. Consequently, the more the dummy resembles a particular machine the less representative it will be of another — which suggests that a practicable approach aims at common features only.

The passive cabinet of the dummy source is equipped with an array of active drivers. The driver array - cabinet assembly constitutes the equivalent acoustical model of the complex machine, Fig. 4. By carefully designing the driver array and adjusting the drivers' source strengths in a suitable manner, it is hypothesised that a similar sound field will be achieved not only at the recording microphones' positions but everywhere inside of an acoustical space.

Due to the restricted volume of the cabinet and the volume of each respective driver, the driver array can not be arbitrarily designed, nor can it continuously cover the dummy's surface. A feasible design requires a sparse driver array where each driver constitutes an elementary velocity distribution on the surface of the dummy source. Matching the sound field of the complex machine as close as possible to the superposition of such elementary velocity distributions, defines the vibration of the dummy source

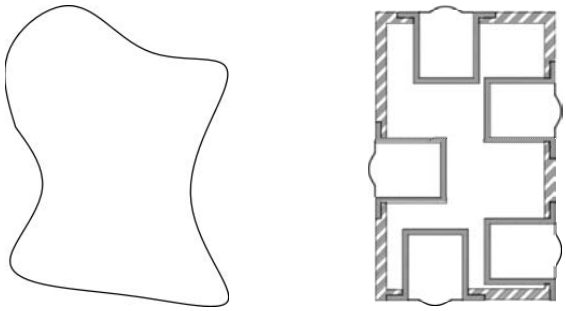

Figure 4: Schematics of a vibrating body, left, which is characterised by a closed cabinet equipped with a driver array, right.

[19]. The approach deviates from existing techniques for which the modelling of sound radiation from a vibrating body requires instead the entire surface to be formed using moving elements [11, 12].

At this point, the question arises as to whether or not it is meaningful to represent the continuous vibration on the irregular surface of the complex machine by a counterpart consisting of a driver array with a limited number of drivers set in a cabinet of simple shape. From the point of view of inverse boundary element methods and holography this is, admittedly, crude. The reconstruction of the exact source velocity distribution is, however, not the purpose of the dummy source. The dummy source serves to reproduce a similar sound field.

There are a number of open questions that need to be answered to make the approach reality: (1) *What is a suitable choice of driver?* The driver determines the expected acoustical behaviour and therefore the modelling of sound radiation of the dummy source; (2) *What is a suitable design of the driver array?* The number of drivers and their positions, needed for accurate reproduction of sound, determine the acoustical layout and the capacity of the dummy source; and (3) *How to match the driver array of the dummy source to the sound field of the complex machine?* There are different principles possible for how the drivers' excitations can be deduced, but beforehand it is not known which criteria is better suited for the purpose of sound prediction. The modelling of a driver - cabinet assembly will be discussed in the next section.

5 THE DRIVER - CABINET ASSEMBLY

Although the dummy source has been conceptualised, a mathematical formulation of the source model is missing. The dummy source is in essence a loudspeaker assembly, and there are several existing models of sound radiation of such a sound source in literature, as will be briefly reviewed here.

Morse and Ingard [20, pp. 343 - 347] proposed the use of a rigid piston in a rigid sphere as a model of sound radiation, provided that the cabinet's aspect ratio allows for it. Svensson and Wendlandt [21] computed sound radiation by a rigid piston in a box using the Rayleigh's integral formulation combined with contributions of edge diffraction. Zotter et al. [22] proposed a model aimed at cabinets shaped in the form of a platonic solid. Their model assumes the driver to be a spherical cap embedded in the surface of a rigid sphere. The free-space sound radiation is expressed in terms of spherical harmonics.

The common assumption between the models is that the driver was a rigid moving surface. Frankort [23] found that such an assumption is in practice reasonable at low frequencies. The assumption of rigidity is nevertheless questionable because the velocity must be lower at the outer ring of the surround than at the diaphragm's connection to the voice-coil. Furthermore, the rigidity of the cabinet is also questionable and cabinet vibration may occur. The dummy source will be conceived in a manner similar to [20, 21, 22] as a closed rigid surface on which is embedded an array of vibrating disks. Unfortunately, a sphere can not be seen as a satisfactory model of diffraction of a complex machine. Therefore analytical modelling is not feasible. The driver - cabinet assembly will be modelled numerically using the substitute source method [24, 25, 26]. Numerical modelling allows for an arbitrary shape of the cabinet.

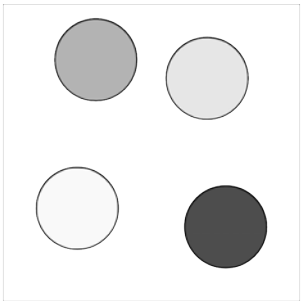

Figure 5: A surface patch of the dummy source with an independent irregularly spaced driver array. The mixed tones illustrates that the drivers are not in-phase with each other.

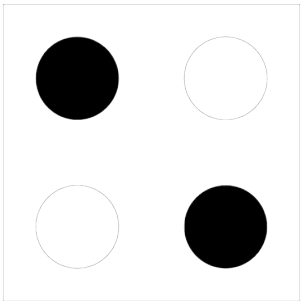

Figure 6: An acoustic lateral quadrupole created by grouping small back-enclosed drivers mounted in a small surface patch: black and white drivers are driven out-of-phase in respect to each other.

The driver will be assumed to be *small* since the difficulty with a large driver is that it is directional and risks to be vibrating in zones [27, pp. 260]. Frankort measured such vibration patterns on a cone [23, pp. 103 - 108]. This implies that the precise shape and velocity of the driver's diaphragm and surround are required to calculate the resulting sound field. Such a complicated approach is not feasible for the construction of a dummy source.

Russel et al. [28] have experimentally demonstrated that a box mounted driver acts as an acoustic monopole when the box is small. By stacking several boxes, with the entire assembly still small, and controlling the phase of the drivers an acoustic monopole, an acoustic dipole and an acoustic quadrupole was demonstrated with measured radiation patterns. This shows *the principle of wave superposition* from a practical point of view. The experiment illustrates that the dummy source can be approached in several ways giving rise to different airborne sound source models.

The dummy's drivers can radiate sound independently of each other, Fig. 5. By superposing such elementary sound fields, a complex composite sound field corresponding to the assembled dummy source can be found. In this case, the degrees of freedom of the dummy source are the same as the number of drivers on its surface. This approach is particularly simple and leads to the simple source formulation of sound radiation.

An alternative approach is to consider the effect of predetermined vibration patterns using several drivers. Such an approach can be used to design a model with higher order sources of sound, Fig. 6. In this case, individual drivers inside of a surface patch of the dummy, or spread across the entire surface of the dummy, can be grouped to form a dipole-like or quadrupole-like sound source, see e.g. [28, Fig. 8, p. 663]. Such higher order models are not considered in this work, but could be subject to further work.

The grouping of the drivers can be done arbitrarily, and does not necessarily lead to a multipole description of the sound field. It is possible, as done in [13], to create a radiation model with e.g. the dummy's faces moving in-phase. Such a model is the result of grouping all the drivers spread across a face of the dummy and attributing to them an identical source strength. A mathematical formulation of sound radiation from the dummy source using small sound sources will be discussed in the next section.

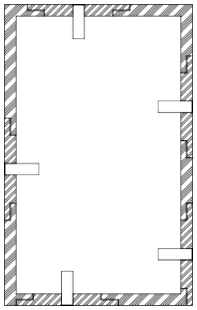

Figure 7: A reciprocal acoustical layout consisting of a rigid closed cabinet and a microphone array.

6 THE SIMPLE SOURCE FORMULATION

It is hereafter taken for granted that the driver array, *flush-mounted* in the surface of the dummy, consists of *small back-enclosed loudspeaker drivers*. Such a driver taken on its own approaches a simple source of sound [20, pp. 309 - 312]. The simple source produces *a spherical wave*, an omnidirectional radiation pattern, in a free-space [20, pp. 309 - 312]. The response of an arbitrary space to a single driver - cabinet layout is nonetheless directional due to cabinet diffraction and acoustical features of the space.

The simple source approaches the concept of an acoustic monopole (point source) in the sense that it has a surface or a volume which is small compared to the acoustic wavelength. Unlike the monopole there is no singularity at the simple source. Like the monopole the simple source is characterised by its position and source strength [20, pp. 309 - 312]. The source model parameter is henceforth called *source strength* or *volume velocity*. Sound radiation by the driver array mounted in the dummy is consequently fully characterised by knowledge of source positions and source strengths. The assumption of a back-enclosed driver is required in order to obtain a spherical radiation pattern in a free-space without the cabinet, to avoid interaction with the air volume inside of the cabinet, and as will be shown later on, to monitor the volume velocity of the driver. The assumption of a flush-mounted driver is intuitive since the driver simulates the effect of surface vibration.

The simple source formulation results in a problem statement suitable for experimental - numerical work with sound sources. There are two advantages of this formulation. First, the equivalent acoustical model can be implemented independently of the loudspeaker driver provided that its diaphragm is small [29]. Second, the formulation allows the use of the principle of vibroacoustic reciprocity [14, pp. 198 - 199] [30, 31, 32]. Since the source and receiver positions become interchangeable, the dummy source can be realised as an array of microphones installed in the surface of a cabinet, Fig. 7. The use of reciprocity for the measurement of transfer impedances is illustrated in Fig. 1 showing a known volume velocity source in the cabin and a reciprocal dummy source in the engine compartment. The use of reciprocity comes down to whether it is more practical in application than direct measurement.

The disadvantage of the formulation is that it requires knowledge of the *impulse response* in the time domain or the *transfer impedance* in the frequency domain of the dummy source, which is not known except for special cases. The transfer impedance of a driver - cabinet assembly has been investigated in detail both experimentally [29] and numerically [24]. Concerning the transfer impedance of the dummy source, the driver can be thought of as an aperture on the cabinet through which sound waves travel similar to the opening of an organ pipe. The transfer impedance is then deduced by knowledge of the volume velocity at the opening of the cabinet and the pressure response of the space.

6.1 Sound radiation by a vibrating body

Sound radiation from a vibrating body is governed by the superposition integral [34, p. 8]. The radiation depends on the acoustical features of the space Ω_0 and the velocity distribution $\hat{\mathbf{v}}_0(\mathbf{s})$ on the housing surface S_0. At a constant angular frequency ω, the complex sound pressure amplitude $\hat{p}_0$ at a (field) point $\mathbf{f}$ is given by

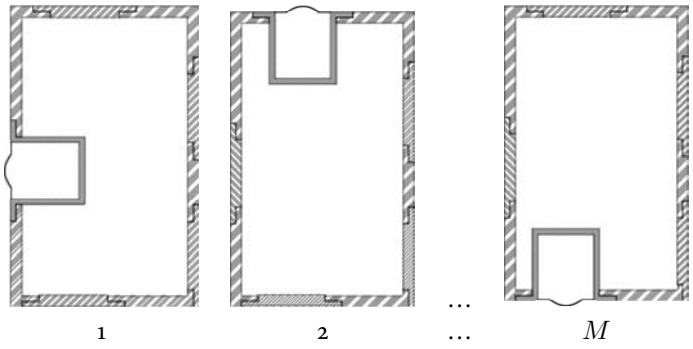

Figure 8: The dummy source decomposed into several single driver - cabinet acoustical layouts.

$$\hat{p}_0(\mathbf{f},\omega) = \int_{S_0} G_0(\mathbf{f} \mid \mathbf{b}_0,\omega)\hat{v}_{0,\perp}(\mathbf{b}_0,\omega)dS_0, \qquad p_0(\mathbf{f},t) = \Re\{\hat{p}_0(\mathbf{f},\omega)\mathrm{e}^{j\omega t}\}, \tag{1}$$

a continuous smear of monopoles across the body surface [34, p. 8]. In this equation, $G_0(\mathbf{f} \mid \mathbf{b}_0)$ is the Green's function and $\hat{v}_{0,\perp}$ is the velocity amplitude at a (boundary) point $\mathbf{b}_0$ on the surface. The hat [$\hat{}$] denotes an amplitude; the zero [$_0$] denotes a quantity belonging to either the original source or the original space; and the perpendicular symbol [$_\perp$] indicates the surface normal.

The superposition integral, Eq. 1, is the bane and the boon of the Green's function approach. Neither the Green's function nor the velocity distribution are known in practice. Thus, the effect of the space and the effect of the forcing vibration are difficult to distinguish in the resulting pressure response. Moreover, Eq. 1 is a Fredholm integral of the first kind, known to cause trouble for inverse methods [18, p. 28 - 29].

6.2 Sound radiation by a dummy source

Sound radiation from the dummy source is given by a superposition summation where each term in the sum corresponds to the Eq. 1 applied to a single driver - cabinet assembly. The principle of wave superposition will be used and the mathematical basis is consequently multiple single driver - cabinet layouts identified from the beforehand designed driver array, Fig. 8. The ensemble of single driver - cabinet layouts will be referred to as an "equivalent sound source". The terminology is, perhaps, in conflict with existing usage which often refers to volumeless sources of sound, such as a dipole. Still the layout serves as an equivalent sound source to the complex machine, and as such the terminology is clear. Eq. 1 is approximated by

$$\hat{p}(\mathbf{f},\omega) \approx \sum_{m=1}^{M} Z(\mathbf{f} \mid \mathbf{s}_m,\omega)\hat{Q}(\mathbf{s}_m,\omega), \qquad \hat{Q}(\mathbf{s}_m,\omega) = \int_S \hat{v}_{m,\perp}dS. \tag{2}$$

Here, the transfer impedance $Z(\mathbf{f} \mid \mathbf{s})$ satisfies the acoustic boundary-value problem of the characterisation space Ω, but with the complex machine replaced by the dummy source. The elementary velocity distribution on the surface of the dummy with only the m^{th} driver in motion, and the other drivers blocked, is denoted by $\hat{v}_{m,\perp}$. The location of the driver at a (source) point on the dummy is denoted by $\mathbf{s}$, and the source strength is denoted by $\hat{Q}$.

The differences between the complex machine and the dummy source have been described. *The dummy source is a driver array - cabinet assembly. The dummy source has a simpler shape than the complex machine, sufficiently representative of diffraction by the machine.* To estimate the transfer impedance of the space, and subsequently the source strengths of the driver array, the dummy source is decomposed into multiple driver - cabinet layouts. The dummy's velocity distribution is considered to be discrete rather than continuous, although each single driver - cabinet assembly forms a continuous velocity distribution on the surface of the dummy source. *The non-zero velocities are localised at the drivers' moving surfaces, which do not continuously form the surface of the dummy source.* It therefore follows that the radiated sound field is

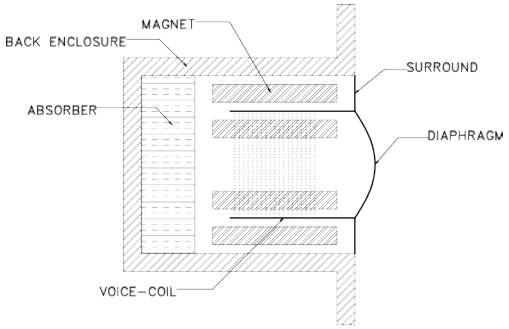

Figure 9: Schematics of a back-enclosed electrodynamic driver.

not similar in the vicinity of the complex machine, but may be similar a distance away from the complex machine.

The electrodynamic driver will be discussed in the next section. The experimental implementation of a simple source of sound is, however, independent of the choice of driver design. The electrodynamic driver has been selected for prototyping a dummy source because of its abundance on the market. An off-the-shelf mid-range driver has been used to implement a simple source as required for experimental work with single driver - cabinet layout.

7 THE ELECTRODYNAMIC DRIVER

Kinsler and Frey [27, Ch. 10] analysed an electrodynamic driver. *The base model is a rigid piston mounted in an infinite baffle and radiating on one side of the baffle.* This simplified analysis serves to introduce the problem of knowing the driver's forcing velocity and radiation pattern.

7.1 Sound radiation

The driver's voice-coil is attached directly to the diaphragm, Fig. 9. The voice-coil is *oscillating* back and forth in the radial uniform magnetic field, perpendicular to the coil winding [27, pp. 249]. Sound radiation by an oscillating rigid piston of radius a with forcing velocity $\hat{v}_\perp$ mounted in an infinite baffle is given by [27, Ch. 7]

$$\hat{p}_{rp} = \frac{j\omega\rho_0 a^2 \hat{v}_\perp}{2r} \mathrm{e}^{-jkr} \left\{ \frac{2J_1(ka\sin\theta)}{ka\sin\theta} \right\}. \tag{3}$$

Here, J_1 denotes the Bessel function of first kind and of order one [27, Ch. 4], $k = \omega/c = 2\pi/\lambda$ is the wavenumber, λ the wavelength, c the speed of sound, ρ_0 the density of air at rest, $\mathbf{r}$ the radial vector from the geometric center of the piston to the field point, $r = \|\mathbf{r}\|_2$ the Euclidean distance, θ is the angle between the outward unit normal of the piston and the radial vector, and ω is the angular frequency. At long wavelengths, at which the diaphragm is small, the radiation pattern can be considered omnidirectional as the bracketed term $\{\ldots\}$ becomes approximately one. Thus for low ka-values, Eq. 3 reduces to the form

$$\hat{p}_h = j\omega\rho_0 \hat{Q}_h \frac{\mathrm{e}^{-jkr}}{2\pi r} \tag{4}$$

of a *pulsating* hemispherical source set in an infinite baffle, $\hat{Q}_h = \pi a^2 \hat{v}_\perp$. This shows that a small rigid piston is only one example of a simple source of sound. In this case the pressure response no longer depends on the details of the vibrating surface and can be expressed by a *point transfer impedance*. Such an impedance Z relates volume velocity amplitude $\hat{Q}$ of the driver located at a source point $\mathbf{s}$ to sound pressure amplitude $\hat{p}$ at a field point $\mathbf{f}$

$$Z(\mathbf{f} \mid \mathbf{s}) = \frac{\hat{p}(\mathbf{f})}{\hat{Q}(\mathbf{s})}. \tag{5}$$

Eq. 5 is in practice what is required to work with the superposition summation in Eq. 2. However, the transfer impedance satisfying the acoustic boundary-value problem of a space is in general not known and has to be measured. The difficulty of such a measurement, as will be shown next, is that the voice-coil velocity, which governs the driver's volume velocity, is affected by the surrounding sound field and is thus not uniquely related to the electrical current through the driver.

7.2 Voice-coil velocity

The driving force f applied on the driver's diaphragm is $f = Bli$ where B is the flux density of the magnetic field, l is the length of the conductor in the voice-coil and i is the current through the voice-coil [27, pp. 249]. A time-harmonic current, $i = \hat{i}e^{j\omega t}$, will create a steady-state velocity of the diaphragm [27, pp. 249]

$$\hat{v}_\perp = \frac{f}{Z_m} = \frac{Bl\hat{i}}{Z_m}. \tag{6}$$

In this equation, the total mechanical impedance Z_m is $Z_m = Z_r + Z_c$ where Z_r is associated with the acoustic radiation loading and Z_c is associated with mechanical behaviour of the moving parts [27, pp. 248].

In practice, a voltage $e = \hat{e}e^{j\omega t}$ is supplied to the terminals of the driver's voice-coil. The steady-state current of a blocked voice-coil is given by the relationship $\hat{i} = \hat{e}/Z_E$. Here, the blocked electrical impedance of the voice-coil is Z_E [27, pp. 249]. The motion of the voice-coil in the magnetic field of the driver generates a motional counter electromagnetic force $\hat{e}_m = \phi\hat{v}_\perp$, where $\phi = Bl$ [27, pp. 250]. Substitution of the diaphragm's velocity gives

$$\hat{e}_m = \frac{\phi^2}{Z_m}\hat{i}. \tag{7}$$

Accounting for this interaction the voice-coil current is given by

$$\hat{i} = \frac{\hat{e} - \hat{e}_m}{Z_E}, \tag{8}$$

which can be rewritten as [27, pp. 250]:

$$\hat{i} = \frac{\hat{e}}{Z_E + \frac{\phi^2}{Z_r + Z_c}} = \frac{\hat{e}}{Z_E + Z_M}, \tag{9}$$

where Z_M is the motional impedance. The motional impedance is in practice never known, as it depends on the sound field in the surrounding space.

Eq. 9 shows that the liaison between mechanical and electrical quantities, even in this ideal analysis, is not independent of the radiated sound field. The forcing velocity is therefore not easy to deduce from the measurement of electrical voltage.

7.3 Experimental characterisation of an instrumented driver

Eq. 9 complicates experimental work with a dummy source. A volume velocity source is required for working with Eq. 2. Several designs for implementing known volume velocity sources have been reported in literature [29, 35, 36, 37, 38, 39]. Common to all of these designs is that an additional transducer producing a signal proportional to either velocity, acceleration or volume displacement is introduced. The relationship to volume velocity can then be either theoretically deduced or measured.

An off-the-shelf mid-range, Morel EM1308, has been used to implement a simple source. Eq. 9 was in this case circumvented by installing a microphone in the driver's back enclosure. The back enclosure was re-sealed using silicone rubber.

Since the sound pressure in the back enclosure is produced by the change of volume, *a one-to-one relationship exists between the pressure and the volume velocity*, irrespective of the radiation loading or internal electro - mechanical links. The problem is that the relationship between the internal pressure and the external volume velocity is not perfectly known theoretically, but has to be measured. The measurement of

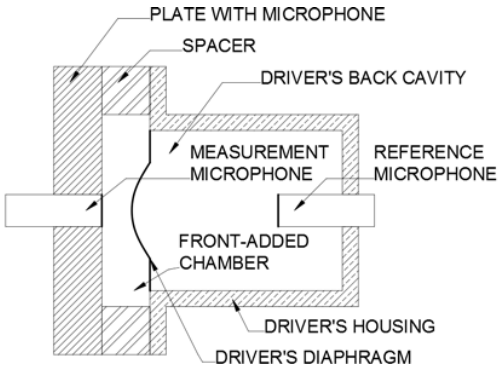

Figure 10: Schematic measurement of the source function using a compression chamber.

the pressure - volume velocity relationship, which calibrates the instrumented driver, has been done using several techniques including a compression chamber and a blocked pipe [29, 39]. Assuming the back enclosure to be an isolated acoustical space, the transfer impedance can be represented as a product of two independent transfer functions: a source function Ψ, which relates internal pressure $\hat{p}_{\text{ref}}$ to volume velocity $\hat{Q}(\mathbf{s})$, and a space function Ω, which relates external pressure $\hat{p}(\mathbf{f})$ to internal pressure $\hat{p}_{\text{ref}}$,

$$Z = \Psi\Omega, \Psi = \frac{\hat{p}_{\text{ref}}}{\hat{Q}(\mathbf{s})}, \Omega = \frac{\hat{p}(\mathbf{f})}{\hat{p}_{\text{ref}}}. \tag{10}$$

The perhaps most straightforward measurement of the source function is by using a front-added compression chamber [29, 39]

$$\Psi = \frac{1}{j\omega}\frac{\rho_0 c^2}{V_0}\frac{\hat{p}_{\text{ref}}}{\hat{p}_e}, \tag{11}$$

which characterises the driver, Fig. 10. Here, $\hat{p}_e$ is the sound pressure in the compression chamber and V_0 the volume at rest of the chamber. The space function can then be measured in any space independently of radiation loading: any change in the driver's diaphragm vibration pattern will be reflected in the internal pressure of the back enclosure. The calibration is discussed in detail in App. III and App. IV. The advantage of the technique is that it *circumvents the difficulties with radiation loading associated with electrodynamic drivers*, because it relies only on acoustic quantities which makes measurement of transfer impedance practicable. The disadvantage is that *any given driver may have quite a small frequency bandwidth in which it effectively behaves as a simple source: the driver becomes inefficient at lower frequencies whereas the driver's radiation pattern becomes directional at higher frequencies*. This can only be mitigated by measuring the transfer impedances using several different sized drivers which approach simple sources at different frequency bands. The entire frequency band of interest can then be covered.

The frequency range for which the instrumented Morel EM1308 behaves as a simple source has been determined from an initial experiment with a flat rectangular baffle in an anechoic room. It was found that the spread in response, measured at several points distributed across the surface of a small half-sphere centred at the point on the axis which intersects with the diaphragm, was pronounced above 1000 Hz. Since the radius of the diaphragm is 30 mm, the upper frequency limit corresponds to about 1/6 of the acoustic wavelength. (The driver has in practice been found to be inefficient below 100 Hz.)

The Morel EM1308 driver has a dome shaped diaphragm. Suzuki and Tichy [40] found that the acoustical center of a convex dome, a point from which the sound field appears to originate, lies at the point on the diaphragm which intersects with the axis. Moreover, a convex dome has a radiation pattern with the principal lobe wider than that of a flat piston. At low frequencies the offset of the acoustical center is of no interest for the measurement of transfer impedance while the wider lobe is beneficial.

Finally, a model of sound radiation by a convex dome set in an infinite baffle has been implemented using the substitute source method, but will not be included in this thesis. The results show that the dome, a half-sphere of the same radius as the mid-range used, is a simple source at the useful frequency range as

expected. Considering it practicable to measure the dummy's transfer impedances, in a frequency range in which the acoustic wavelength goes from much longer than to comparable with the dummy source, the acoustical layout on the surface of the dummy source will be discussed next.

8 THE DRIVER ARRAY

There is no rational way to beforehand specify the number and positions of simple sources on the dummy required to accurately reproduce the sound field of the original source. One possibility is to use inverse methods such as the inverse boundary element method [11, 12, 18] to localise the sound sources and thereafter create an efficient sound synthesis scheme. Such localisation is, however, quite elaborated and may not be adapted to the need of vehicle manufacturers. Instead, the array is for simplicity considered fixed, specified with an upper frequency bound $f_{\max}$. The design *hypothesis* is that an array spread across the surface of the dummy with *two simple sources per shortest acoustical wavelength of interest*, $\lambda_{\min}$, is sufficient for accurate enough sound reproduction.

The introduced criterion is vague and served as a guideline to design a dummy source prototype for the purpose of initial experimental and numerical investigations on the dummy source approach. The assumption will be investigated in this thesis, and consecutive two-dimensional numerical analysis using the substitute source method has suggested that this hypothesis is in fact *a lower limit for the density of the drivers*. Below this limit accurate sound reproduction is difficult to achieve. In [19] an initial case study indicated that the drivers spaced by ca. 30% of the acoustic wavelength is a reasonable trade-off between the number of drivers and the accuracy of the reproduced sound field.

Using the hypothesis as a guideline, the number of simple sources M and the average spacing δ between two adjacent sources are given by

$$M \approx 4S\frac{f_{\max}^2}{c^2}, \qquad \delta \approx \frac{c}{2f_{\max}}, \tag{12}$$

where c is the speed of sound and S is the surface area of the dummy. Below $f_{\max}$, the driver array can at least on a small-scale simultaneously compress and rarefact the air locally in the vicinity of the dummy source as the adjacent drivers can move out-of-phase in respect to each other. The large-scale volume velocity, the net effect on the surrounding air of several drivers being close to each other, can therefore be controlled across the surface of the dummy.

Eq. 12 dimensions the dummy source. It does not, however, indicate the precise position of the drivers required to define the acoustical layout. The design hypothesis is not strict and many equivalent layouts with the same density of drivers can be designed. Such designs are expected to perform equally well using this hypothesis.

Using a fixed acoustical layout, the effective number of sound sources per wavelength increases when the frequency decreases

$$\left(M\Big/\lambda\right)_{\text{eff}} = 2\frac{f_{\max}}{f}. \tag{13}$$

The advantage of such an array is that at long wavelengths, $f \ll f_{\max}$, higher order vibration patterns [28] can be constructed locally across the surface of the dummy. The disadvantage is that nearby sound sources become increasingly difficult to distinguish at the microphone array. Therefore, the estimation of source strengths becomes increasingly ill-posed. A remedy is, as discussed earlier on, to group or switch off the simple sources.

Eq. 12 is quite different from other approaches to sound radiation by vibrating bodies, such as finite element methods where often six elements per shortest structural wavelength of interest are recommended. The reduction in degrees of freedom can be quite substantial. The next issue to be discussed is the measurement of pressure responses of the complex machine.

9 THE MICROPHONE ARRAY

The implementation of the microphone array has to be pragmatic. It is hard, if not impossible, to discuss microphone positioning in a general context. (The following is based on experience from the characterisation of a diesel engine in a test cell.) The characterisation space and peripheral equipment around the complex machine decide where microphones can and can not be positioned. Nevertheless, the design of the microphone array is important since it partially governs, together with the driver array and the frequency, the conditioning of the problem when estimating source strengths [41, Fig. 2 - 3], which will be illustrated in App. I. Some guidelines can be given in this section. The microphones will be split into two mutually exclusive groups. The first group — *the control points* — consists of N microphones and is used to estimate the drivers' source strengths. The second group — *the error points* — is used to validate the dummy source at the E remaining microphones.

The microphones should be matched in phase and amplitude, which has been achieved by use of a compression chamber as described in App. I. In such a chamber the pressure response should practically be uniform. Thus differences between microphones compared to a reference microphone is easy to measure. The reference microphone serves to establish transfer functions which calibrate the other microphones in the array. The procedure removes the mismatch between microphones but not the bias of the reference microphone. The bias is less detrimental than mismatch and thus neglected.

The calibrated microphones should be spread around the complex machine, necessary to record the overall features of the sound field of the complex machine. Such an array avoids focusing with accurate reproduction at and nearby the microphone array only. Needless to say the microphone positions should be marked out in the characterisation space for later reuse when measuring the transfer impedances using the dummy.

Finally, *all time histories should be recorded simultaneously*. The advantage is the circumvention of need for synchronisation between subsequent array recordings [42, 43], moving the array around to scan the sound field, which can be a hurdle in practice if e.g. the time histories are not fully stationary [44, 45, 46]. Simultaneous recording is a prerequisite for working in the time domain [47]. The disadvantage of simultaneous recording is that it limits the total number of microphones $N + E$ to the available number of channels of the data acquisition system. To reduce the influence of measurement errors it is usually required that the number of control microphones are larger than the number of drivers, $M \ll N$. During the estimation of source strengths, an overdetermined set of equations is used [47, 48, 49]. The subsequent validation of the dummy source requires E independent but simultaneous recordings. Independent means in this context that the subset of microphones is *not* used to estimate the source strengths.

Since guidelines for both the driver array on the surface of the dummy source and the microphone array inside of the test cell have been given, and because it is known how to implement a volume velocity source for experimental work the experimental procedure will be discussed next.

10 THE EXPERIMENTAL PROCEDURE

The entire experimental procedure consists of two measurements: (1) the recording of operating sound pressure of the original source in a characterisation space, (2) the measurement of transfer impedances linking each driver on the surface of the dummy source to each microphone previously used to measure the operating responses. The two measurements are illustrated in Fig. 11. The implemented measurement procedure using a dual purpose array will be discussed in App. I.

The measurement of transfer impedances deserves a few remarks. First, a direct approach to the measurement of transfer impedances cause unwanted cabinet vibration, potentially invalidating the measurements at least at cabinet resonances. An alternative approach is to use the principle of vibroacoustic reciprocity [30, 31, 32], which indeed has been used in the experimental work with a dummy source prototype. In this case the dummy source is equipped with a microphone array, and a known volume velocity source is positioned in the characterisation space where there was earlier a microphone to record the pressure response of the original source. Second, it is quite hard to achieve sufficient signal-to-noise ratio at low frequencies using small drivers. This has been mitigated using band-pass filtered pink noise as excitation and a large number of averages when estimating the space function. The success of a transfer function

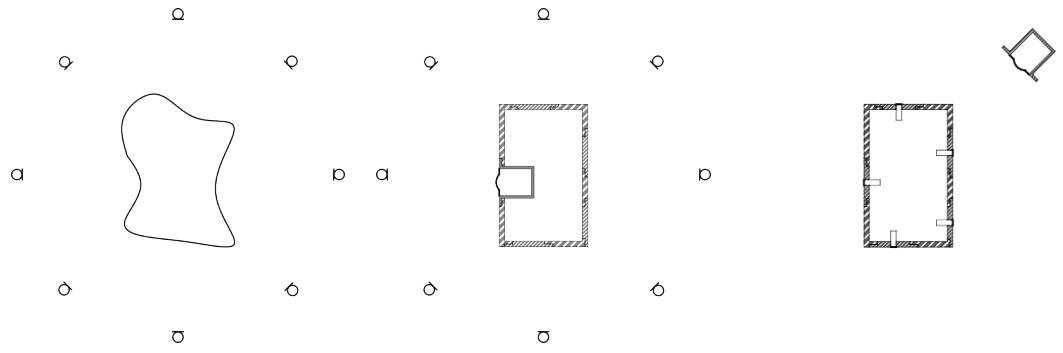

(a) (b) (c)

Figure 11: The dummy source approach illustrated by (a) measurement of pressure response of the complex machine and either (b) direct measurement of transfer impedances or (c) reciprocal measurement of transfer impedances.

measurement is most easily seen by inspection of the coherence between the instrumented driver's internal reference microphone and the microphones in the test cell which should be close to one. Third, a challenge with the measurement of transfer impedances is to ensure minimal changes of the characterisation space when replacing the complex machine with the dummy source. In the experimental work on characterising a diesel engine, it was difficult to keep the peripheral equipment, such as pipes for the water cooling system, exactly in the same location. Even with some changes of the characterisation space it is believed that the overall acoustical features of the space remains the same in the two measurements.

Another aspect which requires a few remarks is that of reproducibility. On the one hand, despite the ease of measuring the operating response of the diesel engine, the reproducibility is poor since a unique time history can not be measured at the same microphone position twice starting and stopping the engine. The reason for this is that the operation (the speed and the torque) of the diesel engine was not controllable enough. Thus the first measurement using an original source can be expected to have poor reproducibility. Considering sound quality assessment of the original source in a listening space other than the characterisation space as the potential use of a dummy source, the use of time histories is unavoidable. In this case (absolute) reproducibility is not interesting since it is the ability to conclude on the sound quality of a given mechanical assembly that is essential. Such an assessment is, however, outside the scope of this thesis. On the other hand the reproducibility of the transfer impedance measurement is excellent provided that the characterisation space does not change between two subsequent measurements.

Considering it feasible to measure both the transfer impedances and the operating sound pressure responses the next issue is to deduce the dummy's source strengths.

11 ESTIMATION OF SOURCE STRENGTHS

The estimation of source strengths is carried out off-line with the help of a personal computer. The problem will be introduced in the frequency domain, and thereafter in the time domain.

11.1 Frequency domain approaches

The basic approach, at a constant frequency, is to relate the sought source strengths to the operating responses by a set of equations. The transfer impedances provide the liaison between the two quantities. Since it is assumed that the number of microphones N is greater than the number of drivers M in the experimental setup, the arrangement results in an overdetermined set of equations which is written

$$\mathbf{Z}\hat{\mathbf{Q}} \approx \hat{\mathbf{p}}. \tag{14}$$

Here, the unknown source strength vector $\hat{\mathbf{Q}}$ in $\mathrm{m}^3\mathrm{s}^{-1}$ of the dummy source ($M \times 1$) is related to the known response vector $\hat{\mathbf{p}}$ in Pa of the original source ($N \times 1$) via the transfer impedance matrix $\mathbf{Z}$ in $\mathrm{kgm}^{-4}\mathrm{s}^{-1}$ of the space ($N \times M$). All of the quantities in Eq. 14 are complex valued. (The complex response of the original source is found from prior processing of the recorded time histories using, for example, the FFT algorithm.)

Since the transfer impedance matrix is not square, a solution can be found using Moore-Penrose pseudoinversion which matches the sound field of the dummy source as closely as possible to the sound field of the original source

$$\min \|\mathbf{Z}\hat{\mathbf{Q}} - \hat{\mathbf{p}}\|_2^2, \tag{15}$$

where the Euclidean norm is denoted by $\| \_ \|_2$. The reconstructed response is given by $\tilde{\hat{\mathbf{p}}} = \mathbf{Z}\hat{\mathbf{Q}}$, and the reconstruction error is quantified by $\|\hat{\mathbf{p}} - \tilde{\hat{\mathbf{p}}}\|_2^2$. Here, tilde [˜] denotes reconstruction.

A first remark is that the approximately equal sign in Eq. 14 is qualified since unavoidable modelling imperfection and measurement errors results in an inconsistent equation system — it has no solution. Instead the best fit solution is used, an intuitive choice. A second remark is that the *inverse problem* is ill-posed [18, Ch. 2.3] since the solution is *not unique* in the sense that several designs of the driver array can be conceived. A third remark is that the transfer impedance matrix becomes *ill-conditioned* at low frequencies. The ill-conditioning is an effect of that the relative spacing between adjacent drivers in the fixed grid design decreases as the acoustical wavelength increases. Consequently, the transfer impedances of adjacent drivers become increasingly similar, which causes numerical instabilities in the matrix inversion. (The numerical solution becomes sensitive to small changes in the response.) The numerical instabilities can be mitigated by preconditioning the problem either by changing the geometry of the experiment, or by altering the formulation of the dummy source.

Finally, in an *initial* attempt to estimate the source strengths it was found that the use of the Moore-Penrose pseudoinverse in Eq. 15 results in useless solutions. The conclusion was reached when attempting to predict the sound pressure at error points in order to validate the approach. Since then it has been found that the problem was due to the ill-conditioning of the problem. Thus, apart from modelling errors and measurement errors there will be inversion errors. The large discrepancy motivated the use of alternative approaches; namely, preconditioning and regularisation. (In practice, both preconditioning and regularisation should be used in the frequency domain.)

11.1.1 Preconditioning

A potential solution to the problem of ill-conditioning at low frequencies is provided by driver grouping — connecting one or more drivers to form a composite sound source for example a quadrupole — since grouping changes both the number of degrees of freedom of the model and the mathematical formulation of the dummy source. The drawback of driver grouping is that it may require a systematic design of the driver array, which may not be practicable. Concerning the implemented prototypes, a regularly spaced array was not feasible because of limitations in the interior volume of the dummy source.

Instead, the design of the driver array has been approached in a cruder way; namely, to turn off drivers at random. In this case a fixed grid of candidate drivers is prescribed across the surface of the dummy, out of which a few actual drivers are selected. All of the candidate drivers are assigned equal probability of being turned off, and an actual driver array is designed drawing M actual drivers out of K prescribed candidate drivers. Thus, several random designs of the driver array can be considered, and the driver array which produces the smallest largest condition number will be employed. The condition number is a function of the driver array, the microphone array and frequency only.

To further improve the conditioning, both the driver array and the microphone array are selected using a Monte Carlo approach. Thus by shuffling a random subset of M drivers and a random subset of N microphones different experimental configurations are realised out of the same physical experiment. Some of the realisations will have significantly smaller largest condition number than others. An example of such a spread in condition number is illustrated in App. I.

The advantage of the proposed preconditioning is that it results in improved accuracy of the dummy source at low frequencies, due to smaller inversion errors, when evaluating the approach at the error mi-

crophones, App. I. The disadvantage is that the randomised driver array is not necessarily well designed to accurately enough reproduce the sound field.

11.1.2 Regularisation techniques

The regularisation techniques will not be thoroughly discussed here, instead the details are given in the appendices. Hansen and O'Leary [48] proposed the use of Tikhonov regularisation with the L-curve as a tool to select the regularisation parameter. Tikhonov regularisation constrains the ordinary least-squares approach by penalising the solution norm

$$\arg\min_{\beta} \|\mathbf{Z}\hat{\mathbf{Q}} - \hat{\mathbf{p}}\|_2^2 + \beta^2 \|\hat{\mathbf{Q}}\|_2^2. \tag{16}$$

The disadvantage here is that the regularisation parameter β needs to be chosen and (in doing so) the physical system is tampered with. This is common to all regularisation procedures. The advantage is that this can mitigate the influence of measurement noise. The L-curve criterion[1], computed using a finite difference scheme, has been applied successfully to validate the dummy source using computed transfer impedances for the case of a simple machine [19]. Tikhonov regularisation and the L-curve will be discussed in detail in App. II. The computation of transfer impedances will be discussed in detail in App. V.

In practice, however, the transfer impedances are measured. This means that the transfer impedance matrix is also perturbed by measurement errors. Therefore, it does not make sense to attribute the measurement errors only to the response vector as is the case with ordinary least squares approaches such as Tikhonov regularisation [50, Ch. 1]. Van Huffel [50, Ch. 2] introduced the total least-squares approach which is formulated as

$$\min_{\tilde{\mathbf{Z}},\,\tilde{\hat{\mathbf{p}}}} \left\| \begin{bmatrix} \mathbf{Z} & \hat{\mathbf{p}} \end{bmatrix} - \begin{bmatrix} \tilde{\mathbf{Z}} & \tilde{\hat{\mathbf{p}}} \end{bmatrix} \right\|_F \quad \text{subject to} \quad \tilde{\mathbf{Z}}\hat{\mathbf{Q}} = \tilde{\hat{\mathbf{p}}}, \tag{17}$$

where the $\| \quad \|_F$ is the Frobenius norm and the approximating matrix is denoted by tilde [˜]. The approach substitutes the physically measured system and response matrix with another approximation matrix using singular value decomposition. The approximation matrix is then solved to find the source strengths. Here, the numerical error is the distance between the measured matrix and the approximating matrix which is measured by the Frobenius norm. In this approach scaling of the column vectors is necessary since the mixed physical quantities are of different order of magnitudes.

Fierro et al. [49] proposed to combine total least-squares with singular value truncation to treat ill-conditioned problems. The disadvantage is that singular value truncation is somewhat crude, and that the truncation level has to be selected. The best choice of truncation level is not obvious, and an attempt using the L-curve criterion will be discussed in App. I. Shephard and Liu [51] have applied truncated total least squares to force estimation and found that it produces results equivalent to or better than Tikhonov regularisation. In this thesis the approach has been found to be quite unstable, with regards to the choice of truncation level, but it produces results fully comparable with that of Tikhonov regularisation. The truncated total least squares approach will be discussed in detail in App. I. The measurement of transfer impedances will be discussed in detail in App. III.

11.2 Time domain approach

Kropp[2] and Larsson [47, 52] proposed the use of an adaptive filter, a modified least mean squares (LMS) algorithm, to estimate e.g. contact forces at the interface between structures. The advantages of estimating source strengths in the time domain, as opposed to in the frequency domain, are that no assumptions are made regarding the nature of the time histories, which can be transient or stationary, and that no matrix inversion is required. The time histories of a diesel engine is known not to be stationary[3] [45, 46], which has been assumed when working in the frequency domain. The fact that matrix inversion is avoided makes the solution more robust to measurement noise. The disadvantage is the increase in computational time.

[1] I acknowledge Q. Leclère and A. Pereira for discussions on regularisation.
[2] I acknowledge W. Kropp whom has helped me with time domain source strength estimation.
[3] I acknowledge Q. Leclère and J. Antoni for discussions on the time histories of rotating machines.

The recorded time histories $\mathbf{p}_n$ are related to the unknown source strengths $\mathbf{q}_m$ through a set of the impulse responses $\mathbf{h}_{nm}$. The impulse responses are not known, and have to be estimated prior to the application of the LMS algorithm.

11.2.1 Impulse response estimation

Each impulse response was estimated from the corresponding transfer impedance already obtained in the frequency domain, where the transfer impedance was estimated using an instrumented driver. The impulse response was back-transformed from the estimated transfer impedance in three steps. The first step is to obtain a symmetric transfer impedance [53, pp. 213 - 214], which is done by setting the frequency component at $f_{\max} = R/2$ — half of the sample rate R — as well as the bias at 0 Hz to be real valued followed by conjugate mirroring. The second step is to apply the inverse Fast Fourier Transform to obtain a set of real valued impulse responses, $\mathbf{Z}_{nm}[j\omega] \xrightarrow{IFFT} \mathbf{h}_{nm}[i/R]$. Here i denotes a sample in the time history and i/R discrete time. The third and final step is to crop the impulse response at N_h samples to be short, yet long enough to significantly decay the response.

11.2.2 Adaptive filtering

The multiple input - multiple output (MIMO) adaptive filter [52] is formulated in vector form but will here be explained by scalar operations. The iterative process is divided into three steps. In each iteration along the recordings, $\forall i_s : N_h \leq i_s \leq N_s$ and $N_s \gg N_h$, is in the first step the n^{th} time history reconstructed, $\tilde{\mathbf{p}}_n$, and in the second step, the corresponding error signal, $\mathbf{e}_n$, is estimated. Each microphone position is treated separately. This is formulated as [52]

$$\tilde{\mathbf{p}}_n[i_s] = \sum_{m=1}^{M} \sum_{i_h=1}^{N_h} \mathbf{h}_{nm}[i_h]\mathbf{q}_{m,\text{old}}[i_s - i_h + 1], \tag{18}$$

$$\mathbf{e}_n[i_s] = \mathbf{p}_n[i_s] - \tilde{\mathbf{p}}_n[i_s]. \tag{19}$$

The first step expresses a summation of the partial contributions of every respective driver identified by convolution summation [53, pp. 492 - 500]. The second step is to extract the error signal between each pair of measured and reconstructed time histories. Thereafter, in the third and final step, each source strength is updated using a separate adaptive filter [52]. In this case the average instantaneous gradient of the N error signals are used to update the source strength. For the m^{th} source strength, $\mathbf{q}_m$, this is formulated as [52]

$$\mathbf{q}_{m,\text{new}}[i_s - N_h + i_h] = \mathbf{q}_{m,\text{old}}[i_s - N_h + i_h] + \frac{\alpha_m}{N} \sum_{n=1}^{N} \mathbf{e}_n[i_s]\mathbf{h}_{nm}[N_h - i_h + 1], \quad \forall i_h : 1 \leq i_h \leq N_h. \tag{20}$$

Here, α_m is a scaling factor of the average instantaneous gradient. As a rule-of-thumb, the scaling factor should be small and decide the stability of the process [47]. The three steps are repeated in each iteration step. The process is initiated by setting the entire vector $\mathbf{q}_{m,\text{old}}$ to zero and at the end of each iteration $\mathbf{q}_{m,\text{old}}$ is overwritten by $\mathbf{q}_{m,\text{new}}$.

The adaptive filter needs to be complemented by stopping criteria. The aim of the adaptive filter is to minimise the mean square error, the difference between the reconstructed and recorded time histories [47, 52]. A normalised measure of the difference between recorded and reconstructed time histories is

$$\left\| \begin{bmatrix} \mathbf{p}_1 \\ \vdots \\ \mathbf{p}_n \\ \vdots \\ \mathbf{p}_N \end{bmatrix} - \begin{bmatrix} \tilde{\mathbf{p}}_1 \\ \vdots \\ \tilde{\mathbf{p}}_n \\ \vdots \\ \tilde{\mathbf{p}}_N \end{bmatrix} \right\|_F \left\| \begin{bmatrix} \mathbf{p}_1 \\ \vdots \\ \mathbf{p}_n \\ \vdots \\ \mathbf{p}_N \end{bmatrix} \right\|_F^{-1}, \tag{21}$$

proposed as a first stopping criterion. Here, $\mathbf{p}_n[i_s/R]$ is the time history of the n^{th} field point. This is used because it is easy to compute. The normalisation is applied because the response can be quite

different depending on the operation of the complex machine, which obfuscates the interpretation of the error. The iterative procedure stops when this normalised error is sufficiently small or, as a second stopping criterion, when a maximum number of iteration steps has been reached. This concludes the discussion on the estimation of source strengths, and in the next section a procedure to validate the dummy source approach is discussed.

12 VALIDATION OF THE DUMMY SOURCE

The source strengths are estimated using a limited number of control microphones (control points) around the original source, which may not be representative of the original sound field. Since the underlying idea for the estimation of source strengths has been to reproduce the original sound field at the control microphones as closely as possible, the dummy source will not only adapt to the original sound field but also to the measurement errors. The small measurement errors may lead to large inversion errors in the estimated source strength distribution. The erroneous source strengths may in turn predict poorly. Consequently, even if the dummy source accurately reproduces the sound field at the control microphones it may fail to reproduce the sound field elsewhere [54, Ch. 3].

It is proposed that the accuracy of the dummy source is checked at E independent microphone positions referred to as error microphones (error points). "Independent" in this context means that the error points are not used to estimate the source strengths. The sound field of the original source has to be measured simultaneously at the control microphones and at the error microphones. The matching between the predicted sound field and the original sound field at the error points is an indicator of the dummy's performance and the fit of the estimated source strengths.

The matching can be assessed by comparing the measured and predicted time histories for each error point when working in the time domain. The matching can also be assessed by listening. In the time domain, the summation of partial contributions of respective drivers can be expressed as

$$\tilde{\mathbf{p}}[i_s] = \sum_{m=1}^{M} \sum_{i_h=1}^{N_h} \mathbf{h}_m[i_h]\mathbf{q}_m[i_s - i_h + 1], \qquad t = i_s/R, \tag{22}$$

a multiple input - single output (MISO) convolution summation [53, pp. 492 - 500] [55, pp. 529 - 531]. The frequency domain instead requires matrix multiplication to estimate the pressure response, but assumes stationary time histories. The complex pressure can then be back-transformed into the time domain [3].

The use of error microphones validates not only the inverse approach but indeed the entire procedure including the measurement and analysis of transfer impedances and pressure responses. This concludes the discussion on various aspects needed for experimentally implementing a dummy source. The key issues are: (1) the design of the equivalent acoustical model, (2) the design of the characterisation experiment, (3) implementing a volume velocity sound source for measuring transfer impedances, and (4) deducing the dummy's source strengths.

The discussion will now change subject. The next section describes how the dummy source approach has been simulated in order to assess the proposed characterisation procedure. The simulations are done using the substitute source method with the method of images [24]. The developed numerical model has been used in a hybrid formulation of the dummy source approach with computed transfer impedances [19].

13 SIMULATION OF THE DUMMY SOURCE APPROACH

The substitute source method, formulated using spherical sound field synthesis [24, 25, 26, 56, 57, 58, 59, 60, 61], is based on the idea that the radiated and diffracted sound field by a vibrating body of volume V can be approximated by superposition of spherical waves originating from within the vibrating body. The superposition aims at reproducing the sound field as accurately as possible outside of the boundary surface of the vibrating body. In the case of free-space radiation, satisfying Sommerfeld's radiation condition [14, pp. 177 - 178], this is achieved by matching all of the spherical waves to the boundary conditions prescribed at many points across the boundary surface of the vibrating body. It is sufficient to prescribe the velocity

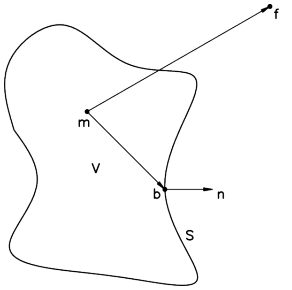

Figure 12: Schematics of the substitute source method using spherical sound fields.

distribution as a boundary condition which guarantees a unique solution to the sound field of the vibrating body [14, pp. 178 - 180]. In reflective spaces such as a half-space, a quarter-space or an eighth-space the method of images [14, pp. 210 - 211] can be combined with the substitute source method to represent reflections. Moreover, the substitute source method can be applied on scattering problems [62, 63, 64], i.e. waves incident on a passive body, which can be used to investigate the similarity between the dummy and the original body. Finally, in [26, 61] alternative mathematical formulations such as the single point multipole expansion and the multiple points multipole expansion are discussed. For simplicity only the spherical sound field synthesis will be considered in this thesis.

Admittedly, other numerical techniques, such as the finite element method, could have been applied equally well. The substitute source method was chosen for two reasons: (1) The technique is similar to the outlined dummy source approach in the sense that superposition is used to find an approximation of the sound field of the vibrating body. However, in the case of the substitute source method the elementary sources are embedded inside of the volume of the vibrating body. *This means that the velocity distribution of the dummy source is numerically represented by an array of monopoles inside of the dummy source. The simple source array on the surface of the dummy source, which defines the vibration of the dummy source, should not be confused with the monopole array needed to compute the sound radiation.*; and (2) The numerical technique can be built and controlled entirely by the user. There is no need for any particular software or dedicated computers.

The substitute source method will be used to simulate both the acoustic transfer impedance of the dummy source and the sound radiation of the original source. The application to a single driver - cabinet assembly — to estimate the transfer impedance — will be discussed in App. V. The approach has been benchmarked against piston radiator theory in an infinite baffle with satisfactory results. The results are not reproduced in this thesis in order to reduce the page count of the thesis. The mathematical formulation of the synthesis procedure will be discussed in the following subsection.

13.1 The substitute source method

Koopmann et al. [57] formulated the spherical sound field synthesis, for a constant frequency sound field, by letting the monopoles be continuously distributed throughout the entire volume of the vibrating body. The sound field outside of the vibrating body is then given by the superposition integral

$$\hat{p}(\mathbf{f}) = j\omega\rho_0 \int_V \hat{q}(\mathbf{m}) G(\mathbf{f} \mid \mathbf{m}) dV, \tag{23}$$

where $\mathbf{m}$ is the monopole position, $\mathbf{f}$ is the field position and $\hat{q}(\mathbf{m})$ is the density of the source strength distribution, Fig. 12. The Green's function [33, Ch. 6]

$$G(\mathbf{f} \mid \mathbf{m}) = \frac{\mathrm{e}^{-jkr}}{4\pi r}, \qquad r = \|\mathbf{f} - \mathbf{m}\|, \tag{24}$$

for radiation into an open space, satisfies the Helmholtz equation

$$(\nabla^2 + k^2) G(\mathbf{f} \mid \mathbf{m}) = -\delta(\mathbf{f} \mid \mathbf{m}) \tag{25}$$

and the Sommerfeld's radiation condition [14, pp. 177 - 178]

$$\lim_{r\to\infty}\left[r\left(\frac{\partial\hat{p}}{\partial r}+jk\hat{p}\right)\right]=0, \tag{26}$$

where $k = \omega/c$ is the wavenumber, ∇ is the gradient and δ is Dirac's delta function [33, pp. 66 - 76]. The Helmholtz equation is a reduced form of the harmonically forced wave equation [33, pp. 397]. The Sommerfeld's radiation condition states that no energy comes back into the acoustic medium from infinity.

The density of the source strength distribution $\hat{q}(\mathbf{m})$ is found by matching the continuous smear of monopoles to reproduce the velocity distribution $\hat{v}_\perp$ on the surface of the vibrating body. The pressure and particle velocity at the surface of the vibrating body is related through the Euler's equation, $j\omega\rho_0\hat{\mathbf{u}} = -\nabla\hat{p}$ assuming $p = \Re\{\hat{p}\mathrm{e}^{j\omega t}\}$ [14, p. 11, p. 15, p. 27][57]. The particle velocity on the surface of the vibrating body is again given by a superposition integral formulation

$$\hat{\mathbf{u}}_\perp(\mathbf{b}) = \int_V \hat{q}(\mathbf{m})\nabla_\perp G(\mathbf{b}\mid\mathbf{m})dV, \tag{27}$$

where $\mathbf{b}$ is a point on the surface S. The derivative of the Green's function $\nabla G(\mathbf{b}\mid\mathbf{m})$ is [14, pp. 180 - 182]

$$\nabla G(\mathbf{b}\mid\mathbf{m}) = \frac{\mathbf{b}-\mathbf{m}}{r}(1+jkr)\frac{\mathrm{e}^{-jkr}}{4\pi r^2}, \qquad r = \|\mathbf{b}-\mathbf{m}\|, \tag{28}$$

which describes the radial particle velocity due to a monopole. This can be used to find the normal derivative, $\nabla_\perp = \nabla\cdot\mathbf{n}$ where $\mathbf{n}$ is the outward unit normal of the surface S, required to approximate the prescribed velocity distribution. The normal derivative is given by

$$\nabla_\perp G(\mathbf{b}\mid\mathbf{m}) = (1+jkr)\frac{\mathrm{e}^{-jkr}}{4\pi r^2}\cos\gamma, \qquad \cos\gamma = \frac{\mathbf{b}-\mathbf{m}}{r}\cdot\mathbf{n}. \tag{29}$$

13.1.1 Boundary conditions

The particle velocity amplitude field $\hat{\mathbf{u}}$, $\hat{\mathbf{u}} = (\hat{u}_1, \hat{u}_2, \hat{u}_3)$, created by the substitute sources has to reproduce the surface vibration amplitude field $\hat{\mathbf{v}}$ in the direction of outward unit normal $\mathbf{n}$ at any point $\mathbf{b}$ on the surface S of the vibrating body [14, pp. 100 - 103, 153 - 207]:

$$\hat{\mathbf{u}}\cdot\mathbf{n} = \hat{\mathbf{v}}\cdot\mathbf{n}. \tag{30}$$

This is the fundamental assumption of the synthesis which enables the computation of the radiated sound field [24, 25, 57, 61].

13.1.2 Method of images

The substitute source method has been formulated in free-space condition, but the method is appropriate also in other acoustical spaces where the Green's function is known. In a reflective space — a realistic condition when testing of vibroacoustic sources is concerned — the acoustic boundary-value problem can be treated using the method of images [14, pp. 210 - 211], Fig. 13.

The method of images deserves a remark. In the substitute source method the monopole array — the positions of the monopoles and the estimated source strengths — aims at matching the normal velocity on the surface of the vibrating body as closely as possible. In a free-space *only* the monopoles inside of the vibrating body will contribute to the reproduction of the normal velocity distribution on the surface of the body. However, in a reflective space such as a half-space *the image sources apply secondary particle velocity fields on the surface of the original vibrating body* [14, pp. 208 - 209]. The failure to account for this phenomenon leads to excessive numerical errors when the vibrating body is positioned close to a hard surface. The monopole array is *strictly valid only in the acoustic space in which it has been constructed*. Installing the vibrating body in another space thus requires a different monopole array in order to satisfy the velocity distribution as closely as possible. The discrete formulation of the synthesis procedure will be discussed in the next subsection.

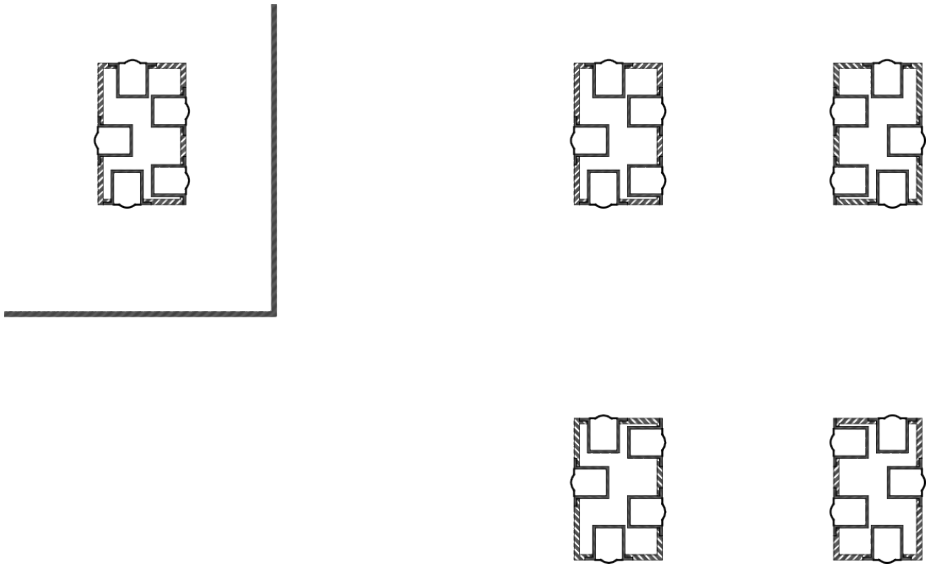

(a) (b)

Figure 13: The dummy source installed in a quarter-space (a) actual boundary-value problem with the vibrating body and two walls stretching to infinity and (b) the method of images in which the walls are replaced by image sound sources set in a free-space.

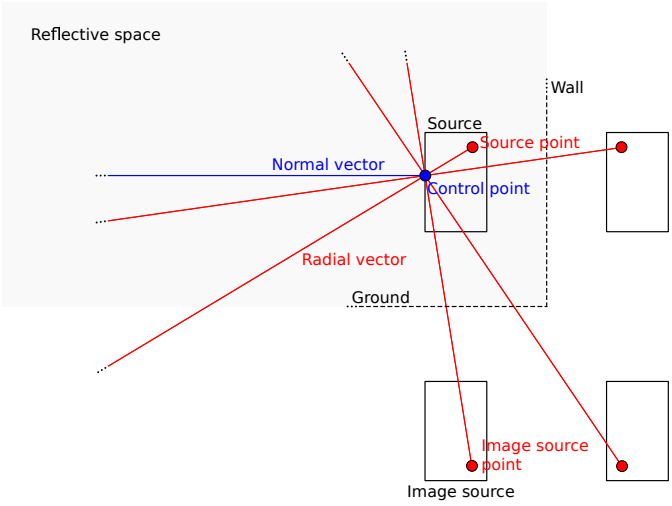

Figure 14: The developed substitute source method combined with the method of images for the computation of sound radiation in a reflective space, illustration in a quarter-space. (Color)

13.1.3 Discrete formulation in a reflective space

As before, the superposition integral has to be reformulated as a superposition summation for numerical analysis of sound radiation. The velocity distribution is prescribed at N surface control points across the surface of the vibrating body. A monopole array is then prescribed at M interior source points inside of the volume of the vibrating body. In order to match the monopole array to the prescribed velocity distribution, the source strength of each substitute monopole is related to the normal velocity at each respective control point. The resulting set of equations can be written

$$\mathbf{T}\hat{\mathbf{Q}} \approx \hat{\mathbf{v}}_{\perp}, \tag{31}$$

using the appropriate transfer function of the space

$$T_{nm} = \frac{1}{4\pi}(1 + jkr_{nm})\frac{\mathrm{e}^{-jkr_{nm}}}{r_{nm}^2}\cos\gamma_{nm} + \frac{1}{4\pi}(1 + jkr_{nm}^{'})\frac{\mathrm{e}^{-jkr_{nm}^{'}}}{r_{nm}^{'2}}\cos\gamma_{nm}^{'} + \ldots. \tag{32}$$

The "appropriateness" of the transfer function comes from that the influence of the image substitute monopoles on the surface of the original vibrating body has been taken into account, Fig. 14. The boundary conditions of the reflective walls are guaranteed using the proposed formulation. The source strengths are found from matrix inversion. It is assumed that the number of control points is greater than the number of source points. The sound pressure at a grid of N field points outside of or on the boundary surface of the vibrating body is then computed from

$$\hat{\mathbf{p}} \approx \mathbf{Z}\hat{\mathbf{Q}}, \tag{33}$$

using the appropriate transfer impedance of the space

$$Z_{nm} = jk\rho_0 c\frac{1}{4\pi}\frac{\mathrm{e}^{-jkr_{nm}}}{r_{nm}} + jk\rho_0 c\frac{1}{4\pi}\frac{\mathrm{e}^{-jkr_{nm}^{'}}}{r_{nm}^{'}} + \ldots. \tag{34}$$

The difficulty with the substitute source method is that a suitable monopole array which sufficiently well describes the prescribed normal velocity is not known beforehand. In the next subsection the design of a suitable monopole array using an optimisation procedure will be discussed.

13.2 Design of the monopole array using a search procedure

The crudest way of positioning substitute sources is across a predetermined support, such as a line or surface [57, 62, 64], or by random positioning [65]. This may or may not lead to numerical instabilities and a poor performance of the method. In this work the monopole array will be constructed out of a set of candidate monopole sources by use of a *search procedure* [24, 25, 26]. There are alternative positioning algorithms, such as genetic algorithms [63, 64, 65] or particle swarm optimisation [66, 67] which may produce better results. This could be subject to further work.

There is no rational way to find out how many substitute sources are needed, nor where they should be located. One reason for this is that the optimal number of sources and their positions depend on both the wavelength and the geometry. This motivates the use of a computational procedure for the design of the monopole array mitigating the risk of poor performance at the cost of time-consuming optimisation. Pavić [25] proposed a search procedure in 2005:

1. A grid of N points — control points — is spread across the surface of the vibrating body. The normal velocity is prescribed at these points. Thereafter is a grid of K points — candidate points — distributed within the volume of the vibrating body.

2. A single point — source point — which produces the best fit to the prescribed velocity distribution is first found among the candidate points. The velocity distribution achieved by this source is then removed from the original velocity distribution which results in the (velocity) residual of the first step.

3. The procedure is then repeated. Among the candidate points which have not been selected the position which provides the best fit to the velocity residual of the previous step is selected. The source strength of all $M \ll N$ selected substitute sources are then updated to best fit the original velocity distribution. The velocity of the array is then removed from the original velocity distribution, which results in the (velocity) residual of the current step.

4. Each subsequent step results in the selection of a new best fit source point among the remaining candidate points. The procedure repeats until either the velocity residual is considered sufficiently small or the number of substitute sources has reached a prescribed maximum.

This is the basic procedure used to compute sound radiation by a driver - cabinet assembly [24]. The practical implementation of the search procedure will be discussed in the following subsection. (The approach has been implemented in GNU Octave under Linux.) This will be followed by a discussion of the performance of the technique.

13.2.1 Implementation of the search procedure

The search procedure has been implemented using a lookup table. The transfer matrix $\mathbf{T}$, in which each element T_{nk} [24, 25] (Eq. 32) relates the normal component of velocity $\hat{\mathbf{v}}_\perp$ of the n^{th} control point, $\mathbf{b}_n$, on the surface of the vibrating body to the source strength, $\hat{\mathbf{Q}}_k$, of the k^{th} candidate monopole position, $\mathbf{m}_k$, inside of the vibrating body, is decomposed into a set of column vectors: $\left\{\mathbf{T}_1,\ \mathbf{T}_2,\ \ldots,\ \mathbf{T}_k,\ \ldots,\ \mathbf{T}_K\right\}$. Each column vector relates a candidate position to the normal velocity on the surface of the vibrating body. In order to determine the best fit candidate position, the source strength and thereafter the residual velocity distribution of each available candidate position needs to be computed in each iteration step. In practice this is done by a lookup table constructed by $\mathbf{T}_k^+ = \mathbf{T}_k^* \Big/ \mathbf{T}_k^*\mathbf{T}_k$ row vectors. The precomputed row vectors are then used to search for the best fit candidate position. The velocity residual $\Delta\hat{\mathbf{u}}$ associated with each candidate source is $\Delta\hat{\mathbf{u}}_{k,i} = \mathbf{T}_k\left(\mathbf{T}_k^+\Delta\hat{\mathbf{u}}_{M,i-1}\right) - \Delta\hat{\mathbf{u}}_{M,i-1}$, where i is the iteration step, which is used to find the best fit candidate source. Here, the subscript $\left[_{M,i-1}\right]$ denotes the residual of the entire monopole array of the previous iteration step, and the subscript $\left[_{k,i}\right]$ the residual of the k^{th} candidate position in the current iteration step. The procedure is initiated by the prescribed normal velocity on the surface of the vibrating body, in place of the velocity residual of the previous step, in the first iteration step. The best fit candidate source position minimises thus in each iteration step the mean square velocity error at the control points

$$\arg\min_k \Delta\hat{\mathbf{u}}_{k,i}^*\Delta\hat{\mathbf{u}}_{k,i}. \tag{35}$$

The lookup table is not meaningful for the source strengths estimation of the resulting array of M substitute sources which is found by matrix inversion of the assembled transfer impedance matrix. The advantage of this approach is that one part of the computation necessary in each iteration step is only computed once before the search procedure is initiated. The search procedure has been found sufficiently accurate, but not satisfactorily fast. The computational cost of the optimisation procedure will be discussed in the following subsection.

13.2.2 Reduction of the computational cost

The disadvantage of the search procedure is that it is quite time-consuming, because the iterative procedure requires in each step a matrix inversion which needs to be repeated for each frequency of interest. Thereafter for each source position on the dummy's surface. To simulate the dummy source approach a multiple driver array needs to be computed in different acoustical spaces. This is not practicable with the above described search procedure. This has been partially mitigated by applying the optimisation procedure of monopole positions at narrow-band center frequencies reducing the computational cost without significant loss of accuracy [24]. Still this reduces only the need of the search procedure, but not the speed of the search procedure itself. Pavić [26] proposed an efficient search procedure selecting in each step a small monopole array, a discrete multipole, instead of a single monopole. This strategy is with some gained perspective recommended for future applications of the substitute source method using the search procedure.

However, for the purpose of simulating the dummy source approach a modified search procedure has been developed. (Such a simulation has been deemed not to be feasible with the original search procedure due to the excessive computational cost.) In total there will be four modifications of the search procedure. The modified approach, which will be called the *fast search procedure*, is rather speculative but has so far been found to construct a monopole array which is fully comparable in accuracy to the original search

procedure. The more speculative approach is valid since the substitute source array, i.e. the number of monopoles and their positions, in itself is of no interest. The two primary questions to be considered when using the substitute source method are: (1) *How well does the substitute sources match the velocity distribution of the vibrating body?*, and (2) *How fast can the substitute source array be constructed?*

To stress the efficiency of the four modifications, the time required for a single optimisation with the search procedure has dropped from roughly *36 000 sec* in 2012 to roughly *36 sec* in 2015, considering a couple of thousand candidate sources and a couple of thousand control points. The two first modifications, exploiting symmetry in the matrix formulation and employing efficient matrix inversion [24], resulted in 800 sec in 2013. The benchmark here is the driver - cabinet assembly in [24] set in a half-space condition at 200 mm from the ground. The first two modifications will be explained in detail in App. V and are not speculative. So far, the results of the fast search procedure are fully comparable with that of the search procedure employed in [24].

There are four reasons the search procedure is slow. The first reason is the matrix inversion used to update the monopole array. Courrieu [68] developed an efficient matrix inversion procedure. This decimates the computation time when compared to the singular value based Moore - Penrose pseudoinverse in GNU Octave. The second reason is that if the method of images is not efficiently handled, the entire sound source should be mirrored, the matrix size explodes. This has been avoided using the symmetry of the radiation problem [24]. This modification reduces the time spent searching and improves numerical accuracy, as the boundary values at the walls are guaranteed. The first two considerations are not speculative, but the computational cost remains high. This motivates further modifications of the search procedure.

The third reason is the way the selection of the best fit source position among the set of available candidate source positions is carried out. Imagine two subsequent computations using the same model of the boundary surface of the vibrating body, the first computation is done with one grid of candidate source positions, which will be called the reference set, and the second computation is done with only a subset of those candidate positions. Clearly, reducing the number of candidate positions from the beginning proportionally reduces the time required for selecting the apparent best fit candidate position in each step in the second computation, but at the risk of having removed the actual best fit in the reference set of candidate positions. There is beforehand no rational reason why a candidate position should be better or worse than another so reducing the set of possible source positions is not a satisfactory solution. This problem has been overcome by in each step only searching trough a random subset of the remaining candidate positions, for example evaluating 500 out of 3000 possible positions. Since there will be many iterations, the entire solution space will eventually be considered. The performance of the final monopole array does not depend on whether or not the best fit monopoles are selected first or last. This limits the time spent searching in each iteration without the risk of removing the actual best fit candidate positions. It was found in an initial investigation that — concerning the monopoles' positions — the modification results in a monopole array which is 75% identical to the monopole array constructed by the original procedure. The new array, however, required 8% more monopoles to reach the same normalized residual velocity at the control points. The time consumption was reduced to about 35%.

The fourth reason is that the original search procedure considers the substitute sources to be joint. Therefore, at the end of each step the entire monopole array is updated which requires matrix inversion. It is argued that it is sufficient to update the monopole array much less frequently, if at all, for example every 25^{th} iteration step which decimates the computation time. The assumption here is that the substitute sources can be treated independently. The search algorithm then superposes the independent sound fields until the numerical error is sufficiently small. This suggests that matrix inversion is potentially not needed for either identifying the monopole array or for the estimation of source strengths. A search without the use of matrix inversion has been found comparably slow to converge, and for this reason it is recommended to update the entire monopole array once in a while. Once the monopole array has been updated, considering the selected monopoles to be joint, the performance will improve. This fourth modification suggests that (if the final array is considered to be joint,) the source strengths of the entire monopole array have to be updated (in a fifth step) once the search has finished, which was previously not necessary.

Even using the fast search procedure the computation of acoustic transfer impedances of a dummy source remains rather time consuming. The entire computation takes between a few hours and a few days depending on the modelling parameters: the number of control points, the number of error points,

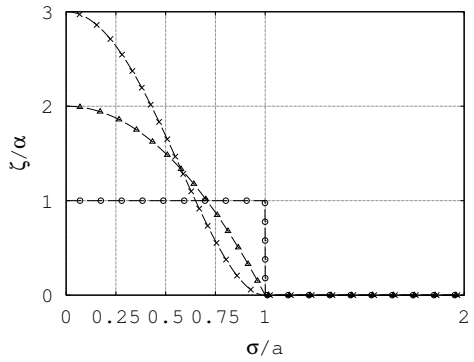

Figure 15: Greenspan profile visualised for three different orders: ∘-marker, zeroth order; △-marker, first order; ×-marker, second order.

the number of candidate points, the largest number of source points, the number of drivers, the frequency range and so on. All of the computations have been made using an ordinary non-dedicated laptop, initially a HP ProBook 6360b (France, 2011) and thereafter a why! W650SZ (Switzerland, 2015). In practice it has been found that, using such a computer, the limit at which the computer starts to be unusable for other tasks is ten thousand candidate source positions inside of the original vibrating body and ten thousand control points on the surface of the original vibrating body. (Several tens of thousands candidate source positions when counting the image sources.) The numbers are believed sufficient for computing sound radiation of a vibrating body, such as a medium-sized loudspeaker, in reflective spaces and at audio frequencies. There was, however, not enough time to fully test the limits of the developed substitute source approach.

A last remark is that numerical instabilities may occur due to an inappropriate choice of source positions [24, 25, 60, 61]. The instabilities can be mitigated by repeated computations, employing a different grid of source points in each computation, until satisfactory reconstruction of the boundary conditions occurs. It has been observed that [24] a small randomisation of the grid of candidate source positions can reduce the number of instabilities using the search procedure. This ends the general discussion on the substitute source method and the method of images. The application of the numerical technique to approximate the acoustic transfer impedance of a single driver - cabinet assembly — a dummy source — will be discussed next.

13.3 Simulation of the transfer impedance of the dummy source

The developed approach to the computation of transfer impedance of a single driver - cabinet assembly will be discussed in detail in appendix V. The approach is not restricted to any particular frequency range and can be used both to estimate the point transfer impedance of a small disk or a general transfer impedance of a large disk when the disk is mounted in the surface of a closed rigid baffle. Prior to the computation, the multiple driver array installed in the surface of the dummy is decomposed into a corresponding set of M single driver - cabinet assemblies, the drivers are located at source positions $\mathbf{s}_1, \ldots, \mathbf{s}_m, \ldots, \mathbf{s}_M$. The computation of the dummy's transfer impedances is carried out for each single driver - cabinet assembly respectively.

In the following the simulation of a point transfer impedance is discussed, which is required by the dummy source approach. The simple source of sound is approached by a vibrating disk which is small compared to the acoustic wavelength, $a \ll \lambda$. A Greenspan [69] distribution $\hat{v}_\perp(\mathbf{s}_m)$ is prescribed across the surface of the disk representing the m^{th} driver. The choice of vibration pattern has been inspired by piston radiator theory [69, 70]. The velocity distribution on the surface S of the single driver - cabinet assembly is [24]

$$\hat{\mathbf{v}}_\perp(\mathbf{s}_m) = \begin{cases} \zeta(\sigma_m),\ 0 \le \sigma_m \le a \\ 0, \text{otherwise on } S. \end{cases} \quad , \qquad \zeta(\sigma) = \alpha(n+1)\left(1 - \frac{\sigma^2}{a^2}\right)^n H(a-\sigma) \tag{36}$$

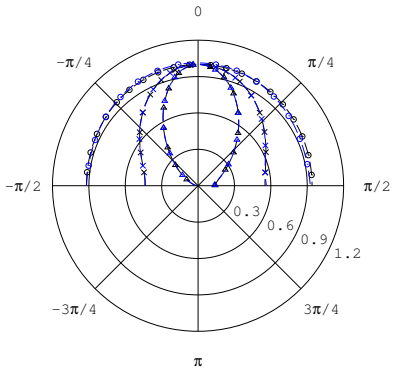

Figure 16: The radiation pattern of a disk with radius 30 mm in an infinite baffle at 1812 Hz (∘-marker), 5442 Hz (×-marker), 9077 Hz (△-marker) evaluated by Rayleigh's integral (black) and by a small monopole array behind the disk (blue) for a Greenspan profile of first order, left side, and second order, right side. (Color)

In this equation, ζ is the Greenspan profile, H is the Heaviside step function, α is a velocity constant, n is the profile order, a the disk radius and σ the distance between a point on the disk and the center of the disk. The velocity distribution for the first few orders are visualised in Fig. 15. The velocity distribution is constrained so that

$$\hat{\mathbf{Q}} = \int_S \hat{\mathbf{v}}_\perp dS = 1, \tag{37}$$

which implies that the velocity constant α must be $\alpha = \frac{1}{\pi a^2}$. The Greenspan velocity distribution is used in place of Dirac's delta function [33, pp. 66 - 70], and represents the effect on the acoustic space of a point source set in the surface of the cabinet for the evaluation of the superposition integral in Eq. 1. Historically, distributions similar to the Greenspan profile have been used to approximate the Dirac's delta in various disciplines of physics [33, pp. 66 - 70]. The Green's function was then understood as the limit when the approximating distribution approaches the delta function, in the case of the Greenspan profile this historical analogy corresponds to $n \to \infty$. In this thesis, however, the acoustic point transfer impedance is understood as the result of the disk being small $a \ll \lambda$ and constrained to the case $n \geq 1$ which is an intuitive notion of a simple source of sound, see e.g. Morse and Ingard [20, pp. 309 - 312]. Whether or not the disk is a simple source of sound can be checked by evaluation of the radiation pattern using the Rayleigh integral [24]. The evaluation of the radiation pattern using the substitute source approach and the Rayleigh integral is seen in Fig. 16. Here, a disk in an infinite baffle for a ka-value of 1, 3 and 5 is illustrated and it is shown that the disk is a hemispherical source at low ka-values. (The principal lobe widens and approaches a non-directional pattern when the ka-value decreases.) Rayleigh's integral will be discussed in App. V. The substitute source approach will be further discussed in App. V.

Moreover, the choice of a higher order Greenspan profile can be motivated due to Gibbs phenomenon. The delta function can not be represented by a finite number of spherical waves coming from inside of the vibrating body. Likewise a rigid piston can not be modelled accurately enough as it has a sharp discontinuity in the velocity along its edge. Instead, a smooth distribution has to be prescribed, $n \geq 1$. The performance of the substitute source approach using a smooth and a sudden velocity profile is illustrated in Fig. 17.

Finally, the substitute source array is validated using both the reconstruction error in the velocity and the total radiated power Π. The power output is separated into contributions by the driver D and the cabinet C. Ideally only the driver contributes to the total radiated power. The power output is obtained by integrating sound intensity across the boundary surface

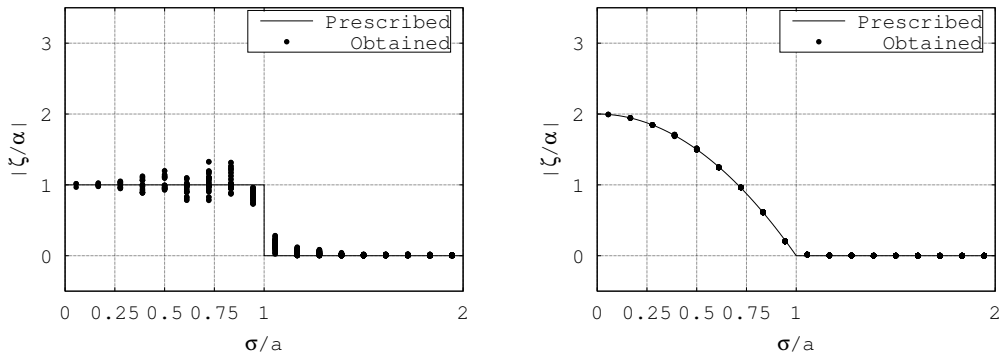

Figure 17: Normalised velocity profile at all control points on and close to the disk in dependence of the prescribed boundary condition: left, zeroth order; right, first order. The disk is set in an infinite baffle and has been modelled by a small monopole array behind its surface.

$$\Pi = \int_S \mathbf{I}\cdot\mathbf{n}\,dS = \int_D \mathbf{I}\cdot\mathbf{n}\,dD + \int_C \mathbf{I}\cdot\mathbf{n}\,dC, \tag{38}$$

$$\equiv \int_D \mathbf{I}\cdot\mathbf{n}\,dD, \tag{39}$$

where the time averaged intensity is given by $\mathbf{I} = 0.5\Re\{\hat{p}\bar{\hat{\mathbf{u}}}\}$ [24]. The bar denotes a complex conjugate. The breakdown is henceforth written $\Pi_S = \Pi_D + \Pi_C$. This leads to a power leakage error which relates the total radiated power with the power output of the driver. The power leakage is quantified in dB by [24]

$$e_C = 10\log_{10}\Pi_D \Big/ \Pi_S. \tag{40}$$

If there is no leakage, the leakage error is zero dB.

Kropp and Svensson [60, pp. 534 - 544] proposed in 1995 a similar technique for approximating the Green's function of a point source in the surface of a vibrating body. Their aim was also to evaluate the sound radiation using the superposition integral in Eq. 1. The computation was done using a time-domain formulation of the substitute source method. There are several differences between the two techniques although the aim is the same. An essential difference between the two techniques is that the dummy source approach is based on piston radiator theory. Moreover, the velocity distribution is enforced both by the use of a search procedure and by prescribing a non-uniform grid of control points on the surface of the single driver - cabinet assembly.

13.4 Simulation of sound radiation by the original source

Sound radiation by the original source is "straightforward" to simulate when compared to the previous simulation of transfer impedance of the dummy source. The reason is that the velocity distribution is in this case smooth and without sudden changes as imposed by a small vibrating disk on an otherwise passive surface. Pavić [25, pp. 13 - 14] proposed a procedure in 2005 in which a randomised monopole array is introduced inside of the vibrating body. The randomisation is carried out in respect to the number of monopoles, the monopoles' positions inside of the vibrating body and the monopoles' complex source strengths. The velocity distribution, $\hat{v}_\perp$, is then identified across the surface of the vibrating body. This serves as a reference source for which the exact velocity distribution and radiated sound field is known.

Unlike in [25] in which this technique was used to benchmark a search procedure, as employed in this thesis, it will now be employed in order simulate sound radiation from the vibrating body in different reflective spaces. Again this is done by prescribing the identified velocity on points spread across the surface of the vibrating body. The search procedure is then used, operating on appropriate outward normal velocity

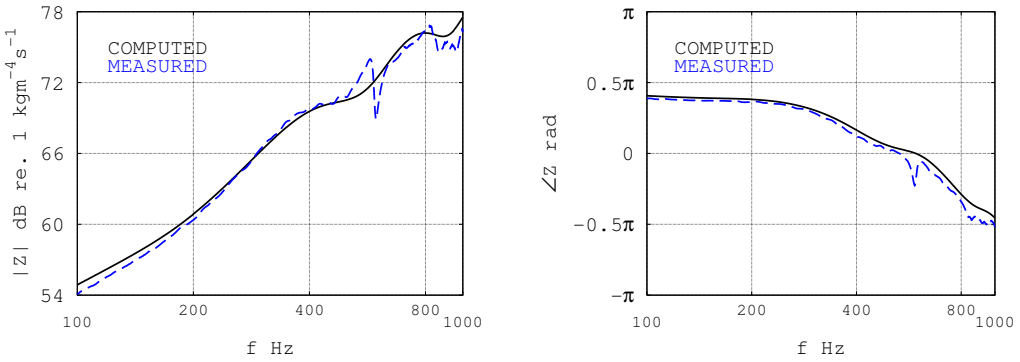

Figure 18: Transfer impedances on the axis of the driver mounted in a closed-box baffle in a semi-anechoic room. Level, left, and phase, right. Legend: blue dashed line measured, black continuous line computed. (Color)

- source strength transfer functions accounting for the reflective space, to identify a monopole array which best approximates the random forcing distribution.

This concludes the discussion on simulation of the dummy source approach using the substitute source method. In the next section a simulated case study will be presented which illustrates the characterisation approach. This will be followed by experimental calibration of a driver, an experimental case study using the diesel engine and an experimental case study using a vibrating box.

14 MAIN FINDINGS

14.1 Numerical findings

The numerical work has been conducted through two case studies: (1) Numerical modelling of a single driver - cabinet assembly, and (2) Numerical assessment of the dummy source approach.

14.1.1 The Single Driver - Cabinet Assembly

The model of a single driver - cabinet assembly has been thoroughly confronted with measured transfer impedances with satisfactory results during the past few years in semi-anechoic condition [19, 24, 38], and is discussed in detail in App. V. Among the measurements, two transfer impedances measured in a semi-anechoic room with the driver - cabinet assembly suspended at a height of 200 mm from the ground will be presented here. The length, width and height of the assembly is 300, 232, 500 mm respectively. (The center of the assembly coincides with the x_3-axis of the space, and the edges of the assembly are aligned with the coordinate system.) In the first example, the microphone is positioned on the axis of the driver in Fig. 18. The driver is positioned at (10, -116, 550) mm, and the microphone is positioned at (10, -281, 550) mm. In the second example, the microphone is positioned on top of the box in Fig. 19. The driver is positioned at (150, 6, 520) mm whereas the microphone is positioned at (0, 0, 995) mm. *It has been concluded that the numerical model is realistic for a small driver mounted in the surface of a closed rigid cabinet. However, to achieve an accurate computation the use of an optimisation procedure, such as the search procedure, is required for the positioning of substitute monopoles.*

14.1.2 The Dummy Source Approach

To show the viability of the dummy source approach, a fictitious original source has been characterised in a reflective space, an eighth-space, using a dummy source with the aim of predicting the sound pressure response in another listening space, a free-space. This enables a comparison between the exact pressure response of the original source and the predicted pressure response of the dummy source. The comparison is done at frequencies involving acoustical wavelengths much longer to several times shorter than

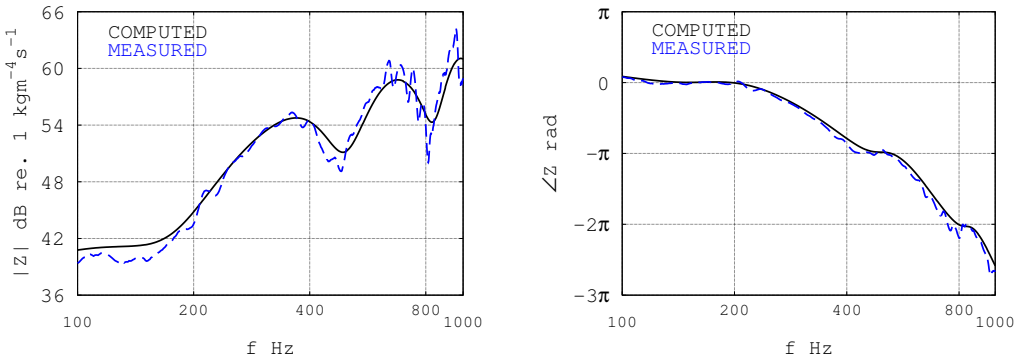

Figure 19: Transfer impedances off the axis of the driver mounted in a closed-box baffle in a semi-anechoic room. Level, left, and phase, right. Legend: blue dashed line measured, black continuous line computed. (Color)

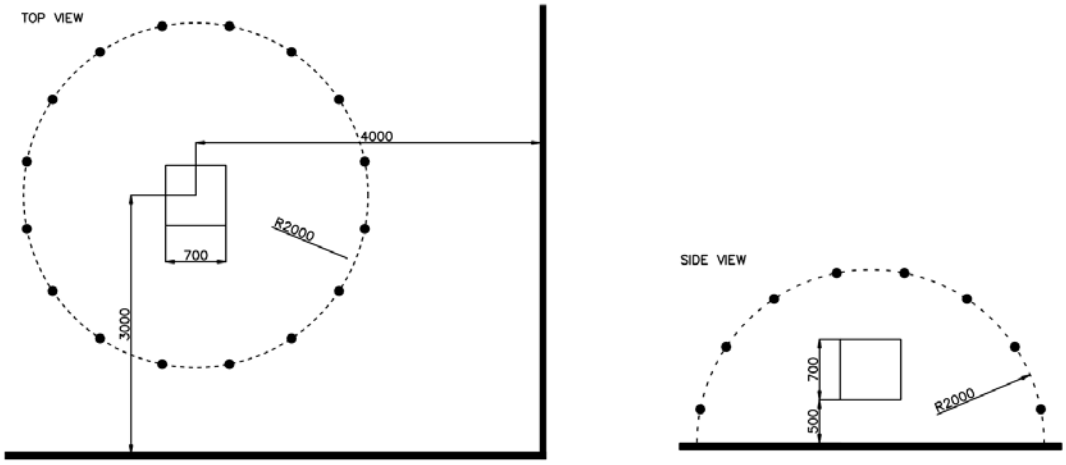

Figure 20: Schematic setup of the characterisation space in the virtual experiment: top view, left; side view, right. Black circles illustrate a microphone array used to estimate the source strengths. All units in mm.

some typical dimension of the original source. The frequency range 20 - 2000 Hz was thus defined. The computation was carried out at 20 logarithmically distributed frequencies.

The original source has the shape of a cube of length 700 mm installed 3000 mm respectively 4000 mm from the corner of a large room measured from its geometrical center while standing at a distance of 500 mm from the floor measured from its lower face, Fig. 20. The velocity of the vibrating sound source is found by scattering a monopole array inside of its surface in a free-space and assigning random complex source strengths. The velocity is then identified across points on its surface which enables synthesis of sound in the eighth-space, Fig. 21. The machine is thereafter enclosed by a fictitious surface, a half-sphere of radius 2000 mm, aligned with the center of the machine while standing on the floor. On the fictitious surface, an array of 128 microphones are (randomly) spread around the sound source.

A dummy source in the shape of a cube of length 700 mm has been conceived. Since there is no difference between the passive bodies of the original source and the dummy source the diffraction is represented exactly. A regularly spaced 3×3 driver array is embedded in the surface of each face of the dummy source with a total of 54 drivers, Fig. 21. This array corresponds to about 2 drivers per wavelength at 735 Hz, which is the expected upper frequency limit of the dummy. Each driver is modelled by a clamped-edge disk, a 2^{nd} order Greenspan profile, with radius 50 mm which is a simple source of sound below about 1000 Hz, ka-value of 0.9, as evaluated by Rayleigh's integral [24]. At 2000 Hz, a ka-value of 1.8, the radiation pattern

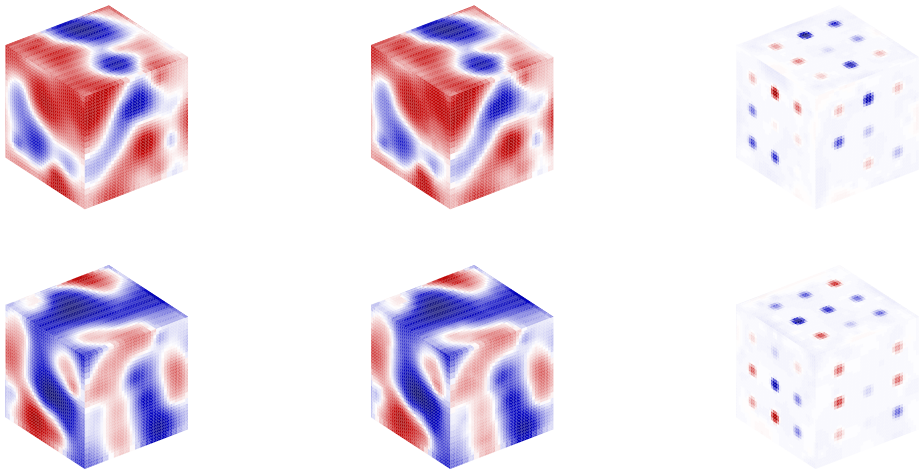

Figure 21: The original source's velocity distribution visualised by, left, prescribed vibration pattern in a free-space and, middle, obtained vibration pattern in an eighth-space at 966 Hz. The corresponding velocity distribution on the dummy source which characterise the original source is visualised to the right. Legend: top, real part; bottom, imaginary part. (Color)

is no more omnidirectional and a beam-like pattern has started to appear. The change in radiation pattern implies that at shorter wavelengths the radiation model of the original source is de facto that of a clamped-edge disk array; i.e., the knowledge of the vibration pattern becomes important and makes experimental implementation difficult. (The resulting sound field is easy to compute, which could be used in further work to characterise sound sources by piston-like models using computed transfer impedances instead of measured point transfer impedances.) A simple source can be achieved by reduction of the radius of the disk. The computations of the disk array are verified by the power leakage through the cabinet [24], the numerical error is typically less than 0.5 dB (up to 1 dB has been observed) for all frequencies and disk positions.

The estimation of the dummy's source strengths was for simplicity done without adding noise to the sound pressure response of the original source at the microphone positions. Due to imperfect substitute source modelling there is, however, still random errors both in the simulated transfer impedances and the pressure response, but this is hard to quantify. Thus, there are two kinds of errors in the simulation results: (1) Imperfect substitute source modelling producing random errors in the transfer impedance matrix as well as in the sound pressure response of the original source, and (2) Imperfect dimensioning of the dummy source, which beforehand makes it physically difficult for the dummy source to reproduce the sound field of the original source above 735 Hz. The two sources of errors can not be separated in the result. The dummy's performance was evaluated at 5041 error points, nodes of a meshed sphere of radius 2000 mm centred on the original source in a free-space. The exact field is known at these nodes. The dummy's performance was also evaluated at 128 control points, positioned across a half-sphere in a eighth-space. The normalised pressure error was estimated as

$$e_p = 10\log_{10}\left(\boldsymbol{\Delta}\hat{\mathbf{p}}^*\boldsymbol{\Delta}\hat{\mathbf{p}}\Big/\hat{\mathbf{p}}^*\hat{\mathbf{p}}\right). \tag{41}$$

The result shows that the dummy source is optimistic in how well it fits to the sound field of the original source in the eight-space at low frequencies, Fig. 22. Nonetheless, the free-space results show that the predicted sound field is similar to the exact sound field up to 2 sources per wavelength. At 2 sources per wavelength the -12 dB error appears to be large but visual inspection of the sound fields suggests that there is some similarity up to about 1.5 sources per wavelength, Fig. 23. At low frequencies the two sound fields are almost indistinguishable to the eye. Moreover, it has been found that the results are still acceptable

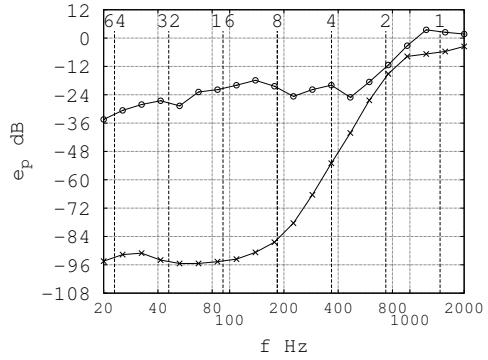

Figure 22: The dummy's performance in terms of normalised pressure error. Legend: ×-marker, eighth-space; ○-marker, free-space. The number of drivers per acoustical wavelength is indicated by dashed vertical lines.

if the number of microphones in the eight-space is halved from 128 to 64 to make the simulation more practicable.

This numerical illustration supports the design hypothesis in Eq. 12 and shows that the sound field a distance away from the source can be represented using a sparse distribution of simple sources set in the surface of a closed rigid baffle. The illustrated dummy source has merely 54 degrees of freedom corresponding to 2 sources per wavelength at 735 Hz. If instead 6 sources per wavelength is prescribed, a 9×9 array on each face with a total of 486 degrees of freedom has to be worked out. Such an array is hardly practicable for experimental characterisation of sound sources since the number of degrees of freedom becomes too high. The illustrated original source is quite large, and larger than the diesel engine used in the experimental work. This simulation is therefore believed to be realistic.

The simulations have been done using the substitute source method with the method of images. The advantage of the numerical technique is that the Helmholtz equation is guaranteed to be satisfied since the computed field is composed of elementary monopole fields, but the disadvantage is that the prescribed boundary conditions are only approximated. Using the substitute source method, it becomes quite involved to ensure that the prescribed boundary conditions are reproduced accurately enough. The accuracy has been verified using both reconstructed normal velocity and power leakage through the cabinet [24]. A key to understanding the behaviour of the obtained velocity is that rapid fluctuations around the prescribed distribution only leads to cancellation of sound [24]. Also, the use of a smooth continuous velocity on a smooth surface is tantamount to accuracy of the substitute source method. The shape of a cube or a box is difficult to compute using spherical wave field synthesis since it has sharp edges.

It is only at the eleventh hour of this research project that a complete numerical case study of the dummy source approach has been feasible, due to the invention of the fast search procedure. To accomplish the same numerical case study with the original search procedure, without any performance enhancements, would take at least five years. Using the search procedure in [24] the computation time would be roughly one month and a half. Instead, the entire case study took less than a weekend to compute using a non-dedicated laptop.

The modelling includes the use of about 30 000 error points spread across the surface of the dummy source, and the dense grid is required in order to compute power leakage from each driver position. It is believed that a rigorous simulation study is on the horizon since the time-consuming transfer impedances of the dummy source only needs to be computed once for a given space. A Monte Carlo approach can be employed to alter the vibration of the original source, which in comparison to the dummy source is much faster to compute. Such a computational study is highly recommended to be carried out in further work on the dummy source approach. This has not been done here due to a lack of time.

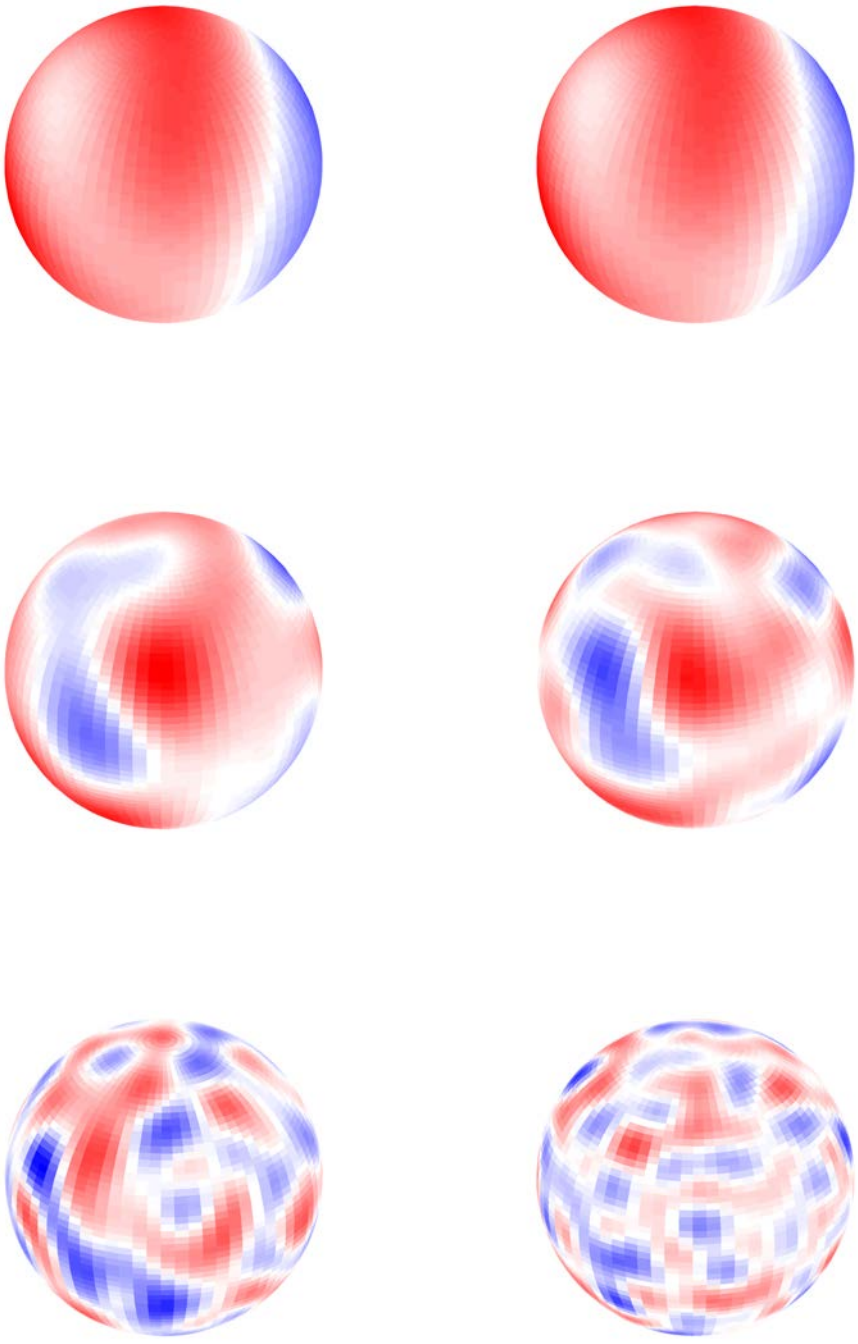

Figure 23: The dummy's performance visualised by, left column, the real part of the exact sound field of the original source and, right column, the real part of the predicted sound field using the dummy source in a listening space other than the calibration space for three different frequencies. Legend: first (top) row, 467 Hz; second row, 966 Hz; third (bottom) row, 2000 Hz. (Color)

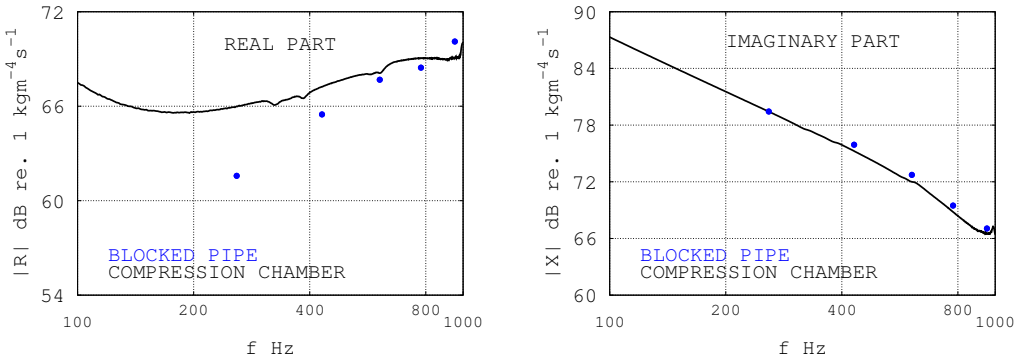

Figure 24: Measured source function of the instrumented mid-range driver. Real part, left, and imaginary part, right. Continuous black line: compression chamber. Blue ∘-marker: blocked pipe. (Color)

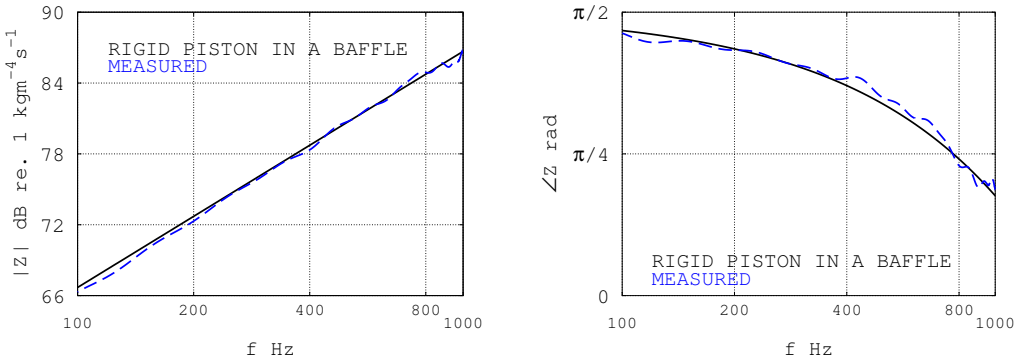

Figure 25: Transfer impedance on the axis of the driver in an anechoic room. Level, left, and phase, right. Modelled: black continuous line; measured using the source function estimated in a blocked pipe, dashed blue line. (Color)

14.2 Experimental results

The experimental work has been conducted through three case studies: (1) Implementation of a known volume velocity source, (2) Characterisation of a diesel engine, and (3) Experimental validation of the dummy source approach.

14.2.1 Calibration of an instrumented driver

The experimental work with a dummy source requires a known volume velocity source for the measurement of transfer impedances, and is discussed in detail in App. III and App. IV. Such a source has been built by use of an instrumented driver characterised with either a blocked pipe or a compression chamber. This particular driver is considered to be small, below 1000 Hz, and the measured source function is shown in Fig. 24. The measurement using a blocked pipe was done about one year after the measurement using a compression chamber. This means that the ambiance might not have been the same in the two measurements, and the time-lag might have changed the driver's mechanical performance. Despite mentioned inconveniences, it was found that the measured source functions are similar. Therefore, the driver can be used to measure transfer impedances. The calibration, performed in small closed spaces, was validated by measuring transfer impedances along the axis of the driver mounted in a flat rectangular baffle inside of an anechoic room, an example is shown in Fig. 25. Finally, the transfer impedances were measured reciprocally in an engine test cell, an example is shown in Fig. 26.

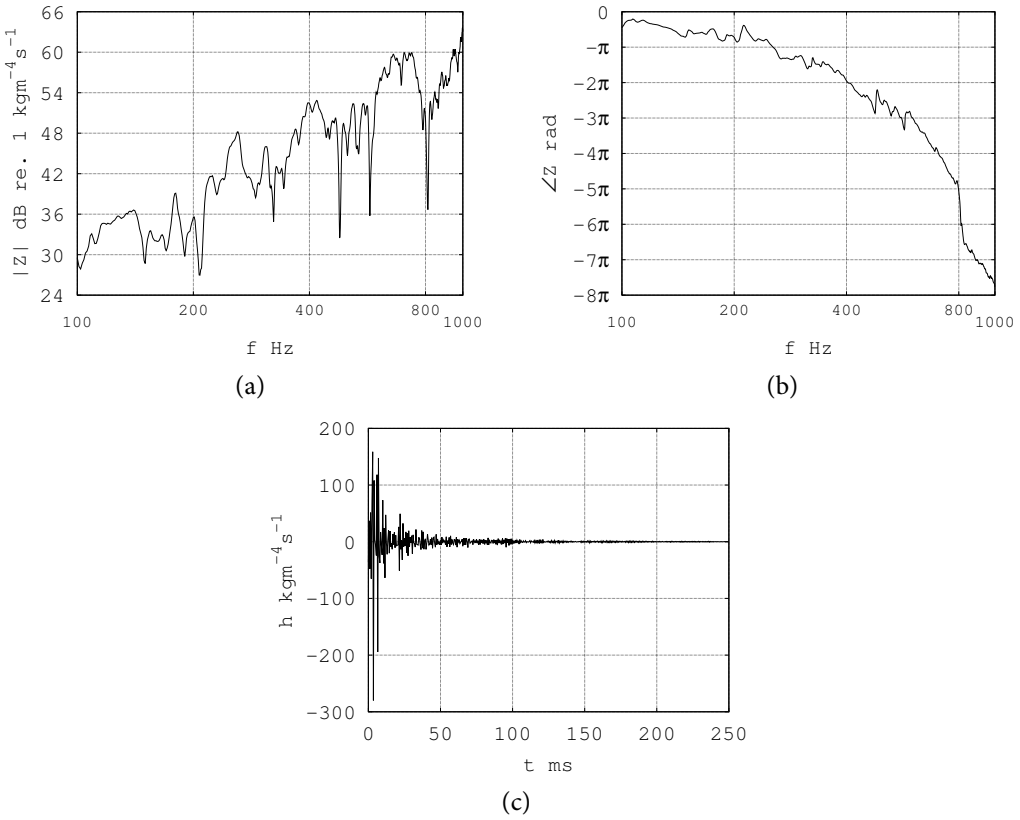

Figure 26: Measured transfer impedance in an engine test cell: (a) level, and (b) phase. The corresponding impulse response is shown in (c).

14.2.2 Characterisation of a diesel engine

The experimental work with a diesel engine was conducted head first, since the engine laboratory of INSA de Lyon was scheduled to be moved (demolished), and is discussed in detail in App. I. The implementation of the dummy source approach is summarised as follows:

1. The diesel engine was started and left in a load regime for a considerable amount of time to approach a steady-state; i.e., mechanical properties, and as a consequence the housing vibration, changes while the engine is heating up. The active water cooling system will after a while stabilise the process (80°C outgoing).

2. The time histories were recorded using a microphone array spread around the diesel engine. A sufficient time duration was recorded, and oversampling was employed.

3. The diesel engine was switched off, and physically removed from the test cell. The dummy source was then installed at the place of the diesel engine in the same test cell.

4. The source strengths of the driver array was related to the operating pressures at the microphone array by reciprocal measurement of transfer impedances in the test cell.

5. The time histories were processed off-line in several steps: (1) band-pass filtering to match the useful frequency band of the known velocity source, (2) calibration to remove differences between the array microphones, and (3) down-sampling to reduce the computational effort using adaptive filtering. The processing was complemented, for the frequency domain estimation of source strengths, by estimating the pressure amplitude at engine harmonics using a tachometer.

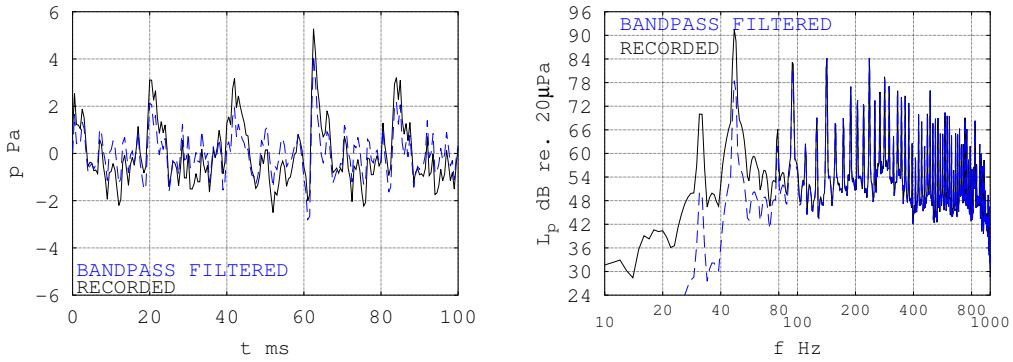

Figure 27: A sample of a recorded operating pressure signal: time domain, left; frequency domain, right. Dashed blue line, band-pass filtered signal used for estimating the source strengths; continuous black line, recorded signal. (Color)

6. The source strengths were estimated from the measured (and processed) time histories and the measured transfer impedances (impulse responses) off-line.

The prototype dummy source was designed as a closed box of dimensions $300 \times 232 \times 500$ mm. The box is smaller than the engine, neglecting the fly wheel and the exhaust muffler. The box was conceived to have an array of 22 drivers spread across its surface satisfying the criteria in Eq. 12 until 1000 Hz. The upper frequency limit of the box was matched to the useful bandwidth of the previously instrumented driver.

The prototype was, however, implemented reciprocally and manufactured as a Plexiglass box equipped with an array of 22 microphones flush-mounted in its surface. Consequently, the transfer impedances were measured reciprocally moving the instrumented driver around at the positions of the microphones previously used to measure the operating responses in the test cell.

Since the performance of the dummy source may depend on the operation of the diesel engine, the unloaded engine was measured at three speeds using a microphone array. The microphone array was installed across a cage surrounding the engine. (The engine was unloaded because a shaft connecting the engine to a brake went into mechanical failure during the experimental work.) The recordings were band-pass filtered, 100 Hz to 1000 Hz in this case, and then down-sampled, to 2000 Hz sample rate, to match the frequency range of the measured impulse responses. The result of the processing is shown in Fig. 27.

The experimental results were hampered, at the time the recordings were made, by the lack of freely available microphones in the laboratory. Merely 16 mixed microphones of different types could be used. The recordings were done before simulation results and processing tools were available. Thus, in retrospect, a too sparse array was installed around the diesel engine. In turn, this limited the dummy source to have only a few drivers on its surface since an overdetermined set of equations has been imposed to mitigate the influence of measurement errors. Out of the 22 drivers only 10 was selected to achieve an overdetermined set of equations.

Such an equivalent acoustical model can not be expected to well reproduce the sound field up to 1000 Hz, which was the upper frequency limit of the calibrated driver. (Above 1000 Hz a directional radiation pattern starts to develop.) According to the design hypothesis, the design should be reasonable up to 700 Hz but since a randomised rather than a uniform acoustical layout has been used the hypothesis may not be valid. During the analysis of the conducted experiments, the engine laboratory was moved and no further experiments could be conducted.

The subsequent analysis using adaptive filtering has provided promising results. A comparison between recorded and predicted time histories at an error point is shown in Fig. 28. The result depends on the (random) selection of source and microphone positions, but good matching at one or both of the error points has been observed for a few realisations. The results have been computed using 10 000 iterations which resulted in an error of about 0.3 at the control points. In practice, the error has been observed not to im-

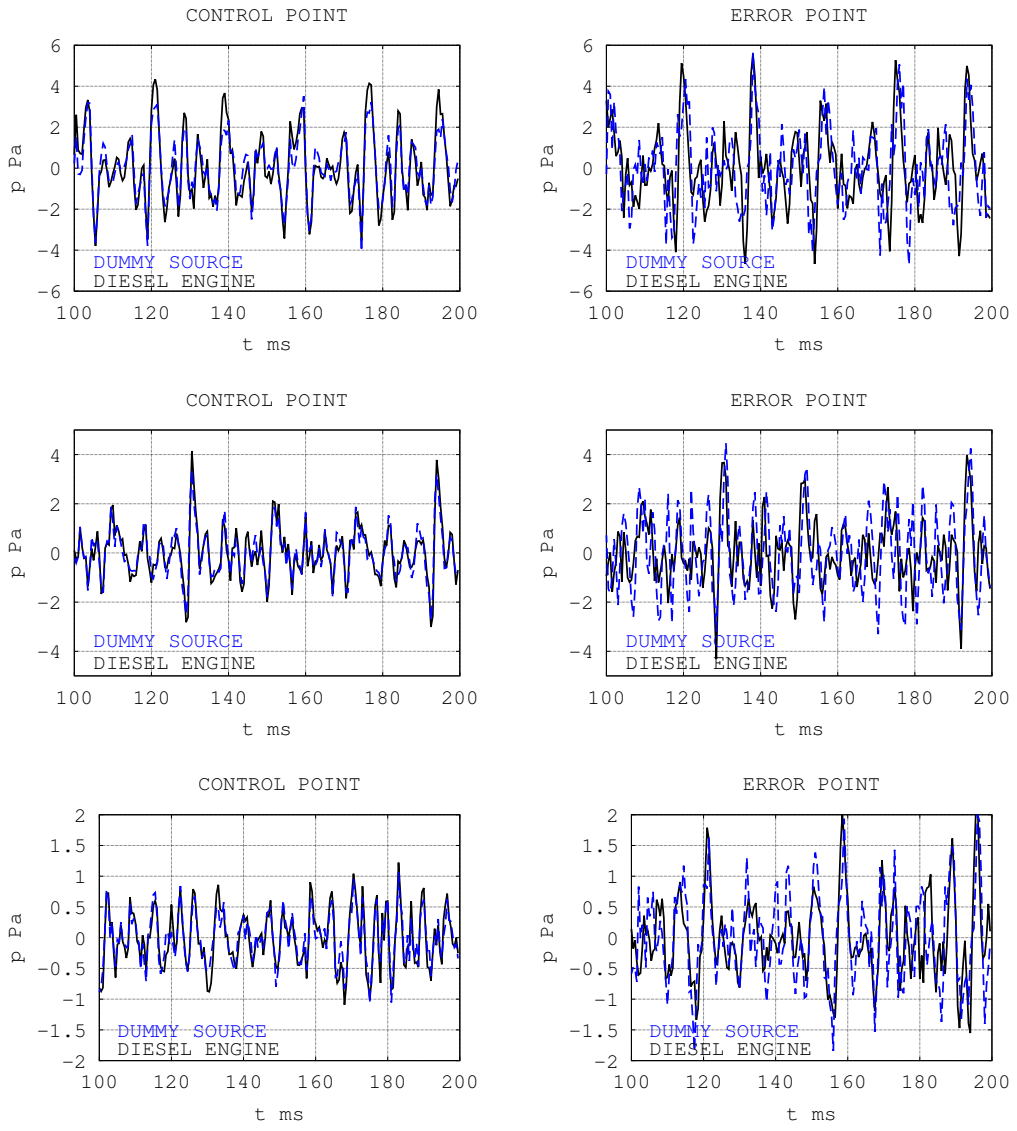

Figure 28: The dummy's performance using the LMS method visualised by, left, reconstruction of a part of a time history at a control point and, right, prediction of a part of a time history at an error point for three different steady-state operations of the complex machine. Continuous black line, diesel engine; dashed blue line, dummy source. Top row, 2160 RPM; middle row, 1890 RPM; bottom row, 1070 RPM. (Color)

prove much after 2 500 iterations. The behaviour likely depends on the choice of scaling factor but this was not elaborated upon due to a lack of time.

The results using adaptive filtering is superior to that achieved using regularisation techniques in the frequency domain, which has been concluded from a direct comparison of the recorded and predicted time histories, from listening and assessment of the frequency content. A comparison in the frequency domain is shown in Fig. 29. The difference between the dummy source and the diesel engine is often within 6 dB, although the error at certain harmonics can be up to 12 dB or more. The differences are audible, and the coloration of the synthesised sound is not quite correct.

Nevertheless, it is believed that with a sufficient number of simultaneous recordings, e.g. 32 or 64 depending on the available data acquisition system, with a uniform microphone array, with all microphones of the same type, the results would be improved. (Unfortunately, the acquisition of such an array was

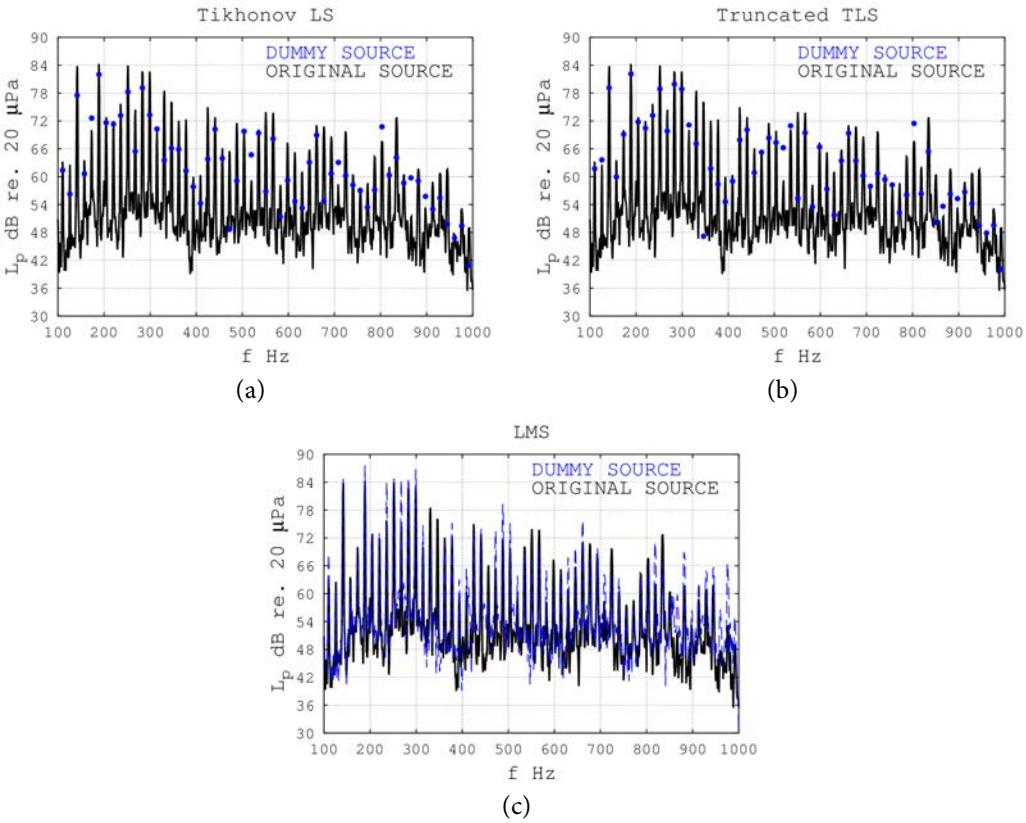

Figure 29: The dummy's performance at an error point illustrated in the frequency domain, at engine harmonics: (a) Tikhonov LS, and (b) Truncated TLS; and as a continuous function of frequency: (c) LMS. Continuous black line, diesel engine; dashed blue line or blue circle, dummy source. The results are shown for the engine speed 1890 RPM. (Color)

not possible.) This would have allowed for 2 drivers per acoustic wavelength or more on the surface of the dummy, as well as provided a sufficient number of time histories for more extensive validation of the dummy source. Consequently, the experimental implementation of a dummy source, for the characterisation of a complex machine in industrial conditions, requires some further work.

14.2.3 Validation of the dummy source approach

The dummy source approach has since been successfully validated in a semi-anechoic test cell using a simple machine, the setup is shown in Fig. 30 and the experiment will be discussed in detail in App. II. The simple machine is a Plexiglass box with a shaker embedded inside of it, connected at two points which are not axially aligned. The shaker was driven by band-pass limited white noise, and the sound field is assumed to be a stationary random process. The box is of the same dimensions as the dummy source prototype which has been used in the preceding experiment with an engine. The objective of this experiment is to characterise the simple machine by a dummy source with 22 drivers distributed across its surface, using the same acoustical layout as employed in the engine experiment. According to the design hypothesis, the dummy source is capable of reproducing the sound field up to 1000 Hz.

Since the size and shape of the simple machine and the dummy source are identical, the sound diffraction is represented exactly. The transfer impedances of the dummy source were computed between 20 and 2000 Hz, in which case the acoustic wavelength goes from much larger to comparable with the size of the simple machine. The ground reflection was modelled using the method of images. The computation of transfer impedances is discussed in App. V. A planar microphone array was moved around the controlled

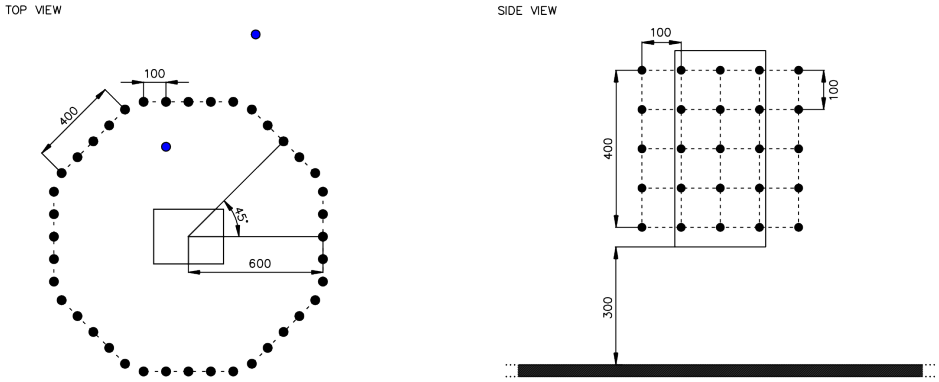

Figure 30: Schematic setup of the validation experiment with a vibrating box: top view, left; side view, right. Black circles illustrate a planar array used to estimate the source strengths, moved around the vibrating box in eight positions, and blue circles illustrate two additional microphones used to validate the dummy source. All units in mm. (Color)

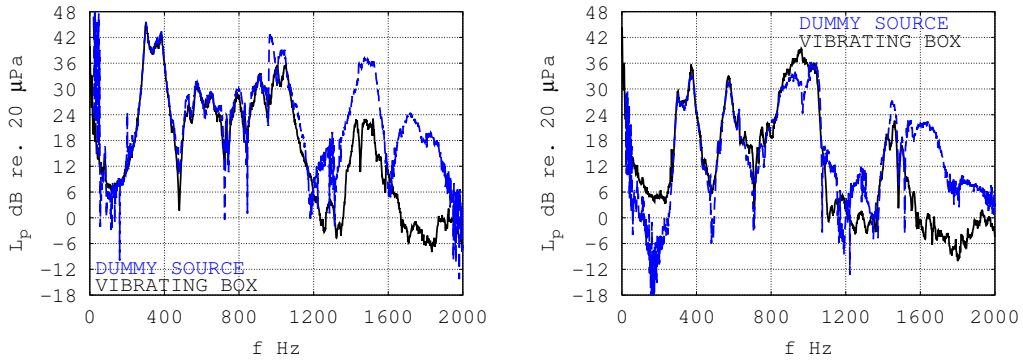

Figure 31: Comparison between the sound pressure level predicted by the dummy source and recorded with a vibrating box at two independent points: left, interior to virtual surface; right, exterior to virtual surface. Continuous black line, vibrating box; dashed blue line, dummy source. (Color)

sound source to produce a large set of measurements spread across a fictitious surface surrounding the simple machine, the measurements were synchronised using a reference signal which is discussed in App. II. The microphones were, as before, split into control points and error points.

The dummy's source strengths was found by Tikhonov regularisation using the L-curve criterion, which is discussed in App. II. A remark, however, is that since an overdetermined set of equations is used to estimate the source strengths, the problem is a non-zero residual problem. This is important in order to compute the curvature of the L-curve, and thus to choose the appropriate regularisation parameter. A second remark is that the selected regularisation parameter has been found to be continuous with frequency, which indicates that the largest curvature criterion is reasonable since the sound field of the vibrating box and the transfer impedances of the dummy source are smoothly changing with frequency.

Satisfactory matching between the measured sound field of the vibrating box and the predicted sound field of the dummy source was obtained at the error points. More importantly, two microphones were positioned in the semi-anechoic room at a distance away from the fictitious surface, so called listening points. Like the error points, the listening points are not used to estimate the source strengths. The results using 32 microphones to estimate the source strengths are shown in Fig. 31. It is seen that the dummy source reproduces the measured sound field between 200 Hz and 1000 Hz in an admirable manner. The discrepancy at low frequencies is likely due to that the simple machine is not an efficient radiator of sound, and thus the measurements suffer from poor signal-to-noise ratio. The discrepancy at higher frequencies

is due to that the density of drivers on the surface of the dummy is insufficient. The results suggest that the design hypothesis is sufficient for accurate enough sound reproduction.

This validation shows the viability of the dummy source approach for experimental work. It also shows the usefulness of the developed substitute source approach for experimental work, in case the characterisation space is uncomplicated enough to permit the use of a simplified numerical model. This concludes the discussion on experimental results which has focused on the implementation of a known volume velocity source, a reciprocal dummy source to characterise a diesel engine, and a virtual dummy source to characterise a vibrating box.

15 CONCLUDING REMARKS

The context of this work is the increasing need of improved operator comfort in heavy-duty vehicles. Due to the complexity of such an industrial problem, this research project has focused on airborne sound characterisation of an active complex machine component: a diesel engine. This is only a first step towards an acoustical prototype of an earth-moving machine. It turns out that the solution to the practical, rather than theoretical, problem at hand is far from obvious.

The complex machine can not be punctiliously represented as it is in reality, and a simplified approach has to be used. This is so since the vibration is distributed across a highly irregular surface which may be of extremely complex pattern. The approach should, however, not be overly simplified and a number of criteria has been devised: (1) Any practicable model has to constrain the number of degrees of freedom, (2) The model has to account for both diffraction and radiation phenomena of the sound source, (3) The model has to be independent of the surrounding space, and (4) The model has to be formal in the sense that the representation of the sound field can be made to be exact. The last criterion is needed to justify the model as a prediction tool. Still an exact representation is not the aim of sound source characterisation. On the contrary, it is believed that a rugged representation is necessary for experimental work.

On the one hand, commonly employed sound source models or descriptions fail one or more of the desired criteria. One such description is in terms of total radiated power. The power output suppresses the radiation pattern and phase information of the sound source. Sound power is, furthermore, not independent but in fact a function of the surrounding space. It is, therefore, for this application, not a meaningful quantity. Neither can an equivalent source approach, using elementary volumeless sources, to sound radiation by vibrating bodies be employed since such a model does not account for sound diffraction. Concerning the diesel engine it is in practice comparable in size to the acoustic wavelength. The change from a semi-anechoic test cell to a small engine compartment is extreme, and it is clear that the volume can not be neglected. This motivates the need of modelling sound diffraction. On the other hand, modern numerical - experimental hybrid approaches, such as the inverse boundary element method or the inverse finite element method, often result in too complicated source models with thousands of degrees of freedom, which is deemed not practicable either. Moreover, models aiming at reproducing the velocity distribution continuously over the surface of the complex machine are not easy to implement experimentally. There is currently a gap between the overly simplified and the overly complicated approaches to the characterisation of airborne sound sources.

This thesis attempts to fill in that gap by proposing *the dummy source approach* to airborne sound source characterisation using a moderate amount of degrees of freedom. The dummy source approach is a general concept and applies to sound sources radiating by housing vibration. It is assumed that the vibration of the complex machine is not sensitive to effects of the surrounding space. This is common to all sound source models based on the normal component of the velocity distribution. The approach may not be general, but it is reasonable for a diesel engine which has high mechanical impedance and is therefore not sensitive to radiation loading. *The active complex machine component has been split into a passive and an active part. The passive part is a closed cabinet of similar size and shape as the complex machine, in this thesis the surface is assumed to be rigid since the diesel engine has a hard surface. The active part is a flush-mounted driver array, in this thesis limited to the case of small back-enclosed drivers.* Such a driver is a simple source of sound determined by its position and source strength. The simple source unifies experimental and numerical modelling. The numerical counterpart is a smooth compact velocity distribution. It is proposed to use at least two simple sources per shortest acoustical wavelength of interest.

The multiple driver - cabinet assembly models both sound diffraction and sound radiation of the complex machine. The approach can be either hybrid, using computed transfer impedances, or fully experimental, using measured transfer impedances.

The dummy source approach is a formal model of sound radiation and sound diffraction from a vibrating body. The sound diffraction is represented exactly if the cabinet is made precisely like the housing of the complex machine it represents. Likewise, the radiated sound field of the dummy source becomes exact if the drivers are made extremely small so that the array is defined continuously across the surface of the cabinet.

The basic assumptions behind the dummy source approach have been verified by simulation using the substitute source method. This includes that a small back-enclosed driver is a simple source, that a closed-box baffle can represent sound diffraction of a more complicated vibrating body, that a flush-mounted simple source array can reproduce the far-field sound of an original source, and that the characterisation is independent of the surrounding. The model of a driver is based on piston radiator theory. The single driver - cabinet assembly model has been confronted to measured transfer impedances using a small back-enclosed driver and an aluminium closed-box baffle with satisfactory results. The dummy source approach has been experimentally validated using a simple vibrating body, a shaker embedded in a box, with satisfactory results. Moreover, the approach is practicable for experimental work since it is rugged. The cabinet can be equipped with handles to be carried around and so on, which allows the dummy source to be easily employed in various environments. The dummy source approach should be subject to further research concerning the optimal design of the acoustical layout and the optimal estimation of the source strengths, but it can already be tested in application as it is outlined in this thesis, with two drivers per shortest wavelength of interest.

This hypothesis implies an array with a moderate amount of degrees of freedom when compared to the inverse boundary element method. In the latter case, small surface elements forming the entire boundary surface is usually considered with six elements per wavelength, as a rule-of-thumb. The dummy source approach can be considered as being equivalent to a(n inverse) boundary element method. However, the point sources are hidden inside of its boundary surface and there is no mesh. The result of the inverse procedure is an equivalent discrete distribution of volume velocity sources on the surface of the dummy. The primary advantage of the proposed formulation is, however, the ability to work fully experimentally.

A known volume velocity source has been constructed using an ordinary small back-enclosed driver equipped with an internal microphone. The driver was calibrated using a front-added volume, such as a blocked pipe. It is recommended to use at least two methods to measure the internal source impedance, the source function, to verify that the characterisation is appropriate. In case the back enclosure is manufactured, with an air cavity of known static volume, the simpler method of Anthony and Elliott [37] can be employed instead.

In practice, there will be modelling or measurement errors in the transfer impedance of the dummy source and measurement errors in the pressure response of the complex machine. Furthermore, the dummy source may be miss-specified in such a way that the number of drivers is not sufficient, or that the driver array is not well distributed across the entire surface. The experiment may in a similar manner be miss-specified so that the number of microphones is not sufficient, or that the microphone array is not well distributed around the complex machine. This complicates the estimation of the source strengths, using control points, and in the frequency domain there is, furthermore, a trade-off between measurement errors and regularisation errors. There are several techniques in the literature to choose the optimal regularisation parameter. I want to stress, however, that, in my opinion, it is more important to ensure that the transfer impedance matrix is physically meaningful in the first place than to apply fancy inversion and regularisation techniques. The most promising source strength estimation technique attempted so far is the LMS algorithm. The advantage is that it avoids matrix inversion altogether and does not require assumptions about the recorded time histories, nor the use of transform methods. The disadvantage is the increase in computation time. The estimated source strengths are validated at independent error points which are not used for source strength estimation. Loosely speaking, many combinations of transfer impedance model and inverse method will be able to reproduce the sound field at the control points, but will fail to predict the same sound field at the error points. A successful check at the error points implies that the transfer impedance model as well as the source strengths are reasonable.

No simple relationship between the various design parameters (driver array, microphone array) in the experimental setup and the performance of the estimated source strengths has been identified. The result seems to be obfuscated, meaning that the results vary from one realisation of the geometry of the problem to another, which is the result of using a Monte Carlo approach for preconditioning the inverse problem. Nonetheless, preconditioning of the problem and (if working in the frequency domain) regularisation of the source strengths is necessary to produce reasonable results at independent error points. An alternative to preconditioning could be to use optimal positioning of the driver array. However, to the best of my knowledge, there is currently no simple off-the-shelf optimisation procedure to design the driver array. There are, however, academic studies based on free-space simulation with point sources concerning the optimal choice of design parameters in regard to the condition number which are difficult, if not impossible, to apply in reality. It is simply not possible to install the microphone array anywhere, due to peripheral equipment in the test cell. It is, likewise, not feasible to design the driver array arbitrarily, due to internal volume conflicts in the dummy source. The design of the driver array, the microphone array and the estimation of source strengths should be subject to further work, but such work must be carried out in realistic circumstances.

One fundamental aspect of acoustics, which was outside the scope of this thesis, is that it is not sufficient to consider only physics in order to solve the industrial problem. One must consider subjective perception of reconstructed sound to assess sound quality. It is evident that the developed dummy source prototype, which handles sound fields up to 1000 Hz, can not be satisfactory for the purpose of listening to diesel engine sound.

To venture further, a dummy source capable of reproducing the sound field up to 4000 Hz, using two drivers per wavelength, would require about 365 drivers for the same surface area on the dummy (0.67 m^2) as used in the experimental case studies. This is a substantial amount of drivers and a numerical model of the transfer impedance of the dummy source, which has been developed, is necessary for the approach to be practicable. If it is possible to use one driver per wavelength for the reproduction of sound, only 90 drivers would be needed. It is believed that a microphone array with e.g. 128 microphones of the same type recording simultaneously around the complex machine is achievable, albeit expensive. Consequently, one may have to let the assumption of an overdetermined set of equations go. Alternatively, the driver array has to be optimised in place of the fixed grid design used in this thesis. The latter could, perhaps, be achieved by an algorithm similar to the search procedure employed to select the substitute sources. The performance of a dummy source from a hearing perspective as well as its feasibility at high frequencies are open questions which should be addressed in future work.

Supplementary material

The supplementary material has been divided into four parts: I, Application to a diesel engine; II, Validation using a vibrating box; III, Measurement of transfer impedances; and IV, Computation of transfer impedances. Each part has been divided into one or more appendices: appendix I is unpublished work, appendix II is an extended version of [19], appendix III is a postprint of [29], appendix IV is a postprint of [39], and appendix V is a postprint of [24]. The reader is invited to jump between appendices, or to skip them entirely, according to their own interest, rather than to read the thesis from cover to cover. No particular reading order is recommended. It is hoped that each part can be read without the need to go trough the rest of the thesis thoroughly.

16 Bibliography

[1] A. T. Moorhouse and G. Pavić, "Virtual Acoustic Prototypes of White Goods Products," In Proc. of the International Congress and Exposition on Noise Control Engineering (Internoise) **33**, pp. N/A (2004).

[2] G. Pavić and A. T. Moorhouse, "Is virtual acoustic prototyping simply a noise prediction tool?," In Proc. of the International Congress and Exposition on Noise Control Engineering (Internoise) **33**, pp. N/A (2004).

[3] A. T. Moorhouse, "Virtual acoustic prototypes: listening to machines that don't exist," Acoustics Australia **33**, pp. 97 - 105 (2005).

[4] G. Pavić, "Noise Sources and Virtual Noise Synthesis," In Proc. of the International Congress and Exposition on Noise Control Engineering (Internoise) **37**, pp. N/A (2008).

[5] Y. Bobrovnitskii and G. Pavić, "Modelling and characterization of air-borne noise sources," J. Sound Vib. **261**, pp. 527 - 555 (2003).

[6] D. Berckmans, B. Pluymers, P. Sas and W. Desmet, "Numerical Comparison of Different Equivalent Source Models and Source Quantification Techniques for Use in Sound Synthesis Systems," Acta Acustica United Ac. **97**, pp. 138 - 147 (2011).

[7] A. T. Moorhouse and G. Seiffert, "Characterisation of an airborne sound source for use in a virtual acoustical prototype," J. Sound Vib. **296**, pp. 334 - 352 (2006).

[8] A. T. Moorhouse, "Simplified calculation of structure-borne sound from an active machine component on a supporting substructure," J. Sound Vib. **302**, pp. 67 - 87 (2007).

[9] A. T. Moorhouse, "In situ measurement of the blocked force of structure-borne sound sources," J. Sound Vib. **325**, pp. 679 - 685 (2009).

[10] G. Pavić, "Air-borne sound source characterization by patch impedance coupling approach," J. Sound Vib. **329**, pp. 4907 - 4921 (2010).

[11] T. S. Vogt, C. Y. Glandier, J. Morkholt, A. Omrani and M. A. Hamdi, "Engine Source Identification using an I-BEM technique," In Proc. of the Euronoise, pp. 1 - 6 (2003).

[12] M. Weber, T. Kletschkowski and B. Samtleben, "Identification of Noise Sources by Means of Inverse Finite Element Method," In Proc. of the COMSOL Conference (2008).

[13] N. Frenne and Ö Johansson., "Acoustic time histories from vibrating surfaces of a diesel engine," Appl. Acoust. **67**, pp. 230 - 248 (2006).

[14] A. D. Pierce, *Acoustics - An Introduction to Its Physical Principles and Applications*, (McGraw-Hill Book Company, 1981), pp. 11, 15, 27, 39 - 47, 100 - 103, 153 - 207, 159 - 171, 177 - 178, 178 - 180, 180 - 182, 198 - 199, 208 - 209, 208 - 211, 210 - 211 and 213 - 215.

[15] I. L. Vér and L. L. Beranek, *Noise and Vibration Control Engineering,* 2^{nd} *ed.*, (John Wiley & Sons, 2006), pp. 71 - 81.

[16] Y. I. Bobrovnitskii, K. I. Mal'Tsev, N. M. Ostapishin, S. N. Panov and J. S. Wood (Translator), "Acoustical model of a machine," Sov. Phys. Acoust. **37**, pp. 570-574 (1991).

[17] Y. I. Bobrovnitskii, "Models of acoustic sources: a survey," In Proc. of the International Congress on Noise Control Engineering (Internoise), pp. N/A (2001).

[18] A. Pereira, "Acoustic imaging in enclosed spaces," Ph.D. Thesis, INSA de Lyon (2013), pp. 9 - 20 and 24 - 28.

[19] A. Lindberg, G. Pavić, and Q. Leclère, "Characterisation of air-borne noise by a dummy source approach," In the Proc. of Noise and Vibration - Emerging Technologies (NOVEM) **5**, pp. N/A (2015).

[20] P. M. Morse and K. U. Ingard, *Theoretical Acoustics*, (McGraw-Hill Book Company, 1968), pp. 309 - 312 and 343 - 347.

[21] U. P. Svensson and K. Wendlandt, "The influence of a loudspeaker cabinet's shape on the radiated power," J. Vibroeng. **3**, pp. 189 - 192 (2000).

[22] F. Zotter, A. Sontacchi and R. Höldrich, "Modeling a Spherical Loudspeaker System as Multipole Source," in the Proc. of Fortschritte der Akustik, pp. 221 - 222 (2007).

[23] F. J. M. Frankort, "Vibration and sound radiation of loudspeaker cones," Ph.D. Thesis, Delft University of Technology (1975), pp. 1 - 15, 103 - 108 and 165 - 166.

[24] A. Lindberg and G. Pavić, "Computation of sound radiation by a driver in a cabinet using a substitute source approach," J. Acoust. Soc. Am. **138**, pp. 1132 - 1142 (2015).

[25] G. Pavić, "An engineering technique for the computation of sound radiation by vibrating bodies using substitute sources," Acta Acustica United Ac. **91**, pp. 1 - 16 (2005).

[26] G. Pavić, "A Technique for the Computation of Sound Radiation by Vibrating Bodies Using Multipole Substitute Sources," Acta Acustica United Ac. **92**, pp. 112 - 126 (2006).

[27] L. E. Kinsler and A. R. Frey, *Fundamentals of Acoustics,* 2^{nd} *ed.*, (John Wiley & Sons, 1962), pp. 153 - 185, 247 - 254, 248, 249, 250, 260.

[28] D. A. Russell, J. P. Titlow and Y.-J. Bemmen, "Acoustic monopoles, dipoles and quadrupoles: an experiment revisited," in Am. J. Phys. **67**, pp. 660 - 664 (1999).

[29] A. Lindberg and G. Pavić, "Measurement of volume velocity of a small sound source," Appl. Acoust. **91**, pp. 25 - 32 (2015).

[30] F. Fahy, "The Vibro-Acoustic Reciprocity Principle and Applications to Noise Control," Acustica **81**, pp. 544 - 558 (1995).

[31] F. Fahy, "Some Applications of the Reciprocity Principle in Experimental Vibroacoustics," Acoust. Phys. **49**, pp. 217 - 219 (2003).

[32] T. Wolde, "Reciprocity Measurements in Acoustical and Mechano-Acoustical Systems. Review of Theory and Applications," Acta Acoustica United Ac. **96**, pp. 1 - 13 (2010).

[33] D. G. Duffy, *Green's Functions with Applications,* 2^{nd} *ed.*, (CRC Press, 2015), pp. 66 - 70, 66 - 76, 397.

[34] M. C. Junger and D. Feit, *Sound, Structures and Their Interaction*, (The MIT Press, 1972), p. 8.

[35] T. Salava, "Sources of the constant volume velocity and their use for acoustic measurements," J. Audio Eng. Soc. **22**, pp. 146 - 153 (1974).

[36] T. Salava, "Acoustic load and transfer functions in rooms at low frequencies," J. Audio Eng. Soc. **36**, pp. 763 - 775 (1988).

[37] D. K. Anthony and S. J. Elliott, "A comparison of three methods of measuring the volume velocity of an acoustic source," J. Audio Eng. Soc. **39**, pp. 355 - 366 (1991).

[38] A. Lindberg and G. Pavić, "Experimental characterisation of a small compression driver," In Proc. of the Congrès Français d'Acoustique (CFA) **12**, pp. 1601 - 1607 (2014).

[39] A. Lindberg and G. Pavić, "Experimental characterisation of a small compression driver using an internal microphone," In Proc. of the International Conference on Noise and Vibration Engineering (ISMA) **26**, pp. 1111 - 1119 (2014).

[40] H. Suzuki and J. Tichy, "Sound radiation from convex and concave domes in an infinite baffle," J. Acoust. Soc. Am. **69**, pp. 41 - 49 (1981).

[41] P. A. Nelson and S. H. Yoon, "Estimation of acoustic source strength by inverse methods: Part I, Conditioning of the inverse problem," J. Sound Vib. **233**, pp. 639 - 664 (2000).

[42] A. Rivola and M. Troncossi, "Zebra tape identification for the instantaneous angular speed computation and angular resampling of motorbike valve train measurements," Mech. Syst. Signal Pr. **44**, pp. 5 - 13 (2014).

[43] L. Yu, J. Antoni and Q. Leclère, "Recovering phase relationships between non-synchronous microphone array measurements," In Proc. of the International Conference on Noise and Vibration Engineering (ISMA), pp. 1415 - 1430 (2014).

[44] W. A. Gardner, A. Napolitano and L. Paura, "Cyclostationarity: Half a century of research," Signal Process. **86**, pp. 639 - 697 (2006).

[45] J. Antoni, "Cyclostationarity by examples," Mech. Syst. Signal Pr. **4**, pp. 987 - 1036 (2009).

[46] Q. Leclère, L. Pruvost and E. Parizet, "Angular and temporal determinism of rotating machine signals: The diesel engine case," Mech. Syst. Signal Pr. **24**, pp. 2012 - 2020 (2010).

[47] W. Kropp and K. Larsson, "Force estimation in the time domain by applying an LMS algorithm," In the Proc. of Noise and Vibration - Emerging Technologies (NOVEM), pp. N/A (2005).

[48] P. C. Hansen and D. P. O'Leary, "The use of the L-curve in the regularization of discrete ill-posed problems, " J. Sci. Comput. **14**, pp. 1487 - 1503 (1993).

[49] R. D. Fierro, G. H. Golub, P. C. Hansen and D. P. O'Leary, "Regularization by truncated total least squares," J. Sci. Comput. **18**, pp. 1223 - 1241 (1997).

[50] S. Van Huffel and J. Vandewalle, *The Total Least Squares Problem - Computational Aspects and Analysis*, (SIAM, 1991).

[51] Y. Liu and W. S. Shephard Jr., "Dynamic force identification based on enhanced least squares and total least-squares schemes in the frequency domain," J. Sound Vib. **282**, pp. 37 - 60 (2005).

[52] W. Kropp and K. Larsson, "Force estimation in the time domain by applying an LMS algorithm," Unpublished document which contains force estimation examples with multiple excitation, pp. N/A (2005).

[53] C. L. Phillips, J. M. Parr and E. A. Riskin, *Signals, Systems and Transforms, 4^{th} ed.*, (Pearson Prentice Hall, 2008), pp. 213 - 214 and 492 - 500.

[54] C. R. Shalizi, *Advanced Data Analysis from an Elementary Point of View*, (Cambridge University Press, 2013).

[55] R. Boulanger and V. Lazzarini, *The Audio Programming Book*, (The MIT Press, 2011), pp. 529 - 531.

[56] L. Cremer, "Die Synthese des Schallfeldes eines beliebigen festen Körpers in Luft mit beliebiger Schnelleverteilung aus Kugelschallfeldern" (Synthesis of the sound field of an arbitrary rigid radiator in air with arbitrary particle velocity distribution by means of spherical sound fields), Acustica, **55**, pp. 44 - 46 (1984).

[57] G. H. Koopmann, L. Song and J. B. Fahnline, "A method for computing acoustic fields based on the principle of wave superposition," J. Acoust. Soc. Am. **86**, pp. 2433 - 2438 (1989).

[58] J. B. Fahnline and G. H. Koopmann, "A numerical solution for the general radiation problem based on the combined methods of superposition and singular-value decomposition," J. Acoust. Soc. Am. **90**, pp. 2808 - 2819 (1991).

[59] L. Song, G. H. Koopmann and J. B. Fahnline, "Numerical errors associated with the method of superposition for computing acoustic fields," J. Acoust. Soc. Am. **89**, pp. 2625 - 2633 (1991).

[60] W. Kropp and P. U. Svensson, "Application of the time domain formulation of the method of equivalent sources to radiation and scattering problems," Acta Acustica United Ac. **81**, pp. 528 - 543 (1995).

[61] M. Ochmann, "The source simulation technique for acoustic radiation problems," Acustica **81**, pp. 512 - 527 (1995).

[62] Y. J. R. Gounot and R. E. Musafir, "On appropriate equivalent monopole sets for rigid body scattering problems," J. Acoust. Soc. Am. **122**, pp. 3195 - 3205 (2007).

[63] Y. J. R. Gounot and R. E. Musafir, "Genetic algorithms: A global search tool to find optimal equivalent source sets," J. Sound Vib. **322**, pp. 282 - 298 (2009).

[64] Y. J. R. Gounot and R. E. Musafir, "Simulation of scattered fields: Some guidelines for the equivalent source method," J. Sound Vib. **330**, pp. 3698 - 3709 (2011).

[65] K. H. Baek and S. J. Elliott, "Natural algorithms for choosing source locations in active control systems," J. Sound Vib. **186**, pp. 245 - 267 (1995).

[66] J. Kennedy and R. Eberhart, "Particle Swarm Optimization," In Proc. of Neural Networks, pp. 1942 - 1948 (1995).

[67] C. S. Obiekezie, D. W. P. Thomas, A. Nothofer, S. Greedy, L. R. Arnaut and P. Sewell, "Complex Locations of Equivalent Dipoles for Improved Characterization of Radiated Emissions," IEEE Transactions on Electromagnetic Compatibility **56**, pp. 1087 - 1094 (2014).

[68] P. Courrieu, "Fast computation of Moore-Penrose inverse matrices," Neural Information Processing - Letters and Reviews **8**, pp. 25 - 29 (2005).

[69] M. Greenspan, "Piston radiator: some extensions of the theory," J. Acoust. Soc. Am. **65**, pp. 608 - 621 (1979).

[70] D. L. Dekker, R. L. Piziali and E. Dong, "Effect of boundary conditions on the ultrasonic beam characteristics of circular disks," J. Acoust. Soc. Am. **56**, pp. 87 - 93 (1974).

Part I

Application to a diesel engine

Appendix I

Experimental characterisation of a diesel engine using a dummy source approach

As a remark to the reader, the experimental work reported in this appendix had to be carried out head first — before numerical results on the proposed dummy source approach was available — since the engine laboratory of INSA de Lyon was scheduled to be moved (demolished). The analysis was partially developed afterwards, and in particular it was towards the end of the research project that the use of total least squares was investigated along side the least mean square algorithm. Notwithstanding the remark, the described implementation of the dummy source approach can serve as a reference for future work.

Abstract

Airborne sound from an internal combustion engine has been characterised using a prototype dummy source. A dummy source is a closed cabinet equipped with a driver array, and serves as an equivalent acoustical model which accounts for both sound radiation and sound diffraction of the original sound source. The prototype was designed as a closed box, made out of Plexiglass plates, and equipped with a flush-mounted microphone array spread across the surface of the box. The microphone array replaces the driver array in the experimental work since the physical assembly was only used to measure transfer impedances reciprocally inside of an engine test cell using a volume velocity source. The drivers' source strengths were deduced from inversion, and computed off-line from the measured transfer impedances and measured operating responses of the engine. The measurement of operating responses was done simultaneously using a microphone array spread around the engine. The identified source strengths characterise the engine, and the prototype can be used to predict both the sound pressure response in the time domain and the sound pressure level in the frequency domain. A comparison between measured and predicted sound pressure at independent measurement points shows the feasibility of the dummy source approach as an industrial characterisation procedure. Despite the simplicity of the experimental work, using merely 10 drivers on the dummy source prototype and 13 microphones in the test cell to estimate the source strengths, the discrepancy at 2 additional microphones is typically within a few dBs at one-third octave bands in the frequency range 100 Hz to 1000 Hz.

1 INTRODUCTION

Prediction of airborne sound from housing vibration of a steady-state industrial source such as a diesel engine is quite some challenge in noise and vibration engineering. Frenne and Johansson [1] compared simplified source models for time domain quantification of partial sources on a diesel engine, the engine represented as a combination of point sources distributed on its surface, for the needs of sound quality assessment. Vogt et al. [2] identified sound sources on the surface of a diesel engine mock-up by an inverse boundary element approach. This optimisation procedure allows for the construction of efficient synthesis models.

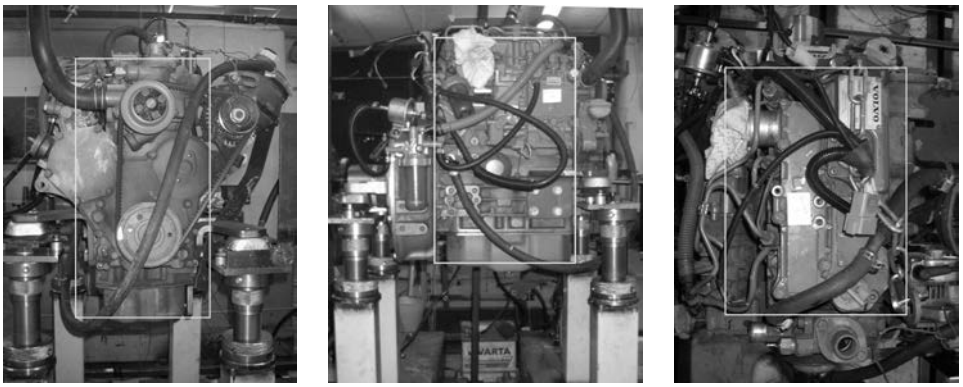

(a) (b) (c)

Figure 1: Comparison of position and size of the dummy source prototype, marked by a grey rectangle, relative to the diesel engine: (a) back view, (b) side view, and (c) top view.

Unlike [1, 2], the dummy source approach has been used to characterise airborne sound from a diesel engine in steady-state operation in a test cell. A *dummy source* is a closed cabinet equipped with a driver array. There are two essential simplifications in the approach: (1) the cabinet has a simpler shape than the original source but is of similar volume, and (2) the cabinet is equipped with a limited number of drivers. To simplify the experimental implementation it is further assumed that the drivers are small compared to the acoustic wavelength; i.e., the cabinet is equipped with a simple source array. It is also assumed that the cabinet is rigid since the engine housing has a hard surface. Consequently, the equivalent acoustical model is in the scope of this work a distribution of simple sources embedded in a rigid surface.

The *dummy source prototype* was designed in the following way: (1) The housing of the diesel engine was modelled as a closed box of similar volume. The box is a low/mid frequency approximation which neglects the presence of for example the fly wheel.; (2) The sound radiation of the diesel engine was modelled using small drivers. Two drivers per shortest acoustical wavelength of interest was prescribed across the surface of the box. The array was designed with a highest frequency of 1000 Hz since this was the frequency limit in which an available known volume velocity source ceased to be a simple source of sound. The driver array - cabinet assembly approximates sound diffraction and sound radiation of the diesel engine. The geometrical shape of the dummy source prototype and the diesel engine is compared in Fig. 1. The prototype, built out of Plexiglass plates and equipped with microphones for reciprocal measurement of transfer impedances is shown in Fig. 2.

The approach requires the double measurement of operating pressure response of the diesel engine and the transfer impedances in the test cell using the dummy source. The response measurement is carried out first, Fig. 3 (a). The dummy source is then introduced in the same test cell, apart from the diesel engine being replaced by the dummy, at the position of the diesel engine. Thereafter, the transfer impedance is measured using a known volume velocity source [4, 5], Fig. 3 (b). The two sets of measurements enables the estimation of the dummy's source strengths, which characterise the diesel engine in a given operation.

The dummy source approach will be discussed in sect. 2. The experimental implementation of the approach is illustrated in sect. 3, which is followed by experimental results in section 4. Finally, concluding remarks are given in sect. 5.

2 THE DUMMY SOURCE APPROACH

The diesel engine is installed in a test cell. The first step (out of three) of the dummy source approach is to measure the operating pressure response of the diesel engine using a microphone array. Thus a number of N microphones are distributed around the diesel engine at field points: $\mathbf{f}_1$, ..., $\mathbf{f}_N$. The microphones are positioned at a distance away from the diesel engine since the dummy source is primarily concerned with global features of the source such as its radiation pattern. All time histories $\mathbf{p}_1[i/R]$, ..., $\mathbf{p}_N[i/R]$ are recorded simultaneously with a sample rate $R \gg 2f_{\max}$ being a few times greater than twice the largest

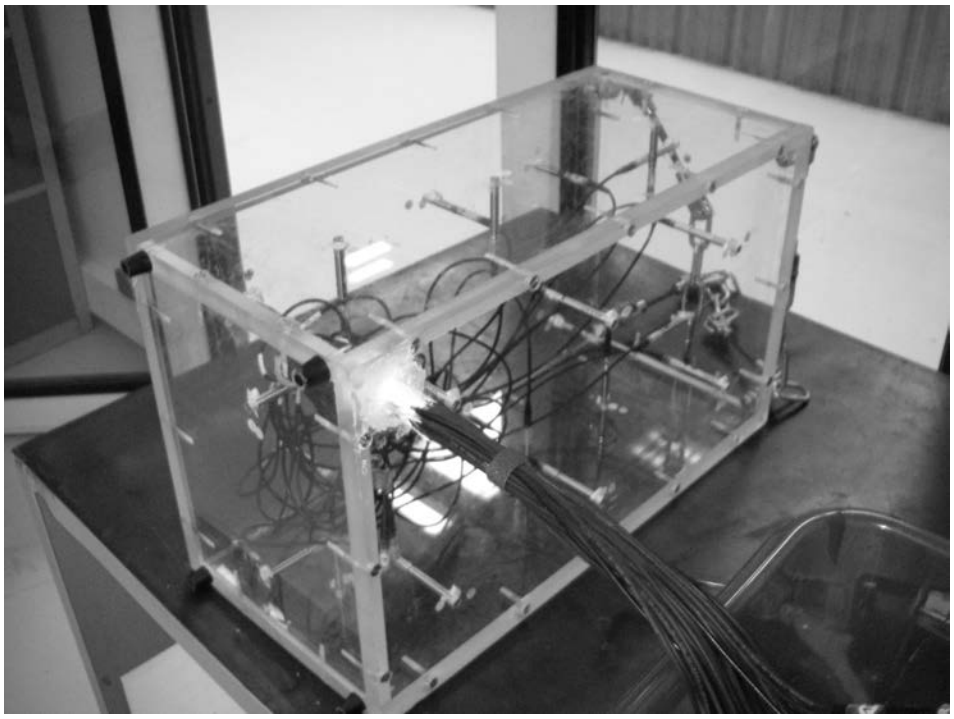

Figure 2: A dummy source prototype was implemented as a microphone array embedded in the surface of a closed Plexiglass box. The prototype was used to characterise a diesel engine.

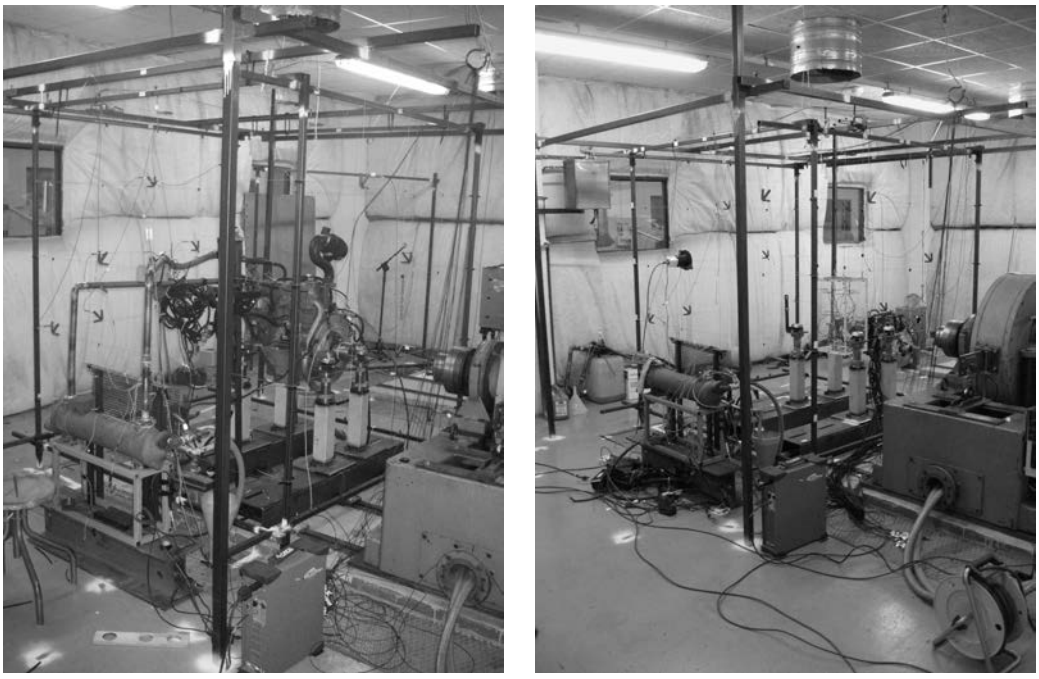

(a) (b)

Figure 3: The dummy source approach illustrated by (a) measurement of the engine's pressure response using an angular reference, and (b) reciprocal measurement of the dummy's transfer impedance using a known volume velocity source.

(a) (b)

Figure 4: Schematic dummy source with (a) a 10 drivers acoustical layout and (b) a 22 drivers acoustical layout.

frequency of interest $f_{\max}$. Although at a constant frequency the complex pressure response of the original source could be directly estimated from the time histories using the Fast Fourier Transform, $\mathbf{p} \xrightarrow{FFT} \hat{\mathbf{p}}$, a Fourier series representation will be used as discussed in sect. 2.1.

Following the measurement of operating responses $p(\mathbf{f}_n)$, the dummy source physically replaces the diesel engine inside of the test cell. The dummy source is placed at the position previously occupied by the diesel engine, and is aligned to the engine's volume. A number of M drivers are spread across the closed surface of the dummy source at source points: $\mathbf{s}_1$, ..., $\mathbf{s}_M$. Since each driver is small compared to the acoustical wavelength, it is characterised by the volume velocity $Q(\mathbf{s}_m)$ it produces and its position only. Consequently, the second step of the dummy source approach is to measure the transfer impedances between all possible driver and microphone combinations in the experiment, $Z(\mathbf{f}_n \mid \mathbf{s}_m)$. Thus the transfer impedance matrix $\mathbf{Z}$ relating each driver of the dummy source to the operating response of the diesel engine is measured. The measurement of transfer impedance requires apart from the installation of the dummy source access to a known volume velocity source.

A first remark on the dummy source is that depending on the acoustic wavelength, and the aspect ratios of the diesel engine, the shape of the dummy source can be a box. A box will be used to prototype a dummy source of a diesel engine at low / mid frequencies. A second remark is that the box can be fitted with different designs of the driver array, and example acoustical layouts are shown in Fig. 4. An array aiming at being regularly spaced with two drivers per shortest acoustical wavelength of interest has been used to implement the dummy source.

The third and final step of the dummy source approach is to estimate the source strengths $\hat{\mathbf{Q}}$ of the driver array. Given the two measurements, the source strengths at a constant frequency are related to the operating pressure through a set of equations

$$\mathbf{Z}\hat{\mathbf{Q}} \approx \hat{\mathbf{p}}. \tag{1}$$

Here, bold upper case denotes a matrix and bold lower case a column vector. The hat [ˆ] denotes peak amplitudes. The source strengths are then estimated using matrix inversion on a computer. The knowledge of the drivers' source strengths characterise the diesel engine in a given steady-state regime. All the quantities in Eq. 1 are complex functions of frequency.

A remark on the estimation of source strengths is that the test cell is assumed to be time invariant although the principle requires substitution of the diesel engine with the dummy source. The replacement does, however, not alter the overall acoustical features of the space if the dummy is representative enough of the diesel engine. A second remark is that the number of microphones is assumed to be greater than the number of drivers, $M \ll N$, so that the resulting equation system is overdetermined. The righteousness of the assumption depends on the actual measurements, but since an underdetermined set of equations, $M \gg N$, can be modified into an overdetermined set of equations — corresponding to a simpler design

of the dummy source with a fewer number of drivers — it is a reasonable starting point for experimental work. An overdetermined set of equations should be used when estimating the source strengths in order to mitigate erroneous contributions in the inversion coming from measurement errors.

Since the transfer impedance matrix $\mathbf{Z}$ is measured its entries are inevitably perturbed by random measurement errors, $\mathbf{Z} = \mathbf{Z}_0 + \mathbf{Z}_\epsilon$. Similarly, the sound pressure response vector $\hat{\mathbf{p}}$ is measured and thus its entries are also inevitably perturbed by random measurement errors, $\hat{\mathbf{p}} = \hat{\mathbf{p}}_0 + \hat{\mathbf{p}}_\epsilon$. Here, the subscript $[_0]$ denotes an underlying physical value and $[_\epsilon]$ random perturbations. The random perturbations are due to among other reasons: (1) modifications of the characterisation space between the response measurement and the subsequent transfer impedance measurement; or (2) presence of uncorrelated sound sources such as exhaust suction and leakage, ventilation, water pouring out of the cooling system, and door slamming; and (3) presence of correlated sound sources due to transmitted vibration to the concrete slab through the resilient mounts. It should here be noted that the characterisation space was an engine test cell with in total three rigs shared with other people which lead to small changes of the room over time. The global features remained, however, the same. This room was quite poorly isolated and door slamming was frequently recorded which led to measurements out-of-office hours to mitigate the problem. The ventilation was turned off during measurements. The vibration of the concrete slab could not be avoided but was mitigated by adjustment of the resilient mounts. The measurement errors are not easy to quantify but *motivates the use of an overdetermined system*. The errors imply that the equation system in Eq. 1 is *incompatible*, it has no solution. A remark is that the conclusion of an incompatible equation system is reasonable even in the case without measurement errors since the dummy source, with a limited number of drivers, should not be expected to be completely capable of reproducing the sound field of the original source, it is a *non zero residual problem*. This may seem like a small detail but will be of importance later on when selecting the so called regularisation parameter. *The measurement errors imply that the estimated complex source strengths which characterise the original source are more or less erroneous,* $\hat{\mathbf{Q}} = \hat{\mathbf{Q}}_0 + \hat{\mathbf{Q}}_\epsilon$*, and it is not beforehand clear how to reduce the contributions of* $\hat{\mathbf{Q}}_\epsilon$.

2.1 Step 1: Measurement of the operating responses

Sound from a diesel engine can be rather complex. One reason for this is random fluctuations in its operation [16]. This occurs because the mixture of diesel fuel and air inside of the engine's cylinders are not perfectly controlled. Apart from the internal mechanics of the diesel engine, which is here considered merely as a vibrating source of sound without consideration of the cause of its vibration, its operation also depends on the applied load which may in turn not be fully controllable. This inherent randomness of the diesel engine's sound is neglected, and it is argued that the dummy should aim at reproducing only the significant features of the sound: the *harmonics*.

For simplicity, a *waveform* representation of sound pressure fluctuations $p(t, \mathbf{f})$ will be sought. This periodic component is sometimes referred to as *the deterministic part* or first order cyclostationarity [16]. Cyclostationarity is a general framework for the time histories of rotating machines such as a diesel engine [17, 18]. Within this framework the time histories are decomposed into its deterministic and random parts. The deterministic part represents the expected value of the sound during one cycle, in the temporal or angular domain depending on how the time histories are treated, and will be referred to as the waveform from now on. Formally, a waveform is expressed by

$$p(\mathbf{f}, t) = \sum_{n=0}^{\infty} \Re\{\hat{p}_n(\mathbf{f}) \mathrm{e}^{j\omega_n t}\}, \qquad \omega_n = (2\pi/T_0)(n+1), \tag{2}$$

a *Fourier series* [19, p. 74 - 75]. Here, T_0 is the period and $\hat{p}_n$ denotes the complex amplitude of the n^{th} harmonic and the fundamental angular frequency is $\omega_0 = 2\pi/T_0$. The random part is neglected, but is in general defined as the residual between the original pressure fluctuations and the deterministic part. The identified waveforms in combination with the dummy's transfer impedances are used to estimate the dummy's source strengths.

A comparison between a measured time history of sound from a diesel engine and the reconstructed time history using a waveform representation is seen in Fig. 5. Apart from visual inspection, the reconstructed time history is compared against the measured time history in terms of its sound pressure level.

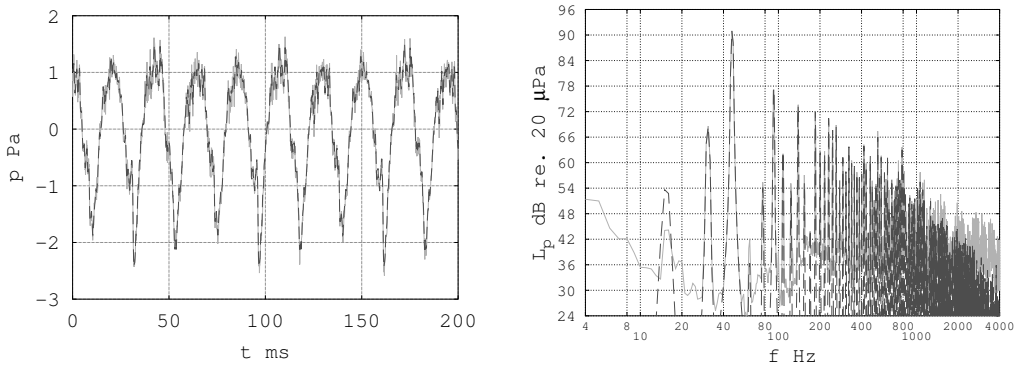

(a) (b)

Figure 5: Sound from a diesel engine (a) time history, and (b) sound pressure level. Legend: light gray continuous line, measured, dark gray dashed line, reconstructed using a waveform.

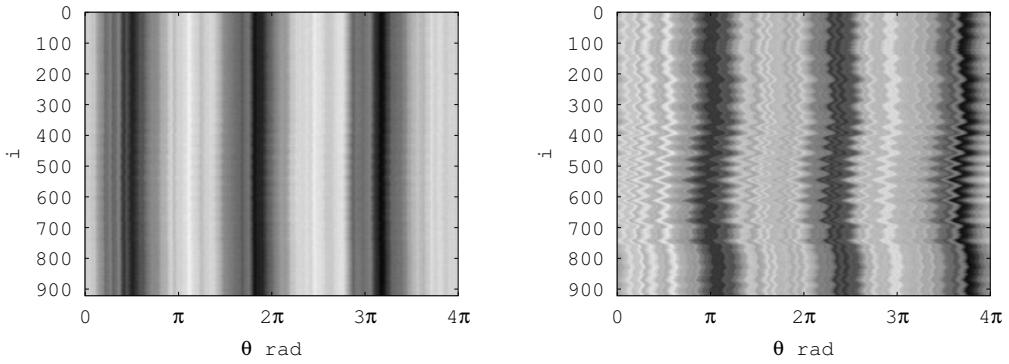

(a) (b)

Figure 6: Cyclic representation of diesel engine noise $p/\max(|p|)$ at one point in the angular domain with (a) successful syncronisation and (b) unsuccessful syncronisation. Colorscale: black, negative sign; white, positive sign.

The waveform representation is not perfect, when the frequency increases the level decreases as compared to the measured time history. The discrepancy in level is not an artefact of Eq. 2, but of the cyclic averaging used to estimate the waveform. The accuracy of the imperfect averaging suffice, however, for this application since the transfer impedances could only be estimated in a limited frequency band. An instrumented driver was used to measure transfer impedances, and the available driver was inefficient below 100 Hz and ceased to be omnidirectional above 1000 Hz [4].

The advantage of a waveform is an elegant representation of the sound pressure response $p(\mathbf{f},\ t)$ from a diesel engine which is suitable for sound synthesis [20, Ch. 4, 6]. The disadvantage is the cyclic averaging which is not straightforward since the cycle duration varies in time. The averaging requires the time history $p[\mathbf{f},\ i/R]$ where $i = 0, \ldots, N-1$ to be divided into M blocks, $p_1, \ldots, p_M$. Each block corresponds to a cycle of different time duration $N_1, \ldots, N_M$ because the operation of the diesel engine is not perfect. Consequently, it is not obvious how to perform the block averaging in time. Here, brackets $[\ldots]$ denotes discrete representation whereas parentheses $(\ldots)$ denotes continuous representation. The current sample is denoted by i, the number of samples by N, and the sample rate by R. This should not be confused with the truncation level i, the number of microphones N, and the number of substitute sources M.

The problem of varying duration of the cycles has been overcome by resampling the time history into the *angular domain*. The angular domain is a function of the instantaneous angular speed over time in respect to an angular reference on the rotating machine. Hence, the angle $\theta[i/R]$ is introduced in respect

to a pulse train with several pulses per revolution recorded with a tachometer. This has been achieved using zebra tape [21] installed on the diesel engine's crankshaft. The waveform is then extracted in the angular domain [16]. In angle $p(\mathbf{f},\ \theta)$ the response is periodic and for the case of a four-stroke diesel engine the wave repeats itself every 4π of the crankshaft's rotation, Fig. 6. The waveform is then identified by averaging the observed response over all cycles. This is then transformed into the frequency domain, Eq. 2. The procedure is repeated for each time history. The relative phase between the engine harmonics at various microphone positions around the diesel engine remains synchronised, since the angular waveforms are aligned to a "missing tooth". The missing tooth is an effect of the zebra tape which is not fully periodic with the rotation of the crankshaft since there is a gap at the tape's ends. The advantage of the angular domain is that all blocks are of equal duration. The disadvantage is that the optical tachometer and zebra tape assembly requires calibration.

Finally, the result is checked in time and frequency domains. Once the waveform has been identified in the angular frequency domain, and recognising that one cycle in the angular domain corresponds to one time-averaged cycle in the frequency domain, the corresponding time histories are obtained from Eq. 2 using the same sample rate and the same number of samples as the measured signal. An example of a reconstructed time history compared to a measured time history is shown in Fig. 5. An additional check of the decomposition into a Fourier series is done by Parseval's theorem [19, pp. 74 - 75]

$$(p^2(t))_{\text{av}} = \lim_{T\to\infty} \frac{1}{T} \int_{-T/2}^{T/2} p^2(t) \approx \frac{1}{N} \sum_{i}^{N} p^2[i/R], \tag{3}$$

$$(p_r^2(t))_{\text{av}} = \sum_{n=0}^{\infty} |\hat{p}_n|^2, \tag{4}$$

stating that the time-average intensity of the original time histories is equal to the sum of the individual intensity of the identified harmonics. The ratio of $(p_r^2(t))_{\text{av}}/(p^2(t))_{\text{av}}$ was found to be typically in the range of $92\% - 99\%$ if the synchronisation of the cycle blocks are aligned. At measurement points were the synchronisation was visually not satisfactory the ratio drops and is often below 75%. This has been used as an indication of outliers.

2.2 Step 2: Measurement of the transfer impedances

An ordinary electrodynamic driver has been used to implement a known volume velocity source. Since the driver's diaphragm has low mechanical impedance the volume velocity it produces depends strongly on the acoustic environment. To overcome this problem the driver's source strength is deduced using a signal from an internal microphone [4, 5]. The transfer impedance is split into two independent transfer functions: a source function and a space function. A driver's diaphragm is characterised by its source function. The volume velocity at the front of the driver's diaphragm, and thereby the source function, can be assessed in specific spaces where further substitution is possible. This can be achieved using a compression chamber or a blocked pipe [4, 5]. The advantage of these techniques are that no assumptions regarding the driver's diaphragm shape or velocity distribution are made. The identified source function is then applied in other spaces where the transfer impedance has to be measured.

2.2.1 Interpolation of the transfer impedances

The operating responses are represented by a Fourier series, but the harmonics f_n are not directly corresponding to the frequency resolution of the transfer impedances. Thus interpolation is necessary in order to estimate the source strengths. The interpolation requires finding both the nearest lower frequency f_l and nearest upper frequency f_u in the transfer impedances which bounds an harmonic at $f_l \le f_n \le f_u$. The transfer impedance matrix at f_n is then obtained by weighting

$$\mathbf{Z}(f_n) = w_1\mathbf{Z}(f_l) + w_u\mathbf{Z}(f_u), \quad w_l = 1 - \frac{f_n - f_l}{f_u - f_l}, \quad w_u = 1 - \frac{f_u - f_n}{f_u - f_l}. \tag{5}$$

2.3 Step 3: Estimation of the source strengths

Eq. 1 can be solved approximately in a least squares sense but some care should be taken. Ordinary least squares attributes the measurement errors to the pressure response vector [9, Ch. 1 - 2] which does not correspond to the actual situation which has to be dealt with. An attempt to overcome this contradiction between actual measurement errors and attributed measurement errors by a least squares approach is by use of total least squares [9, Ch. 1 - 2].

Total least squares has advantages and disadvantages. The advantage is that the technique accounts for measurement errors in the transfer impedance matrix which leads to a more realistic problem formulation when the dummy's transfer impedances are indeed measured. The measurement of transfer impedances is taken as a premise for implementations in industrial condition, since the development of a numerical model of sound propagation from a dummy source set in a space similar to the one shown in Fig. 3 requires some effort. Thus it is reasonable to begin deploying the dummy source approach using measured transfer impedances. On the other hand an appropriate numerical model results in better understanding of the sound field inside of the test cell.

Eq. 1 is an ill-posed problem [7, 10] for which small changes in the measured response $\hat{\mathbf{p}}_\epsilon$ can lead to large changes in the estimated source strengths $\hat{\mathbf{Q}}_\epsilon$. This problem has been overcome in literature by introducing additional constraints which leads to a less sensitive solution. The disadvantage of total least squares is that in its basic formulation it amplifies the smaller singular values and is therefore not suitable for ill-posed problems [10]: it is more sensitive to noise than ordinary least squares. Fierro et al. [10] overcame this problem by a modified approach called the truncated total least squares (*Truncated TLS*). This work was complemented by Sima and Van Huffel [11] who proposed two techniques for an optimal selection of truncation level. The truncated total least squares approach will be used to deduce the dummy's source strengths.

The use of truncated total least squares was not evident but arrived upon while struggling to estimate the source strengths in the frequency domain. The source strengths were initially estimated using the Moore - Penrose pseudoinverse which utterly failed to produce satisfactory results when used to predict the sound pressure level at independent points. The failure sparked a second attempt using Tikhonov regularised least squares (*Tikhonov LS*) combined with the L-curve and the largest curvature criterion [7]. Tikhonov LS will be discussed in App. A. Tikhonov LS has since been applied successfully on a vibrating box for experimental validation of the dummy source approach using computed transfer impedances [3]. When applied on a diesel engine the L-curve's were, however, often found to be concave. A concave L-curve implies either that the complex pressure response is pure noise, which is not the case when the inversion is carried out at engine harmonics, or that no regularisation is needed [7]. The conclusion is not reasonable since it implies an identical solution to the previously attempted pseudoinverse. It was hypothesised that the behaviour of the L-curve was due to that ordinary least square techniques does not account for measurement errors in the transfer impedances, which inspired the search for an alternative inversion technique. It should be noted that truncated total least squares has been previously applied in vibroacoustics. Liu and Shepard Jr. [12] applied the truncated total least squares to dynamic force identification in the frequency domain. They found that the Truncated TLS can produce better results than Truncated LS and Tikhonov LS when the frequency response functions are indeed measured.

Unfortunately, the Truncated TLS approach is — in my opinion — quite complicated. A final attempt was done using the least mean square algorithm (*LMS algorithm*) [13] in the time domain. The advantage of this approach is that: (1) no assumptions are made regarding the nature of the time histories, (2) there is no need of a frequency transform method, and (3) there is no need of matrix inversion. The disadvantage is that the optimisation procedure is time consuming. The LMS algorithm is discussed in App. B.

2.3.1 Total least squares

Van Huffel and Vandewalle [9, Ch. 2] define the total least squares approach as the minimisation of

$$\min_{\tilde{\mathbf{Z}},\,\tilde{\hat{\mathbf{p}}}} \left\| \begin{bmatrix} \mathbf{Z} & \hat{\mathbf{p}} \end{bmatrix} - \begin{bmatrix} \tilde{\mathbf{Z}} & \tilde{\hat{\mathbf{p}}} \end{bmatrix} \right\|_F \quad \text{subject to} \quad \tilde{\mathbf{Z}}\hat{\mathbf{Q}} = \tilde{\hat{\mathbf{p}}}, \tag{6}$$

and once a minimising solution $\begin{bmatrix}\tilde{\mathbf{Z}} & \tilde{\hat{\mathbf{p}}}\end{bmatrix}$ has been found the $\hat{\mathbf{Q}}$ satisfying $\tilde{\mathbf{Z}}\hat{\mathbf{Q}} = \tilde{\hat{\mathbf{p}}}$ is the total least squares solution. Here, the Frobenius norm is denoted by $\| \ \|_F$ and is defined as [9, Ch. 1]:

$$\|\mathbf{Z}\|_F = \sqrt{\sum_{n=1}^{N}\sum_{m=1}^{M}|Z_{nm}|^2}, \tag{7}$$

which is used as a measure of the difference between the original matrix and the approximating matrix denoted by tilde [˜]. Eq. 6 attempts to keep the overall properties of the acoustical system and its response while neglecting small differences. The latter is, hypothetically, originating from measurement errors. The total least squares problem can alternatively be formulated as [9, Ch. 2]:

$$\begin{bmatrix}\mathbf{Z} & \hat{\mathbf{p}}\end{bmatrix}\begin{bmatrix}\hat{\mathbf{Q}} \\ -1\end{bmatrix} \approx \mathbf{0}. \tag{8}$$

2.3.2 Truncated total least squares

Since Eq. 1 is an ill-posed problem the total least squares approach is not applicable. Fierro et al. [10] proposed truncated total least squares in which the smaller singular values are fully discarded as a regularisation procedure for the treatment of ill-posed problems. This approach will be used, and is here briefly explained. The first step is the use of singular value decomposition [9, Ch. 2]:

$$\begin{bmatrix}\mathbf{Z} & \hat{\mathbf{p}}\end{bmatrix} = \mathbf{U}\mathbf{\Sigma}\mathbf{V}^* = \sum_{m=1}^{M+1}\mathbf{u}_m\sigma_m\mathbf{v}_m^*. \tag{9}$$

Here, $\mathbf{U}$ and $\mathbf{V}$ are unitary matrices and $\mathbf{\Sigma}$ a diagonal matrix whose entries are the singular values $\sigma_1 > \ldots > \sigma_{M+1}$. The $\mathbf{u}$ and $\mathbf{v}$ are corresponding column vectors. The second step is to split the matrix $\mathbf{V}$ $[M+1, M+1]$ into four parts for a given truncation level i such that

$$\mathbf{V} = \begin{array}{c} \\ M \\ 1 \end{array}\begin{array}{c} \begin{array}{cc} i & M-i+1 \end{array} \\ \begin{bmatrix}\mathbf{V}_{11} & \mathbf{V}_{12} \\ \mathbf{V}_{21} & \mathbf{V}_{22}\end{bmatrix} \end{array}. \tag{10}$$

The truncation level is, in practice, chosen to be lower than the number of drivers. Fierro et al. [10] have shown that the source strengths are estimated by:

$$\hat{\mathbf{Q}}_i = -\mathbf{V}_{12}\mathbf{V}_{22}^{+} = -\mathbf{V}_{12}\mathbf{V}_{22}^{*}\|\mathbf{V}_{22}\|_2^{-2}. \tag{11}$$

If the norm $\|V_{22}\|_2$ is near zero, the use of truncated total least squares is not applicable [10]. In this case, in [10], it has been suggested that the norm can be constrained not to be lower than a prescribed threshold value.

Fierro et al. [10] has shown that Eq. 11 is a regularised solution of Eq. 1. A regularised solution should account for the larger singular values of $\mathbf{Z}$ while oppressing the smaller ones. The smaller singular values corresponds to an increasing number of sign changes in the solution [11]. These oscillations are sensitive to noise and can be arbitrarily amplified in the solution and should therefore be filtered out. Eq. 11 can be expressed as [10, 14]:

$$\hat{\mathbf{Q}}_i = \sum_{m=1}^{M} f_m \frac{\mathbf{u}_m'^{*}\hat{\mathbf{p}}}{\sigma_m'}\mathbf{v}_m'^{*}, \tag{12}$$

where the prime refers to the singular value decomposition of $\mathbf{Z}$ and the filter factors f_m are given by

$$f_m = \sum_{h=i+1}^{M+1}\frac{v_{M+1,h}^2}{\|\mathbf{V}_{22}\|_2^2}\frac{\sigma_m'^2}{\sigma_m'^2-\sigma_h^2}. \tag{13}$$

In [10, 14] it is shown that the first i filter factors form a monotonically increasing series starting from one, that is the first few singular values are actually amplified by the solution, whereas the last $M-i$ filter factors gradually goes to zero as the distance to σ_i increases. This implies that Eq. 11 is a regularised solution of Eq.

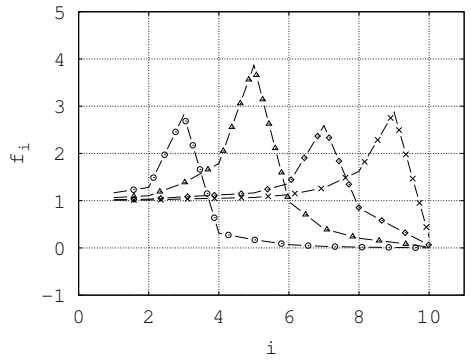

Figure 7: Sample filter factors for truncated total least squares for different choice of truncation level at 3, ∘-marker, 5, △-marker, 7, ◊-marker, and 9, ×-marker, singular values.

6. This behaviour is different from truncated least squares for which the filter factors are either one or zero and is illustrated in Fig. 7. This can be compared with Fig. 4 in [11, p. 1113] which gives yet another example of the amplification effect. It should perhaps be mentioned that in [14] there is an alternative technique for the regularisation of total least squares based on Tikhonov regularisation. This could be an idea for future work on the estimation of source strengths using measured transfer impedances.

2.3.3 Scaling

Before total least squares or truncated total least squares is applied it is recommended to scale the matrix $\begin{bmatrix}\mathbf{Z} & \hat{\mathbf{p}}\end{bmatrix}$ such that the signal-to-noise ratio is roughly equal in each entry [9, Ch. 3]. This is difficult to achieve in practice as the measurement errors are unknown. In [12] the truncated total least squares approach was applied with success without scaling for force identification. Nevertheless the response column vector has a different physical unit and can therefore be of a different order of magnitude than the transfer impedance column vectors. This suggest that the absolute measurement errors are rather different in the response vector.

To overcome this problem, the matrix is scaled such that each column is of unit norm. The applied scaling of Eq. 1 exemplified on a two drivers dummy with three microphone measurements takes the form [9, pp. 90 - 92]:

$$\left[\begin{bmatrix} Z_{11} & Z_{12} & \hat{p}_1 \\ Z_{21} & Z_{22} & \hat{p}_2 \\ Z_{31} & Z_{32} & \hat{p}_3 \end{bmatrix}\begin{bmatrix} \alpha_1 & 0 & 0 \\ 0 & \alpha_2 & 0 \\ 0 & 0 & \alpha_3 \end{bmatrix}\right]\left[\begin{bmatrix} 1/\alpha_1 & 0 & 0 \\ 0 & 1/\alpha_2 & 0 \\ 0 & 0 & 1/\alpha_3 \end{bmatrix}\begin{bmatrix} \hat{Q}_1 \\ \hat{Q}_2 \\ -1 \end{bmatrix}\right] = \begin{bmatrix} 0 \\ 0 \\ 0 \end{bmatrix} \tag{14}$$

which has been scaled such that

$$\alpha_1 = \frac{1}{\sqrt{Z_{11}^2 + Z_{21}^2 + Z_{31}^2}}, \ \ldots, \ \alpha_3 = \frac{1}{\sqrt{\hat{p}_1^2 + \hat{p}_2^2 + \hat{p}_3^2}}. \tag{15}$$

Once the total least squares solution to the scaled equation system is known, the dummy's source strengths can be back scaled.

2.3.4 Choice of truncation level

To apply Eq. 11 in practice, the truncation level has to be chosen. Sima et al. [11] proposed two approaches to select the truncation level: generalised cross validation and generalised information criterion. The disadvantage of the proposed cost functions are that they depend on knowledge of the filter factors derived by Fierro et al. [10], Eq. 13. The formulation involves singular value decomposition of both $\mathbf{Z}$ and $\begin{bmatrix}\mathbf{Z} & \hat{\mathbf{p}}\end{bmatrix}$ and is quite complicated. Furthermore, the generalised information criterion and the generalised cross validation has been found to select only the very first few singular values when applied on the data from

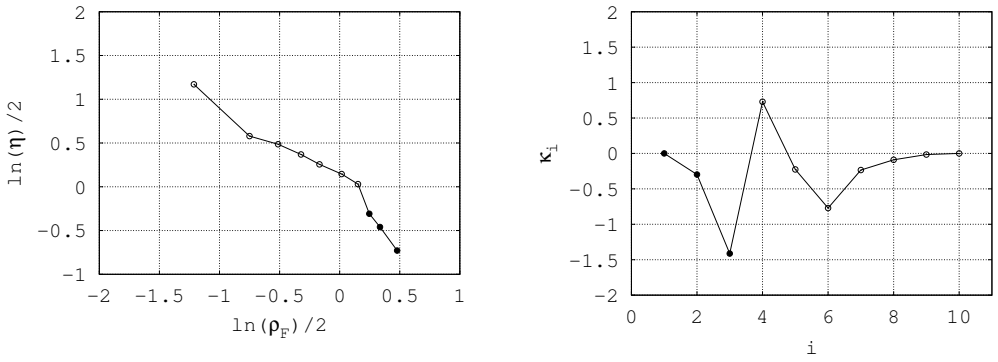

(a) (b)

Figure 8: The truncation level's influence (a) the L-curve in logarithmic scale and (b) its curvature in linear scale. (Included singular values marked by filled circles.)

the two performed experiments with a diesel engine. This results in severe underestimation of the sound pressure level and is therefore not an appropriate choice. Moorhouse [15] observed a similar behaviour with the truncated singular value decomposition and proposed that the drop in pressure level should be corrected for. Here, it is argued that more singular values should be accounted for instead.

Hansen [7] introduced the L-curve and the largest curvature criterion for use in Tikhonov regularised least squares. The L-curve is a logarithmic plot of the residual Euclidean norm versus the solution Euclidean norm for various choices of filtering parameter. Euclidean norms will hereafter be denoted by $\| \ \|_2$ or simply by $\| \ \|$ if there is no ambiguity. Fierro et al. [10] suggested that a similar treatment is possible for the selection of truncation level in truncated total least squares. Fierro et al. [10] defined the residual norm and the solution norm as:

$$\rho_F \equiv \left\| \begin{bmatrix} \mathbf{Z} & \hat{\mathbf{p}} \end{bmatrix} - \begin{bmatrix} \tilde{\mathbf{Z}} & \tilde{\hat{\mathbf{p}}} \end{bmatrix} \right\|_F^2, \tag{16a}$$

$$\eta \equiv \|\hat{\mathbf{Q}}_i\|_2^2, \tag{16b}$$

Thus the L-curve is given by $(\ln(\rho_F)/2, \ln(\eta)/2)$ and corresponds to the minimisation problem in Eq. 6. This definition is sensitive to the scaling, and the truncation level is selected before the source strengths are scaled back. As the truncation level is increased, starting from the first singular value, the residual norm will ideally decrease up to a point were there will be amplification of the solution norm. Thereafter the solution norm will dominate the curve's shape. This will create a trade-off were the solution norm is small and the residual norm is small which can be found by minimising the curve's curvature. Minimising because an increase of truncation level, the filtering parameter, corresponds to accounting for more singular values in the solution. This is the opposite case to Tikhonov regularised least squares were an increase of the regularisation parameter filters out more singular values. The curvature κ is estimated in regards of the truncation level i. The smallest curvature criterion is given by

$$i_\kappa = \arg\min_i \kappa[i], \qquad \kappa[i] = \frac{\rho_i' \eta_{ii}'' - \rho_{ii}'' \eta_i'}{((\rho_i')^2 + (\eta_i')^2)^{3/2}}. \tag{17}$$

Here, prime $[']$ and bis $['']$ corresponds to the first and second order derivative with regards to the truncation level i. This stopping criterion has often been found to occur after the point in which the spatial averaged sound pressure level is correct, but before the part in which the solution norm is increased. An example of the L-curve, Eq. 16, and the stopping criterion, Eq. 17, is shown in Fig. 8. Another advantage is that this is easy to compute since it does not require the double use of the singular value decomposition.

3 EXPERIMENTAL IMPLEMENTATION

The dummy source approach requires the measurement of both the operating responses and the transfer impedances. To facilitate the experimental work an array which can be used for both purposes was developed. An issue with the array was that mixed microphones were used to measure operating responses, so the microphone array had to be calibrated. Another issue with the measurement of operating responses was the installation of an angular reference since the diesel engine is moving in regards to the test cell. The solution was to attach the tachometer to the same frame of reference as the crankshaft of the diesel engine.

3.1 The dual purpose array

The estimation of source strengths requires that the sound pressure responses have been measured simultaneously across a fictitious surface which enclose the diesel engine. Neither the shape of the microphone array, nor the number of microphones is of importance to the dummy source approach — provided that the number of microphones is greater than the number of drivers. The design of the microphone array is in practice constrained by the test cell and peripheral equipment close to the diesel engine. As an example of such peripheral equipment the diesel engine should normally be connected to an engine brake, and requires an exhaust system, and a water cooling system. The additional equipment restricts the available space around the diesel engine and constrains therefore the design of the microphone array. In the test cell of INSA de Lyon, the geometry was such that it was suitable to construct a box like fictitious surface.

Needless to say, the microphones' positions across the fictitious surface should be marked out for the measurement of operating responses. The marked positions has to be recovered easily and accurately for the subsequent measurement of transfer impedances. The microphones' positions were locked in the test cell by the use of a "cage" in the shape of an open box: a rectangular tube structure equipped with a wire mesh on each outer face except along the concrete slab. The microphones were positioned at the crossings of the wires using plastic fixtures. Since a reciprocal approach was used to measure transfer impedances, a microphone array representing the driver array was mounted in the surface of the dummy source prototype. The transfer impedances were measured with a known volume velocity source mounted, one position at a time, at the microphones' positions on the cage previously used to measure operating responses using an additional plastic fixture. The fixtures allowed the geometrical center of the microphones and the volume velocity source to coincide. *Since the cage is used both to measure the operating responses of the diesel engine and the transfer impedances of the test cell it has been named a dual purpose array.* The fixtures and their usage are shown in Fig 9.

The position of the cage relative to the test cell was marked out by white spray on the floor, Fig. 3. After the sound pressure responses had been measured the cage was partially dismantled, which allowed for the diesel engine to be removed and the dummy source prototype to be installed at the position of the diesel engine, Fig. 1. Once the dummy source prototype was in place the cage was rebuilt and repositioned at the same place.

3.2 Microphone calibration

The implemented dual purpose array suffered from a specific issue: at the moment of measurements the laboratory had one planar array with many microphones of the same kind but without additional cables. In addition there was also a set of freely available microphones of various kinds with cables. Therefore a mixed microphone array with 16 microphones, using all of the freely available microphones in the laboratory, was used to record the response of the diesel engine. At the same time a second set of cables were ordered to construct the dummy source using the microphones in the planar array. A dummy source with 22 drivers was conceived which makes it more practical to measure all of the transfer impedances corresponding to one microphone position at the fictitious surface at once. Also, it is easier to move the driver around on the fictitious surface than to change its position on the dummy. The experimental procedure resulted in a need of calibrating the mixed microphone array against a microphone of the same kind as used to measure the dummy's transfer impedances. This is so because the sensitivity of the microphones can vary which introduce random errors in the measured sound pressure.

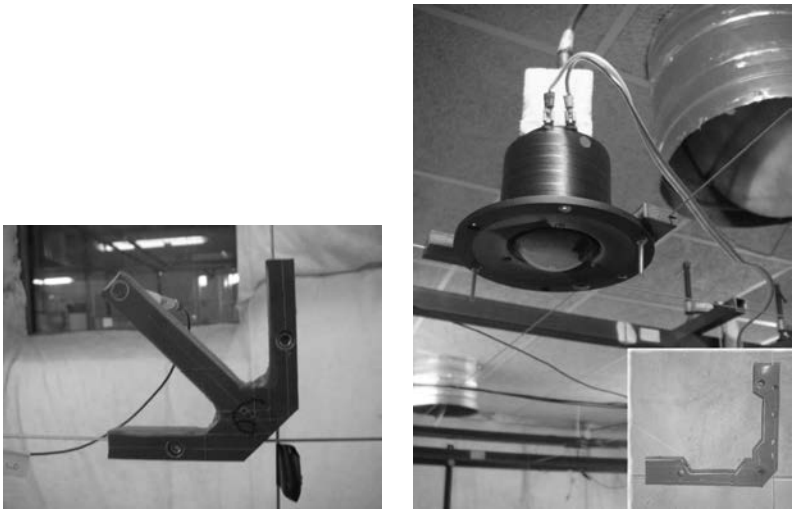

(a) (b)

Figure 9: Plastic fixtures used to install either microphones or a driver onto a wire grid across a fictitious surface. The fixtures facilitate the measurement of (a) the operating responses of the diesel engine and (b) the transfer impedances of the test cell (plastic fixture is shown in the lower right corner).

Figure 10: A driver connected to a small cavity was used to calibrate the measurement microphones against a reference microphone.

The mixed microphones were calibrated using a small compression chamber. This chamber was made out of an air cylinder enclosed by an aluminium fixture but open at one end. The open end was sealed by a loudspeaker driver excited by bandpass limited white noise. The closed end was fitted with two holes adjusted to precisely fit the microphones. Inside of the closed cavity there was one reference microphone, of the same kind as used to measure the dummy's transfer impedances, and one measurement microphone to be calibrated, Fig. 10. Both microphones were flush-mounted. Because the cavity is small such that the acoustic wavelength is much larger than the dimensions of the cavity the pressure inside of the cavity is expected to be uniform. Therefore the two microphones should measure the same response. The calibration consists therefore of measuring a transfer function between the two microphones. The frequency response of the measurement microphone is then corrected by multiplication in the frequency domain with this transfer function.

Figure 11: The diesel engine's speed was monitored from the crankshaft rotation using zebra tape and an optical encoder.

3.3 The diesel engine

The four-strokes Yanmar 3TNV76-WVE diesel engine, used in this case study, has 3 cylinders. Since a four-stroke engine is characterised, each respective cylinder ignites every second revolution of the crankshaft. The waveform of a recorded time history is therefore expected to be periodic in angle for a 4π rotation of the crankshaft. (The camshaft makes one revolution at the time as the crankshaft makes two revolutions.) The crankshaft is an accessible rotating part of the diesel engine, outside of the housing of the engine, and therefore suitable for the installation of a tachometer. An optical tachometer (Oros TAC-001) was used, which requires the use of "zebra tape" to create a pulse train relating the time to the angular position of the shaft. Each and every other stripe of the zebra tape alternates between glossy white and glossy black.

Thus a piece of "zebra tape" was put around the crankshaft, Fig. 11. The piece of the zebra tape was aligned as perpendicular to the crankshaft's direction as possible, and the length was adjusted to the crankshaft's circumference but slightly shorter. The gap creates "a missing tooth" effect which serves as an absolute angular reference.

Since the operational diesel engine is moving in comparison to the engine test cell, the optical encoder has to be mounted on the engine's housing to be in the same frame of reference as the rotating crankshaft. Moreover to measure the optical sensor has to be mounted close to the zebra tape (a few millimetres), and perpendicular to both the crankshaft and the zebra tape. The installation of the optical tachometer was achieved using a steel fixture, Fig. 11.

4 EXPERIMENTAL RESULTS

The experiment was conducted with a Yanmar 3TNV76-WVE engine in steady-state operation inside of a test cell. The experimental work was aided by a custom made "cage array" of dimensions $1725 \times 1650 \times 1970$ mm enclosing the diesel engine. The cage structure was made out of 25×25 mm hollow steel tubes. A steel wire was used to create a grid at the outer surface of the cage. The wire was laid out in a stringing pattern to achieve a regular grid of 400 mm spacing, suspended through holes in the tubes drilled with a distance of 100 mm. The grid served as a fictitious surface for both measuring the engine's response and measuring the dummy's transfer impedances. In the wire crossings custom made plastic fixtures were used to suspend either measurement microphones or a known volume velocity source, Fig. 9.

A preliminary measurement showed that the diesel engine's vibration, measured with accelerometers glued to the housing, change dramatically during the first 30 mins of operation. The change in vibration implies that steady-state operation has not yet been reached, which is likely due to the temperature

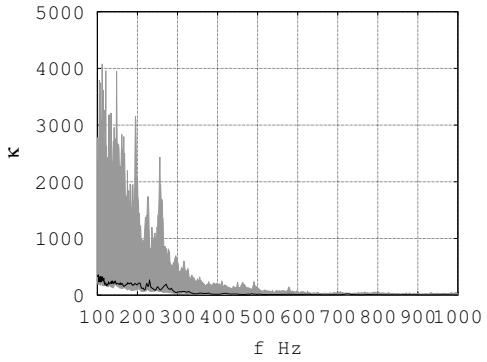

Figure 12: Region of condition number, gray color, for a random selection of 10 drivers and 13 microphones for 1000 different experimental setups. The selected setup for estimating source strengths with the smallest largest condition number as function of frequency is marked by a black line.

dependence of the engine's materials. The engine was therefore warmed up during 45 mins prior to the measurement of the operating responses using a microphone array. The responses were recorded at three different engine speeds: idle, in between, and full throttle. It should be stated that the engine was unloaded because a shaft connecting the diesel engine to a brake went to mechanical failure in the preliminary measurements. The choice of regime does not influence the assessment of the dummy source approach.

The operating responses were measured simultaneously in 15+1 field points using the setup in Fig. 3 (a). The microphones were distributed with 3 microphones at each face of the cage. The last microphone was positioned further away from the source and was initially thought of as an additional measurement point to validate the approach. Unfortunately, the added microphone could not be taken into account in the analysis. The sound pressure response, at the added point, was not enough synchronised with the angular reference provided by the tachometer. The added point was therefore treated as an outlier, and neither used for the estimation of source strengths nor for the validation of the approach. The remaining 15 points were randomly split into a group of 13 control points and 2 error points. The control points are used to estimate the source strengths, whereas the error points are used to validate the approach.

The transfer impedances where then measured reciprocally using an implemented dummy source prototype and a known volume velocity source, Fig. 3 (b). The dummy source prototype, a box of dimensions $300 \times 232 \times 500$ mm, was equipped with 22 microphones (i.e. drivers), Fig. 4 (b). The box was made out of six 12 mm thick Plexiglass plates. Since it was decided to use a reciprocal approach to measure transfer impedances, the plates were penetrated at the 22 drivers geometrical centers using a $\varnothing 1/4$ inch drill. The diameter was precisely adjusted to the flush-mounted microphones and silicone rubber was applied, in the interior of the box, to block the position of the microphones.

Out of the 22 prescribed drivers on the surface of the box, a simplified dummy source with 10 drivers was identified by a Monte Carlo approach minimising the largest condition number

$$\underset{\{\mathbf{s}_1,\ldots,\mathbf{s}_M\}_i,\{\mathbf{f}_1,\ldots,\mathbf{f}_N\}_i}{\arg\min} \|\kappa_i(\omega)\|_\infty, \tag{18}$$

where the norm $\| \ \|_\infty$ refers to the largest absolute value of its argument, Fig. 12. Here i refers to the random shuffling of microphones and drivers. This was done by in each iteration shuffling both the 13 control points out of 15 field points and the 10 source points out of 22 candidate source points used. The condition number was then computed at each frequency of interest. The process was repeated 1000 times and the combination which produced the smallest largest condition number was selected.

All results are concerned with the prediction of sound pressure response and sound pressure level at the error points. The geometry of the experiment, control points and source points, remains identical in all of the examples. The error points is an independent group of simultaneous measurements which are not used to estimate the dummy's source strengths. It has been found that the dummy reconstructs the measured response and level well at the control points, the microphone positions which have been used

to estimate the source strengths, but this is not an indication of how well the dummy source prototype predicts.

The results will be given for Moore - Penrose pseudinverse, Tikhonov LS [7], Truncated TLS [10] and the LMS algorithm [13]. The LMS algorithm has been applied directly on the original time histories, without making any assumption about the recordings such as a waveform representation, apart from band-pass filtering and downsampling to fit the frequency bandwidth of the measured transfer impedances. The transfer impedances have been back-transformed to impulse responses using the inverse Fast Fourier Transform.

4.1 The performance of the dummy source prototype

It is not straightforward to compare the different source strength estimation techniques. The frequency domain techniques have been computed using the engine harmonics only, whereas the time domain method produce results at all frequencies. To compare the estimation methods the measured time histories and the predicted time histories — either back transformed from predicted waveform amplitudes in the frequency domain or obtained directly from convolution with the source strengths in the time domain — were first faded-in and faded-out. The fading was done to mitigate end effects appearing with the LMS algorithm, but is also useful for comparing each predicted time history against the corresponding measured time history by listening. The fading was done using a Tukey window, which creates a smooth change when listening to the different time histories. The windowed time histories are of length 2.7 s using a sample rate of 2000 Hz.

The measured time histories have been bandpass filtered to match with the bandwidth of the measured transfer impedances and the corresponding impulse responses. The filtering has been motivated on the control points for deducing the source strengths with the LMS algorithm. Nonetheless the harmonic content used for the frequency domain methods are extracted from the band-pass filtered time histories at the control points. Therefore all of the source strength estimation techniques should be expected to produce nearly the same result close to the engine harmonics.

4.1.1 Sound pressure response

A comparison between measured and predicted time histories using a jury is out of scope for the purpose of an initial assessment of the dummy source approach, but a rudimentary comparison was done (by the author) out of curiosity. First, the time histories were normalised to an equal mean square value. (The normalisation was needed to avoid clipping effects.) Second, for each respective source strength estimation technique a pairwise listening comparison has been done. The result is, however, subjective and the following is solely based on my opinion.

A pairwise comparison has been done by listening in a specific sequence: recorded, Moore - Penrose pseudoinverse; recorded, Tikhonov LS; recorded, Truncated TLS; recorded, LMS. The listening sequence was designed for simplicity, and the listening sequence was used for each each engine speed and at each error point.

Unfortunately, in my opinion none of the predicted time histories sounds fully like the corresponding measured time history. The frequency domain methods sound artificial since the engine is not exactly running at a constant speed. The coloration of the sound was audible different, but at least the change of engine speed or error point can be noticed. (The predicted sound is clearly that of an engine though.)

In my opinion, the time history predicted using the LMS algorithm is the one which sometimes audible matches the measured time history at the error points. The audible results at the control points were, however, using the LMS method sounding rather similar to the measured. (The matching at control points should be expected.) Interestingly enough, the result depends strongly on the random shuffling of the drivers and it was observed that on one "lucky shuffle" the audible results matched even at the error points. (The tendency in matching is equally true for the frequency domain methods if they are compared to the engine harmonics only; i.e., against the estimated deterministic part of the sound.)

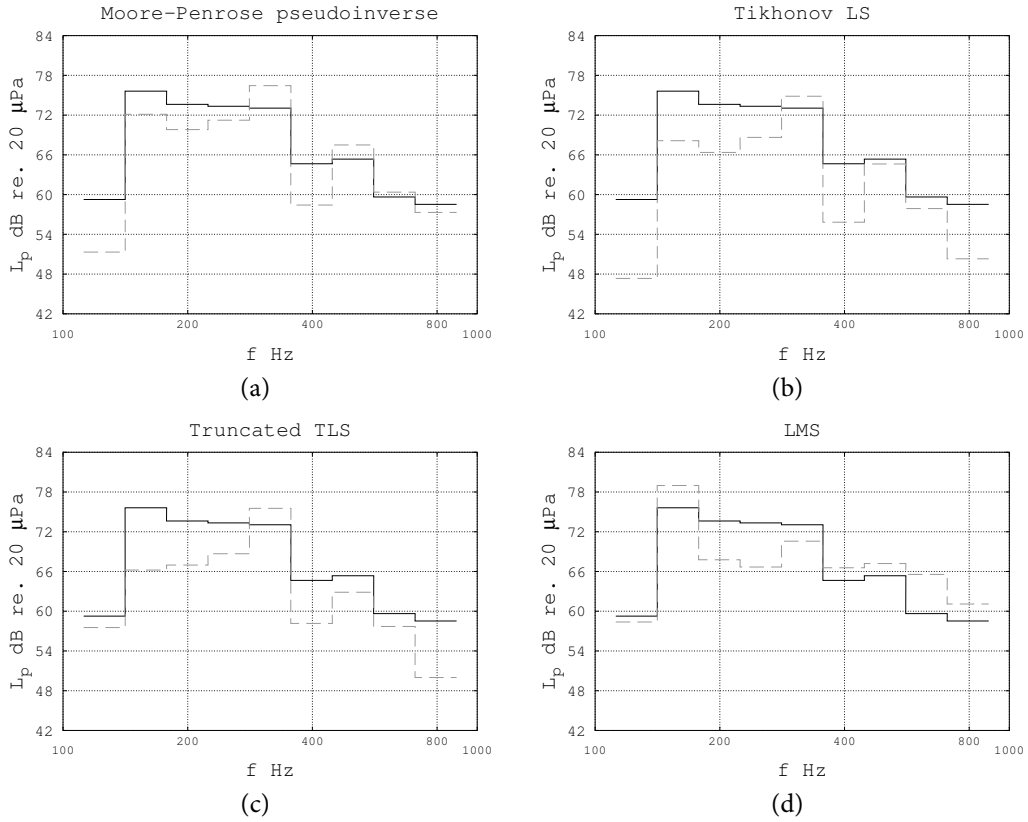

Figure 13: Sound pressure level in one-third octave band of the band-pass filtered measured time history, black continuous, and corresponding predicted time history, gray dashed, at one error point at 2160 RPM for four different source strength estimation techniques: (a) Moore-Penrose pseudoinverse, (b) Tikhonov LS, (c) Truncated TLS and (d) LMS.

4.1.2 Sound pressure level

A frequency domain comparison at the error points has been done by assuming the predicted and recorded time histories to be stationary random processes and thereafter computing a corresponding set of autospectra at each error point and for each engine speed. The level difference in autospectra between the predicted time history and the recorded time history in one-third octave band is seen at one error point for each engine speed in Fig. 13, 14 and 15. Concerning narrow-band results, which are not shown, the level difference is in the case of the frequency domain techniques large in-between the engine harmonics as expected and this should be ignored. (The difference should be large as no frequency content exist in the predicted time histories in-between the engine harmonics.) The surprising outcome, considering the two error points, is that Moore-Penrose, Tikhonov LS and Truncated TLS are performing more or less equally well. This is due to the preconditioning of the problem.

Initial computations, which were done without preconditioning manually selecting the 10 drivers and the 13 microphones, showed that the result using the Moore-Penrose is very sensitive to the condition number and can produce large errors at the error points at low frequencies: up to 50 dB at a harmonic. This does not happen at control points as expected. The Tikhonov LS using the L-curve technique to choose the regularisation parameter has been found to often be concave in this experiment: this means that it falls back on the Moore-Penrose pseudoinverse as no regularisation is the optimal choice. It was initially found that the Truncated TLS produced the better matching at the error points at the engine harmonics. Especially so when averaging over the two error points.

Using preconditioning, the typical narrow-band errors seems to be ±6 dB to ±12 dB at a given engine

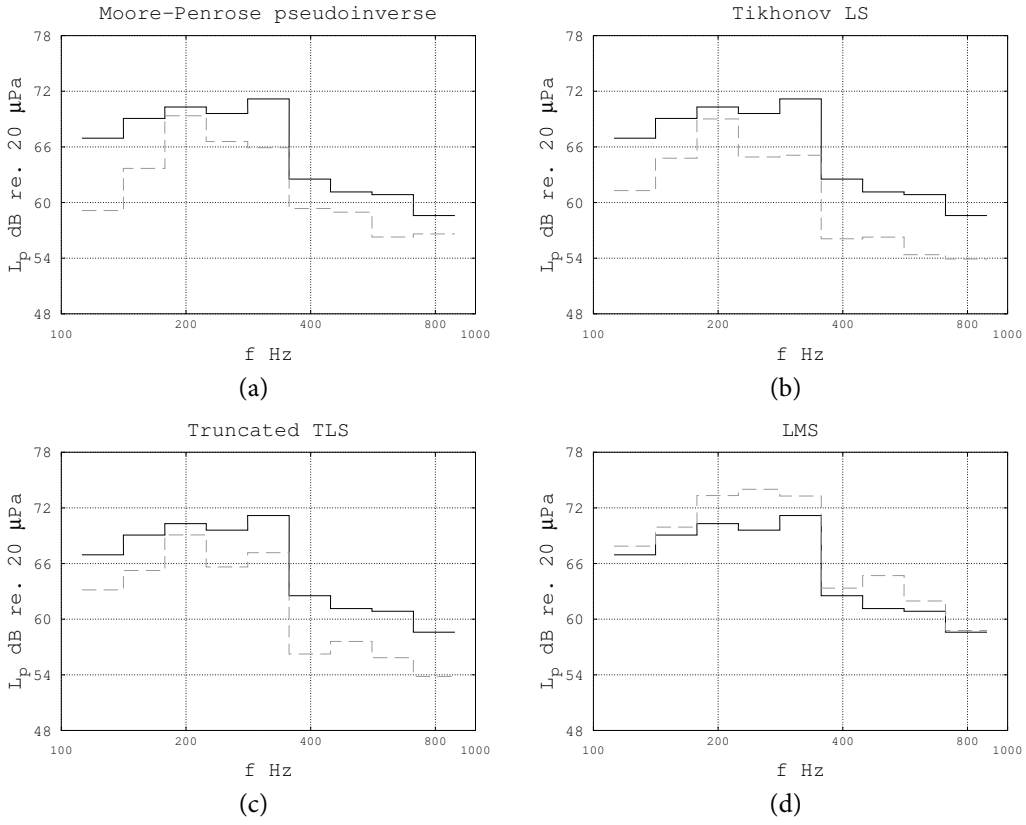

Figure 14: Sound pressure level in one-third octave band of the band-pass filtered measured time history, black continuous, and corresponding predicted time history, gray dashed, at one error point at 1890 RPM for four different source strength estimation techniques: (a) Moore-Penrose pseudoinverse, (b) Tikhonov LS, (c) Truncated TLS and (d) LMS.

harmonic at a given error point. Still large level differences up to 30 dB occurs occasionally. The difference in sound pressure level should be seen in view of the limited number of control points and source points used in the experiment. More than a doubling of the number of drivers, to 22 drivers, is necessary in order to achieve two drivers per shortest acoustical wavelength of interest. Numerical results suggest that such a dense array is required to expect satisfactory results.

In turn such a complicated dummy source prototype requires more microphones around the diesel engine, and future experiments with a dummy source should be designed from scratch so that the number of microphones is greater than the number of drivers. The results should be expected to improve using 32 microphones across the surface of the cage, which was the limit of the available data acquisition system, but there was no funding to acquire such an array. In any case no more experiments could be carried out since the former engine laboratory was demolished.

The performance of the LMS technique is similar to the frequency domain methods. In this case, however, the result exists at all frequencies so the overall error is smaller. Surprisingly, it seems that there is a systematic error of a few dB at one of the error points for all three engine speeds. The bias suggest, perhaps, a problem with the estimated set of impulse responses related to this error point.

4.2 Discussion

The dummy source approach has been applied on a diesel engine. Since the transfer impedances have been measured, measurement errors in the matrix should be accounted for when estimating the source strengths. It has been observed that whereas the dummy source prototype can satisfactorily reproduce the

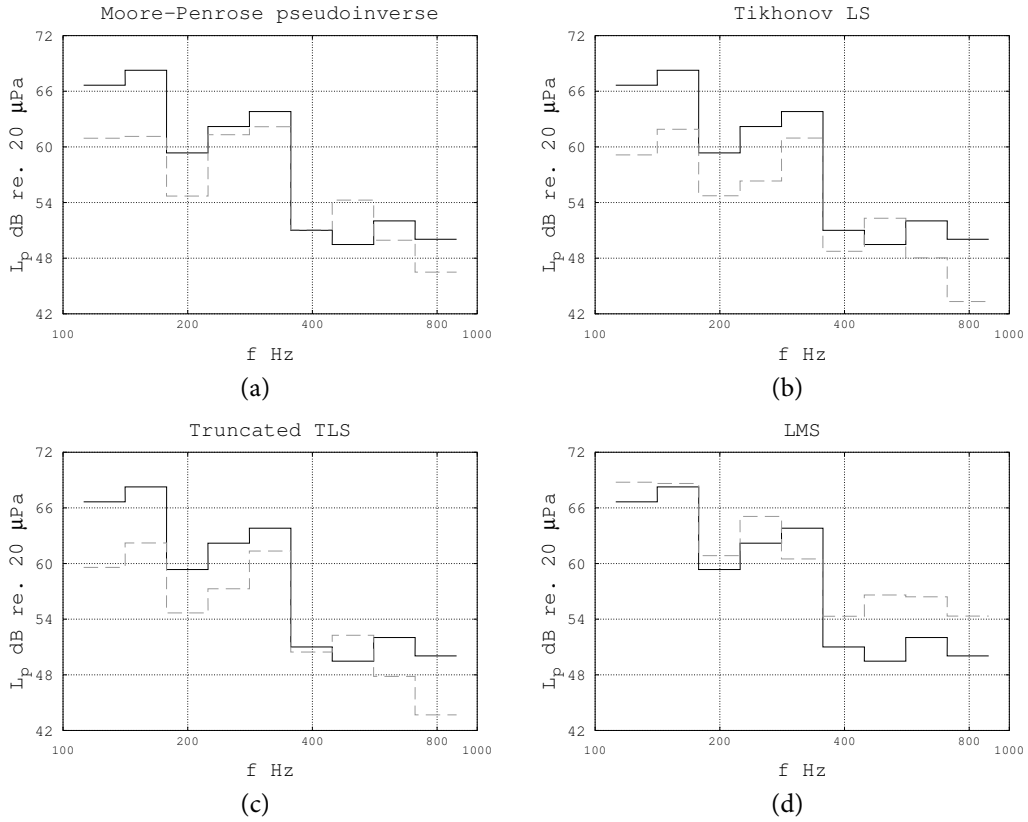

Figure 15: Sound pressure level in one-third octave band of the band-pass filtered measured time history, black continuous, and corresponding predicted time history, gray dashed, at one error point at 1070 RPM for four different source strength estimation techniques: (a) Moore-Penrose pseudoinverse, (b) Tikhonov LS, (c) Truncated TLS and (d) LMS.

sound pressure level of the diesel engine at the control points, this does not imply that the identified sound sources are applicable for the prediction of sound pressure level elsewhere.

The influence of measurement errors can be mitigated using regularisation: physical regularisation, for example turning off drivers; or mathematical regularisation, introducing additional criteria in the inverse computation. The mathematical regularisation is done by filtering out smaller singular values, but to the best of my knowledge the filtering lacks physical meaning. The physical system is approximated by a fictitious system which is less sensitive to random perturbations. *The use of regularisation techniques has been found to dramatically improve the accuracy of the predictions at error points when the condition number is above a few hundreds for the conducted experiment, but the need of regularisation can be mitigated by preconditioning.*

The experimental work was hampered by a limited number of microphones. The dummy source prototype should not be expected to produce satisfactory results with less than 2 drivers per shortest acoustical wavelength of interest. The design criterion requires 22 drivers at 1000 Hz, but instead only a random subset of 10 drivers could be used. The reduction of the number of drivers was necessary in order to achieve an overdetermined equation system, and to have two independent measurement points which was used to check the results. The typical error at an engine harmonic is less than 6 dB but may rise up to 12 dB. The discrepancy is, perhaps, satisfactory in view of the simplicity of the experiment.

The predicted time histories does capture a change of operation of the engine as well as a change of listening position in the test cell. When compared to the recorded time histories there are audible differences which should be subject to further work.

The objective performance of the dummy source depends on the applied random shuffling of source,

control and error points. A future experiment with a greater number of microphones around the diesel engine, e.g. 64 microphones, would not only be useful to further assess the dummy source approach on industrial sources but, hopefully, show that satisfactory matching, within a few dB, is possible. The two error points in this experiment are too few to make meaningful statistics. Still the result suggests that the dummy source approach can be used, given further work, as a prediction tool of airborne sound from a complex industrial source.

5 CONCLUDING REMARKS

An experimental modelling concept — the dummy source approach — which is believed to be applicable for prediction of sound pressure response from surface vibration of an original source has been assessed and implemented in practice. The developed modelling is based on substitution of the original source with a closed rigid cabinet — the dummy — being of similar volume but simpler shape. The dummy intrinsically accounts for diffraction from the original source. Sound radiation by the original source is modelled by superposition of waves created by a number of drivers embedded in the dummy's surface. The source strengths of the driver array characterise the original source.

The dummy source approach is carried out in three steps. In the first step, the operating responses are measured at microphones spread around the original source. In the second step, the dummy source is introduced in the test cell at the place of the diesel engine, and the transfer impedances are measured. The transfer impedances and the operating responses enables the inverse computation of the drivers' source strengths. In the third step, the source strengths are estimated.

To the best of the author's knowledge, no simple optimisation procedure exists for finding the number of drivers and their positions needed for satisfactory sound reproduction. The problem of designing a suitable driver array has been overcome by use of a fixed grid array with two drivers per shortest acoustic wavelength of interest.

The dummy source prototype has been implemented using reciprocity as a microphone array embedded in the surface of a Plexiglass box, and the transfer impedances of the test cell was measured using an electrodynamic driver positioned in the test cell. The driver had been instrumented and equipped with an internal microphone.

In the experimental work a microphone array with a restricted number of microphones had to be used, which is required to be practicable in industrial conditions. To mitigate the influence of measurement errors, however, it is usually required that the number of microphones are greater than the number of drivers. Unfortunately, in the conducted experiment this was not the case. The actual driver array was therefore selected out of the fixed grid using a Monte Carlo approach which minimised the condition number (and selected 10 out of 22 drivers).

A few remarks regarding the source strength estimation in the frequency domain should be given. The harmonic response of a diesel engine has been found quite difficult to handle from the point of view of applying the L-curve and the largest curvature criterion. There is an idea in the acoustic community that the regularisation parameter should be continuous with frequency, when the transfer impedance and the excitation is smooth, for a successful regularisation parameter selection technique. This is often used as a check of the regularisation tool. Clearly, this idea does not apply on harmonic excitation and it is therefore hard to judge if the selected parameter is reasonable. As a matter of fact the L-curve has often been found concave at the harmonics were the signal is strong, so no regularisation should be applied theoretically, but also in-between the harmonics where the signal is weak, and so the solution should be fully suppressed theoretically.

The typical error has been found to be around 6 to 12 dB at a given frequency, independent of the inversion technique and of the regime of the diesel engine. However, if preconditioning is not applied the difference in sound pressure level can become excessive — in particular for the Moore - Penrose pseudoinverse technique. The results are satisfactory in view of the simplicity of the experiment.

Among the techniques used to estimate the source strengths, the LMS algorithm has been judged to be the most promising one. The conclusion was made when comparing the measured and predicted time histories at independent error microphones in terms of sound pressure level and by listening. The two

primary advantages of this technique are: (1) the estimation does not involve matrix inversion, and (2) no assumption is made regarding the nature of the time history.

A TIKHONOV LEAST SQUARES

P. C. Hansen and D. P. O'Leary [7] proposed the use of Tikhonov regularisation with the L-curve as a tool to select the regularisation parameter. Tikhonov regularisation constrains the ordinary least-squares approach by penalising the solution norm

$$\arg\min_{\beta} \|\mathbf{Z}\hat{\mathbf{Q}} - \hat{\mathbf{p}}\|_2^2 + \beta^2 \|\hat{\mathbf{Q}}\|_2^2. \tag{19}$$

The computation of the L-curve is based on singular value decomposition [23, pp. 16 - 20] for which the transfer impedance matrix

$$\mathbf{Z} = \sum_{i=1}^{\min N,\, M} \mathbf{u}_i \sigma_i \mathbf{v}_i^*, \tag{20}$$

is written as a summation of left and right singular vectors $\mathbf{u}_i$, $\mathbf{v}_i$ and singular values σ_i [8]. The asterisk [*] denotes a complex conjugate transpose. The source strength vector is given by

$$\hat{\mathbf{Q}} = \sum_{i=1}^{\min N,\, M} f_i \frac{\mathbf{u}_i^* \hat{\mathbf{p}}}{\sigma_i} \mathbf{v}_i, \qquad f_i = \frac{\sigma_i^2}{\sigma_i^2 + \beta^2}, \tag{21}$$

where f_i is the filter factor [8]. Hansen and O'Leary [7] proposed the L-curve to assess the filtering. The L-curve is a plot of the residual norm versus the solution norm in logarithmic scale. The squared residual norm ρ is given by

$$\rho(\beta) = \|\mathbf{Z}\hat{\mathbf{Q}} - \hat{\mathbf{p}}\|_2^2 = \sum_{i=1}^{\min N,\, M} \left((1 - f_i)\mathbf{u}_i^* \hat{\mathbf{p}}\right)^2 + \|\Delta\hat{\mathbf{p}}_\perp\|_2^2, \tag{22}$$

and the squared solution norm η is given by

$$\eta(\beta) = \|\hat{\mathbf{Q}}\|_2^2 = \sum_{i=1}^{\min N,\, M} \left(f_i \frac{\mathbf{u}_i^* \hat{\mathbf{p}}}{\sigma_i}\right)^2, \tag{23}$$

when expressed as a function of the singular value decomposition [7, 8]. The perpendicular symbol [$_\perp$] denotes pressure outside of the dummy's range. There is a part of the pressure vector $\hat{\mathbf{p}}$, and thereby the residual norm, which can not be explained by superposition of waves from the dummy's driver array. Due to miss-specification of the driver array and measurement errors, the residual $\|\Delta\hat{\mathbf{p}}_\perp\|_2$ is not zero in the overdetermined case. The residual influences the L-curve's shape and should not be neglected in the analysis. The L-curve is computed by prescribing a grid of filtering parameters covering the entire range of singular values. The best guess corresponds to the value being closest to the corner of the L-curve, which can be found by the largest curvature criterion [7].

A.1 The curvature of the L-curve

A simplified approach to compute the L-curve, defined by $(\hat{\rho}(\beta)/2, \hat{\eta}(\beta)/2)$ as given by Eq. 22 and Eq. 23 respectively, and its curvature is proposed here. The computation is performed by prescribing N guesses of the filtering parameter β over the entire logarithmic space of singular values in the transfer impedance matrix. Here, the hat [$\hat{}$] is used to denote a logarithmic value $\hat{\rho} = \ln\rho$, and as before ρ is the squared residual norm and η is the squared solution norm. The range of guesses was prescribed starting from below the lowest logarithmic singular value, "underfiltering", and going to above the largest logarithmic singular value, "overfiltering". The guesses are prescribed using an uniform spacing δ in the logarithmic space of filtering parameters, $\hat{\beta}$. Thus the guesses are non-uniform in a linear scale and concentrated at lower values.

A reasonable guess, which corresponds to the L-curve's corner, was chosen among the prescribed values, using the largest curvature κ criterion [7]:

$$\beta_\kappa = \arg\max_\beta \kappa(\beta), \qquad \kappa(\beta) = \frac{\hat{\rho}'_\beta \hat{\eta}''_{\beta\beta} - \hat{\rho}''_{\beta\beta} \hat{\eta}'_\beta}{((\hat{\rho}'_\beta)^2 + (\hat{\eta}'_\beta)^2)^{3/2}}, \tag{24}$$

Here prime [$'$] and bis [$''$] corresponds to the first and second order derivative with regards to the filtering parameter β. Because the prescribed guesses are uniformly spaced in a logarithmic space, it is unfeasible to differentiate with regards to the filtering parameter. The first order logarithmic derivative at the i^{th} guess can be expressed as [22, p. 137, 409]:

$$\hat{\rho}'_\beta = \frac{\partial \hat{\rho}}{\partial \hat{\beta}} \frac{\partial \hat{\beta}}{\partial \beta} = \frac{1}{\beta} \hat{\rho}'_{\hat{\beta}}, \tag{25}$$

where the unknown first order derivative is approximated by

$$\hat{\rho}'_{\hat{\beta}}[i] \approx \frac{\hat{\rho}[i+1] - \hat{\rho}[i-1]}{2\delta}, \qquad i = 2, \ldots, N-1. \tag{26}$$

The second order logarithmic derivative with regards to the filtering parameter can be expressed in a similar manner [22, p. 137, 409]:

$$\hat{\rho}''_{\beta\beta} = \frac{\partial^2 \hat{\rho}}{\partial \hat{\beta}^2} \left(\frac{\partial \hat{\beta}}{\partial \beta} \right)^2 + \frac{\partial \hat{\rho}}{\partial \hat{\beta}} \frac{\partial^2 \hat{\beta}}{\partial \beta^2}, = \frac{1}{\beta^2} \left(\hat{\rho}''_{\hat{\beta}\hat{\beta}} - \hat{\rho}'_{\hat{\beta}} \right), \tag{27}$$

where the unknown second order derivative is approximated by

$$\hat{\rho}''_{\hat{\beta}\hat{\beta}}[i] \approx \frac{\hat{\rho}[i+1] - 2\hat{\rho}[i] + \hat{\rho}[i-1]}{\delta^2}, \qquad i = 2, \ldots, N-1, \tag{28}$$

and the unknown first order partial derivative is identical to the one that has been approximated earlier on. The expressions are valid inside of the discretised space, and the extremes are neglected as the curve's corner should lie inside of the range of singular values. The logarithmic derivatives of the solution norm can be estimated in an analogous manner.

B LEAST MEAN SQUARE

Kropp and Larsson [13] proposed the use of an adaptive filter, a modified least mean squares (LMS) algorithm, to estimate e.g. contact forces at the interface between structures. In the time domain, the recorded time histories $\mathbf{p}_n$ are related to the unknown source strengths $\mathbf{q}_m$ through a set of the impulse responses $\mathbf{h}_{nm}$. (The impulse responses are not known, and has to be estimated prior to the application of the LMS algorithm. The impulse responses has been estimated from back-transformation of the measured transfer impedances.)

The multiple input - multiple output adaptive filter [13] is formulated in vector form but will here be explained by scalar operations. The iterative process is divided into three steps. In each iteration along the recordings, $\forall i_s : N_h \leq i_s \leq N_s$ and $N_s \gg N_h$, is in the first step the n^{th} time history reconstructed, $\tilde{\mathbf{p}}_n$, and in the second step, the corresponding error signal, $\mathbf{e}_n$, is estimated. Each microphone position is treated separately. This is formulated as [13]

$$\tilde{\mathbf{p}}_n[i_s] = \sum_{m=1}^{M} \sum_{i_h=1}^{N_h} \mathbf{h}_{nm}[i_h] \mathbf{q}_{m,\text{old}}[i_s - i_h + 1], \tag{29}$$

$$\mathbf{e}_n[i_s] = \mathbf{p}_n[i_s] - \tilde{\mathbf{p}}_n[i_s]. \tag{30}$$

The first step expresses a summation of the partial contributions of every respective driver identified by convolution summation [24, pp. 492 - 500]. The second step is to extract the error signal between each

pair of measured and reconstructed time histories. Thereafter, in the third and final step, is each source strength updated using a separate adaptive filter [13]. In this case the average instantaneous gradient of the N error signals are used to update the source strength. For the m^{th} source strength, $\mathbf{q}_m$, this is formulated as [13]

$$\mathbf{q}_{m,\text{new}}[i_s - N_h + i_h] = \mathbf{q}_{m,\text{old}}[i_s - N_h + i_h] + \frac{\alpha_m}{N} \sum_{n=1}^{N} \mathbf{e}_n[i_s]\mathbf{h}_{nm}[N_h - i_h + 1], \quad \forall i_h : 1 \leq i_h \leq N_h. \tag{31}$$

Here, α_m is a scaling factor of the average instantaneous gradient. As a rule-of-thumb, the scaling factor should be small and decides the stability of the process [13]. The three steps are repeated in each iteration step. The process is initiated by setting the entire vector $\mathbf{q}_{m,\text{old}}$ to zero and at the end of each iteration $\mathbf{q}_{m,\text{old}}$ is overwritten by $\mathbf{q}_{m,\text{new}}$.

The adaptive filter needs to be complemented by stopping criteria. The aim of the adaptive filter is to minimise the mean square error, the difference between the reconstructed and recorded time histories [13]. A normalised measure of the difference between recorded and reconstructed time histories is

$$\left\| \begin{bmatrix} \mathbf{p}_1 \\ \vdots \\ \mathbf{p}_n \\ \vdots \\ \mathbf{p}_N \end{bmatrix} - \begin{bmatrix} \tilde{\mathbf{p}}_1 \\ \vdots \\ \tilde{\mathbf{p}}_n \\ \vdots \\ \tilde{\mathbf{p}}_N \end{bmatrix} \right\|_F \left\| \begin{bmatrix} \mathbf{p}_1 \\ \vdots \\ \mathbf{p}_n \\ \vdots \\ \mathbf{p}_N \end{bmatrix} \right\|_F^{-1}, \tag{32}$$

proposed as a first stopping criterion. Here, $\mathbf{p}_n[i_s/R]$ is the time history of the n^{th} field point. This is used because it is easy to compute. The normalisation is applied because the response can be quite different depending on the operation of the original source which obfuscates the interpretation of the error. The iterative procedure stops when this normalised error is sufficiently small or, a second stopping criterion, when a maximum number of iteration steps has been reached.

6 Bibliography

[1] N. Frenne and Ö. Johansson, "Acoustic time histories from vibrating surfaces of a diesel engine," Appl. Acoust. **67**, pp. 230 - 248 (2006).

[2] T. S. Vogt, C. Y. Glandier, J. Morkholt, A. Omrani, and M. A. Hamdi, "Engine source identification using an I-BEM technique," In Proc. of the Euronoise, pp. 1 - 6 (2003).

[3] A. Lindberg, G. Pavić, and Q. Leclère, "Characterisation of air-borne noise by a dummy-source approach," In Proc. of Noise and Vibration - Emerging Technologies (NOVEM), pp. N/A (2015).

[4] A. Lindberg and G. Pavić, "Experimental characterisation of a small compression driver using an internal microphone," In Proc. of the International Conference on Noise and Vibration Engineering (ISMA), pp. 1111 - 1119 (2014).

[5] A. Lindberg and G. Pavić, "Measurement of volume velocity of a small sound source," Appl. Acoust. **91**, pp. 25 - 32 (2015).

[6] Q. Leclère, G. Pavić, and S. Greffe, "Quantification of airborne and structureborne engine noise in a coach under real operating conditions," In Proc. of the International Conference on Noise and Vibration Engineering (ISMA), pp. 3203 - 3211 (2008).

[7] P. C. Hansen and D. P. O'Leary, "The use of the L-curve in the regularization of discrete ill-posed problems," J. Sci. Comput. **14**, pp. 1487 - 1503 (1993).

[8] P. C. Hansen, "The L-curve and its use in the numerical treatment of inverse problems," In *Computational Inverse Problems in Electrocardiology, ed. P. Johnston, Advances in Computational Bioengineering*, pp. 119 - 142 (WIT Press, 2000).

[9] S. Van Huffel and J. Vandewalle, *The Total Least Squares Problem - Computational Aspects and Analysis*, (SIAM, 1991).

[10] R. D. Fierro, G. H. Golub, P. C. Hansen, and D. P. O'Leary, "Regularization by truncated total least squares," J. Sci. Comput. **18**, pp. 1223 - 1241 (1997).

[11] D. M. Sima and S. Van Huffel, "Level choice in truncated total least squares," Comput. Stat. Data Anal. **52**, pp. 1103 - 1118 (2007).

[12] Y. Liu and W. S. Shepard Jr., "Dynamic force identification based on enhanced least squares and total least-squares schemes in the frequency domain," J. Sound Vib. **282**, pp. 37 - 60 (2005).

[13] W. Kropp and K. Larsson, "Force estimation in the time domain by applying an LMS algorithm," In Proc. of Noise and Vibration - Emerging Technologies (NOVEM), pp. N/A (2005).

[14] P. C. Hansen and D. P. O'Leary, "Regularization algorithms based on total least squares," In *Recent Advances in Total Least Squares Techniques and Errors-in-Variables Modeling, ed. S. Van Huffel*, (SIAM, 1997), pp. 127 - 137.

[15] A. T. Moorhouse, "Compensation for discarded singular values in vibro-acoustic inverse methods," J. Sound Vib. **267**, pp. 245 - 252 (2003).

[16] Q. Leclère, L. Pruvost, and E. Parizet, "Angular and temporal determinism of rotating machine signals: The diesel engine case," Mech. Syst. Signal Pr. **24**, pp. 2012 - 2020 (2010).

[17] W. A. Gardner, A. Napolitano, and L. Paura, "Cyclostationarity: Half a century of research," Signal Process. **86**, pp. 639 - 697 (2006).

[18] J. Antoni, "Cyclostationarity by examples," Mech. Syst. Signal Pr. **23**, pp. 987 - 1036 (2009).

[19] A. D. Pierce, *Acoustics - An Introduction to Its Physical Principles and Applications*, (McGraw-Hill Book Company, 1981).

[20] R. Boulanger and V. Lazzarini, *The Audio Programming Book*, (The MIT Press, 2011).

[21] A. Rivola and M. Troncossi, "Zebra tape identification for the instantaneous angular speed computation and angular resampling of motorbike valve train measurements," Mech. Syst. Signal Pr. **44**, pp. 5 - 13 (2014).

[22] L. Råde and B. Westergren, *Mathematics Handbook for Science and Engineering,* 5^{th} *ed.*, (Studentlitteratur, 2004).

[23] G. H. Golub, *Matrix Computations*, (The John Hopkins University Press, 1983).

[24] C. L. Phillips, J. M. Parr and E. A. Riskin, *Signals, Systems and Transforms,* 4^{th} *ed.*, (Pearson Prentice Hall, 2008), pp. 213 - 214 and 492 - 500.

Part II

Validation using a vibrating box

Appendix II

Characterisation of air-borne noise by a dummy source approach

The following appendix is an *extended* version of "Characterisation of air-borne noise by a dummy-source approach" published in the proceedings of Noise and Vibration - Emerging Technologies (NOVEM) (April 2015). The appendix A has been added to show how the L-curve's curvature has been computed. Also, there are additional remarks on the use of principal component analysis. Finally, some illustrations have been remade for improved clarity.

Abstract

A proper characterisation of noise of a vibrating source has to take into account both radiation from the source and diffraction by its body in order to enable prediction of sound pressure of the source when inserted into a given acoustical space. A particular technique, named the dummy source approach, has been developed with the aim of characterising real noise sources. Here the original source is replaced by a closed rigid cabinet of similar size and shape - the dummy - equipped with several small flush-mounted drivers. The noise of the original source is measured first in a number of control points and the source strengths of the drivers are then identified by inversion. Once a source is experimentally characterised by its dummy, further noise prediction steps can be carried out in a fairly straightforward manner since the source is represented by a simple shape and its excitation is of monopole type. The paper introduces the concept of the dummy source and discusses criteria of its acoustical layout. A characterisation procedure is then carried out via a virtual experiment aimed at validating the approach. The approach is finally validated by experimental results.

1 INTRODUCTION

Synthesis of air-borne noise radiated by steady-state vibration of an industrial source such as a diesel engine is quite some challenge in noise and vibration engineering. Recently sound synthesis methods have been in development, aimed at either sound auralisation [1] or virtual noise prototyping [2, 3]. In [3] sound radiation by an electric engine was modelled using sound pressure - force transfer functions. The forces were quantified by a mobility approach in which the original source was characterised by free velocities. Frenne and Johansson [4] compared simplified source models for time-domain quantification of partial sources on a diesel engine, the latter represented by a combination of several point sources distributed on its surface. Vogt et al. [5] identified sound sources on the surface of a diesel engine mock-up by an inverse boundary element approach. This optimisation procedure allows for the construction of efficient synthesis models. The purpose of this paper is to discuss basic aspects of air-borne noise characterisation using a so called dummy. The dummy can then be applied as a black-box source model in a synthesis scheme.

At low frequencies, for which the source is small compared to the acoustic wavelength, the source can be characterised as a monopole, a dipole, a quadrupole, or a combination of such volumeless sources [6]. At high frequencies, for which the body is large compared to the wavelength, the source can be characterised

by its power output [7]. In the mid-frequency range, a model of a source can be based on its normal velocity distribution [5]. This is applicable if the mechanical impedance of the housing is high; i.e., the housing vibration does not depend on the acoustic environment.

Bobrovnitskii and Pavić [8] proposed an alternative airborne characterisation technique based on blocked pressure and source impedance across an enclosing surface. These source quantities were defined in terms of analytical spherical functions, but the technique requires a spherical chamber to be carried out in practice. Pavić later proposed [9] a further refined source model based on patch averaged blocked pressure, and patch averaged source impedance. In this case the measurement of blocked pressure is not restricted to a chamber of any particular shape. The advantage of the developed approaches is that they are general and can be applied to any noise source. The disadvantage is that the measurement of blocked pressure is rather cumbersome in practice.

In this paper an approach in which the original source is replaced by a particular substitute source, the dummy source, is proposed. The dummy is a rigid closed cabinet of similar but simpler shape than the original source. The dummy accounts for both radiation and diffraction by the source. Sound radiation by the dummy is achieved by a number of M drivers spread across its surface. The response of each driver of surface D is governed by the source strength amplitude $\hat{Q}$ it produces, the acoustic features of the observation space Ω, and diffraction by the dummy's body. The dummy source implies that the integral formulation of sound radiation [10, p. 8] is approximated by

$$\hat{p}(\mathbf{f}) \approx \sum_{m=1}^{M} Z(\mathbf{f} \mid \mathbf{s}_m)\hat{Q}(\mathbf{s}_m), \qquad \hat{Q}(\mathbf{s}_m) = \int_{D_m} \hat{v}_\perp dD_m. \tag{1}$$

Here, the transfer impedance (Green's function) $Z(\mathbf{f} \mid \mathbf{s})$ satisfies the conditions at the boundaries of the observation space but with the original source replaced by the dummy. Thus the original source is characterised by its dummy and its excitation is provided by a lookup table of frequency source strengths $\hat{Q}_1, \ldots, \hat{Q}_M$. The latter are obtained by an inverse technique. The synthesis of sound, e.g. at the operator's ear in a machine compartment, may be carried out given an additional transfer impedance describing sound propagation from the dummy's driver array to the ear's position.

2 THE DUMMY SOURCE APPROACH

There are several steps in the proposed approach. The first step is the design of the dummy. On the closed rigid surface S of the dummy a driver array of M simple sources with centres at $\mathbf{s}_1, \ldots, \mathbf{s}_M$ are prescribed. The geometric centres will be referred to as source points. The second step is the sampling of sound radiated by the vibrating body. This is done using a microphone array of N control points, located at $\mathbf{f}_1, \ldots, \mathbf{f}_N$ around the source. The third step is to establish the dummy's transfer matrix. This matrix relates each simple source on the dummy's surface to each field point in the observation space. The fourth step is the inversion which may be ill-conditioned. Tikhonov regularisation is applied to improve conditioning but any other suitable regularisation technique can be employed. The check of the dummy source is finally done by predicting the sound pressure at E error points scattered around the original source.

2.1 Design hypothesis

There is at beforehand no rational way to specify the number and positions of simple sources on the dummy. A hypothesis is that at least two sources per acoustic wavelength on the surface of the dummy are sufficient to reproduce far-field sound pressure of a vibrating body. This is different from other approaches such as e.g. boundary elements were often at least six elements per shortest acoustical or structural wavelength is required. The number of required sources M, and the average spacing δ between two adjacent source positions are roughly given by

$$M \approx 4S\frac{f_{\max}^2}{c^2}, \qquad \delta \approx \frac{c}{2f_{\max}} \tag{2}$$

where c is the speed of sound and S is the surface area of the dummy. Using the introduced criteria, a fixed grid of simple sources is prescribed. An acoustical layout, as used in this paper in section 4, with

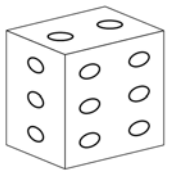

Figure 1: Schematic driver array set in a dummy's surface.

22 drivers embedded in the surface of a closed rigid box - the dummy - is shown in Fig. 1. This satisfies the introduced criterion until 1000 Hz. The exact positions of the substitute sources are not so important as different layouts of identical number of sources will perform in a similar manner. Note the squared frequency dependence of the number of substitute sources needed by Eqs. 2 for the reproduction of sound. This hypothesis will be tested in two case studies.

2.2 Source identification

At a constant frequency, the pressure amplitudes at microphones in the observation space are put in a vector $\hat{\mathbf{p}}$ $(N \times 1)$, and the unknown source strengths of the dummy's drivers are put in a vector $\hat{\mathbf{Q}}$ $(M \times 1)$. The transfer impedance matrix $\mathbf{Z}$ $(N \times M)$ is estimated using either repeated measurements or computations. Reciprocity may be used. The dummy's source strength distribution is quantified, at a constant frequency, by finding the solution to

$$\mathbf{Z}\hat{\mathbf{Q}} \approx \hat{\mathbf{p}}, \tag{3}$$

using a constrained least-squares approach [11, 12, 13]. To introduce the dummy source concept, it is here assumed that a smooth fit to the original sound field requires more control points than source points; i.e., $M \ll N$. The optimal number of microphones and their positions in the observation space represent a subject of its own which lies outside the scope of this paper.

Eq. 3 has no unique solution. This problem is overcome by being as close as possible in reproducing the original sound field while avoiding excessive source strengths of the simple sources. Such a trade-off can be expressed as

$$\hat{\mathbf{Q}} = \arg\min_{\beta} \|\mathbf{Z}\hat{\mathbf{Q}} - \hat{\mathbf{p}}\|_2^2 + \beta^2 \|\hat{\mathbf{Q}}\|_2^2, \tag{4}$$

where β is the filtering parameter [12]. Hansen and O'Leary [11] proposed the L-curve to assess the filtering parameter. The best guess of filtering parameter corresponds to the value being closest to the corner of the L-curve, which can be identified by the largest curvature criterion [11]. Similar to the approach in [14], the curvature is found from central finite difference quotients. If the curve is concave, the Moore-Penrose pseudoinverse is used which finds the best fit solution to $\min \|\mathbf{Z}\hat{\mathbf{Q}} - \hat{\mathbf{p}}\|_2^2$. The computation of the curvature of the L-curve is discussed in App. A.

2.3 Transfer impedances

An element of the transfer impedance (Green's function) matrix $\mathbf{Z}$ in Eq. 3, is given by

$$Z_{nm} = Z(\mathbf{f}_n \mid \mathbf{s}_m) = \frac{\hat{p}(\mathbf{f}_n)}{\hat{Q}(\mathbf{s}_m)}, \tag{5}$$

which respects the conditions at the boundaries of the observation space but with the original source replaced by the dummy. This function is not known. Two distinct approaches to the estimation of the dummy's transfer impedances are briefly described: (1) a numerical substitute source approach accounting

for semi-anechoic condition of the surrounding space, and (2) an experimental approach using a source of known volume velocity. As a rule an experimental approach should be preferred since numerical modelling is difficult.

The two approaches are roughly equivalent inside of a semi-anechoic room. This has been deduced from repeated measurements with a dummy. Through the measurements it has been found that computed transfer impedances correspond in sound pressure level and phase to the experimental transfer impedances. Examples of experimental and numerical setups are shown in Fig. 2, and a sample transfer impedance is shown in Fig. 3. The deviations between computation and measurement are believed to be due to vibration of the dummy or imperfect room features. The characterisation method is described in [15].

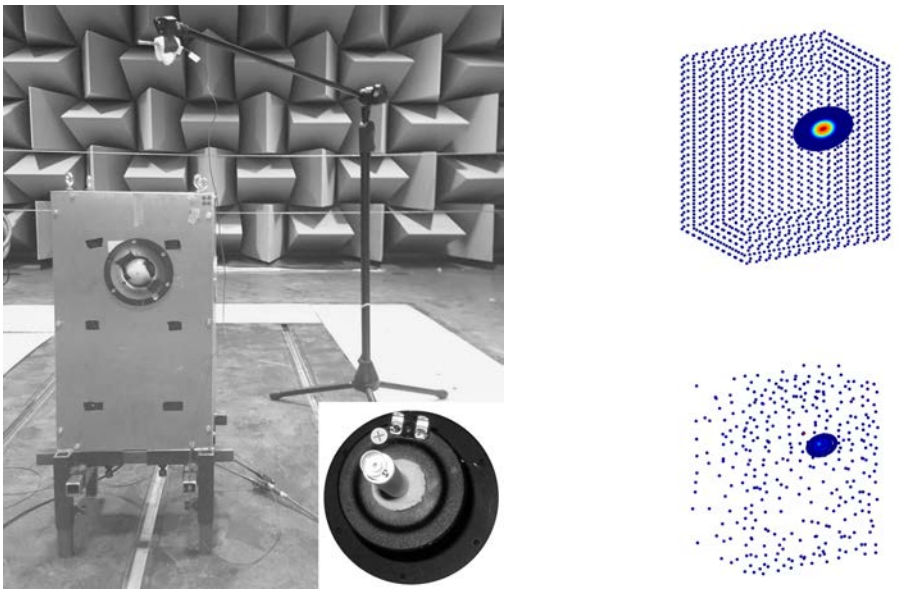

(a) (b)

Figure 2: Transfer impedance (a) measurement with a box using an instrumented driver shown in the lower right corner, and (b) computer model using a substitute source approach: upper part, points of prescribed velocity across the dummy's surface; lower part, positions of substitute monopole sources within the dummy at 525 Hz. (Color)

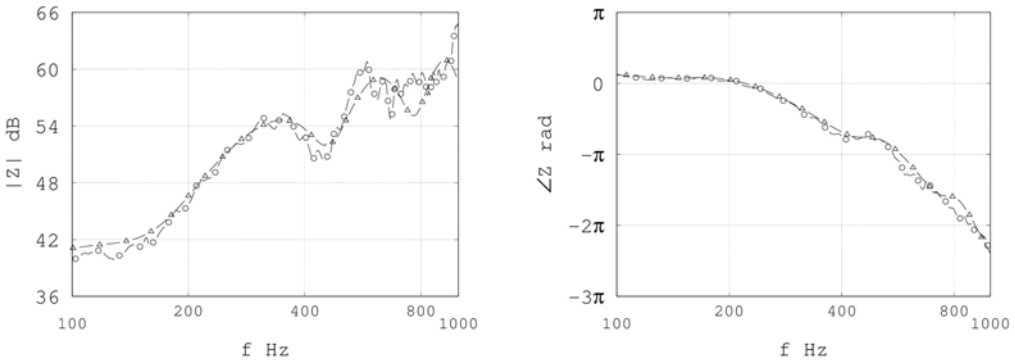

(a) (b)

Figure 3: Example transfer impedance (a) level dB re. 1 kg·m^{-4}·s^{-1} and (b) phase, legend: ∘ measured, △ computed.

2.3.1 Computation of transfer impedances

The dummy's cabinet surface C is assumed not to vibrate and acts only as an obstacle to the propagating sound. It follows that the normal component of particle velocity across the cabinet should vanish [6, pp. 100 - 103]. Let the driver be modelled by a circular disk of radius a in axisymmetric motion [16, 17]. A Greenspan [17] velocity profile $\zeta(\sigma)$ of the form

$$\zeta(\sigma) = \frac{1}{\pi a^2}(n+1)\left(1-\frac{\sigma^2}{a^2}\right)^n, \tag{6}$$

which produce unit source strength is prescribed across the disk. Here, σ denotes the distance from a point $\mathbf{b}$ on the surface of the disk to the disk's geometric centre and n is the profile order. The normal velocity for the dummy's m^{th} simple source is

$$\mathbf{v}_\perp(\mathbf{s}_m) = \begin{cases} \zeta(\sigma_m),\ 0 \le \sigma_m \le a \\ 0, \text{otherwise on } S. \end{cases} \tag{7}$$

The radiated sound is computed using superposition of waves created by volumeless sources located inside of the dummy's surface [18, 19, 20, 21]. The particle velocity amplitude field created by the substitute sources has to reproduce the surface vibration amplitude field in the outward normal direction at any point on the closed surface of the dummy [18, 19]. The substitute source locations are chosen by a search algorithm [20] operating on a prescribed set of candidate source positions spread out within the entire dummy. This is the technique used in the computation of sound radiation. The computation is repeated for each source position on the dummy surface.

2.3.2 Measurement of transfer impedances

An experimental implementation of a simple source can be a small back-enclosed driver. A driver's diaphragm has low mechanical impedance and its volume velocity depends strongly on the acoustic environment. To overcome this problem the driver's source strength is deduced using a signal from an internal microphone [22, 23, 24]. The transfer impedance in Eq. 5 is split into two independent transfer functions: a source function and a space function. A driver's diaphragm is characterised by its source function. The volume velocity at the front of the driver's diaphragm, and thereby the source function, can be assessed in specific spaces where further substitution is possible. This can be achieved using a compression chamber or a blocked pipe [25, 26]. The advantage of these techniques are that no assumptions regarding the driver's diaphragm shape or velocity distribution are made. The identified source function is then applied in other spaces where the transfer impedance has to be measured.

3 NUMERICAL VALIDATION

The concept of a dummy source concerns any source radiating by vibration of its closed solid surface. The characterisation of air-borne noise aims at far-field radiation, and conserves only basic features: power output, directivity, and diffraction by the original source.

The matching between the sound field created by the original source and its dummy is here analysed in a two-dimensional case. The original source of irregular shape and its dummy of simple rectangular shape are shown in Fig. 4. This dummy will be equipped with a number of drivers positioned around its perimeter in an as equidistant way as possible. The size of the dummy, 500×350 mm, gives it an area equal to that of the original source; its centre coincides with the geometric centre of the original source.

The original source is constructed from a large number of line sources, the two-dimensional equivalent of monopoles, of randomly selected source strengths randomly scattered within the original source's contour [20]. The particle velocity of this field normal to the contour is identified. This velocity is thereafter taken as the normal vibration velocity of the original source since the field created by the internal line sources exactly matches the field created by the vibrating source outside its contour. The radiated field is then computed in a number of control points around the source. These points correspond to microphone positions in a real measurement setup.

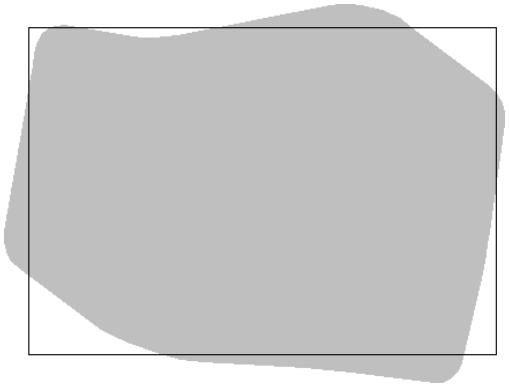

Figure 4: Schematics of the original source, grey area, and the dummy source's contour, black line, used for numerical evaluation.

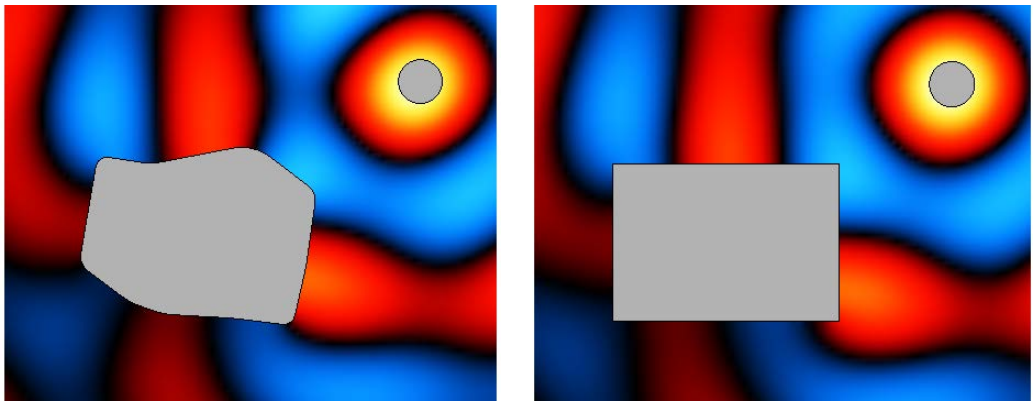

Figure 5: Scattering of sound by the original source, left, and by the dummy, right, at 500 Hz. Blue, negative; red, positive. (Color)

Next the transfer impedances are computed between the pressure at control points and the unit source strengths at the drivers' positions. This computation is done using a technique described in [20]. The transfer impedance matrix obtained in this way is then used in an inverse computation to produce the source strengths of each driver. The field radiated by the dummy is finally obtained by superposing the individual fields of all the drivers. In the next sections basic results concerning sound scattering and sound radiation at a single frequency is given.

3.1 Sound scattering

Figures 5 compares the instantaneous values of pressure fields created by an external cylindrical source incident on the passive original source and the passive dummy at 500 Hz. The bodies are here acting only as obstacles to the propagating wave. A good matching between the two scattered fields is seen as expected. Close to the bodies the matching deteriorates somewhat due to the fine grained differences in the geometrical shapes, but the global features of the fields are the same. This illustrates that a field can be approximated by replacing the original body with its dummy. Diffraction of waves by the original source is therefore inherently taken into account by the dummy.

3.2 Sound radiation

Figures 6 compares the instantaneous values of pressure fields created by the original source and the dummy at 500 Hz. The control points were distributed along a rectangular line 3 times larger than the con-

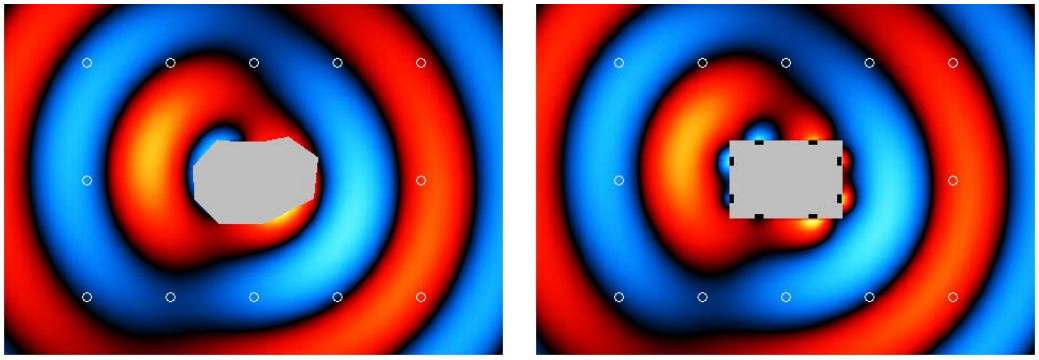

Figure 6: Radiation of sound by the original source, left, and by the dummy, right, at 500 Hz. White circles: control points; black spots: drivers. (Color)

Frequency (Hz)	Original source (W/m)	Dummy (W/m)
250	0.084	0.081
500	0.30	0.30
1000	0.91	0.92

Table II.1: Power output by the two sources at some characteristic frequencies.

tour line of the dummy source. The spacing between the control points was set to 62% of the wavelength, and the spacing between the drivers was set to 31% of the wavelength. These values were found to represent a reasonable trade-off between simplicity and accuracy, and were also applied at 250 and 1000 Hz.

The figures show a rather good matching of the two fields. Very close to the source the matching deteriorates due to high near-field gradients, but further away it improves a lot. The radiated powers of the original source and its dummy match extremely well, as shown in the Tab. II.1.

4 EXPERIMENTAL VALIDATION

A box of dimensions $300 \times 232 \times 500$ mm was used as original source. The box was made out of six 12 mm thick Plexiglass plates, and excited using an electrodynamic shaker mounted inside of the box. This shaker was fed with low passed white noise. The vibrating box was mounted on a turn table at a height of 300 mm from the floor inside of a semi-anechoic room. The box was rotated such that 8 different 5×5 planar array recordings with an angular step of 45° were achieved. The array was positioned 600 mm from the box centre and the spacing between microphones was 100 mm. The height of the array was adjusted to coincide with the vibrating box. This resulted in 200 measurement points which were randomly split into 128 control points and 70 error points. Additional measurements were done at two listening points lying inside and outside of the virtual surface. The experimental setup is shown in Fig. 7.

A dummy of identical dimensions as the box was computer modelled. On the surface of the dummy a driver array with 22 sources was defined using Eq. 2. This fulfils the hypothesis of at least 2 sources per wavelength until 1000 Hz. The simple sources are spread across all faces of the dummy. The dummy was placed at a height of 300 mm from the ground in a virtual half-space, and thereafter the transfer impedances were computed using the approach outlined in section 2.3.1. The floor was modelled using the mirror image technique.

4.1 The box's response

The measured sound pressure is expressed at a constant frequency as a pressure spectral density matrix $\mathbf{G}_{pp}$ $(N \times N)$ [27, pp. 391 - 409]. This is related to the unknown source strength spectral density matrix $\mathbf{G}_{QQ}$ $(M \times M)$ by the transfer impedance matrix $\mathbf{Z}$ as [13]:

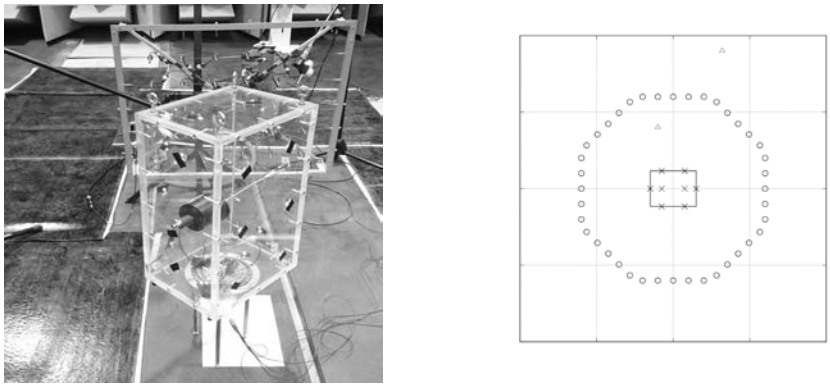

(a) (b)

Figure 7: Setup inside of a semi-anechoic room (a) array recording of the vibrating box using a turn table with the position of the substitute sources marked by black tape, and (b) schematic setup of control and error points (∘), source points (×) and listening points (△) projected onto a plane.

$$\mathbf{G}_{pp} \approx \mathbf{Z}\mathbf{G}_{QQ}\mathbf{Z}^{*}, \tag{8}$$

for which the solution is obtained for each frequency of interest. To apply Tikhonov regularisation, Eq. 8 has been recast on the form of Eq. 3 by use of principal component analysis [28]:

$$\mathbf{G}_{pp} = \mathbf{\Theta}\boldsymbol{\lambda}\mathbf{\Theta}^{*}, \tag{9}$$

which is express an eigendecomposition of the cross-spectral density matrix. The column vectors in $\mathbf{\Theta}$ are called eigenvectors and the diagonal of $\boldsymbol{\lambda}$ are called eigenvalues. The k^{th} principal component is given by

$$\mathbf{p}_k = \boldsymbol{\theta}_k\sqrt{\lambda_k}, \tag{10}$$

where $\boldsymbol{\theta}_k$ is the eigenvector and λ_k the eigenvalue respectively. The corresponding principal source strengths are found for each such component. The cross-spectral source strength matrix can then be reconstructed. The advantage of this approach is that the same numerical treatment can be applied on both Eq. 8 and Eq. 3. The disadvantage is that repeated matrix inversions for each principal component of interest are necessary. In practice however only the strong eigenvalues are accounted for when estimating the source strengths.

4.1.1 Synchronisation

Using several repeated array measurements synchronisation is required. In the specific case of the vibrating box this has been achieved by a reference signal. The n^{th} measurement signal was synchronised using one reference signal r, the complex pressure amplitude is then given by

$$\hat{p}_n = \sqrt{2G_{nn}}\frac{G_{nr}}{|G_{nr}|}, \qquad \mathbf{G}_{pp} \approx \frac{1}{2}\hat{\mathbf{p}}\hat{\mathbf{p}}^{*}, \tag{11}$$

which can be used to approximate the full pressure spectral density matrix. The voltage signal feeding the shaker was used as a reference signal. Synchronisation was only carried out at control and error points. The pressure auto-spectral density at the listening points were computed separately from the time signals to check the results [27].

4.2 The dummy's source strengths

The dummy's source strengths were estimated from the measured pressure, Eq. 11, at the microphones using the outlined regularisation technique, Eq. 4, combined with computed transfer impedances of the

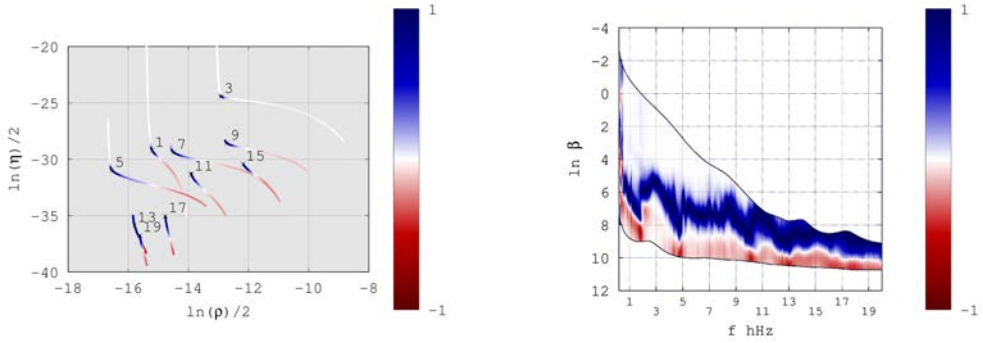

Figure 8: L-curves, left, with normalised curvature $\kappa/\max(|\kappa|)$ at 1, 3, …, 19 hHz with the largest curvature indicated by an ×-marker, and a map, right, of normalised curvature as function of filtering parameter and frequency. (Color)

dummy source, Eq. 7. Sample L-curves, the range of singular values and the curvature as function of frequency are shown in Fig. 8.

The selected filtering parameter is nearly continuous between 100 Hz and 2000 Hz. This indicates that the largest curvature criterion is applicable. It is seen that the transfer matrix is increasingly ill-conditioned with decreasing frequency, motivating the use of a regularisation technique. At higher frequencies there are small differences in the identified source strengths from that obtained by Moore-Penrose pseudoinversion.

4.3 Performance at error points

Once the vibrating box was characterised its dummy was used to predict the sound pressure at 70 independent error points. The error points are located at the same array as the control points, but they were not used in the inversion, and are used to check the dummy's performance. A first check is the dummy's far-field power output. This is related to the spatial averaged pressure at the error points. A comparison between the predicted and measured spatial averaged pressure, as well as pressure in one point, is shown in Fig. 9. Good matching between the box and the dummy is seen in the range 200 - 1000 Hz. Going below 200 Hz the box is not an efficient radiator of sound, while the room likely ceases to be semi-anechoic. This may explain the deviation in the dummy's behaviour at low frequencies apart from problems coming from inversion. The matching is however rather good down to about 80 Hz. Surprisingly, the matching in the range 1000 Hz to 2000 Hz is good suggesting that the hypothesis about the number of drivers, Eq. 2, may be unnecessarily penalising in this particular case. The results indicates that the dummy can be used to predict both the power output and the pressure response.

4.4 Performance at listening points

To further investigate the performance of the dummy, predictions are made at listening points not located at the virtual surface of the array used to characterise the dummy. The result is shown in Fig. 10. Contrary to the case of error points, there are large level differences at some frequency ranges between the box and its dummy. It is seen that the radiated pressure by the dummy is reasonably close to the one radiated by the vibrating box between 200 Hz and 1000 Hz. This suggest that the hypothesis of 2 sources per smallest wavelength of interest is potentially applicable.

5 CONCLUDING REMARKS

A modelling concept believed to be applicable for prediction of noise radiated by a vibrating source of complex geometry has been proposed. The developed model is based on substitution of the real source with a closed rigid cabinet - the dummy - being of similar but simple shape. The dummy intrinsically models

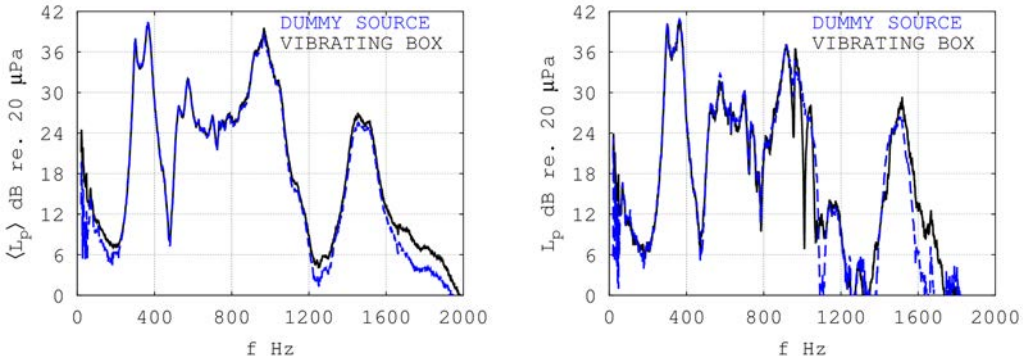

Figure 9: Performance at error points: left, spatial averaged pressure response; right, pressure response at one error point. Continuous black line, vibrating box; dashed blue line, dummy source. (Color)

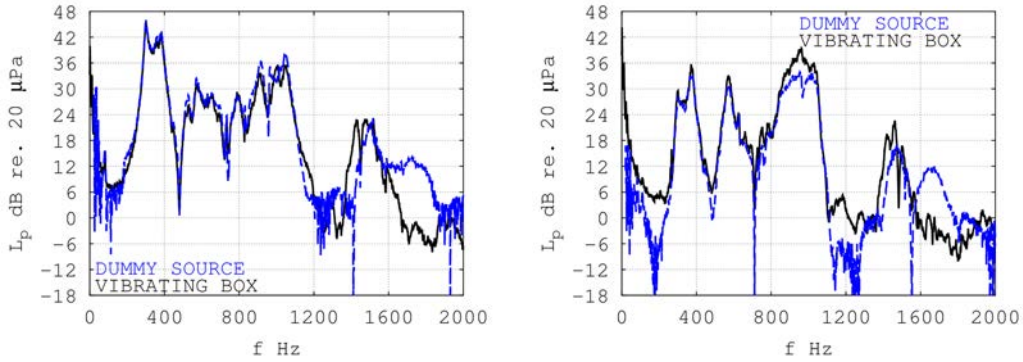

Figure 10: Performance at listening points: left, interior to virtual surface; right, exterior to virtual surface. Continuous black line, vibrating box; dashed blue line, dummy source. (Color)

diffraction by the original source. Sound radiation by the original source is modelled by superposition of waves created by a number of drivers embedded in the dummy's surface. The dummy aims at preserving far-field radiation characteristics of the original source while simultaneously accounting for diffraction by the source.

The source strengths of the dummy's drivers are obtained by an inverse technique. At first response measurements are done using control microphones spread around the original source. Thereafter the dummy is introduced in the same environment at the place of the original source, and the dummy's transfer impedances relative to the control microphones are identified. Knowing the dummy's transfer impedances and the pressure response of the original source enables the inverse computation of the drivers' source strengths using a constrained least-squares approach.

To the best of the authors' knowledge, no simple optimisation procedure exists for finding the number of drivers and their positions needed for satisfactory sound reproduction. This problem has been overcome by use of a fixed array using two sources per acoustic wavelength. An optimised driver array would perform better, but it would also depend on the specific source and its operation. On the contrary, it is believed that a single dummy equipped with a fixed driver array may represent an entire class of real sources of similar size and shape in various operational conditions. This enables a comparison of different industrial sources mounted in a mechanical assembly.

Two different techniques for establishing the dummy's transfer impedances have been briefly described: (1) a numerical approach based on superposition of monopoles suitable for semi-anechoic conditions, and (2) an experimental approach applicable anywhere. The computational model of a driver in a cabinet above a rigid ground has been validated experimentally.

So far no conclusive findings about the number of drivers per acoustic wavelength has been made. In the experimental validation it seems like less than two sources per acoustic wavelength may be sufficient to match the power output. In simulations not presented in this paper, up to four sources per wavelengths have been required to accurately reproduce the sound field when the volume velocity of the original source is negligible. Thus, the design of the dummy's source array depends on the source in question and may require some trial and error engineering.

Finally, the approach has been validated experimentally in a semi-anechoic room using a medium-sized vibrating box as original source. The predicted and measured response shows satisfactory matching.

Acknowledgements

This work was co-funded by Volvo Construction Equipment. The funding and discussions with Nicklas Frenne and Catalin Badau are gratefully acknowledged. The work was carried out at Laboratoire Vibrations Acoustique at INSA de Lyon in France, a member of the Centre Lyonnais d'Acoustique. The experimental work has been greatly assisted by Patrick Blachier. Antonio Pereira has helped with comments about inversion.

A THE CURVATURE OF THE L-CURVE

P. C. Hansen and D. P. O'Leary [11] proposed the use of Tikhonov regularisation with the L-curve as a tool to select the regularisation parameter. The computation of the L-curve is based on singular value decomposition [29, pp. 16 - 20] for which the transfer impedance matrix

$$\mathbf{Z} = \sum_{i=1}^{\min N,\, M} \mathbf{u}_i \sigma_i \mathbf{v}_i^*, \tag{12}$$

is written as a summation of left and right singular vectors $\mathbf{u}_i$, $\mathbf{v}_i$ and singular values σ_i [12]. The asterisk [*] denotes a complex conjugate transpose. The source strength vector is given by

$$\hat{\mathbf{Q}} = \sum_{i=1}^{\min N,\, M} f_i \frac{\mathbf{u}_i^* \hat{\mathbf{p}}}{\sigma_i} \mathbf{v}_i, \qquad f_i = \frac{\sigma_i^2}{\sigma_i^2 + \beta^2}, \tag{13}$$

where f_i is the filter factor [12]. Hansen and O'Leary [11] proposed the L-curve to assess the filtering. The L-curve is a plot of the residual norm versus the solution norm in logarithmic scale. The squared residual norm ρ is given by

$$\rho(\beta) = \|\mathbf{Z}\hat{\mathbf{Q}} - \hat{\mathbf{p}}\|_2^2 = \sum_{i=1}^{\min N,\, M} \left((1 - f_i)\mathbf{u}_i^* \hat{\mathbf{p}}\right)^2 + \|\Delta\hat{\mathbf{p}}_\perp\|_2^2, \tag{14}$$

and the squared solution norm η is given by

$$\eta(\beta) = \|\hat{\mathbf{Q}}\|_2^2 = \sum_{i=1}^{\min N,\, M} \left(f_i \frac{\mathbf{u}_i^* \hat{\mathbf{p}}}{\sigma_i}\right)^2, \tag{15}$$

when expressed as a function of the singular value decomposition [11, 12]. The perpendicular symbol [$_\perp$] denotes pressure outside of the dummy's range. There is a part of the pressure vector $\hat{\mathbf{p}}$, and thereby the residual norm, which can not be explained by superposition of the dummy's simple sources. Due to miss-specification of the simple source array as well as measurement noise this is not zero in the overdetermined case. This influences the L-curve's shape and should not be neglected in the analysis. The L-curve is computed by prescribing a grid of filtering parameters covering the entire range of singular values. The best guess corresponds to the value being closest to the corner of the L-curve, which can be found by the largest curvature criterion [11].

A simplified approach to compute the L-curve, defined by $(\hat{\rho}(\beta)/2, \hat{\eta}(\beta)/2)$ as given by Eq. 14 and Eq. 15 respectively, and its curvature is proposed here. The computation is performed by prescribing N guesses of the filtering parameter β over the entire logarithmic space of singular values in the transfer impedance

matrix. Here, the hat [ˆ] is used to denote a logarithmic value $\hat{\rho} = \ln \rho$, and as before ρ is the squared residual norm and η is the squared solution norm. The range of guesses was prescribed starting from below the lowest logarithmic singular value, "underfiltering", and going to above the largest logarithmic singular value, "overfiltering". The guesses are prescribed using an uniform spacing δ in the logarithmic space of filtering parameters, $\hat{\beta}$. Thus the guesses are non-uniform in a linear scale and concentrated at lower values.

A reasonable guess, which corresponds to the L-curve's corner, was chosen among the prescribed values, using the largest curvature κ criterion [11]:

$$\beta_\kappa = \arg\max_\beta \kappa(\beta), \qquad \kappa(\beta) = \frac{\hat{\rho}'_\beta \hat{\eta}''_{\beta\beta} - \hat{\rho}''_{\beta\beta} \hat{\eta}'_\beta}{((\hat{\rho}'_\beta)^2 + (\hat{\eta}'_\beta)^2)^{3/2}}, \tag{16}$$

Here prime [′] and bis [″] corresponds to the first and second order derivative with regards to the filtering parameter β. Because the prescribed guesses are uniformly spaced in a logarithmic space, it is unfeasible to differentiate with regards to the filtering parameter. The first order logarithmic derivative at the i^{th} guess can be expressed as [30, p. 137, 409]:

$$\hat{\rho}'_\beta = \frac{\partial \hat{\rho}}{\partial \hat{\beta}} \frac{\partial \hat{\beta}}{\partial \beta} = \frac{1}{\beta} \hat{\rho}'_{\hat{\beta}}, \tag{17}$$

where the unknown first order derivative is approximated by

$$\hat{\rho}'_{\hat{\beta}}[i] \approx \frac{\hat{\rho}[i+1] - \hat{\rho}[i-1]}{2\delta}, \qquad i = 2, \ldots, N-1. \tag{18}$$

The second order logarithmic derivative with regards to the filtering parameter can be expressed in a similar manner [30, p. 137, 409]:

$$\hat{\rho}''_{\beta\beta} = \frac{\partial^2 \hat{\rho}}{\partial \hat{\beta}^2} \left(\frac{\partial \hat{\beta}}{\partial \beta} \right)^2 + \frac{\partial \hat{\rho}}{\partial \hat{\beta}} \frac{\partial^2 \hat{\beta}}{\partial \beta^2}, = \frac{1}{\beta^2} \left(\hat{\rho}''_{\hat{\beta}\hat{\beta}} - \hat{\rho}'_{\hat{\beta}} \right), \tag{19}$$

where the unknown second order derivative is approximated by

$$\hat{\rho}''_{\hat{\beta}\hat{\beta}}[i] \approx \frac{\hat{\rho}[i+1] - 2\hat{\rho}[i] + \hat{\rho}[i-1]}{\delta^2}, \qquad i = 2, \ldots, N-1, \tag{20}$$

and the unknown first order partial derivative is identical to the one that has been approximated earlier on. The expressions are valid inside of the discretised space, and the extremes are neglected as the curve's corner should lie inside of the range of singular values. The logarithmic derivatives of the solution norm can be estimated in an analogous manner. The results of the differentiation has been checked against a local low order polynomial fit with good results. An alternative approach based on the singular value decomposition can be found in [12].

6 Bibliography

[1] D. Berckmans, B. Pluymers, P. Sas, and W. Desmet, "Numerical comparison of different equivalent source models and source quantification techniques for use in sound synthesis systems," Acta Acustica United Ac. **97**, pp. 138 - 147 (2011).

[2] A. T. Moorhouse and G. Seiffert, "Characterisation of an airborne sound source for use in a virtual acoustical prototype," J. Sound Vib. **296**, pp. 334 - 352 (2006).

[3] A. T. Moorhouse, "Simplified calculation of structure-borne sound from an active machine component on a supporting substructure," J. Sound Vib. **302**, pp. 67 - 87 (2007).

[4] N. Frenne and Ö. Johansson, "Acoustic time histories from vibrating surfaces of a diesel engine," Appl. Acoust. **67**, pp. 230 - 248 (2006).

[5] T. S. Vogt, C. Y. Glandier, J. Morkholt, A. Omrani, and M. A. Hamdi, "Engine source identification using an I-BEM technique," In Proc. of the Euronoise, pp. 1 - 6 (2003).

[6] A. D. Pierce, *Acoustics - An Introduction to Its Physical Principles and Applications*, (McGraw-Hill Book Company, 1981).

[7] I. L Vér and L. L. Beranek, *Noise and Vibration Control Engineering,* 2^{nd} *ed.*, (John Wiley & Sons, 2006).

[8] Y. Bobrovnitskii and G. Pavić, "Modelling and characterization of airborne noise sources," J. Sound Vib. **261**, pp. 527 - 555 (2003).

[9] G. Pavić, "Air-borne sound source characterization by patch impedance coupling approach," J. Sound Vib. **329**, pp. 4907 - 4921 (2010).

[10] M. C. Junger and D. Feit, *Sound, structures and their interaction*, (The MIT Press, 1972).

[11] P. C. Hansen and D. P. O'Leary, "The use of the L-curve in the regularization of discrete ill-posed problems," J. Sci. Comput. **14**, pp. 1487 - 1503 (1993).

[12] P. C. Hansen, "The L-curve and its use in the numerical treatment of inverse problems," In *Computational Inverse Problems in Electrocardiology, ed. P. Johnston, Advances in Computational Bioengineering*, pp. 119 - 142, (WIT Press, 2000).

[13] P.A. Nelson and S. H. Yoon, "Estimation of acoustic source strength by inverse methods: Part I, Conditioning of the inverse problem," J. Sound Vib. **233**, pp. 639 - 664 (2000).

[14] J.-L. Le Carrou, Q. Leclère, and F. Gautier, "Some characteristics of the concert harp's acoustic radiation," J. Acoust. Soc. Am. **127**, pp. 3203 - 3211 (2010).

[15] A. Lindberg and G. Pavić, "Experimental characterisation of a small compression driver," In Proc. of the Congrés Français d'Acoustique (CFA), pp. 1601 - 1607 (2014).

[16] D. L. Dekker, R. L. Piziali, and E. Dong, "Effect of boundary conditions on the ultrasonic beam characteristics of circular disks," J. Acoust. Soc. Am. **56**, pp. 87 - 93 (1974).

[17] M. Greenspan, "Piston radiator: Some extensions of the theory," J. Acoust. Soc. Am. **65**, pp. 608 - 621 (1979).

[18] L. Song, G. H. Koopmann, and J. B. Fahnline, "A method for computing acoustic fields based on the principle of wave superposition," J. Acoust. Soc. Am. **86**, pp. 2433 - 2438 (1989).

[19] M. Ochmann, "The source simulation technique for acoustic radiation problems," Acustica **81**, pp. 512 - 527 (1995).

[20] G. Pavić, "An engineering technique for the computation of sound radiation by vibrating bodies using substitute sources," Acta Acustica United Ac. *91*, pp. 1 - 16 (2005).

[21] G. Pavić, "A technique for the computation of sound radiation by vibrating bodies using multipole substitute sources," Acta Acustica United Ac. *92*, pp. 112 - 126 (2006).

[22] T. Salava, "Sources of the constant volume velocity and their use for acoustic measurements," J. Audio Eng. Soc. **22**, pp. 146 - 153 (1974).

[23] T. Salava, "Acoustic load and transfer functions in rooms at low frequencies," J. Audio Eng. Soc. **36**, pp. 763 - 775 (1988).

[24] D. K. Anthony and S. J. Elliott, "A comparison of three methods of measuring the volume velocity of an acoustic source," J. Audio Eng. Soc. **39**, pp. 355 - 366 (1991).

[25] A. Lindberg and G. Pavić, "Experimental characterisation of a small compression driver using an internal microphone," In Proc. of the International Conference on Noise and Vibration Engineering (ISMA), pp. 1111 - 1119 (2014).

[26] A. Lindberg and G. Pavić, "Measurement of volume velocity of a small sound source," Appl. Acoust. **91**, pp. 25 - 32 (2015).

[27] J. S. Bendat and A. G. Piersol, *Random Data - Analysis and Measurement Procedures*, (John Wiley & Sons, 1986).

[28] Q. Leclère, G. Pavić, and S. Greffe, "Quantification of airborne and structureborne engine noise in a coach under real operating conditions," Proc. of the International Conference on Noise and Vibration Engineering (ISMA), pp. 3203 - 3211 (2008).

[29] G. H. Golub, *Matrix Computations*, (The John Hopkins University Press, 1983).

[30] L. Råde and B. Westergren, *Mathematics Handbook for Science and Engineering,* 5^{th} *ed.*, (Studentlitteratur, 2004).

Part III

Measurement of transfer impedances

Appendix III

Measurement of volume velocity of a small sound source

The following appendix is based on "Measurement of volume velocity of a small sound source" published in Applied Acoustics (Vol. 91, April 2015).

Abstract

Two methods for measuring volume velocity of a back-enclosed driver, that make no assumptions about the shape or the vibration distribution of the driver's diaphragm, are investigated: a compression chamber and a blocked pipe. Both methods were implemented on an off-the-shelf driver using a microphone installed in the driver's cavity. The relationship between the pressure inside of the driver's cavity and the volume velocity of the driver's diaphragm was established by measurement. The two methods produced similar results.

1 INTRODUCTION

An engineering implementation of a simple source can be a small back-enclosed driver, provided that its driving surface is small compared to the wavelength and vibrates in phase [1]. In such a case the pressure response does not depend on the details of the vibrating surface and can be expressed by a point transfer impedance Z. Such an impedance relates volume velocity amplitude $\hat{Q}$ of the driver located at a source point $\mathbf{s}$ to sound pressure amplitude $\hat{p}$ at a field point $\mathbf{f}$

$$Z(\mathbf{f} \mid \mathbf{s}) = \frac{\hat{p}(\mathbf{f})}{\hat{Q}(\mathbf{s})}. \tag{1}$$

All the quantities in Eq. 1 are complex functions of frequency, and hat [ˆ] is used to denote amplitude [2]. The driver becomes increasingly inefficient when the frequency decreases, whereas at higher frequencies it develops pronounced directivity and thereby ceases to be a simple source [1]. In the mid-frequency range the transfer impedance can be measured, independently of the choice of driver, provided that the volume velocity of the source is known.

The need for a volume velocity source has been motivated by the demand for quantifying radiation by vibroacoustic sources. The principle of such a characterisation is to replace the complex vibroacoustic source by a simpler substitute source for use in noise synthesis. It is presumed that the radiation can be modelled by superposition of simple sources set in a rigid closed baffle of similar volume and shape as the original source. Such a characterisation critically depends on the knowledge of the source volume velocities.

One way of measuring volume velocity of a driver is to measure the velocity of the voice-coil, and multiply it with the projected surface of the driver's diaphragm in the direction parallel to its motion. The velocity of the voice-coil may be deduced by knowledge of the blocked electrical impedance and the

motional impedance of the driver [1]. The measurement of motional impedance can thus be used for an estimation of volume velocity assuming that the diaphragm moves as a rigid body. This requires prior knowledge of the blocked electrical impedance which can be found by e.g. casting the driver's moving parts into an epoxy resin [3]. Thus a second driver is needed for the measurement of motional impedance. This makes the method sensitive to differences between the two drivers [3]. Furthermore the motional impedance depends on the ambient space. Therefore the approach is rather cumbersome, and the supply voltage is not proportional to volume velocity.

Several designs for implementing volume velocity sources have been reported [4, 5, 6]. Common to all of these designs are that an additional transducer producing a signal proportional to either velocity, acceleration or volume displacement is used. The relationship to volume velocity can then be either deduced by theory or measured.

Three different designs of volume velocity sources have been reviewed by Salava [4]. The first design is based on use of a supplementary porous acoustic resistor. The advantage of the design is that it can be assembled quickly, but the disadvantage is that for accurate measurements careful calibration of the resistor is necessary and the resistor may not be linear in regards to the volume velocity [4]. The second design uses a microphone which provides a signal proportional to volume displacement. The disadvantage of the design is that in order to obtain a signal directly proportional to volume velocity a derivative circuit is required [4]. The third design is to equip a rigid piston, driven by an electrodynamical transducer, with a measuring voice-coil [4]. The advantage of the design is that the output signal is proportional to the velocity of the voice-coil, but the disadvantage is that it assumes mechanical rigidity of the moving parts which is not met in practice [4].

A more recent design described by Salava [5] uses two coupled drivers put together face-to-face: one acting as an exciter, and the other as a sensor. The exciting driver is in a rigid enclosure, and given that there is no supply voltage in the measuring and radiating driver's voice-coil the output voltage is proportional to its velocity. Another design is to equip the diaphragm with an accelerometer [5]. The relationship between the volume velocity and the transducer's signal is however not known, and experimental calibration is carried out in a free-space. The disadvantage of such a calibration is that it requires access to an anechoic room.

Anthony and Elliott [6] have investigated two designs of known volume velocity sources. One of the designs is based on the previously mentioned method by Salava, and uses two identical drivers put together face-to-face. The volume velocity can be estimated by summing up individual contributions of smaller patches each considered to be in rigid motion. The calibration is based on measurement of multiple point velocity - voice-coil voltage transfer functions using laser velocimetry. The volume velocity was then expressed in terms of an effective area. The disadvantage of such a calibration is that the effective area is not straightforward to measure, and the method requires access to a Laser Doppler Vibrometer. The second design uses an internal microphone installed in the driver's back cavity of precisely known volume which had to be designed and manufactured. Here the volume velocity was deduced from the internal pressure assuming a compliance law theoretically valid for small cavities of rigid walls. The two designs were compared using a single-point velocity as a reference measurement of volume velocity.

In this study the latter technique using an internal microphone was applied on a small off-the-shelf driver. In this case the calibration between pressure and volume velocity was not modelled, as done in [6], but instead had to be measured in dependence of frequency due to the presence of internal damping material and the effect of cavity resonances. Such a calibration is advantageous because the features of the driver's back cavity do not have to be known and may vary with frequency. The disadvantage is the need to independently measure the volume velocity which has turned out not to be a trivial task.

Four different calibration methods were compared in [7]. The first calibration was based on the laser velocimetry, as done in [6]. The technique was found difficult to apply on curved surfaces such as dome shaped diaphragms. Therefore the volume velocity was deduced from a single point velocity measurement in the centre of diaphragm. This requires rigidity of the diaphragm which is not met in practice. The second calibration was performed in a free-space, as done in [5], but using a large flat baffle to avoid radiation from the driver's enclosure. The accuracy of the measured data was found to suffer from baffle diffraction.

The inconveniences have prompted the authors to find alternative ways to calibrate the source. Two novel methods were thus conceived: a compression chamber technique and a blocked pipe technique. The

key advantage of the two methods, which will be described in detail in this paper, is that no assumptions are made regarding the shape or the vibration distribution of the driver's diaphragm.

2 METHOD

The principle of measuring transfer impedance based on an internal microphone is discussed in section 2.1. The transfer impedance is split into two transfer functions: a source function and a space function. A driver is characterised by its source function. In order to estimate the source function volume velocity has to be measured. The two methods for measuring the driver's volume velocity are discussed further on in section 2.2.

2.1 Internal pressure technique

If the volume of air inside the back cavity of the driver is tightly closed, and if its back enclosure is small and rigid, then sound pressure p inside of the cavity is effectively proportional to volume velocity Q of the diaphragm when it compresses and expands the interior air, $p \propto Q$. The assumption of a tightly closed cavity may not be fully true: drivers are often equipped with either a small vent or a porous diaphragm for the compensation of changing ambient pressure. Such a compensation is however practically ineffective where sound pressure is concerned and needs not be accounted for.

Using an internal microphone, the transfer impedance, Eq. 1, can be rewritten in a form suitable for experimental work. The transfer impedance will be split into two independent transfer functions: a source function Ψ which relates internal pressure $\hat{p}(\mathbf{i})$ to volume velocity $\hat{Q}(\mathbf{s})$ and a space function Ω which relates external pressure $\hat{p}(\mathbf{f})$ to internal pressure $\hat{p}(\mathbf{i})$

$$Z \equiv \Psi\Omega, \Psi = \frac{\hat{p}(\mathbf{i})}{\hat{Q}(\mathbf{s})}, \Omega = \frac{\hat{p}(\mathbf{f})}{\hat{p}(\mathbf{i})}. \tag{2}$$

Here $\mathbf{i}$ denotes the position of the internal reference microphone. A driver's diaphragm is characterised by its source function which is theoretically governed by compliance-like behaviour of the air inside of its back cavity. This transfer function depends on ambient factors such as temperature and will be discussed in detail in section 2.2.1. This characterisation procedure is therefore approximate as it depends on the ambiance.

2.1.1 Modelling the source function by a polynomial

A compliance-like behaviour implies that the source function is inversely proportional to frequency. A measured source function Ψ may in practice not have such an ideal behaviour and can be perturbed by noise. A remedy is to fit the source function to a polynomial

$$j\omega\tilde{\Psi} = \psi_0 + j\omega\psi_1 - \omega^2\psi_2 + \ldots, \tag{3}$$

of order N using a least squares fit were tilde [$\tilde{}$] denotes a fitted estimate [8]. The angular frequency is denoted by ω and the imaginary unit is denoted by j. A model of the source function is required in order to interpolate the data, as will be discussed in conjunction with the blocked pipe method in section 2.2. If the order N of the model is chosen too high, the polynomial over-fits the acquired data. A concern was therefore how to choose the order of the polynomial.

2.1.2 Interpreting the source function as a filter

A small volume inside the driver's back cavity may be represented as a filter [1]. Since the distance between the internal microphone and the diaphragm is small compared to the wavelength, $\|\mathbf{i} - \mathbf{s}\| \ll \lambda$, and assuming that the pressure inside of the cavity is spatially uniform at low frequencies the sound pressure at the driver's surface is $p(\mathbf{s}) \approx p(\mathbf{i})$. As the cavity has its own resonance frequencies the compliance-type behaviour will be valid at frequencies well below the first cavity resonance. At these frequencies the source function can be represented as an impedance of a damped one-degree of freedom system

$$\tilde{\Psi} \approx \frac{\hat{p}(\mathbf{s})}{\hat{Q}(\mathbf{s})} = \frac{1}{j\omega C} + R + j\omega M, \tag{4}$$

where the frequency independent and real valued constants are a compliance C, resistance R and inertance M [1]. The damping in the cavity, created by the incorporated absorbing layer, is accounted for in the resistance R. This impedance model, Eq. 4, suggests that the polynomial, Eq. 3, should be of second order.

2.2 Volume velocity estimation

The volume velocity, and thereby the source function, can be assessed in specific space conditions. In this investigation two spaces are considered: the first is a small compression chamber, and the second is interior of a closed pipe.

2.2.1 Compression chamber method

Let the driver's diaphragm be coupled to a small loss-less chamber of impenetrable surface such that the chamber's cavity is compressed and expanded by the vibrating diaphragm. Inside of the cavity density and pressure are related by

$$\frac{p}{p_0} = \left(\frac{\rho}{\rho_0}\right)^{\gamma}, \tag{5}$$

where the instantaneous pressure p is given by the sum of ambient pressure p_0 and sound pressure p_e [1]. The instantaneous density is denoted by ρ, the density at rest is denoted by ρ_0 and the ratio of specific heats is denoted by γ. The velocity is taken to be positive when the diaphragm moves into the volume V, in which case the internal air is compressed. The mass inside the chamber is conserved, and the volume velocity is related to the change of volume $dV = V_0 - V$ by $Q = \frac{\partial}{\partial t} dV$ given by

$$Q = \frac{\partial}{\partial t} V_0 \left[1 - \left(\frac{p_0}{p_0 + p_e}\right)^{\frac{1}{\gamma}}\right]. \tag{6}$$

The volume at rest, denoted V_0, should be known. The sound pressure is much smaller than the ambient pressure, and the equation can therefore be linearised using the following power series expansion [8]:

$$(1+x)^{\alpha} = 1 + \alpha x + \frac{\alpha(\alpha-1)}{2!} x^2 + \ldots. \tag{7}$$

If only the first two terms are taken into account the volume velocity, in the frequency domain, becomes

$$\hat{Q} = j\omega \frac{V_0}{\gamma p_0} \hat{p}_e. \tag{8}$$

Thus in the compression chamber's cavity sound pressure is proportional to volume displacement. Recall that the speed of sound is $c^2 = \gamma p_0/\rho_0$ [2]. Substituting γp_0 with $\rho_0 c^2$ and changing sign, considering expansion as positive sign, yields the result of Anthony and Elliot [6]. Introducing a pressure reference $\hat{p}_{\text{ref}}$ in the driver's back cavity yields the source function

$$\Psi = \frac{1}{j\omega} \frac{\rho_0 c^2}{V_0} \frac{\hat{p}_{\text{ref}}}{\hat{p}_e}. \tag{9}$$

The frequency range of this technique is limited by cavity resonances: the limiting frequency should be well below of the first resonance frequency to justify the hypothesis of uniform pressure distribution.

2.2.2 Blocked pipe method

Sound propagating in a cylinder of air with a radius a and length l inside of a rigid pipe at frequencies below the first cut-on frequency can be idealised as forth and back travelling plane waves [1]. The pressure fluctuation $\hat{p}$ inside the pipe is excited by the driver at the termination $x = l$. The particle velocity amplitude $\hat{u}$ at a cross-section x ($0 \leq x \leq l$) is

$$\hat{p} = \hat{A}_+ \mathrm{e}^{-jkx} + \hat{A}_- \mathrm{e}^{jkx}, \tag{10a}$$

$$\hat{u} = \frac{1}{\rho_0 c} \left(\hat{A}_+ \mathrm{e}^{-jkx} - \hat{A}_- \mathrm{e}^{jkx} \right). \tag{10b}$$

where $\hat{A}_+$ and $\hat{A}_-$ are the pressure amplitudes of two waves and k is the wavenumber. The subscript + denotes forth going waves, in the direction of the x-axis and taken to be towards the driver, and − back going waves, in the opposite direction. A non-planar centrally symmetric driver's diaphragm may excite many duct waves. At frequencies below the first cut-on frequency only plane waves will propagate and substantially contribute to volume velocity while other waves will decay. For a circular duct of radius a, the first cut-on frequency is given by $ka < 1.8$ [2].

Let the pipe termination at $x = 0$ be sealed by a rigid surface with a flush-mounted microphone embedded in it. The overtones of a closed pipe are given by $f_n = nf_0 = nc/(2l)$ where n is a positive integer. At half-order frequencies equal to $f_{n-0.5} = (n - 0.5)f_0$ the relationship between volume velocity $\hat{Q}$ at the driver and the blocked pressure $\hat{p}_b$ at the termination can be found from Eq. 10 to be

$$\hat{Q} = j(-1)^{n-1} \frac{\pi a^2}{\rho_0 c} \hat{p}_b. \tag{11}$$

No assumption regarding the shape or the vibration of the driver's diaphragm has been made in the above. The advantage of this expression is its independence of the distance between the driver and the blocked end. Such a distance is difficult to define if the driver has not a flat diaphragm. The source function for a blocked pressure in a pipe at the half-order frequencies $f_{n-0.5}$ is then

$$\Psi = -j(-1)^{-n+1} \frac{\rho_0 c}{\pi a^2} \frac{\hat{p}_{\mathrm{ref}}}{\hat{p}_b}. \tag{12}$$

3 EXPERIMENTS

A Morel EM1308 driver was bought off-the-shelf, a small hole was drilled in its back enclosure, and a microphone was fixed inside its back cavity using silicone rubber, Fig. 1. This particular driver has a convex dome-shaped diaphragm with a radius of 30 mm. The excitation signal was created by a noise generator, filtered through an analog filter, and then amplified. Thus in measurements of transfer functions the driver was fed with a band-pass limited white noise and a frequency estimate was obtained from the recorded signals by use of spectral densities [9]. A schematics of such a setup is shown in Fig. 2. In preceding experiments it was found that the limit of diaphragm displacement makes the driver inefficient below 100 Hz. The driver acts as a simple source up to about 1000 Hz. The frequency range of the analysis has thus been limited to the 100 Hz - 1000 Hz band.

The volume velocity estimation methods are discussed in section 3.1. The characterised driver is tested by measuring known transfer impedances in section 3.2.

3.1 Volume velocity estimation

Both experimental setups were realised by a front-added closed volume of air as shown in Fig. 3. Their practical implementation were however different.

In the first measurement, the compression chamber was made small to allow the use of simple pressure - volume velocity laws. It was assembled by two rectangular aluminium plates of 16 mm thickness clamped together face-to-face. In the first plate there was a $\varnothing 1/4$ inch hole, precisely adjusted to the microphone

Figure 1: View of the implemented driver's back enclosure equipped with a fixated reference microphone.

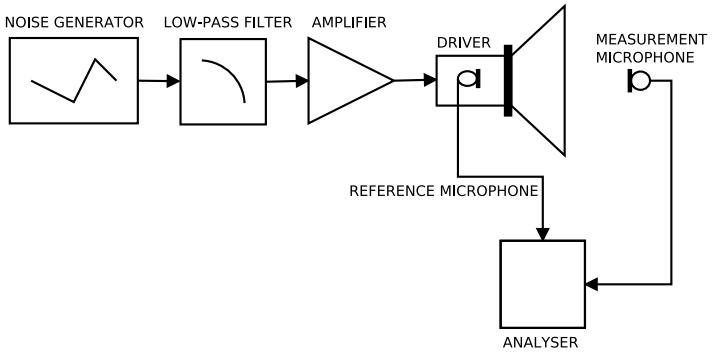

Figure 2: Schematic setup of transfer function measurements. The driver is fed with band-passed white noise and the microphones signals are recorded by a data acquisition system and thereafter the pressure - pressure relationship can be computed off-line.

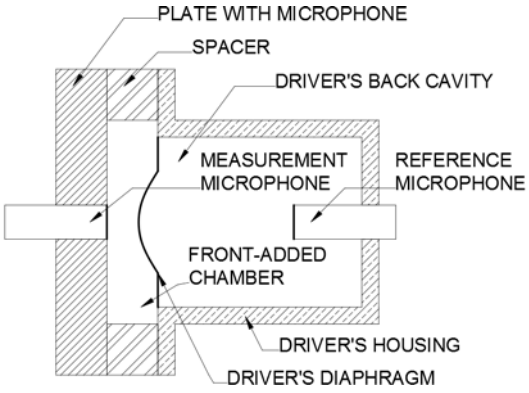

Figure 3: Schematic setup of source function measurement using a compression chamber. This layout also applies to the experimental setup using a blocked pipe, with the spacer replaced by the pipe.

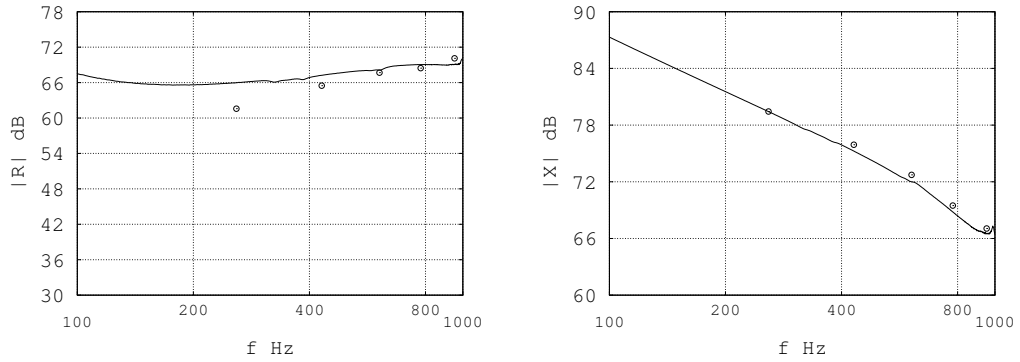

Figure 4: Measured source function, $\tilde{\Psi}$. Left: real part; right: imaginary part. Continuous line: compression chamber. ∘-marker: blocked pipe.

used to measure sound pressure in the chamber's cavity. In the second plate acting as a spacer there was a ∅80 mm cylindrical cut-out, an open air volume for fitting the driver. The centred driver was mounted with its diaphragm and rim entering the spacer cut-out. The cavity volume at rest was estimated using granular material of known density required to fill the cavity. Finally, the emptied cavity was sealed by the end plate equipped with a flush-mounted microphone. The assembly was done in such a way that the microphones were aligned to the axis of the driver.

In the second measurement, a blocked pipe was used as a cavity. It was made out of Plexiglas of internal radius 50 mm and internal length 990 mm. The pipe was sealed at one end by a circular Plexiglas plate in which there was a $\varnothing 1/4$ inch hole, precisely adjusted to the flush-mounted microphone used to measure sound pressure at the blocked end of the pipe. At the other end the centred driver was mounted in such a way that its diaphragm and rim could move freely.

3.1.1 Estimating the source function

The measured source functions are shown in Fig. 4. A fair comparison between the measurement methods would require that the experiments were done in a controlled environment. However, the measurement using a blocked pipe Ψ_{bp} was done one year after the measurement using a compression chamber Ψ_{cc}. This means that the ambiance was not the same in the two measurements, and the time-lag might have changed the driver's mechanical performance. Despite mentioned inconveniences, it was found that the measured source functions are similar except in the real part at the first half-order frequency in the measured 100 - 1000 Hz range. In this case, it is observed that the real part is a few dB under the measured value in the compression chamber. Note that the measurements agree well in the imaginary part of the source function. The similarities between the measurements, in view of measurement uncertainties such as the estimation of volume at rest of the compression chamber and the time-lag, suggests that the estimation of volume velocity is robust.

The fitted source functions, shown in Fig. 5, tend to agree in the imaginary part. It is seen that the frequency behaviour of the imaginary part is dominated by a compliance law as expected. Nonetheless, the transformation to a lumped element filter is not straightforward. The real part, which should have theoretically been zero, is frequency dependent and shows large mismatch between the two measurements. Due to the lack of a sufficiently long pipe to cover low frequency measurements, the large discrepancy of the real part at low frequencies is due to a poor extrapolation outside the polynomial fit range.

The difference between the two measurements was assessed from the quotient Δ between fitted source functions, $\Delta = \tilde{\Psi}_{\mathrm{bp}}/\tilde{\Psi}_{\mathrm{cc}}$. The differences in level and in phase are shown in Fig. 6. The differences are small, less than 1 dB and 0.1 rad, and either of the two characterisation method looks well adapted to the measurement of transfer impedances. The level difference in the real part R at low frequencies in Fig. 5 does not influence the overall difference in level because the imaginary part X of the fitted source functions dominates as expected $R \ll X$, $|\Delta| \approx |X_{bp}|/|X_{cc}|$.

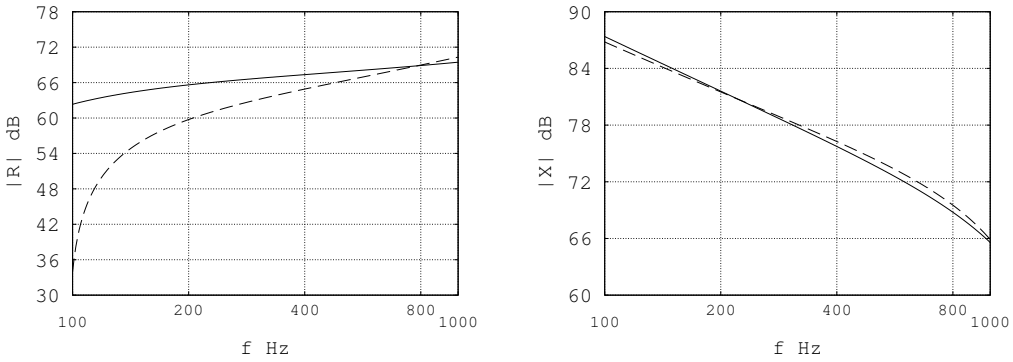

Figure 5: Fitted source function, $\tilde{\Psi}$. Left: real part; right: imaginary part. Continuous line: obtained from compression chamber measurement. Dashed line: obtained from blocked pipe measurement.

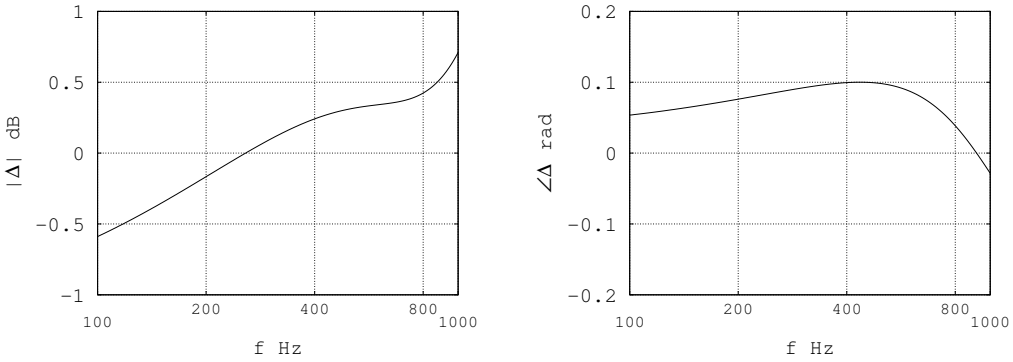

Figure 6: The quotient between the obtained source function using the blocked pipe method and the compression chamber method. Left: level; right: phase.

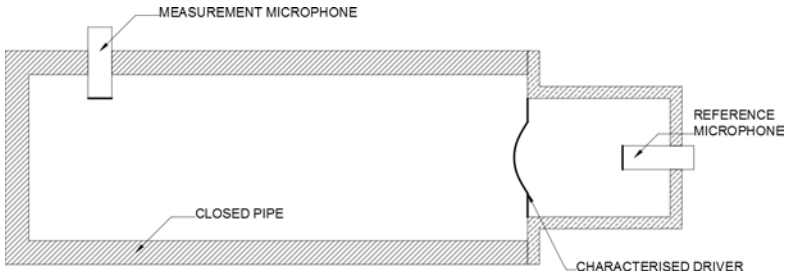

Figure 7: Schematic setup of space function measurement in a closed pipe.

3.2 Measurement of transfer impedances

The characterisation should not depend on the external loading of the driver. The two characterisation methods satisfy this requirement in principle. One way of checking the accuracy of the obtained source function is to measure transfer impedances in rather dissimilar spaces. The sound pressure in two such spaces was investigated; namely, inside of a closed pipe and in an anechoic room.

3.2.1 Driver set in a closed rigid pipe

The pipe previously used for estimating the source function was also used for measuring transfer impedance. A schematics of the experimental setup is seen in Fig. 7. This setup was modelled as a rigid piston

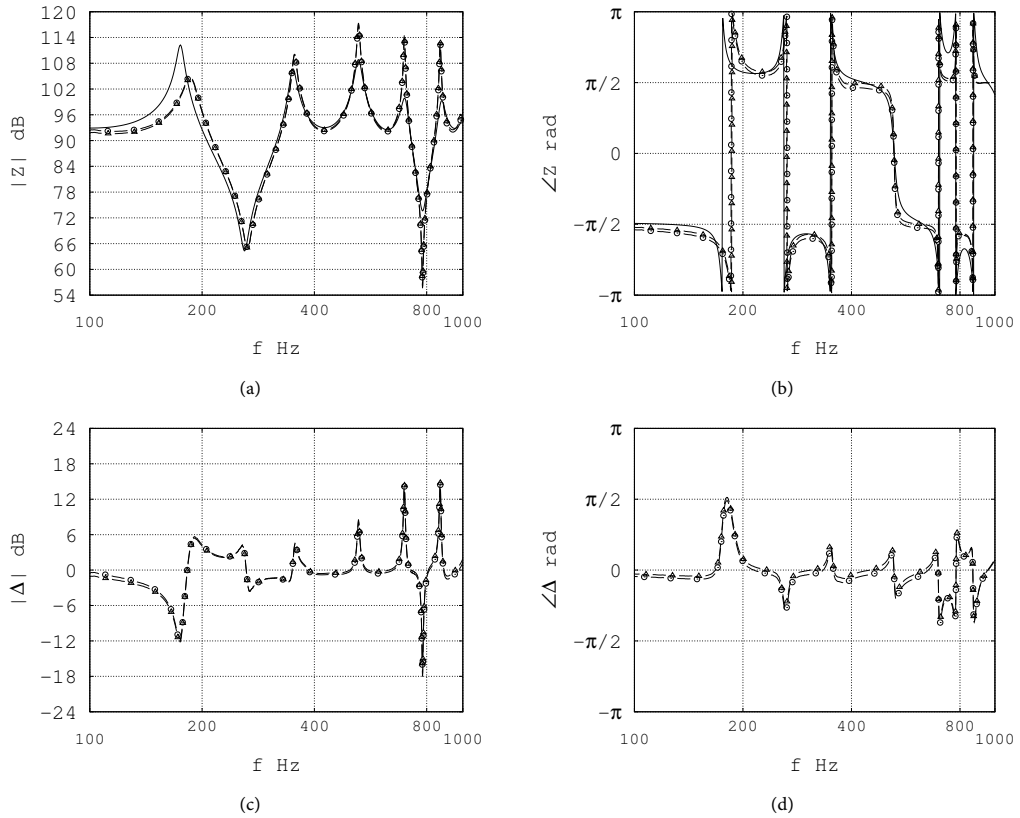

Figure 8: Sample transfer impedance measured in a blocked pipe: (a) level and (b) phase. Modelled: continuous line; measured using a compression chamber, ∘-marker, or a blocked pipe, △-marker. The quotient between measured and modelled estimates: (c) level and (d) phase.

in a pipe assuming travelling plane waves in analogy to section 2.2.2. The transfer impedance between the rigid piston at $x = l$, taking positive velocity when the piston is moving into the pipe, and a pickup at x, due to forth and back travelling plane waves, is given by

$$Z = -j\frac{\rho_0 c}{\pi a^2}\frac{\cos kx}{\sin kl}. \tag{13}$$

This can be deduced from Eq. 10 by setting $u(x = 0) = 0$ and $u(x = l) = -1/(\pi a^2)$. The assumption of a flat circular disk is not realistic due to the convex dome on the real driver, therefore the plane of the rigid piston is not well defined in the model. Furthermore the equivalent length of the pipe may be frequency-dependent as a result of non-planar excitation. Damping is introduced in the model by a complex speed of sound $c' = c(1 + j\eta/2)$ where the loss-factor η is a frequency dependent parameter [10]. For simplicity, the measured transfer impedance is compared to a fictitious pipe of 980 mm length and 4% loss-factor. The pickup was at 330 mm. The speed of sound is taken to be 343 ms^{-1} and the density of air 1.2 kgm^{-3}.

The modelled transfer impedance and its measured counterpart are shown in Fig. 8. The agreement in magnitude, away from the resonances, and in phase is quite satisfactory considering the inconveniences in the modelling. The frequency shift of the fundamental tone may be due to the existence of non plane waves inside the pipe. The first few overtones are correctly positioned, but the magnitude of the modelled transfer impedance is not quite correct due to unknown loss-factor. The matching confirms that the characterisation is consistent with measurement and that the driver can be used to measure transfer impedances.

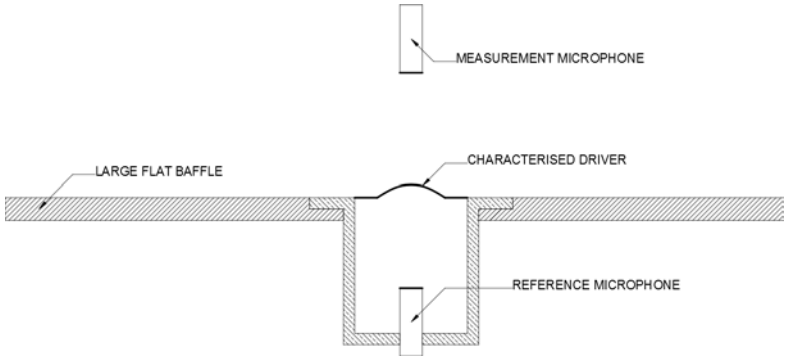

Figure 9: Schematic setup of space function measurement in an anechoic room.

3.2.2 Driver set in a rectangular flat baffle in an anechoic room

The driver was set in a large flat rectangular baffle 1350×1650 mm, made out of medium-density fibreboard and placed roughly in the centre of a large anechoic room. The driver was slightly offset with respect to the centre of the baffle. The experimental setup is seen in Fig. 9 and can be modelled at lower frequencies as a rigid piston in an infinite baffle. The transfer impedance on the axis of a rigid piston is [1]:

$$Z = -\frac{\rho_0 c}{\pi a^2}\left(\mathrm{e}^{-jk\sqrt{z^2+a^2}} - \mathrm{e}^{-jkz}\right), \tag{14}$$

here a is the piston's radius and z is the distance from the piston's center to the field point. This model is not fully realistic because it neglects edge effects of the finite baffle, which should be negligible only at wavelengths much smaller than the baffle size. Another issue with the simple model is that the convex dome-shaped diaphragm on the physical driver should not have the same near-field behaviour as a rigid piston, and the acoustic centre of the dome is moved towards the microphone pickup.

An example of a transfer impedance is shown in Fig. 10. The response was measured 50 mm from the baffle. The measured transfer impedance follows the computed one of a rigid piston. The agreement in magnitude and phase between measured and modelled transfer impedances looks satisfactory. It shows that the driver can be used to measure transfer impedances, and that the characterisation is reasonably invariant to external loading. This also suggests that the two calibration methods are comparable with free-space calibration.

In this particular experiment the measured space function contained small amplitude fluctuations with frequency. The behaviour is perhaps due to scattering from alien objects or imperfect baffle diffraction. The measured space function has been smoothed by a polynomial fit prior to estimating the transfer impedance. This has reduced the fluctuations while still representing the correct tendencies in the raw data.

4 DISCUSSION

The authors were looking for a practical measurement technique of transfer impedances using an ordinary driver. None out of several designs of known volume velocity sources found in the literature [3, 4, 5] has proved to be fully adequate for this task. The volume velocity of a driver can not be measured directly, and each design relies on a transducer producing an output which can be related to volume velocity. Such a transducer can be e.g. an additional measuring voice-coil or an accelerometer [4, 5]. The disadvantage of such transducers is that they make the assumption of rigidity which is not met in practice. Another design is to equip a driver with an internal microphone [6]. The microphone should theoretically produce a signal proportional to volume displacement of the driver's diaphragm. This cannot be achieved in an ordinary back-cavity design because of the presence of cavity damping and resonance.

Unlike in [6], the methods developed in this work require the internal microphone to be calibrated experimentally. It has been proposed in [6] that calibration can be carried out by summing up individual contributions of surface patches. Apart from requiring specific equipment, the disadvantage of such calibration is that the surface patches are considered to be in rigid motion and are quantified by a single point

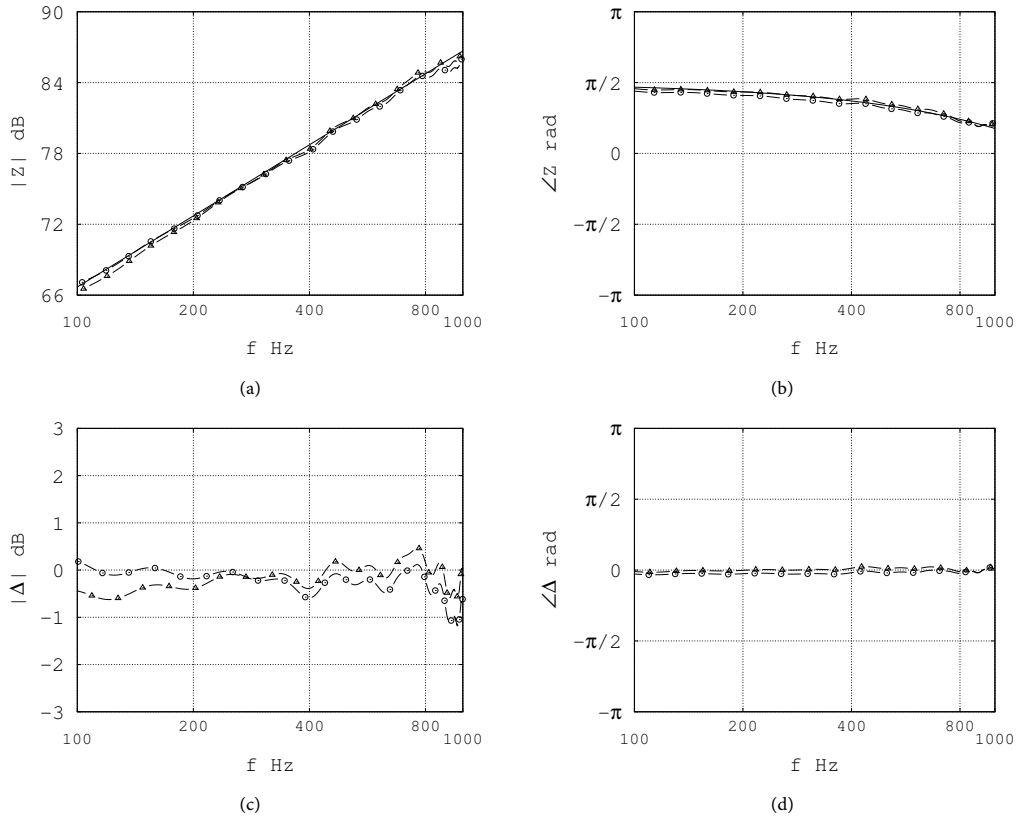

Figure 10: Sample transfer impedance measured in an anechoic room: (a) level and (b) phase. Modelled: continuous line; measured using a compression chamber, ∘-marker, or a blocked pipe, △-marker. The difference between measured and modelled estimates: (c) level and (d) phase.

velocity measurement. This calibration technique was found to be cumbersome in the case of a curved surface [7]. An alternative as done in [5] is free-space calibration. The advantage is that this technique is based on a simple law. The disadvantage of such an approach is that it requires access to an anechoic room. Furthermore it has been found that free-space calibration may suffer from radiation by the driver's back enclosure [7]. This can be shielded off by use of a baffle but risks to create unwanted diffraction phenomena.

The advantage of the two methods developed are that neither requires any specific equipment nor access to specific laboratory space. Perhaps the biggest advantage is that no assumption about the vibrating surface is needed, which is a property shared with the free-space calibration. The disadvantage of the compression chamber method is that in order to go up in frequency a very small calibration chamber is required. This makes the method sensitive to precise estimation of the calibration volume. The measurement using the blocked pipe method can be done only at discrete frequencies and thus requires interpolation. In order to reduce the frequency spacing and decrease the lower frequency limit of measurement a long pipe is necessary which may be a disadvantage. Thus, the two methods are complementary in the frequency domain.

Despite mentioned inconveniences the differences between the two calibration methods was found to be small. The identified source functions were applied in a in an anechoic room with satisfactory matching to modelled transfer impedances. This suggest that the two methods can be used as an alternative to free-space calibration.

5 CONCLUSIONS

Two calibration methods of a small volume velocity source have been developed. The source can be any small driver equipped with a sealed back cavity into which a microphone is installed. The calibration consists in finding the relationship between the sound pressure in the back cavity, measured by the microphone, and the volume velocity of the source produced by the driver's diaphragm. This relationship, which is theoretically given by a $1/f$ law for a small loss-less cavity, was found to deviate from it thus requiring an independent measurement of volume velocity. The latter is done in front of the diaphragm in an external cavity of rigid walls which allows obtaining the volume velocity from simple sound pressure measurements. Thus the entire calibration procedure consists in simultaneous measurement of two sound pressure signals. The external cavity used is either a small compression chamber of known volume or a long blocked tube. In both cases the relationship between the volume velocity and the measured sound pressure has been formulated in such a way to avoid dependence on either the geometry or the velocity distribution of the driver's diaphragm. Calibration by the two methods produced similar results. The volume velocity, once obtained by calibration, was then employed to compute transfer impedances in a closed pipe and in an anechoic room. The matching between the computed and measured transfer impedances was found satisfactory, suggesting that the two calibration methods are sufficiently accurate for use in engineering applications.

Acknowledgements

This work was co-funded by Volvo Construction Equipment. The funding is gratefully acknowledged. The free-space measurement was done at Applied Acoustics at Chalmers University of Technology in Sweden with the help of Patrik Andersson. The work was carried out at Laboratoire Vibrations Acoustique at INSA de Lyon in France, a member of the Centre Lyonnais d'Acoustique umbrella organization.

6 Bibliography

[1] L. E. Kinsler and A. R. Frey, *Fundamentals of Acoustics,* 2^{nd} *ed.*, (John Wiley & Sons, 1962).

[2] A. D. Pierce, *Acoustics - An Introduction to its Physical Principles and Applications*, (McGraw-Hill Book Company, 1981).

[3] F. J. M. Frankort, "Vibration and sound radiation of loudspeaker cones," Ph.D. Thesis, Delft University of Technology (1975).

[4] T. Salava, "Sources of the constant volume velocity and their use for acoustic measurements," J. Audio Eng. Soc. **22**, pp. 146 - 153 (1974).

[5] T. Salava, "Acoustic load and transfer functions in rooms at low frequencies," J. Audio Eng. Soc. **36**, pp. 763 - 775 (1988).

[6] D. K. Anthony and S. J. Elliott, "A comparison of three methods of measuring the volume velocity of an acoustic source," J. Audio Eng. Soc. **39**, pp. 355 - 366 (1991).

[7] A. Lindberg and G. Pavić, "Experimental characterisation of a small compression driver using an internal microphone," In Proc. of the International Conference on Noise and Vibration Engineering (ISMA), pp. 1111 - 1119 (2014).

[8] L. Råde and B. Westergren, *Mathematics Handbook for Science and Engineering,* 5^{th} *ed.*, (Studentlitteratur, 2004), pp. 232, 404.

[9] J. S. Bendat and A. G. Piersol, *Random Data - Analysis and Measurement Procedures*, (John Wiley & Sons, 1986).

[10] E. Skudrzyk, *The Foundations of Acoustics - Basic Mathematics and Basic Acoustics*, (Springer - Verlag, 1971).

Appendix IV

Experimental characterisation of a small compression driver using an internal microphone

The following appendix is based on "Experimental characterisation of a small compression driver using an internal microphone" published in the proceedings of the International Conference on Noise and Vibration Engineering (ISMA) (September 2014).

Abstract

A test of a small compression driver in an anechoic room suggested that it can be seen as a simple source at low frequencies. A simple source is characterised only by the volume velocity it produces. The estimation of volume velocity should not depend on external loading. The driver was therefore characterised using an internal pressure signal. The volume velocity was estimated using four idealisations: adiabatic process in a small closed chamber, travelling plane waves in a pipe, a free-space transfer impedance and a rigid diaphragm. The four methods produced similar results.

1 INTRODUCTION

A simple source is any source of sound which in a free-space creates an outgoing spherical wave. An approximate realisation of a simple source is a small compression driver. The basic requirements are that the driver is small compared to the wavelength and that its entire surface moves in phase [1]. In such a case the radiated pressure does not depend on the details of the vibrating surface and can be expressed by a point transfer impedance Z. Such an impedance relates volume velocity $\hat{Q}$ of the driver located at $\mathbf{s}$ to sound pressure $\hat{p}$ at $\mathbf{f}$

$$Z = \frac{\hat{p}(\mathbf{f})}{\hat{Q}(\mathbf{s})}. \tag{1}$$

The transfer impedance can be measured independently of the choice of driver provided that its volume velocity is known. A driver becomes inefficient when the frequency decreases, whereas at higher frequencies a driver develops pronounced directivity and thereby ceases to be a simple source [1].

Several methods have been reported for measuring volume velocity of small drivers. One approach is to measure the blocked electrical impedance of the driver and to deduce the velocity of the diaphragm, considered as a rigid surface, from the supply voltage [2]. Different concepts of constant volume velocity sources and their implementation have been described by Salava [3]. Anthony and Elliott [4] have compared two concepts of implementing known volume velocity sources: an implementation of Salava's source using two identical drivers put together and an implementation using an internal pressure microphone in the driver enclosure. They used laser velocimetry as a reference measurement of volume velocity.

In this study an off-the-shelf loudspeaker driver is used as a small sound source. The volume velocity is identified by measuring the sound pressure inside the driver's back cavity. The relationship between internal pressure and external volume velocity by the diaphragm is unknown and has to be found out.

The implementation of a known volume velocity source has been inspired by the demand for quantifying radiation of sound from vibroacoustic sources. The principle of the characterisation is to replace a complex vibroacoustic source by a simpler physically realisable substitute source for use in noise synthesis. It is presumed that the radiation by a vibroacoustic source can be represented by superposition of simple sources set in a rigid closed baffle of similar volume and shape as the original source. Such a characterisation critically depends on the knowledge of the source volume velocities.

2 INTERNAL PRESSURE METHOD

If the volume of air inside of the driver is tightly closed, and if its back enclosure is rigid, then sound pressure p inside of the enclosure is proportional to volume velocity Q evaluated at the front side when the oscillating diaphragm compresses and expands the interior air, $p \propto Q$. Using an internal microphone the transfer impedance, Equation 1, can be rewritten in a form suitable for experimental work. The transfer impedance will be split into two independent transfer functions; a so called source function Ψ which relates internal pressure $\hat{p}(\mathbf{i})$ to volume velocity $\hat{Q}$ and a space function Ω which relates external pressure $\hat{p}(\mathbf{f})$ to internal pressure $\hat{p}(\mathbf{i})$

$$Z = \frac{\hat{p}(\mathbf{i})}{\hat{Q}(\mathbf{s})} \frac{\hat{p}(\mathbf{f})}{\hat{p}(\mathbf{i})} = \Psi\Omega. \tag{2}$$

Here $\mathbf{i}$ denotes the position of the internal microphone. The source function $\Psi = \hat{p}(\mathbf{i})/\hat{Q}(\mathbf{s})$ characterises the loudspeaker driver and is theoretically governed by a compliance-like behaviour of the air inside of the back enclosure. Such a pressure-velocity relationship depends on the ambiance. The knowledge of the source function, once measured, is therefore approximate.

A compliance-like behaviour implies that the source function is inversely proportional to the frequency, $\Psi \propto 1/f$. In practice, the estimated source function $\tilde{\Psi}$ may not have such an ideal behaviour and contains noise. A remedy is to fit the source function to a polynomial

$$j\omega\tilde{\Psi} = \psi_0 + j\omega\psi_1 - \omega^2\psi_2 + \ldots, \tag{3}$$

of order N using a least squares approach. Tilde [˜] denotes that the source function is a modelled (fitted) estimate. If the order is chosen too high, the polynomial is over-fitted to the raw data.

3 ESTIMATION OF VOLUME VELOCITY

A simple source is characterised by the volume velocity it produces. Considering that the driver is normally used when flush-mounted in a closed baffle, the volume velocity of a physical driver is obtained by integration of normal component of velocity $\hat{\mathbf{v}} \cdot \mathbf{n}$ over the vibrating surface of the front D; i.e, the diaphragm and rim. This neglects the contribution of the vibrating back enclosure. Formally, volume velocity of the driver at $\mathbf{s}$ is [1]:

$$\hat{Q}(\mathbf{s}) = \int_D \hat{\mathbf{v}} \cdot \mathbf{n} \, dD. \tag{4}$$

The volume velocity, and thereby the source function, can be measured in specific conditions. In this investigation four measurement methods, carried out in four different spaces, are considered: the first is a compression chamber, the second is interior of a closed pipe, the third is in an anechoic chamber and the fourth is based on Laser Doppler Velocimetry in a room. In measurements of the source function Ψ the driver was fed with a band-pass limited white noise and an estimate of the source function was obtained from the recorded signals using spectral densities [5].

3.1 COMPRESSION CHAMBER METHOD

Consider a volume V of air inside of an impenetrable surface. Let the volume be compressed and expanded by a vibrating source which constitutes one part of the enclosure; i.e., the driver is flush-mounted with its diaphragm inside of a small closed undamped chamber. Density and pressure are related by

$$\frac{p}{p_0} = \left(\frac{\rho}{\rho_0}\right)^{\gamma}, \tag{5}$$

where the instantenous pressure p is given by the sum of ambient pressure p_0 and sound pressure p_e [1]. The instantenous density is denoted by ρ, the density at rest is denoted by ρ_0 and the ratio of specific heats is denoted by γ. The velocity is taken to be positive when the diaphragm moves into the volume, in which case the volume is compressed. The volume at rest is denoted by V_0. The mass inside of the chamber is conserved. The sound pressure is much smaller than the ambient pressure, and a linearised relationship, in the frequency domain, is

$$\hat{Q} = j\omega \frac{V_0}{\gamma p_0} \hat{p}_e. \tag{6}$$

It is seen that sound pressure is proportional to volume velocity inside of the compression chamber. It may be noted that the speed of sound is $c^2 = \gamma p_0/\rho_0$ [6]. Introducing internal pressure p_{ref} in the driver's enclosure yields the source function

$$\tilde{\Psi}_{\text{cc}} = \frac{1}{j\omega} \frac{\rho_0 c^2}{V_0} \frac{\hat{p}_{\text{ref}}}{\hat{p}_e}. \tag{7}$$

The frequency range of the technique is limited by the appearance of the first cavity resonance: the limiting frequency should be well below this frequency.

3.2 PIPE METHOD

Sound propagating in a cylinder of air with a radius a and length l inside of a rigid closed pipe at frequencies below the first cut-on frequency can be idealised as forth and back travelling plane waves [1]. The pressure fluctuation inside the pipe is excited by the driver at the termination $x = l$. The particle velocity amplitude $\hat{u}$ at a cross-section x ($0 \leq x \leq l$) is

$$\hat{u} = \frac{1}{\rho_0 c} \left(\hat{A}_+ \mathrm{e}^{-jkx} - \hat{A}_- \mathrm{e}^{jkx} \right), \tag{8}$$

where $\hat{A}_+$ and $\hat{A}_-$ are the pressure amplitudes of two waves and k is the wavenumber. The subscript + denotes forth going waves, in the direction of the x-axis and taken to be towards the driver, and − back going waves, in the opposite direction. For a circular duct of radius a, the plane waves assumption is valid away from discontinuities, at frequencies satisfying $ka < 1.8$ which is the cut-off value of first higher propagation mode [6].

Let the pipe termination at $x = 0$ be sealed by a rigid surface with a flush-mounted microphone embedded in it. The overtones of a closed pipe are given by $f_n = nf_0 = n\frac{c}{2l}$ where n is a positive integer. At frequencies equal to $f_{n-0.5} = (n - 0.5)f_0$ the complex relationship between volume velocity $\hat{Q}$ at the driver and the blocked pressure $\hat{p}_b$ at the termination can be found from Equation 8 to be

$$\hat{Q} = j(-1)^{n-1} \frac{\pi a^2}{\rho_0 c} \hat{p}_b. \tag{9}$$

No assumption regarding the shape or the vibration of the driver's diaphragm has been made in the above. The advantage of this expression is its independence of the distance between the driver and the blocked end. Such a distance is difficult to define if the driver has not a flat diaphragm. The source function for a blocked pressure in a pipe at the half-order frequencies $f_{n-0.5}$ is then

$$\tilde{\Psi}_{\text{bp}} = -j(-1)^{-n+1} \frac{\rho_0 c}{\pi a^2} \frac{\hat{p}_{\text{ref}}}{\hat{p}_b}. \tag{10}$$

3.3 ANECHOIC CHAMBER METHOD

Volume velocity can be estimated from pressure measurements in any space presuming that the transfer impedance is known; e.g., in a free-space the far-field pressure of a small driver can be assumed to be that of a simple source. A single measure of radiated sound pressure response $\hat{p}$ is sufficient to deduce the volume velocity $\hat{Q}$, which is inversely proportional to the transfer impedance Z. Hence, the volume velocity is

$$\hat{Q} = \frac{1}{Z}\hat{p}, \tag{11}$$

Measurements were done in an anechoic room using a large flat baffle. Measurements directly in a free-space would have been possible, but the back enclosure of the driver vibrates and radiates unwanted sound. It was considered that radiation from the diaphragm and from the back enclosure can be separated by the use of a baffle. The experimental setup approximates an hemispherical source set in an infinite baffle, and the transfer impedance is [1]:

$$Z = \frac{jk\rho_0 c}{2\pi}\frac{\mathrm{e}^{-jkr}}{r}. \tag{12}$$

The source function in a half-space, assuming that the source is a hemispherical source in an infinite baffle, is therefore

$$\tilde{\Psi}_{\mathrm{ac}} = Z\frac{\hat{p}_{\mathrm{ref}}}{\hat{p}} = \frac{jk\rho_0 c}{2\pi}\frac{\mathrm{e}^{-jkr}}{r}\frac{\hat{p}_{\mathrm{ref}}}{\hat{p}}. \tag{13}$$

3.4 DIRECT METHOD

The surface of the diaphragm and rim can be divided into non-overlapping patches of surface $D_1, \ldots, D_N$ forming the entire vibrating surface D. Using Laser Doppler Velocimetry the contribution of each surface patch can be summed up, and the volume velocity of the driver is given by

$$\hat{Q} = \sum_{i=1}^{N} \hat{v}_{\perp,i} D_i. \tag{14}$$

Such an estimate follows from direct discretisation of Equation 4. The normal velocity is denoted by $[_\perp]$.

From a practical point of view it is not straightforward to quantify the normal velocity. The reason is that the tested driver has a convex dome-shaped diaphragm. Measuring perpendicular to the surface is therefore prohibited. Because the diaphragm is small, one can consider a projection of the diaphragm onto the baffle, a circle of radius a, in which the driver is set. The only point on the diaphragm where the laser beam does not deflect, when measuring perpendicular to the baffle, is on the axis. The diaphragm had to be treated by putting a small piece of reflective tape on its axis, shown in Figure 1. The tape changes the mechanical properties of the diaphragm, and was left in its place after the measurement. Assuming that the driver can be modelled as an oscillating rigid surface it is sufficient to measure the normal velocity in a single point. Hence, the volume velocity estimate becomes

$$\hat{Q} = \pi a^2 \hat{v}_\perp. \tag{15}$$

The point velocity estimate is not quite realistic as the true vibration of the diaphragm is not accounted for; e.g., it is known that the normal velocity has to be lower at the rim than in the middle of the diaphragm even below break up. The point estimate is therefore biased. Once the diaphragm breaks up the point velocity estimate is not useful, but above the cut-on the driver ceases to be a simple source anyway and the characterisation is therefore not valid, independently of the choice of volume velocity estimation method. The source function, assuming a rigid surface, becomes

$$\tilde{\Psi}_{\mathrm{dm}} = \frac{1}{\pi a^2}\frac{\hat{p}_{\mathrm{ref}}}{\hat{v}_\perp}. \tag{16}$$

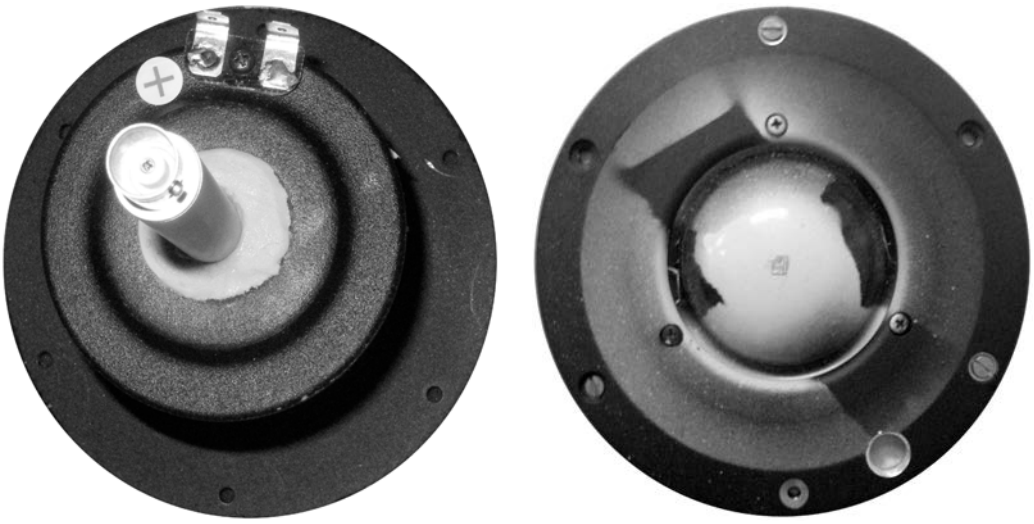

(a) (b)

Figure 1: Loudspeaker driver (a) enclosure equipped with measuring microphone and (b) diaphragm treated with reflective tape.

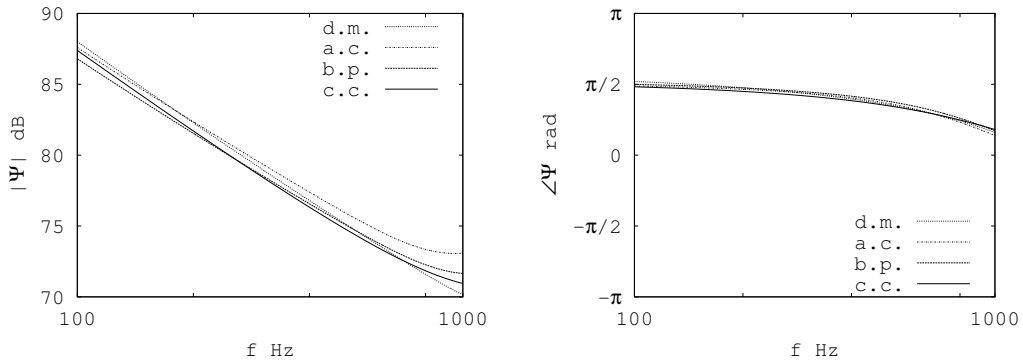

(a) (b)

Figure 2: Fitted source function estimates using different characterisation methods (a) level and (b) phase, legend: d.m. direct method, a.c. anechoic chamber, b.p. blocked pipe, c.c. compression chamber.

4 IMPLEMENTATION AND MEASUREMENT OF VOLUME VELOCITY

A microphone was inserted inside of a back-enclosed driver, shown in Figure 1. The driver has a convex dome-shaped diaphragm with a radius of 30 mm. The excitation signal was created by a noise generator, filtered through an analog filter, and then amplified. In preceding experiments it was found that the driver is not efficient below 100 Hz and acts as a simple source up to about 1000 Hz in which case the diameter corresponds to 1/6 of the wavelength.

A fair comparison between the estimation techniques would require that the experiments were done in a controlled environment. However, the measurement using a blocked pressure in a pipe was done about one year after the measurement using a compression chamber which might have changed the driver's mechanical performance. The fitted source functions $\hat{\Psi}$, using a polynomial of order two, are shown in Figure 2. There is a spread in magnitude between the methods, whereas the phase largely agrees.

The source function measured in an anechoic chamber, at a distance of 500 mm from the baffle, seems to be overestimating the level. The discrepancy increases with frequency, and compared with the estimate obtained using a compression chamber the level difference is about 2 dB at 1000 Hz. The reason for the

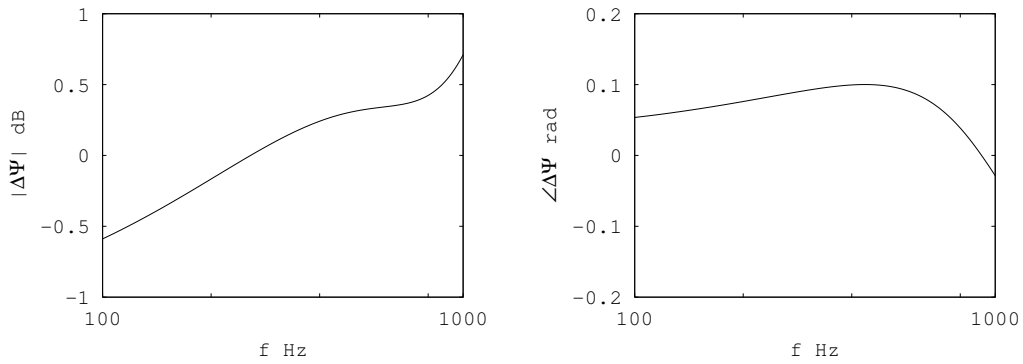

(a) (b)

Figure 3: Difference between fitted source function estimates using a blocked pipe and a compression chamber (a) level and (b) phase.

discrepancy should be further investigated.

The source function measured using a point velocity estimate is comparable with the ones given by a compression chamber and a blocked pipe. The point velocity estimate is slightly above in magnitude at low frequencies and does not show the same deviation from a compliance-law due to inertance at high frequencies as found by the other methods.

The remaining two methods, that of a blocked pipe and a compression chamber, tend to agree with each other. These two source functions agree in the imaginary part, which is dominated by a compliance law at low frequencies. The real part is frequency dependent and disperses more between the two measurements. The deviation from zero real part may be a consequence of damping treatments inside of the driver enclosure. To better assess the difference of the two types of measurements the ratio between the fitted source functions was taken $\Delta\Psi = \hat{\Psi}_{\text{bp}}/\hat{\Psi}_{\text{cc}}$. The difference in magnitude, given by $20\log_{10}|\Delta\Psi|$, and phase is shown in Figure 3. The difference is small, less than 1 dB and 0.1 rad. Either of the two characterisation method looks thus well adapted to the estimation of transfer impedances.

5 MEASUREMENT OF TRANSFER IMPEDANCES

The characterisation should not depend on the external loading of the driver. One way of checking the obtained source function is to measure transfer impedances in rather different spaces. The sound pressure in two different spaces was investigated; namely, inside of a closed pipe and in an anechoic room. Out of the four characterisation methods results are shown for the source function obtained in a compression chamber.

5.1 Driver set in a closed rigid pipe

The driver was set in one termination of a closed cylindrical pipe of radius 50 mm and length 990 mm made out of Plexiglas. The dome shaped diaphragm neither did fit snugly into the pipe nor was it perfectly centred. The experimental setup was modelled as a rigid piston in a pipe assuming travelling plane waves. The transfer impedance between the rigid piston at $x = l$, taking positive velocity when the piston is moving into the pipe, and a pickup at $x = z$ is given by

$$Z = -j\frac{\rho_0 c}{\pi a^2}\frac{\cos kz}{\sin kl}. \tag{17}$$

The assumption of a flat circular disk is not realistic due to the convex dome on the real driver. Therefore the plane of the rigid piston is not well defined in the model. The equivalent length of the pipe may be frequency-dependent as a result of non-planar excitation. Damping is introduced in the model by a complex speed of sound $c' = c(1 + j\eta/2)$ where the damping factor η should be a frequency dependent

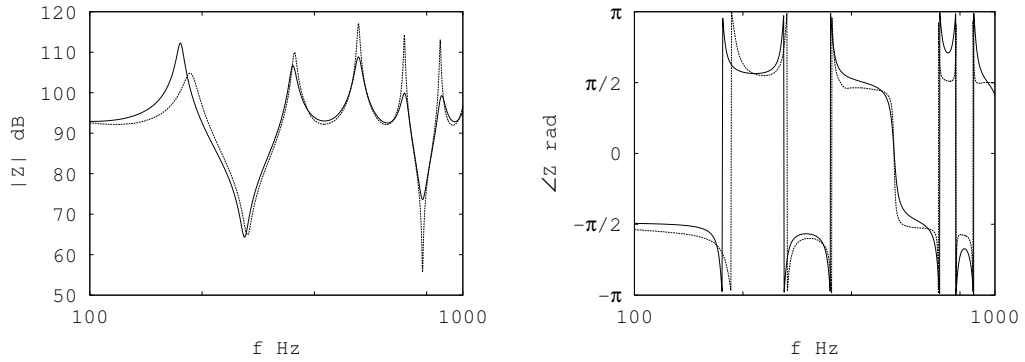

(a) (b)

Figure 4: Modelled, continuous line, and measured, dashed line, transfer impedance estimates in a closed pipe, (a) level and (b) phase.

parameter. For simplicity, the measured transfer impedance is compared to a fictitious pipe of 980 mm length and 4% damping factor.

The presumed transfer impedance and its measured counterpart are shown in Figure 4. The agreement in magnitude, away from resonances, and phase is in general quite satisfactory. The fundamental tone is shifted in frequency which may be due to the uncertainty of the pipe's length, or existence of non plane waves inside of the pipe. The first few overtones are correctly positioned, but the magnitude of the modelled transfer impedance is not quite correct due to assumption of constant damping factor.

5.2 Driver set in a rectangular flat baffle in an anechoic room

The driver was set in a large flat rectangular baffle 1350×1650 mm, made out of medium-density fibreboard, roughly in the centre of a large anechoic room. The driver was slightly offset with respect to the centre of the baffle. The sound pressure response was measured on the axis of the driver, 50 mm away from the baffle. The experimental setup can be modelled as a rigid piston in an infinite baffle. The on-axis transfer impedance of a rigid piston is

$$Z = -\frac{\rho_0 c}{\pi a^2}\left(\mathrm{e}^{-jk\sqrt{z^2+a^2}} - \mathrm{e}^{-jkz}\right), \tag{18}$$

this model may be more realistic than the assumption of a hemispherical source, Equation 12, near the source [1]. This model is still not quite realistic because it neglects edge effects of the finite baffle, which should be negligible only at wavelengths much smaller than the baffle size. Another issue with the simple model is that the convex dome-shaped diaphragm on the physical driver should not have the same near-field behaviour as a rigid piston, and the acoustic centre of the dome is moved towards the microphone pickup.

The measured transfer impedance, shown in Figure 5, follows the one of a rigid piston. The matching in magnitude and phase between measured and modelled transfer impedances looks satisfactory.

6 CONCLUSIONS

Four techniques were used to characterise a small driver in terms of its volume velocity. The volume velocity is measured using a microphone mounted in the driver's back cavity. Two techniques, using a blocked pipe or a compression chamber, were found to be well suited for estimating the pressure - velocity factor. The advantage of these two methods is that no assumptions is made regarding the shape of the diaphragm. The relationship between pressure and volume velocity, which should have been theoretically a $1/f$-function has been found to slightly deviate from it. Because the compression chamber and

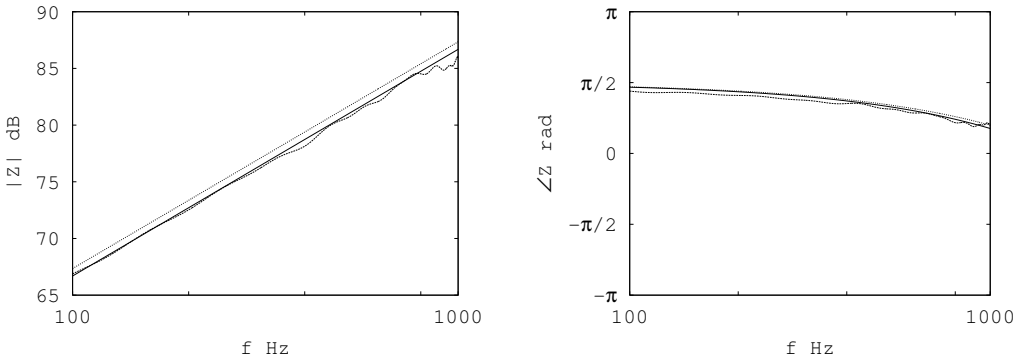

(a) (b)

Figure 5: Transfer impedance estimates in a free-space, (a) level and (b) phase. Continuous line: modelled rigid piston in a baffle; dotted line: modelled hemisphere in a baffle; dashed line: measured.

blocked pipe methods yield similar results in rather different spaces, the characterisation is shown to be independent of external loading.

Acknowledgements

This work was co-funded by Volvo Construction Equipment. The funding is gratefully acknowledged. The free-space measurement was done at Chalmers Tekniska Högskola in Sweden with help of Patrik Andersson and Börje Wijk.

7 Bibliography

[1] L. E. Kinsler and A. R. Frey, *Fundamentals of Acoustics,* 2^{nd} *ed.*, (John Wiley & Sons, 1962).

[2] F. J. M. Frankort, "Vibration and sound radiation of loudspeaker cones," Ph.D. Thesis, Delft University of Technology (1975).

[3] T. Salava, "Sources of the constant volume velocity and their use for acoustic measurements," J. Audio Eng. Soc. **22**, pp. 146 - 153 (1974).

[4] D. K. Anthony and S. J. Elliott, "A comparison of three methods of measuring the volume velocity of an acoustic source," J. Audio Eng. Soc. **39**, pp. 355 - 366 (1991).

[5] J. S. Bendat and A. G. Piersol, *Random Data - Analysis and Measurement Procedures*, (John Wiley & Sons, 1986).

[6] A. D. Pierce, *Acoustics - An Introduction to its Physical Principles and Applications*, (McGraw-Hill Book Company, 1981).

Part IV

Computation of transfer impedances

Appendix V

Computation of sound radiation by a driver in a cabinet using a substitute source approach

The following chapter is based on "Computation of sound radiation by a driver in a cabinet using a substitute source approach" published in the Journal of the Acoustical Society of America (Vol. 138, August 2015).

Abstract

Sound radiation by a driver set in a rigid closed cabinet is modeled analytically using the principle of wave superposition. The driver - cabinet assembly is replaced by an array of volumeless substitute sources — monopoles — confined within its surface. The role of substitute sources is to reproduce the sound field exterior to the surface as closely to the original field as possible. The frequency dependent positions and strengths of substitute monopoles are optimized by an iterative search procedure aimed at matching the prescribed surface boundary conditions of the original source. The time-consuming optimization of monopole positions is carried out at narrow-band center frequencies reducing the computational cost without significant loss of accuracy. The consistency of computed results is verified by checking the power output through the cabinet surface. Modeling is done for anechoic and semi-anechoic conditions. The model has been validated experimentally in a semi-anechoic room with satisfactory results using a mid-range driver set in a closed-box baffle.

1 INTRODUCTION

A loudspeaker consists of one or more drivers set in a cabinet. Sound radiated by such an assembly is governed not only by the acoustical features of the drivers and the surrounding space but also by diffraction from the cabinet. The extent to which the sound is diffracted depends primarily on the ratio between the cabinet's size and the acoustic wavelength[1]. Diffraction is negligible at wavelengths much longer than the cabinet's dimensions in which case the sound wave created by a driver appears to originate from a point source. On the contrary, at short wavelengths the cabinet acts as an infinite baffle. Both cases can be modeled using simple analytical formulae[2, pp. 153 - 185]. In-between these two extremes, i.e. at wavelengths comparable to the cabinet size, analytical modeling needs simplifications. An example of a simplified model is superposition of a monopole field and a dipole field [3]. To account for short wavelengths the analytical solution of either a piston[4, pp. 343 - 347] or a resilient cap[5] set in a rigid sphere can be used provided that the cabinet's aspect ratio allows for it. However, in most cases numerical modeling will be required.

A general model of a driver set in the surface of a closed rigid cabinet will be outlined in this paper. The driver will be considered to be small but the modeling approach is not limited to any particular driver's size or shape. The vibration pattern of the driver's radiating surface is inspired by works on piston radiators[6, 7]. The modeling will be demonstrated on a closed-box baffle representative of medium-sized loudspeaker designs.

Whereas the computation of sound radiation by a given driver - cabinet assembly can be done by commercially available software based on the finite element method or the boundary element method a lesser known method will be used: namely, the substitute source method[8, 9, 10]. This method provides an engineering tool for the computation of sound radiation which is well adapted to certain acoustical spaces, e.g. semi-anechoic spaces. The model can as a consequence relatively easily be extended to account for the presence of large hard reflecting surfaces which are sometimes encountered in practice. The method is based on superposition of waves created by volumeless sources, so called substitute sources. The substitute sources are adjusted in amplitude and phase to match the normal vibration on the assembly's surface. In [9] it is proved that the superposition integral is equivalent to the Helmholtz integral.

In the present work the substitute sources will be confined within the volume closed by the assembly's surface. The positions of the substitute sources are found via a convenient search procedure[11]. Alternatively, in simple cases the sources can be positioned across an internal surface[9, 12] or other selection approaches such as genetic algorithms[13] or particle swarm optimization[14] can be employed. The superposition principle can also be formulated directly in the time domain [15].

An advantage of the substitute source method, using sources positioned inside of the assembly, is that the computational errors regarding pressure and particle velocity are related to each other and can be quantified by the normal velocity error at the assembly's surface[12]. This was illustrated using the notion of an "error wave" resulting from the difference between prescribed and obtained normal velocity. It was found that the normal velocity error serves as an indicator of the magnitude of the error wave. Therefore as long as the substitute sources closely match the prescribed vibration the radiated field is nearly correct[12]. Finally, the method does not rely upon any particular software. The authors have implemented it in open source GNU Octave under Linux. This autonomy gives transparency to the approach: the user carries out the computation entirely by himself and is, as a consequence, in control of modeling details.

The substitute source positions are selected by the search algorithm from a non-uniform grid of candidate points. The density of these grid points varies in dependence of the velocity distribution over the surface of the assembly. In the vicinity of high gradients of normal velocity, i.e. close to the driver, the grid is denser than elsewhere. The cost function used in the search is the difference between the prescribed normal vibration velocity across the surface of assembly and the normal acoustical velocity created by the substitute sources. The described procedure was employed due to its ease of implementation and familiarity to the authors. Furthermore the power leakage through the cabinet, theoretically equal to zero, is employed as an additional check of the strengths of the substitute sources.

The outlined model is an offspring of research on airborne characterization of a complex machine radiating noise by vibration of its housing. The model is conceived for engineering applications, such as sound synthesis aimed at either auralization[16] or virtual prototyping[17], in which the industrial source has to be characterised by measurement. This can be done by a dummy source approach[18]. In this approach the housing is represented by a rigid closed cabinet of similar volume but simplified overall shape. The dummy is equipped with an array of small drivers. Such an acoustical counterpart is supposed to produce a sound field close to that of the original source by accounting for both radiation and diffraction. The identification of the source strength of each driver requires the knowledge of the field radiated by a driver mounted in a cabinet (transfer impedance) which is the principal subject of this paper. However, the approach can be used in other applications such as loudspeaker design.

The modeling principles are described first, section 2. This is followed by two case studies of sound radiation by a driver embedded in a closed-box baffle. The first case study, section 3, is a numerical study of radiated sound pressure and sound power in anechoic and semi-anechoic conditions. In the second case study, section 4, computed transfer impedances are validated experimentally.

2 NUMERICAL MODEL OF A DRIVER - CABINET ASSEMBLY

The driver - cabinet assembly will be modeled as a closed box of dimensions l_1, l_2 and l_3 set in a free-space. The center of the box $\mathbf{x}$ is placed at the origin $\mathbf{\Omega}$ of the space, i.e. $\mathbf{x} = (0, 0, 0)$, and the edges of the box are aligned with the coordinate system defined by orthonormal vectors $\mathbf{e}_1$, $\mathbf{e}_2$ and $\mathbf{e}_3$. On one face of the otherwise passive surface of the box is embedded a vibrating circular disk of radius a centered in a point

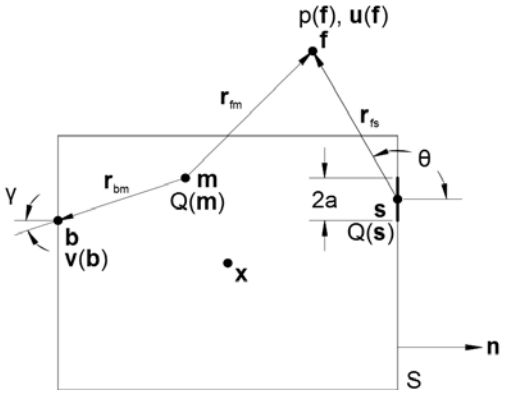

Figure 1: Schematic representation of a vibrating flat circular disk set in a rigid closed cabinet.

s. This point will be referred to as the source position. The active disk with the passive enclosure form the driver - cabinet assembly. A schematic representation of the radiation model is shown in Fig. 1.

The assembly is replaced by an array of monopoles confined within the volume defined by its surface. Assuming sinusoidal time variations, pressure amplitude $\hat{p}$ and particle velocity amplitude $\hat{\mathbf{u}}$ at a reception point $\mathbf{f}$ in a free-space due to an array of M monopoles located at $\mathbf{m}_1, \ldots, \mathbf{m}_M$ are given by

$$\hat{p}(\mathbf{f}) = \sum_{m=1}^{M} jk\rho_0 c \frac{\hat{Q}_m}{4\pi} \frac{\mathrm{e}^{-jkr_m}}{r_m}, \tag{1a}$$

$$\hat{\mathbf{u}}(\mathbf{f}) = \sum_{m=1}^{M} \frac{\mathbf{r}_m}{r_m} \frac{\hat{Q}_m}{4\pi} (1 + jkr_m) \frac{\mathrm{e}^{-jkr_m}}{r_m^2}, \tag{1b}$$

where $\hat{Q}_m$ is the volume velocity and the subscript m denotes a monopole [2, pp. 153 - 185]. The hat [ˆ] denotes an amplitude, the imaginary unit is denoted by j, the wavenumber k is given by ω/c where ω is the angular frequency, the density at rest of the ambient fluid is denoted by ρ_0, and the speed of sound is denoted by c. The distance between the m^{th} source and the reception point is $r_m = \| \mathbf{r}_m \|$ where $\mathbf{r}_m = \mathbf{f} - \mathbf{m}_m$. It is further assumed that the radiated sound pressure is of small amplitude, and that sound propagation takes place in a lossless homogeneous medium.

The particle velocity amplitude field $\hat{\mathbf{u}}$, $\hat{\mathbf{u}} = (\hat{u}_1, \hat{u}_2, \hat{u}_3)$, created by the substitute sources has to reproduce the surface vibration amplitude field $\hat{\mathbf{v}}$ in the direction of outward unit normal $\mathbf{n}$ at any point $\mathbf{b}$ on the surface S of the box[19, pp. 100 - 103, 153 - 207]

$$\hat{\mathbf{u}} \cdot \mathbf{n} = \hat{\mathbf{v}} \cdot \mathbf{n}. \tag{2}$$

This is the fundamental assumption of the synthesis, which together with Eqs. 1 enables the computation of the radiated sound field [9, 10, 11].

2.1 Search procedure

Except in special cases, any finite number of substitute sources will be unable to exactly reproduce the original sound field. The objective thus is to find a solution which produces a tolerable numerical error. Since the computational effort increases with the number of substitute sources involved, a tradeoff should be found between the number of sources and the numerical accuracy.

There is no rational way of finding how many substitute sources are needed, nor where they should be located. Moreover, the optimal number of sources and their positions are both wavenumber and geometry dependent. Therefore the substitute sources are chosen out of a prescribed set of candidate sources spread out in the entire vibrating body [11].

The volume inside of the surface of the box where substitute sources can be positioned will be referred to as the "solution space". The substitute sources are found by a "greedy search"[11] where the best source

positions are selected from a group of K preset candidate points $\mathbf{m}_1, \ldots, \mathbf{m}_K$ inside of the surface. The particle velocity is monitored across the surface in a number of control points. The best fit corresponds to the candidates producing the sound field which most closely matches the prescribed velocity at the control points. This velocity is assumed to be zero all over the surface S except at the disk surface D. The modeling error is the difference between prescribed normal velocity at control points and that obtained from the selected substitute sources.

The normal velocity prescribed at control points $\mathbf{b}_1, \ldots, \mathbf{b}_N$ at the surface of the box is represented by a vector $\hat{\mathbf{v}}_\perp$ $(N \times 1)$ with its n^{th} element given by $\hat{v}_{\perp,n} = \hat{\mathbf{v}}(\mathbf{b}_n) \cdot \mathbf{n}(\mathbf{b}_n)$. The subscript $[_\perp]$ indicates motion perpendicular to the surface. In order to find the source strength distribution $\hat{\mathbf{Q}}$ $(M \times 1)$ at the end of the M^{th} iteration step, $1 \leq M \ll K$, all selected monopoles are tuned to best reproduce the prescribed normal velocity $\hat{\mathbf{v}}_\perp$. This is done by finding the solution to

$$\mathbf{T}\hat{\mathbf{Q}} \approx \hat{\mathbf{v}}_\perp \tag{3}$$

by a least squares approach [20]; i.e., $\hat{\mathbf{Q}} = \mathbf{T}^+\hat{\mathbf{v}}_\perp$ were the plus $[^+]$ denotes a pseudoinverse. The number of control points is chosen to be several times larger than the number of monopoles in order to produce a smooth matching across the surface, $M \ll N$. Each element in the transfer matrix $\mathbf{T}$ $(N \times M)$ corresponds to the outward normal component of particle velocity at $\mathbf{b}_n$ originating from a monopole of a unit volume velocity at $\mathbf{m}_m$. An element of $\mathbf{T}$ reads:

$$T_{nm} = \frac{1}{4\pi}(1 + jkr_{nm})\frac{\mathrm{e}^{-jkr_{nm}}}{r_{nm}^2}\cos\gamma_{nm}. \tag{4}$$

The radius vector is given by $\mathbf{r}_{nm} = \mathbf{b}_n - \mathbf{m}_m$ and γ_{nm} is the angle between the normal vector $\mathbf{n}_n$ and the radius vector. In general there is no exact solution to Eq. 3. The difference between prescribed and obtained normal components of velocity, $\hat{\mathbf{u}}_\perp = \mathbf{T}\mathbf{T}^+\hat{\mathbf{v}}_\perp$, is given by the residual vector, $\Delta\hat{\mathbf{u}}_\perp = \hat{\mathbf{u}}_\perp - \hat{\mathbf{v}}_\perp$. This residue can be expressed by a single value as a normalized residual velocity in dB given by

$$e_u = 10\log_{10}\frac{\Delta\hat{\mathbf{u}}_\perp^*\Delta\hat{\mathbf{u}}_\perp}{\hat{\mathbf{v}}_\perp^*\hat{\mathbf{v}}_\perp}. \tag{5}$$

The asterisk $[^*]$ denotes a complex conjugate transpose. The value e_u is used in each search step as a cost function to select the best fit monopole, and to quantify the performance of the array.

An accurate computation reproduces the normal velocity almost correctly at control points but the error in-between these points could be large if the density of control points is insufficient [12]. Therefore the comparison between prescribed and obtained normal velocity will be made at error points across a denser grid than that of control points. A schematic representation of control and error points is shown in Fig. 2.

2.2 Velocity distribution

Normal motion of a driver can be fairly complex. The moving surface of a driver consists of a diaphragm and a surround supposing that the frame does not move. Frankort[21, pp. 1 - 15 and 165 - 166] has shown that sound radiation by a cone-shaped diaphragm can be modeled at low frequencies as being generated by a rigid piston and that axisymmetric vibration is a reasonable assumption.

A physical driver is more realistically approximated by a profile other than uniform as the normal velocity at the surround has to be lower than in the center of the diaphragm. Let the vibrating surface of the driver be a circular disk of radius a in axisymmetric but non-uniform motion. The normal velocity profile on the disk $\hat{\mathbf{v}} \cdot \mathbf{n} = \zeta(\sigma)H(a-\sigma)$ depends only on the distance σ from a point $\mathbf{b}$ on the disk to the center of the disk at $\mathbf{s}$, $\boldsymbol{\sigma} = \mathbf{b} - \mathbf{s}$. The Heaviside step function is denoted by H. Greenspan[7] considered normal velocity profiles of the form

$$\zeta(\sigma) = \frac{1}{\pi a^2}(n+1)\left(1 - \frac{\sigma^2}{a^2}\right)^n, \tag{6}$$

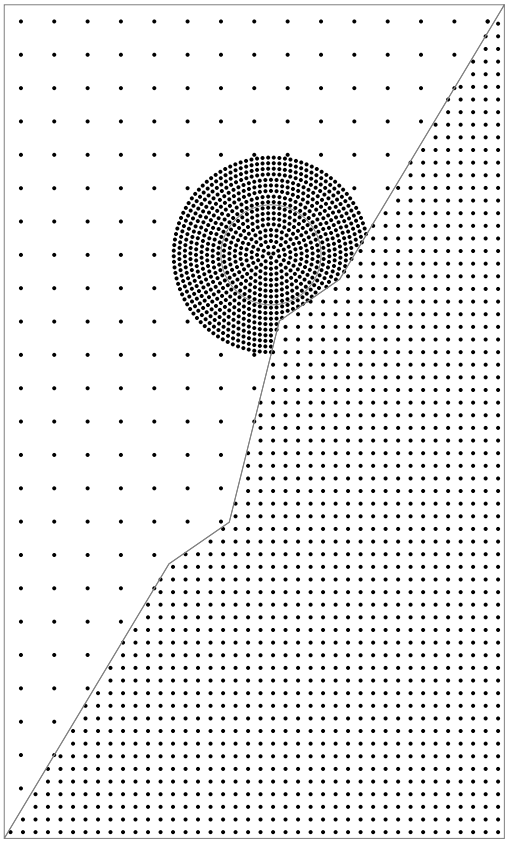

Figure 2: Schematic representation of the box face with the disk: upper-left, control points; lower-right, error points.

which produce unit volume velocity. The profile order n is an integer. The zeroth order corresponds to a rigid piston $\zeta(\sigma) = \alpha$ where the velocity constant is $\alpha = 1/(\pi a^2)$. The first order corresponds to a simply supported disk and the second order to a clamped-edge disk.

Motion of a physical driver can cause vibration on the cabinet which in turn will radiate sound. This phenomenon is here neglected; the cabinet surface is assumed not to move and to act only as an obstacle to the propagating sound. At a rigid surface the normal component of particle velocity should vanish[19, pp. 100 - 103], $\hat{\mathbf{v}} \cdot \mathbf{n} = 0$.

2.3 Discrete representation

Modeling of a driver in a cabinet by the substitute source method requires a double selection: that of control and error points across the surface of the box as well as that of candidate source points in the solution space. A non-uniform distribution of control points is used on the surface S of the box by taking densely spaced control points on the disk D and more sparsely spaced control points on the cabinet C. A similar non-uniform distribution of candidate source points is prescribed in the solution space with a higher density close to the circular disk. The increase in density of control and candidate points close to or at the disk is done in view of significant velocity change in-between vibrating and passive surface regions. Once the substitute sources have been positioned and their volume velocities computed, the computation is verified in densely distributed error points on the surface S. A schematic representation of candidate points is shown in Fig. 3.

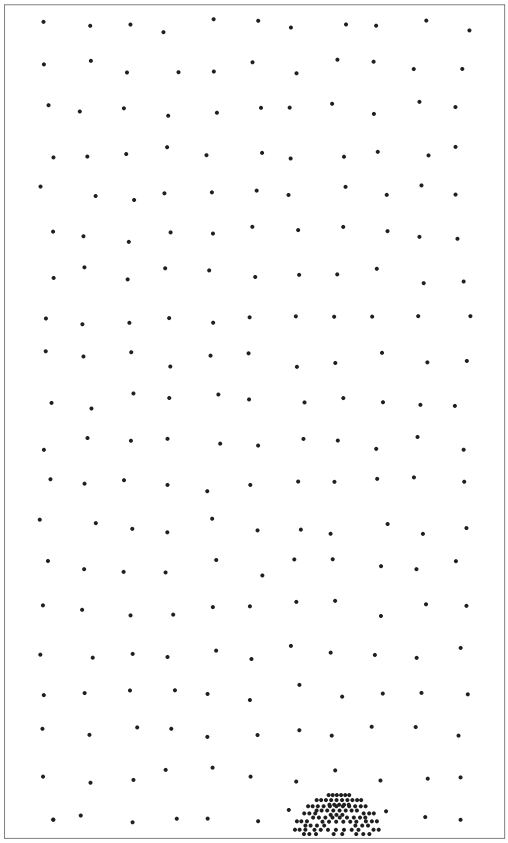

Figure 3: Schematic representation of candidate points through a layer of the solution space.

2.3.1 Control points

Control points were prescribed on the box by joining high density points on the driver with low density points on the cabinet.

The surface D of the driver was represented by a circular disk of radius $A \geq a$ partitioned by annular sector surface patches. Only the active disk section of radius $\sigma \leq a$ represents the vibrating surface. A passive annulus $a < \sigma \leq A$ complements the circular disk and sets the velocity profile to zero. The non-overlapping patches were chosen to be of almost equal areas such that the entire surface of the disk was formed. This was achieved by keeping a constant radial step and rounding the number of circumferential steps to a closest integer. A control point was positioned in the center of each patch.

The surface C of the cabinet was divided into non-overlapping rectangular patches forming the entire surface S of the box. The patches were of about the same area, and a point was put in the center of each patch. No points were put along the edges as the normal vector is not well defined there. The points representing the cabinet were taken to be all points on the box not lying in the circular disk.

2.3.2 Candidate points

Candidate points, located in the interior of the box surface, were created in an analogous manner; i.e., by selecting a high density of points near the disk and lower density elsewhere. A dense grid of candidate points over the entire volume of the box would have led to a large computation effort at no major improvement of computation accuracy.

The dense candidate points were located within a ball centered at the disk center and divided into concentric spheres of uniformly decreasing radius. Each sphere was divided into surface patches of about the same area. A candidate point was put in the center of each patch. Only the ball points interior to the box were kept.

The rest of the candidate points in the solution space were placed on a uniform base-grid outside of the half-ball volume. Thereafter the two groups were merged.

2.3.3 Error points

If the spacing between control points is too large the obtained normal velocity between control points might deviate a lot from what it should be without penalizing the normalized residual velocity. This may produce an effect of secondary radiation from the cabinet body potentially invalidating the computation.

The computation is checked using error points in-between control points. Since the prescribed normal velocity is known at the surface of the box the residual $\Delta u = u_\perp - v_\perp$ can be evaluated anywhere across this surface. The entire box surface was divided into very small non-overlapping surface patches of nearly identical areas. Error points were distributed at the center of the patches. Thus the reconstruction error can be assessed as discussed in section 2.4.

The patches associated to error points serve to evaluate the sound power output of the box. This is used to quantify power leakage as discussed in section 2.5.

2.4 Reconstruction error

The computation of normal velocity is little time consuming compared to the search procedure. Thus a dense grid of error points on the box can be afforded. The reconstruction error in dB is given by Eq. 5, evaluated at error points, and quantifies the overall performance of the computation.

2.5 Power leakage

The power output can be separated into contributions by the driver D and the cabinet C. The total radiated power is obtained by integrating sound intensity across the surface

$$\Pi = \int_S \mathbf{I}\cdot\mathbf{n}\,dS = \int_D \mathbf{I}\cdot\mathbf{n}\,dD + \int_C \mathbf{I}\cdot\mathbf{n}\,dC, \tag{7}$$

where the time averaged intensity is given by $\mathbf{I} = 0.5\Re\{\hat{p}\bar{\hat{\mathbf{u}}}\}$ [19, pp. 39 - 47]. The bar denotes a complex conjugate and $\Re\{\ldots\}$ the real part.

The breakdown is henceforth written $\Pi_S = \Pi_D + \Pi_C$. The total radiated power should be contributed only by the vibrating circular disk, $\Pi_S = \Pi_D$, while the power contributed by the surface C should ideally be zero. The field created by substitute sources cannot make the power through the baffle completely vanish. This power leakage can be estimated by transforming the integrals above into discrete sums over the surface patches already defined. The powers through the entire surface Π_S and the one contributed by only the circular disk Π_D are approximated by

$$\Pi_S \approx \sum_S \langle\mathbf{I}\rangle\cdot\mathbf{n}\,dS, \qquad \Pi_D \approx \sum_D \langle\mathbf{I}\rangle\cdot\mathbf{n}\,dD. \tag{8}$$

The chevrons $\langle\ldots\rangle$ denote that a value representative for the entire patch is used. Such a value can be obtained by taking the intensity in the center points of the patches. All patches that have at least one node inside of the prescribed circular disk are taken as belonging to the disk. The power leakage is quantified in dB by

$$e_C = 10\log_{10}\frac{\Pi_D}{\Pi_S}. \tag{9}$$

If there is no leakage, the leakage error is zero dB.

2.6 Power deviation

Apart from the discussed reconstruction error and power leakage, it is interesting to quantify: (1) the lower frequency limit at which the closed-box baffle approximates an infinite baffle, and (2) the upper frequency limit for which the disk approximates a simple source. At frequencies beyond the first limit sound radiation

may be modeled using an infinite baffle, e.g. by applying the Rayleigh integral formula[19, pp. 213 - 215]. This limit can be found from the deviation in power output from a circular disk set in a closed-box baffle, Π_S, and an infinite baffle, Π_∞. The power deviation is given in dB by

$$\Delta\Pi = 10\log_{10}\frac{\Pi_S}{\Pi_\infty}. \tag{10}$$

The total power radiated by a disk in an infinite baffle depends on the disk vibration but at low ka-values the power output of a rigid piston, a simply supported disk and a clamped-edge disk are governed by the same leading term [7]. This term corresponds to the power output of a pulsating hemisphere

$$\Pi_h = \frac{\rho_0 c k^2}{4\pi}\hat{Q}_h^2 \tag{11}$$

where $\hat{Q}_h = \pi a^2 \alpha$ is the volume velocity [2, pp. 153 - 185]. This power output will be used as a reference of power output of a disk in an infinite baffle, $\Pi_\infty \approx \Pi_h$. For the second limit, the power deviation between Π_∞ and Π_h indicates that the disk is no longer a simple source and should not be used to compute transfer impedances. The power output for the case of an infinite baffle, Π_∞, will be discussed in App. A.

2.7 Remarks on modeling

The operation with the matrix $\mathbf{T}$ relating M monopoles to N control points used by the search algorithm, in Eq. 3, might suffer from numerical instabilities at certain frequencies causing intolerably large reconstruction error. The origins of these instabilities are not fully understood at this stage, and should be subject to further work, but suggest an algorithm difficulty in selecting a monopole array suitable for the searched frequency. A remedy against the instabilities is to modify the grid of the candidate points. This can be done by changing the spacing Δ between points in the base-grid.

The total number of candidate points is roughly given by $K \approx V/\Delta^3$ where V is the box volume. It follows that grid refinement highly penalizes the computation time. An alternative technique is to replace the regular spacing by an irregular one without altering the number of candidate points. Such a grid can be obtained by offsetting each point in the regular base-grid in a random direction by a small random distance. The positions of the candidate points lying in the half-ball do not need to be randomized because the grid in this zone is not uniform anyway.

This concludes the description of the numerical model of free-space radiation by a driver in a cabinet. In the following part two case studies will be presented: a numerical one with the modeling extended to the case of half-space radiation, §3, and an experimental one, §4.

3 SOUND RADIATION FROM A CLOSED-BOX BAFFLE

A box of dimensions 300 × 232 × 500 mm equipped with a vibrating disk of radius 30 mm was modeled. This is representative of medium-sized off-the-shelf loudspeaker designs. At the disk surface a smooth velocity profile was prescribed (a clamped-edge disk). This disk is expected to be a simple source for the computation of transfer impedances.

3.1 Numerical setup

The frequency range was chosen between 10 Hz and 1000 Hz with a step of 1 Hz. Since the optimized monopoles' positions depend on the frequency, a particular technique was applied to avoid too lengthy searches at each frequency. The entire frequency range was divided into 50 Hz bands and the search was done at band center frequencies: 25, 75, ... and 975 Hz. These frequencies are henceforth called search frequencies. In each band the volume velocity distribution was thus computed at a number of frequencies, henceforth called band frequencies, using the fixed monopoles' positions identified at the corresponding search frequency. This procedure greatly reduces the computation time and is common to all computations presented further on. Stop criteria of the search algorithm were chosen to be, whichever comes first, a maximum number of 500 monopoles or a normalized residual velocity lower than -40 dB.

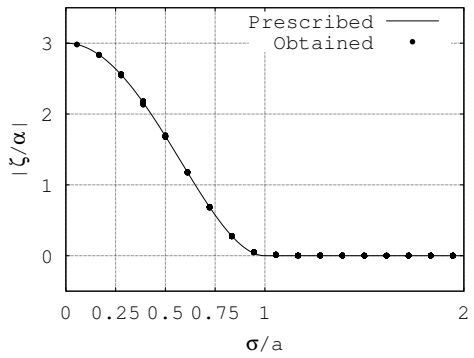

Figure 4: Obtained normalized velocity profile at all control points on the circular disk in a free-space at 1000 Hz when the piston is in s.p. 1.

Control points on the cabinet were spaced at approximately 20 mm, resulting in about 20 points per wavelength at 1000 Hz. The control points on the disk were rendered with a spacing of approx. 3 mm = $a/9$, giving about 100 points per wavelength at 1000 Hz. This resulted in ca 2600 control points at the box's surface whereof 250 on the vibrating disk and 750 on the passive annulus. The spacing between candidate points of the regular base-grid was chosen to be 25 mm, while an approximate spacing of 5 mm = $a/6$ was used in the ball. This resulted in ca 2700 candidate sources whereof 750 in the ball. If instead a spacing of 30 mm is used in the base-grid, this results in ca 1900 candidate points. An irregular base-grid was created from the regular one by adding a random offset of 5 mm to each candidate point. All simulations are based on an irregular base-grid unless otherwise stated. The box surface was divided into approx. 12000 non-overlapping rectangular error patches with one error point in the center of each patch. This resulted in a spacing between error points of approx. 7.5 mm, giving 40 points per wavelength at 1000 Hz.

3.2 Radiation in a free-space

The performance of the numerical model is evaluated using three different source positions; namely, s.p. 1 $(10, -116, 100)$, s.p. 2 $(150, 6, 70)$, and s.p. 3 $(50, 18, -250)$ in mm. This is followed by an analysis of the radiated sound field.

3.2.1 Performance

By increasing the number of substitute monopoles the normalized residual velocity approaches slowly the target threshold of -40 dB. This threshold however could rarely be reached at all frequencies which made the search stop at 500 selected monopoles. The normalized residual velocity, Eq. 5, did not exceed -34 dB at 1000 Hz for any of three source positions. The computation accuracy in the disk area was assessed by inspecting the velocity profiles obtained by substitute sources. The reconstructed velocity profiles on the disk as function of frequency were found to be in excellent agreement with the prescribed clamped-edge profile. An example is shown in Fig. 4.

Using the error points the reconstruction error typically descends to -25 ± 5 dB depending on source point and frequency. The obtained normal velocity can be observed by plotting the patch center velocities on the box surface. An example of the obtained normal velocity map is shown in Fig. 5. As expected, the velocity amplitude is strong within the disk area and virtually zero away from it.

The reconstruction error displays maxima near the box edges at the face containing the vibrating disk and near the vibrating disk. The velocity residual is lower than 0.1α; i.e., about 3% of the maximal velocity amplitude of the disk. Since the cabinet surface is much larger than the disk surface it may contribute to sound radiation even if its vibration amplitude is small. To evaluate the erroneous contribution by the cabinet, due to imperfect modeling, the radiated power was evaluated using Eq. 8. The power leakage, Eq. 9, was found to be small, less than 0.5 dB for all of three source positions and all frequencies. This shows

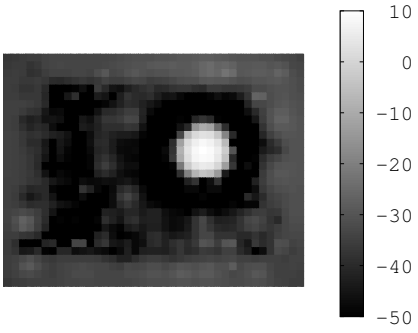

Figure 5: Obtained normalized normal velocity $|u_\perp/\alpha|$ in dB at surface patches on the face with disk at 1000 Hz. Box in a free-space, disk in s.p. 3.

that the substitute sources sufficiently well represent the original source and can thus serve to predict the sound field.

This far the vibrating disk was meant to simulate a simple source. The preceding analysis was therefore limited to wavelengths longer than the diameter of the disk. The substitute source technique is however not limited to any particular wavelengths. The computation of a disk in source position one was thus continued up to 10 kHz; i.e., to wavelengths shorter than the disk. As before, an irregular base-grid was used. In this case 1000 band frequencies were logarithmically distributed, starting at 10 Hz and ending at 10 kHz.

The normalized residual velocity on the box rarely exceeded -30 dB. The reconstruction error was however rather large beyond 1300 Hz, above -20 dB, and peaks to -15 dB at around 5 kHz. This shows the limits of the computation. The power leakage was however less than 0.5 dB and its tendency was to decrease with frequency. This indicates that the computed normal velocity rapidly fluctuates across the cabinet's surface without contributing much to the radiated sound due to the cancellation effect.

At short wavelengths the disk becomes a directional source whereas the closed-box baffle acts as an infinite baffle. The performance at higher frequencies will be further assessed by comparing the directivity of a disk in an infinite baffle and in a closed-box baffle.

3.2.2 Comparison with an infinite baffle

The sound radiated by a disk in an infinite baffle was computed using the Rayleigh integral as discussed in App. A. In the case of a box source, the radiation pattern was evaluated along a circle of 1 m radius centered at the disk center and lying in the $\mathbf{e}_1\mathbf{e}_2$-plane. In the case of an infinite baffle, the radiation pattern was evaluated along a half-circle of radius 1 m. The results have been normalized by the response of a hemispherical source.

A comparison between the two kinds of baffles are shown in Fig. 6. At low frequencies it is seen that the box-mounted disk behaves as a spherical source, with its acoustic center moved out of the box, while the infinite baffle turns it into a hemispherical source. At high frequencies it is seen that the closed-box baffle acts virtually as an infinite baffle. In-between the two extremes the case of a closed box-baffle approximates the radiation pattern of an infinite baffle at moderate angles from the disk axis. It is also seen that the baffle makes the vibrating disk a directional source as expected.

3.3 Radiation in a half-space

Radiation by a box suspended in a semi-anechoic room is influenced only by ground reflection if the absorbing materials on walls and ceiling are efficient. Where testing of vibroacoustic sources is concerned such a half-space is more readily available than a free-space. The model of a half-space will be developed in this section. This model will be confronted to measured transfer impedances in section 4.

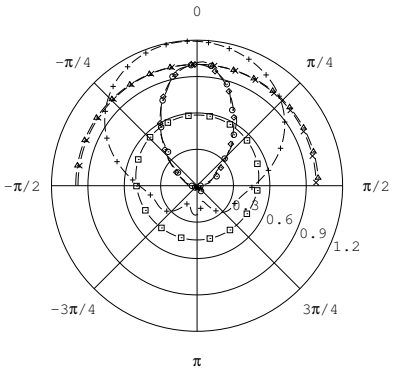

Figure 6: Polar radiation pattern of a clamped-edge disk in either an infinite baffle (i.b.) or in s.p. 1 of the closed-box baffle (c.b.b.). Legend: △ i.b. 100 Hz, □ c.b.b. 100 Hz, × i.b. 1000 Hz, + c.b.b. 1000 Hz, ◇ i.b. 10000 Hz, ∘ c.b.b. 10000 Hz.

3.3.1 Extending the numerical model: ground reflection

The ground will be simulated by an infinite rigid baffle on which normal velocity vanishes. Let the origin of coordinates lie on the infinite baffle coinciding with the $\mathbf{e}_1\mathbf{e}_2$-plane. The box is suspended at a height h from the baffle such that its center is given by $\mathbf{x} = (0, 0, h + 0.5l_3)$. The box edges are aligned with the coordinate system.

The infinite baffle can be modeled as an acoustic mirror, replacing the original surface problem in a half-space by one with the original box and its mirror image in a free-space [19, pp. 208 - 211]. Such an image box is obtained if all points $\mathbf{b} = (b_1, b_2, b_3)$ on the original box surface are mirrored to corresponding points given by $\mathbf{b}' = (b_1, b_2, -b_3)$. This applies both to the control and error points. In the same manner the prescribed velocity $\hat{\mathbf{v}}(\mathbf{b}) = (\hat{v}_1, \hat{v}_2, \hat{v}_3)$ in a point on the original surface is changed on the mirror surface to $\hat{\mathbf{v}}(\mathbf{b}') = (\hat{v}_1, \hat{v}_2, -\hat{v}_3)$. Thereafter each of the original box candidate points $\mathbf{m}_1, \ldots, \mathbf{m}_K$ are attributed a corresponding image candidate point $\mathbf{m}'_1, \ldots, \mathbf{m}'_K$ such that the k^{th} point is $\mathbf{m}'_k = (m_1, m_2, -m_3)_k$.

The half-space model requires no modification of the substitute source approach but involves a transfer matrix $\mathbf{T}$ four times larger than that in a free-space. To reduce the computational effort without compromising accuracy the search algorithm selects here a candidate monopole simultaneously with its image in each step and attributes to both an identical volume velocity. The symmetry of the radiation problem requires that, when an irregular base-grid is used, the randomization is applied to the primary source points before mirroring. Each element in the transfer matrix relates normal velocity at a control point $\mathbf{b}_1$, $\ldots$, $\mathbf{b}_N$ on the surface of the original box, to volume velocity of a pair $\{\mathbf{m}_1, \mathbf{m}'_1\}_1, \ldots, \{\mathbf{m}_K, \mathbf{m}'_K\}_K$ of monopoles. Such an element is given by

$$\begin{aligned} T_{nm} = &\frac{1}{4\pi}(1 + jkr_{nm})\frac{\mathrm{e}^{-jkr_{nm}}}{r_{nm}^2}\cos\gamma_{nm} \\ &+\frac{1}{4\pi}(1 + jkr'_{nm})\frac{\mathrm{e}^{-jkr'_{nm}}}{r'^2_{nm}}\cos\gamma'_{nm}, \end{aligned} \tag{12}$$

where $\mathbf{r}'_{nm} = \mathbf{b}_n - \mathbf{m}'_m$ and γ'_{nm} is the angle between the outward normal vector $\mathbf{n}_n$ of the original control point and the radius vector of the mirrored source, $\mathbf{r}'_{nm}$. The image box control points can be suppressed because no information is added to the solution. Using this formulation, the matrix size does not change with the inclusion of ground reflection. The mirror approach therefore does not penalize the computation time.

3.3.2 Comparing the performance in a free-space and a half-space

A box identical to the one used in free-space conditions was modeled. The analysis extended to all three disk positions combined with two suspension heights: either 200 mm or 530 mm from the ground. The

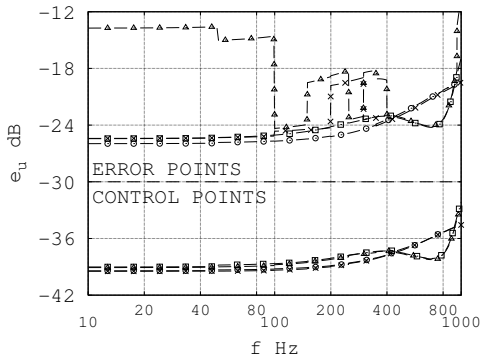

Figure 7: Velocity error for source point 3 in a free-space, using a regular base-grid (×) or an irregular base-grid (○), and in a half-space with the box suspended at 200 mm, using an irregular base-grid with spacing of either 25 mm (△) or 30 mm (□). Upper part: error points; lower part: control points.

stopping criteria of the search procedure were set to a maximum of 500 pairs of monopoles or a -40 dB velocity error whichever encountered first.

Numerical instabilities have been observed in both free-space and half-space conditions using a regular base-grid. As a result, the reconstruction error exhibits discrete jumps with frequency. An irregular base-grid makes most of the instabilities disappear.

By suspending the box from the ground, the substitute monopoles were found to sufficiently well represent the prescribed boundary conditions if the disk is either at source position 1 or 2. The largest reconstruction error was found to attain ca -20 dB in the worst case. Thus, the accuracy of the computation in a half-space condition is similar to that obtained in a free-space condition.

The source position 3, with the driver directed towards the ground, with the box at a height of 200 mm has been found difficult to compute and a mere randomization of the candidate points was not sufficient to improve accuracy. This is believed to be due to near-field interference of the source and the image boxes. A remedy was found by altering the average spacing in the base-grid from 25 mm to 30 mm. Thus repeated computations with different spacings may be necessary to obtain stable results, implying that a sparser base-grid can outperform a denser base-grid.

An example of velocity error at control points and error points as function of frequency for source position 3 is shown in Fig. 7. The jumps are not visible in the normalized residual velocity, showing that the accuracy at control points tells little about what happens in-between them.

3.3.3 Sound radiation

The radiated sound field was computed across a 2 × 2 m square surface placed through the box center, and a spatial resolution of 20 mm was used. The results show that at low frequencies the box and its image appear as a single source. The apparent source has its acoustical center moved out from the boxes towards the reflecting plane. In this case the box is acoustically transparent and does not perturb the propagating waves. Once the wavelength approaches the box dimensions, the box and its image radiate sound much more independently of each other. Constructive and destructive interference from the two fields is created. Transfer impedance level in the $\mathbf{e}_2\mathbf{e}_3$-plane at 1000 Hz is seen in Fig. 8. The interference together with cabinet diffraction is seen by the presence of undulations in the computed transfer impedances.

3.4 Discussion

A difficulty in applying the substitute source method is the lack of an intuitive design of the substitute source array. To overcome this problem a particular search procedure has been used. This requires repeated matrix inversion at each frequency of interest which makes the entire computation rather time consuming. Using an ordinary laptop (HP ProBook 6360b) an array of 500 substitute monopoles was identified in around 13 min at best. If instead an array of 300 monopoles was created, the procedure took 5 min, revealing

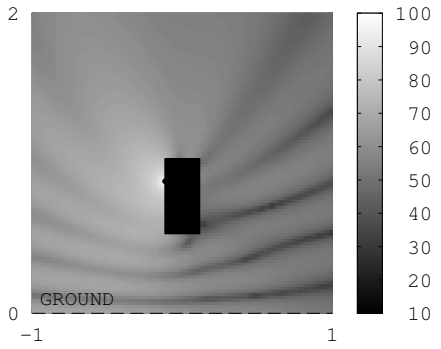

Figure 8: Transfer impedance level dB re. 1 kg·m^{-4}·s^{-1} between a box suspended at 530 mm, indicated by a black rectangle, and its image, not seen, when the disk is in s.p.1. The source point projected onto the plane is marked by a black half-circle, and the ground is marked by a dashed black line.

a square-law dependence on the number of monopoles. To reduce the computation time the frequency scale was divided into bands while the search was carried out at the band center frequencies. The identified source positions were then applied to all the frequencies within the band. Furthermore the original single-step formulation, where the search identifies one substitute source position per iteration step, was replaced in the case of a half-space by a search of a mirrored pair of positions resulting at the end in quadruple reduction of the transfer matrix involved. The entire computation for a single source layout takes several hours on an ordinary laptop.

The method cannot accurately enough model a rigid piston as a driver, as it fails to reproduce a steep change in normal velocity between the piston and the baffle. A similar problem exists close to the sharp edges of the box. Rounding corners and edges results in increased accuracy.

In the next study the half-space radiation model will be verified against measured transfer impedances.

4 TRANSFER IMPEDANCES IN A SEMI-ANECHOIC ROOM

A small driver can be used to simulate a simple source[22]. In this case the radiated field may be expressed by a (point) transfer impedance Z. The latter relates the volume velocity amplitude $\hat{Q}$ of the driver, located at $\mathbf{s}$, to the sound pressure amplitude $\hat{p}$ at $\mathbf{f}$

$$Z(\mathbf{f} \mid \mathbf{s}) = \frac{\hat{p}(\mathbf{f})}{\hat{Q}(\mathbf{s})}. \tag{13}$$

The measurement of transfer impedance requires the use of a known volume velocity driver[22, 23, 24, 25].

Measurements were done in an engine test cell. In spite of the walls being covered by sound absorbing layers, the cell was far from an ideal semi-anechoic room. Moreover it contained reflectors, such as an engine brake and technical equipment, which impairs its performance. One section of the concrete floor was missing and covered by a metallic grid. Despite these drawbacks, the cell maintained basic features of a semi-anechoic room as it is rather large and has a hard floor.

4.1 Hardware

An off-the-shelf mid-range driver, a Morel EM1308, was used as a simple source. The measurement of volume velocity was made using a reference microphone sealed into the driver's back cavity[25, 22]. The pressure - volume velocity calibration was done using a blocked pipe[22].

A closed-box baffle of dimensions 300 × 232 × 500 mm, i.e. of the same dimensions as used in the previous computation, was made out of six aluminum plates of 16 mm thickness. In two of the plates a Ø80 mm driver hole was cut-out at the position of the source positions 1 and 2 as defined in section 3. The projected area of the driver's diaphragm onto the surface of the cabinet corresponds to a disk of radius 30

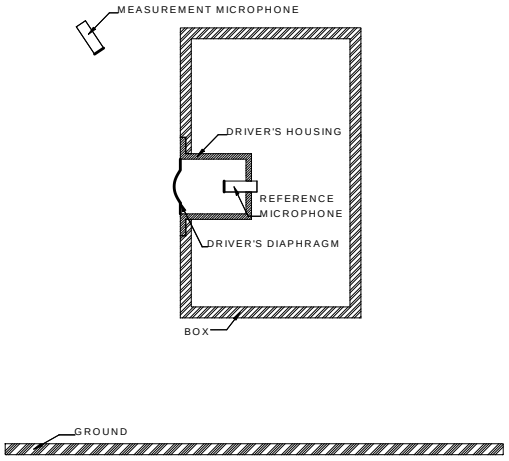

Figure 9: Schematic setup of the box inside of an engine test cell.

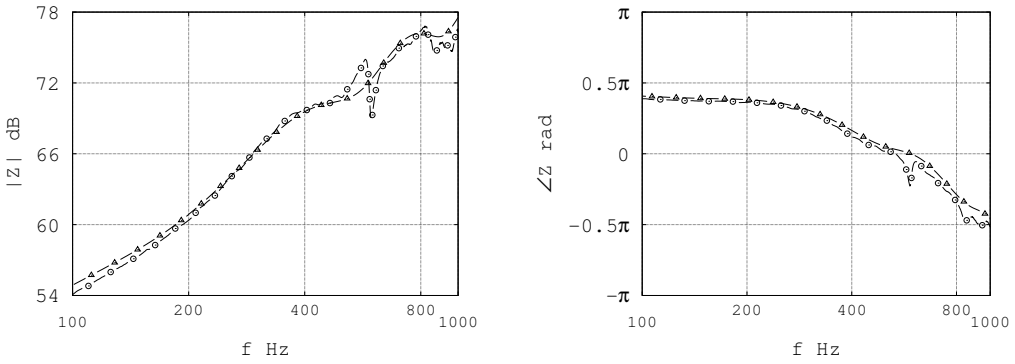

(a) (b)

Figure 10: Transfer impedances on the axis of the driver in s.p. 1 (a) level dB re. 1 kg·m^{-4}·s^{-1} and (b) phase, legend: ∘ measured, △ computed.

mm. Cable holes in the cabinet were sealed using silicone rubber. The box was mounted at a height of 200 mm on a frame made out of 25 × 25 mm hollow rectangular steel profiles.

The driver was fed from a bandpass filtered white noise generator. Frequencies below 100 Hz are omitted because the sound pressure level was too low with respect to background noise. An upper frequency limit was set to 1000 Hz because the driver is too large to act as a simple source above this frequency. The setup is shown in Fig. 9.

4.2 Validation

An example of measured and computed transfer impedances 165 mm away from the box along the driver's axis is shown in Fig. 10. The difference between the measured and computed sound pressure levels is less than 1 dB below 500 Hz, and the measured transfer impedance fluctuates around the predicted value. Around 600 Hz there is a dip where the difference in level is about 3 dB, believed to come from radiation by the box resonance. The computed and measured transfer impedances match rather well.

A second example of transfer impedances taken above the box, $(0, 0, 995)^t$ in mm, is shown in Fig. 11. Below about 400 Hz the prediction agrees with measurements within 3 dB. The level of the measured transfer impedance is fluctuating around its computed counterpart, which is believed to come from the imperfect room properties as well as from box vibration. The level difference is less than 6 dB for all frequencies. Measured and predicted phases match very well.

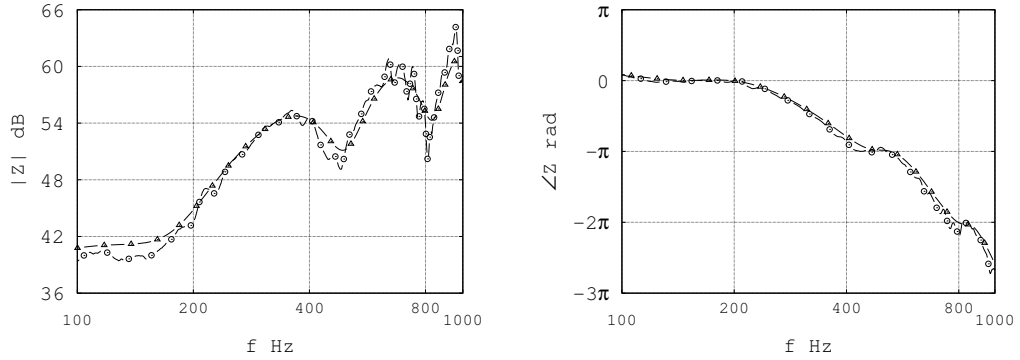

(a) (b)

Figure 11: Transfer impedances above the box with driver in s.p. 2 (a) level dB re. 1 $kg{\cdot}m^{-4}{\cdot}s^{-1}$ and (b) phase, legend: ○ measured, △ computed.

Measured transfer impedances contain effects of non-ideal room conditions and an imperfect realization of a rigid box. Despite practical and numerical shortcomings measured and computed transfer impedances look coherent.

5 CONCLUDING REMARKS

The paper discusses how free-space radiation by a vibrating disk set in a rigid closed baffle can be computed using an array of monopoles. The strengths of monopoles are computed for the best matching of radiated normal particle velocity to prescribed normal velocity across the surface of the driver - cabinet assembly. The computation is carried out by an incremental search procedure which uses pseudo-inversion of an analytical transfer matrix linking the monopole positions to control points at the surface. The search picks up convenient monopole positions from a grid of candidate points distributed in the interior of the surface. The quality of the results obtained is evaluated by two types of errors: (1) the difference between the prescribed and obtained normal velocities at the surface, and (2) the power output from the monopole array leaking through the passive baffle.

It was found that the grid of candidate positions should be made non-uniform, by considerably increasing its density close to the driver. Similarly the spacing of control points over the surface used in the search procedure should be much smaller across the disk than elsewhere. In some cases the grid with regular spacing produces instability of results which can be remedied by using small randomization of candidate positions. The finally attained result can be verified using additional, densely spaced error points across the boundary.

In a numerical case study the accuracy of radiation modeling by a medium-sized closed-box baffle is studied. To reduce the computation time the analyzed frequency range was divided in bands, with the search algorithm applied only at band center frequencies. The boundary velocity error was found to be typically in-between -30 and -20 dB. The power leakage was very small, indicating little influence of velocity error to the far-field radiation. It has been furthermore shown how the synchronized mirroring of substitute sources can be used for field modeling in the presence of a hard floor at no additional computational cost.

Finally a validation of the approach was made by comparing the computed transfer impedance in a semi-anechoic space to measurements. In spite of non-ideal anechoic conditions in the measurement room, the computation has produced satisfactory matching.

Acknowledgements

This work was funded by Volvo Construction Equipment. The funding is gratefully acknowledged. The work was carried out at Laboratoire Vibrations Acoustique at INSA de Lyon in France, a member of the Centre Lyonnais d'Acoustique. The experimental work has been greatly assisted by Patrick Blachier.

A SOUND RADIATION BY A CIRCULAR DISK IN AN INFINITE BAFFLE

To compute transfer impedances it is necessary that the disk is a simple source. Generally a disk does not have the spherical radiation pattern of a simple source [2, pp. 153 - 185]. It is known that at a considerable distance $r \gg a$ from a disk of radius a set in an infinite baffle the pressure amplitude $\hat{p}_\infty$ is of the form

$$\hat{p}_\infty = jk\rho_0 c \frac{\hat{Q}}{2\pi} \frac{\mathrm{e}^{-jkr}}{r} \Big\{ \dots \Big\}. \tag{14}$$

The braced term $\{\dots\}$ depends on the disk's vibration pattern and is a function of the radiation angles ϕ, θ [6, 7]. This term has to be one for a spherical radiation pattern. As long as this term does not change significantly over the inclination angles $0 - \pi/2$ an axisymmetrically moving disk approximates a simple source.

The radiated sound by a disk with a non-uniform velocity profile in an infinite baffle is computed by the Rayleigh integral[19, pp. 213 - 215]. The integral express a superposition of a continuous layer of monopoles set in the disk's surface, and is given in polar coordinates by

$$\hat{p}_\infty(\mathbf{f}) = \frac{j\omega\rho_0}{2\pi} \int_0^{2\pi} \int_0^a \zeta(\sigma) \frac{\mathrm{e}^{-jkr(\sigma,\phi)}}{r(\sigma,\phi)} \sigma \, d\sigma d\phi \tag{15}$$

where the angle ϕ describes a rotation around the disk's axis. Here, the distance is taken from an elementary source at the disk's surface at $\mathbf{m}(\sigma, \phi)$ to one field point at $\mathbf{f}$. This integral has been computed by iterated numerical integration using the trapezoidal rule[26].

The braced term in Eq. 14 can be estimated by evaluating the response at several points $\mathbf{f}(r, \theta)$ on a large half-circle originating at the disk center and being parallel with the disk normal. The radiation pattern is obtained by normalizing the disk response with the response of a hemispherical source of equal volume velocity.

The disk's power output in the far-field can be computed from the time-averaged radial intensity[19, pp. 39 - 47], $I_r = |\hat{p}|^2/(2\rho_0 c)$, through a half-sphere enclosing the disk and is given by

$$\Pi_\infty = \frac{\pi}{\rho_0 c} \int_0^{\pi/2} |\hat{p}_\infty(r, \theta)|^2 r^2 \sin\theta \, d\theta. \tag{16}$$

Here, the distance is computed from the disk center. Such a surface of revolution can be created from the half-circle previously used to assess the radiation pattern.

6 Bibliography

[1] H. F. Olson, "Direct Radiator Loudspeaker Enclosures," J. Audio Eng. Soc. **0**, 34, 36, 38 and 59 - 64 (1951).

[2] L. E. Kinsler and A. R. Frey, *Fundamentals of Acoustics, 2^{nd} ed.*, (John Wiley & Sons, 1962), pp. 153 - 185 and 247 - 254.

[3] J.-H. Chang and F. Jacobsen, "Experimental validation of sound field control with a circular double-layer array of loudspeakers," J. Acoust. Soc. Am. **133**, pp. 2046 - 2054 (2013).

[4] P. M. Morse and K. U. Ingard, *Theoretical Acoustics*, (McGraw-Hill Book Company, 1968), pp. 343 - 347.

[5] R. M. Aarts and A. J. E. M. Janssen, "Sound radiation from a resilient spherical cap on a rigid sphere," J. Acoust. Soc. Am. **127**, pp. 2262 - 2273 (2010).

[6] D. L. Dekker, R. L. Piziali, and E. Dong, "Effect of boundary conditions on the ultrasonic beam characteristics of circular disks," J. Acoust. Soc. Am. **56**, pp. 87 - 93 (1974).

[7] M. Greenspan, "Piston radiator: some extensions of the theory," J. Acoust. Soc. Am. **65**, pp. 608 - 621 (1979).

[8] L. Cremer, "Die Synthese des Schallfeldes eines beliebigen festen Körpers in Luft mit beliebiger Schnelleverteilung aus Kugelschallfeldern" (Synthesis of the sound field of an arbitrary rigid radiator in air with arbitrary particle velocity distribution by means of spherical sound fields), Acustica, **55**, pp. 44 - 46 (1984).

[9] G. H. Koopmann, L. Song, and J. B. Fahnline, "A method for computing acoustic fields based on the principle of wave superposition," J. Acoust. Soc. Am. **86**, pp. 2433 - 2438 (1989).

[10] M. Ochmann, "The source simulation technique for acoustic radiation problems," Acustica **81**, pp. 512 - 527 (1995).

[11] G. Pavić, "An engineering technique for the computation of sound radiation by vibrating bodies using substitute sources," Acta Acustica United Ac. **91**, pp. 1 - 16 (2005).

[12] L. Song, G. H. Koopmann, and J. B. Fahnline, "Numerical errors associated with the method of superposition for computing acoustic fields," J. Acoust. Soc. Am. **89**, pp. 2625 - 2633 (1991).

[13] Y. J. R. Gounot, R. E. Musafir, "Genetic algorithms: A global search tool to find optimal equivalent source sets," J. Sound. Vib. **322**, pp. 282 - 298 (2009).

[14] C. S. Obiekezie, D. W. P. Thomas, A. Nothofer, S. Greedy, L. R. Arnaut, and P. Sewell, "Complex Locations of Equivalent Dipoles for Improved Characterization of Radiated Emissions," IEEE Transactions on Electromagnetic Compatibility **56**, pp. 1087 - 1094 (2014).

[15] W. Kropp and P. U. Svensson, "Application of the time domain formulation of the method of equivalent sources to radiation and scattering problems," Acta Acustica United Ac. **81**, pp. 528 - 543 (1995).

[16] D. Berckmans, B. Pluymers, P. Sas, and W. Desmet, "Numerical comparison of different equivalent source models and source quantification techniques for use in sound synthesis systems," Acta Acustica United Ac. **97**, pp. 138 - 147 (2011).

[17] A. T. Moorhouse and G. Seiffert, "Characterisation of an airborne sound source for use in a virtual acoustical prototype," J. Sound Vib. **296**, pp. 334 - 352 (2006).

[18] A. Lindberg, G. Pavić, and Q. Leclère, "Characterisation of air-borne noise by a dummy source approach," In the Proceedings of Noise and Vibration - Emerging Technologies (NOVEM), pp. N/A (2015).

[19] A. D. Pierce, *Acoustics - An Introduction to its Physical Principles and Applications*, (McGraw-Hill Book Company, 1981), pp. 39 - 47, 100 - 103, 153 - 207, 208 - 211 and 213 - 215.

[20] P. Courrieu, "Fast computation of Moore-Penrose inverse matrices," Neural Information Processing - Letters and Reviews **8**, pp. 25 - 29 (2005).

[21] F. J. M. Frankort, "Vibration and sound radiation of loudspeaker cones," Ph.D. Thesis, Delft University of Technology (1975), pp. 1 - 15 and 165 - 166.

[22] A. Lindberg and G. Pavić, "Measurement of volume velocity of a small sound source," Appl. Acoust., **91**, pp. 25 - 32 (2015).

[23] T. Salava, "Sources of the constant volume velocity and their use for acoustic measurements," J. Audio Eng. Soc. **22**, pp. 146 - 153 (1974).

[24] T. Salava, "Acoustic load and transfer functions in rooms at low frequencies," J. Audio Eng. Soc. **36**, pp. 763 - 775 (1988).

[25] D. K. Anthony and S. J. Elliott, "A comparison of three methods of measuring the volume velocity of an acoustic source," J. Audio Eng. Soc. **39**, pp. 355 - 366 (1991).

[26] L. Råde and B. Westergren, *Mathematics Handbook for Science and Engineering,* 5^{th} *ed.*, (Studentlitteratur, Lund, 2004), p. 232 and 404.

INSA INSTITUT NATIONAL DES SCIENCES APPLIQUÉES LYON

FOLIO ADMINISTRATIF

THÈSE SOUTENUE DEVANT L'INSTITUT NATIONAL DES SCIENCES APPLIQUÉES DE LYON

NOM : LINDBERG
(avec précision du nom de jeune fille, le cas échéant)

DATE de SOUTENANCE : 28/09/2015

Prénoms : Anders Sven Axel

TITRE :

Airborne Noise Characterisation of a Complex Machine using a Dummy Source Approach

NATURE : Doctorat

Numéro d'ordre : 2015ISAL0082

Ecole doctorale : MEGA

Spécialité : Acoustique

RESUME : La caractérisation des sources sonores dues aux vibrations est un défi dans le domaine du bruit et des vibrations. Dans cette thèse, une approche expérimentale pour caractériser la propagation du son d'une machine complexe a été étudiée. Pour caractériser de manière appropriée la source sonore placée dans un environnement quelconque, il a été indispensable de prendre en compte les phénomènes de rayonnement et de diffraction. Cela permet de prédire une pression acoustique. Une technique particulière, appelée source mannequin, a été développée pour répondre à cette problématique. Le mannequin est une enceinte fermée de taille similaire mais qui a une forme simplifiée par rapport à la machine complexe, et sert de modèle de diffraction sonore. Le mannequin est équipé d'une série de haut-parleurs alignés dans le prolongement de la surface de l'enceinte. La superposition du champ acoustique créé par chaque haut-parleur modélise le rayonnement acoustique de la machine complexe.

Cette thèse introduit donc le concept de source mannequin et traite de trois problèmes émanant de la mise en pratique de celui-ci : (1) l'estimation du transfert d'impédance dans l'espace (fonction de Green), (2) les spécifications de l'enceinte et de la série de haut-parleurs, et (3) l'estimation des sources équivalentes en termes de débit volumique. L'approche est étudiée au travers de cas d'études expérimentaux et numériques.

MOTS-CLÉS : rayonnement acoustique par un corps vibrant, diffraction du son par un corps vibrant, principe de superposition, estimation des fonctions de transfert d'impédance, estimation de débit volumique des sources équivalentes, approche par source mannequin, approche par la fonction de Green.

Laboratoire (s) de recherche : Laboratoire Vibrations Acoustique

Directeur de thèse : Goran PAVIC

Président de jury : Charles PEZÉRAT

Composition du jury :

Goran PAVIC, Prof. Emer., INSA de Lyon, Directeur de Thèse
Anders NILSSON, Prof. Emer., Università degli Studi di Brescia, Rapporteur
Paul SAS, Prof., Katholieke Universiteit Leuven, Rapporteur
Charles PEZÉRAT, Prof. & Université de Maine, Examinateur
Quentin LECLÉRE, MCF HDR, INSA de Lyon, Examinateur